16+

ISSN 1028-4427 (Print)
ISSN 2542-131X (Online)

Гений Ортопедии
Orthopaedic Genius

Том 31
№ 3
2025

Научно-теоретический и практический журнал
Основан в память академика Г.А. Илизарова

Курган

Учредитель и издатель журнала:

федеральное государственное бюджетное учреждение «Национальный медицинский исследовательский центр травматологии и ортопедии имени академика Г.А. Илизарова» Министерства здравоохранения Российской Федерации

Издание журнала осуществляется при поддержке Ассоциации по изучению и применению метода Илизарова России (A.S.A.M.I. Россия)

Журнал включен в перечень научных специализированных изданий ВАК, в которых могут публиковаться основные результаты диссертационных работ на соискание ученой степени кандидата наук, ученой степени доктора наук (3.1.8 – травматология и ортопедия)

Журнал включен в Реферативный журнал и Базы данных ВИНИТИ

Сведения о журнале ежегодно публикуются в международной справочной системе по периодическим и продолжающимся изданиям «Ulrich's Periodicals Directory»

Журнал включен в библиографические и реферативные базы данных РИНЦ и SCOPUS

Журнал включен в электронные информационные ресурсы базы данных EBSCO

Электронная версия журнала размещена на сайтах

http://ilizarov-journal.com
http://elibrary.ru
http://cyberleninka.ru

Адрес: 640021, Россия, г. Курган, ул. М. Ульяновой, 6
Телефоны: (3522) 43-06-94 – редакция
(3522) 23-42-60 – реклама
Интернет: http://ilizarov-journal.com/
Email: genius@ilizarov.ru

Оригинал-макет изготовлен ОИАиВР ФГБУ «НМИЦ ТО имени академика Г.А. Илизарова» Минздрава России

Журнал зарегистрирован Федеральной службой по надзору в сфере связи, информационных технологий и массовых коммуникаций ПИ № ФС77-68207 от 30 декабря 2016 года

Территория распространения: Российская Федерация, зарубежные страны

Язык: русский, английский

Издается 6 раз в год

Цена свободная

Original Articles

Clinical Case

Review Article

Anniversaries

Obituary

Оригинальные статьи

Клинический случай

Обзорная статья

Юбилей

Некролог

Original article
https://doi.org/10.18019/1028-4427-2025-31-3-269-278

Results of supracondylar osteotomy and bone fixation with the Ilizarov apparatus for cubitus varus and valgus deformities

R. Kaul✉, M. Prasad, N. Akhoon

Base Hospital Delhi Cantt, New Delhi, India

Corresponding author: Rajiv Kaul, drrajivkaul@gmail.com

Abstract

Introduction Cubitus varus denotes the inward deviation of the supinated forearm on the extended elbow. In cubitus valgus, the forearm is angled away from the body with the arm fully extended. Both deformities manifest clinically as an abnormal carrying angle, along with a cosmetically unsightly appearance, with or without restricted range of motion (ROM).

The **aim** of the study is to evaluate the results of one-stage supracondylar corrective osteotomy and bone fixation using the Ilizarov apparatus in varus and valgus deformities of the elbow joint, using the angulation-translation principle (osteotomy rule 2); to determine the effect of this method on the humerus-elbow-wrist angle (HEW), ODD and lateral prominence index (LPI).

Materials and Methods A total of 12 patients, age ranging from 7–24 years, who presented with cubitus varus of ⩾ 10° (n = 9) and cubitus valgus (n = 3) of ⩾ 20°, were included in the study. All patients underwent acute correction using a mini-incision, supracondylar osteotomy and fixation with the Ilizarov frame.

Results The mean time to union was 14.2 weeks (range, 11–18 weeks). The average duration of follow-up was 24 months. Functional outcome was graded as excellent in 9 cases (75 %), good in 2 (17 %) cases and poor in 1 case (8 %) using the grading system of Oppenheim. For cubitus varus, the mean HEW angle improved significantly, from (–15.5 ± 4.2) pre-operatively to (8.2 ± 1.5) post-operatively. For cubitus valgus, the mean HEW angle was (28.3 ± 5.3) pre-operatively, which improved to (14.1 ± 3.1) post-operatively, which was statistically significant. Complications encountered included superficial pin-tract infection in 1 case, lateral condylar prominence in 1 case and complete radial nerve palsy in 1 case.

Discussion Conventional methods of treatment of cubitus varus or valgus include various corrective osteotomies, typically stabilized with internal fixation. Despite being successful, a substantial number of distressing complications have been reported with the use of internal fixation. The mandatory requirement of post-operative immobilization, resulting in stiffness and disuse atrophy, is a deterrent to the use of internal hardware, which can be easily circumvented by the versatility of the Ilizarov apparatus.

Conclusion External fixation with the Ilizarov apparatus is a versatile means of correction of cubitus varus and valgus. It precisely achieves the desired carrying angle and cosmetic appearance of the elbow. It facilitates residual adjustments in under/over-corrected scenarios. The stability is indisputable. Early joint mobilization leads to an improved functional outcome.

Keywords: cubitus varus, cubitus valgus, osteotomy rules, Ilizarov fixator, deformity correction

For citation: Kaul R, Prasad M, Akhoon N. Results of supracondylar osteotomy and bone fixation with the Ilizarov apparatus for cubitus varus and valgus deformities. *Genij Ortopedii*. 2025;31(3):269-278. doi: 10.18019/1028-4427-2025-31-3-269-278.

INTRODUCTION

Supracondylar fractures are the most common fractures encountered in paediatric population, accounting for 50–70 % of elbow injuries [1]. Treatment can vary from conservative management to open reduction with or without pinning, depending upon the fracture geometry [2, 3]. Cubitus varus is the most common angular deformity, presenting as late sequel to poorly-treated or untreated supracondylar fractures in children [4]. The main reason for development of this deformity is a varus tilt along with internal rotation and medial displacement of the distal fragment, resulting in an abnormal carrying angle [5]. Cubitus valgus, on the other hand, is a rather uncommon deformity arising most often from a lateral condylar non-union or malunion, with or without ulnar nerve symptoms [6]. The indications for corrective surgery include an undesirable cosmetic deformity or a limitation of elbow motion or both. Numerous osteotomies have been described for the treatment of cubitus varus and valgus [7]. The goal of correction is to address not only the coronal component, but the rotational and sagittal plane deformity, if any. Prevention of joint stiffness, by virtue of a stable fixation, and early mobilization is highly desirable.

The choice of osteotomy as well as of fixation methods is a topic of contention till date. Most surgeons prefer a lateral closing wedge osteotomy for cubitus varus for its technical simplicity and reproducibility [8]. Cubitus valgus is frequently addressed with a dome osteotomy along with ulnar nerve transposition [9]. Problems associated with acute corrective osteotomies include under- or over-correction, failure of fixation, neuropraxia, unsightly scars, re-fractures at the osteotomy site, joint stiffness, and infection [10]. The introduction of the Ilizarov method of a low-energy osteotomy, combined with gradual distraction, offered the unique ability to perform post-operative titration of angular correction, as well as early joint mobilization [10].

The **aim** of the study is to evaluate the results of one-stage supracondylar corrective osteotomy and bone fixation using the Ilizarov apparatus in varus and valgus deformities of the elbow joint, using the angulation-translation principle (osteotomy rule 2); to determine the effect of this method on the humerus-elbow-wrist angle (HEW), ODD and lateral prominence index (LPI).

MATERIALS AND METHODS

Twelve patients, in the age range from 7 to 24 years, who presented with either cubitus varus or valgus, and desired surgical correction, were included in this retrospective study. We retrieved hospital records, radiographs, and clinical photographs from 2020 to 2024, of individuals who underwent deformity correction using a percutaneous, low-energy osteotomy, and bone fixation with an Ilizarov frame application, and analysed various clinical and radiological parameters, using Microsoft Excel 2024 (v.16). Those with an incomplete database or follow-up were excluded from the study. The objectives of the study were to assess the bearing of this method on the Humerus-Elbow-Wrist (HEW) angle, the Lateral Prominence Index (LPI) and elbow range of motion (ROM). Preoperative clinical examination included recording of the carrying angle and ROM, using a goniometer. The internal rotation element was assessed using the Yamamoto method [11]. The three-point bony relationship and inter-condylar distance measurements were recorded in all cases, although their clinical relevance is a matter of debate [12]. The HEW angles were measured on anteroposterior radiographs of both upper extremities, in addition to the LPI [7, 13]. In normal individuals, the LPI is predominantly a negative value, due to naturally-existing slight medial condylar prominence. All pre-operative planning and software simulation was performed using the Bone Ninja iPad mobile application [14].

Surgical technique

The Ilizarov frame design consisted of two rings, one proximal at the level of the mid-arm, and one distal at the level of the elbow joint (Fig. 1 a, b). The orientation of the distal ring was parallel to the distal humeral articular surface, whereas that of the proximal ring was perpendicular to the diaphysis (Fig. 1 b). The rings were connected to each other using juxta-articular hinges mounted on connecting rods, and a medially placed distraction assembly, orthogonally, as shown in the figure 1, b. Two counter-opposed olive wires and one 5-mm Shanz pin, inserted along the safe corridors, were used to affix the distal ring (Fig. 2 a). The medial wire was inserted with the elbow in semi-extended position, palpating the ulnar nerve, and ensuring the wire entry anterior to the nerve. The proximal ring was affixed with two 5-mm Shanz pins and a wire. A 1-cm skin incision was sufficient to perform a low-energy osteotomy using the multiple drill-hole method (Fig. 2 b) [15]. The osteotomy was distracted acutely and an angulation-translation was performed, using the juxta-articular hinges (Fig. 2 c). Once satisfactory correction was confirmed under fluoroscopy, the osteotomy was compressed and the nuts tightened (Fig. 2 d). For larger deformities of more than 15° of angular correction, anterior transposition of the ulnar nerve was contemplated, both in cubitus varus and valgus. Any residual deformity detected in post-op radiographs was corrected subsequently.

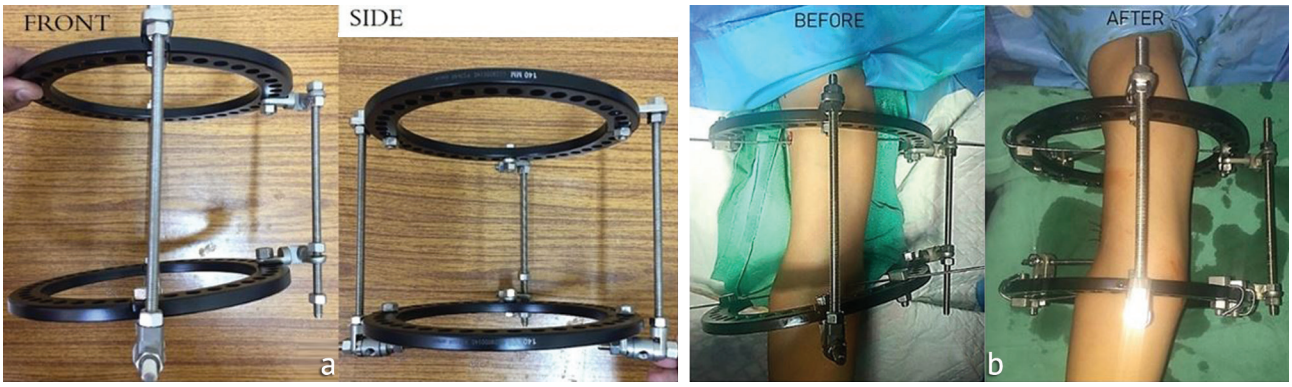

Fig. 1 Pre-assembled frame design: (a) front view showing juxta-articular hinge placement, and side view, showing the motor/distraction assembly; (b) intra-operative images of frame orientation before and after the osteotomy

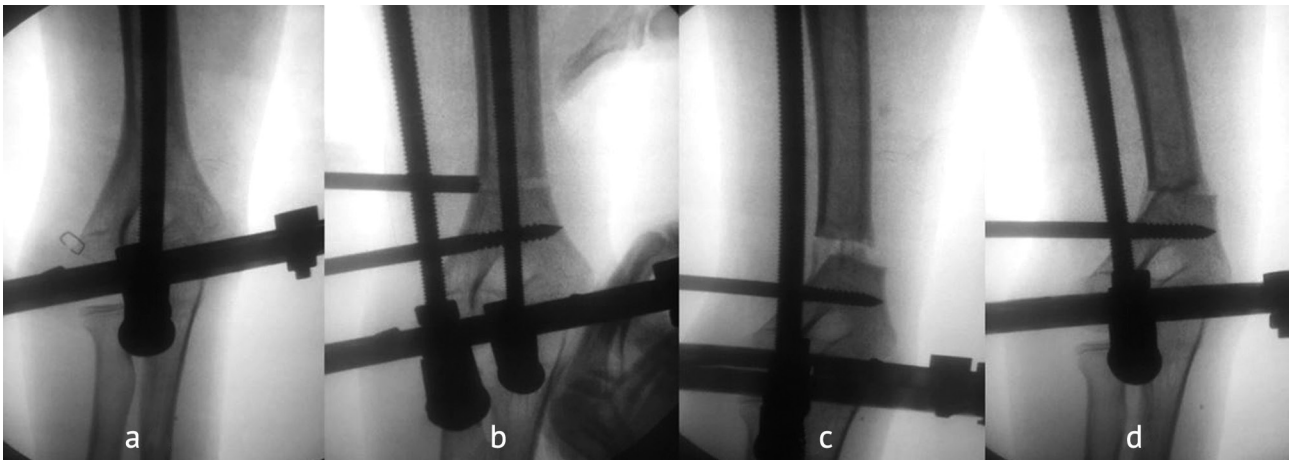

Fig. 2 The Ilizarov frame assembly: (a) orientation of distal ring with counter-opposed olives; (b) multiple drill-hole osteotomy; (c) acute distraction followed by angulation of the osteotomy; (d) compression of the osteotomy after satisfactory alignment

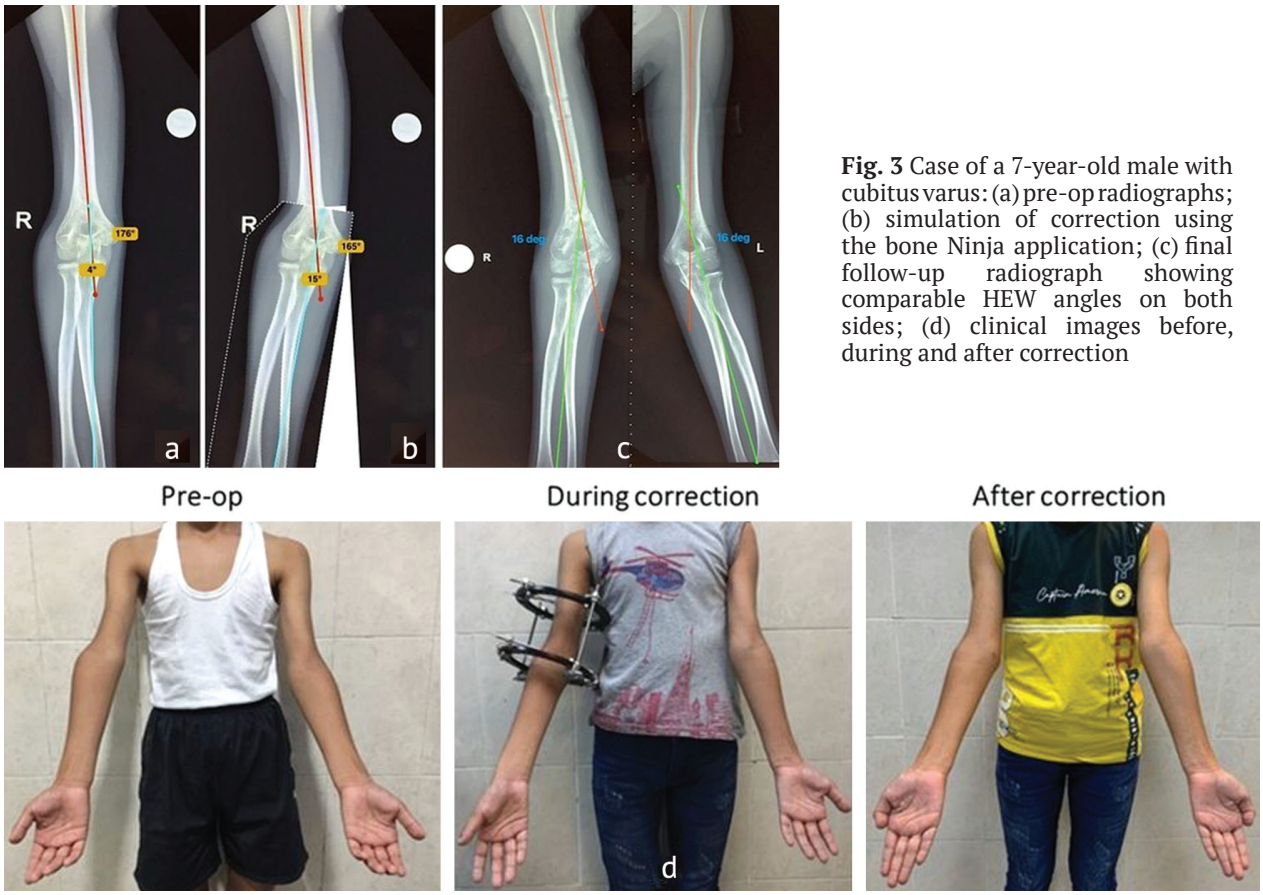

Fig. 3 Case of a 7-year-old male with cubitus varus: (a) pre-op radiographs; (b) simulation of correction using the bone Ninja application; (c) final follow-up radiograph showing comparable HEW angles on both sides; (d) clinical images before, during and after correction

For skeletally mature patients with closed physes, a mini-Ilizarov assembly was used, which was less cumbersome as compared to the standard Ilizarov frame. Two 5-mm Shanz pins were placed percutaneously in the distal humerus from the lateral side, in the same plane, parallel to the joint line (Fig. 4 a), and two pins were placed in the mid-third of the humerus, perpendicular to the shaft, but in different planes, subtending an angle of around 45° when viewed from above (Fig. 5 b, d). The biplanar placement of pins was planned to circumvent the course of the radial nerve and increase the stability of fixation. The pins in the distal segment were mounted on a swivel-type Rancho cube (Fig. 5 d, circled in red), to allow angulation of the distal fragment following the osteotomy, which was performed precisely as described above. It is noteworthy to state here, that while performing all acute corrections, translation precedes angulation, in accordance with osteotomy rule 2 (Fig. 4 c, d) [16].

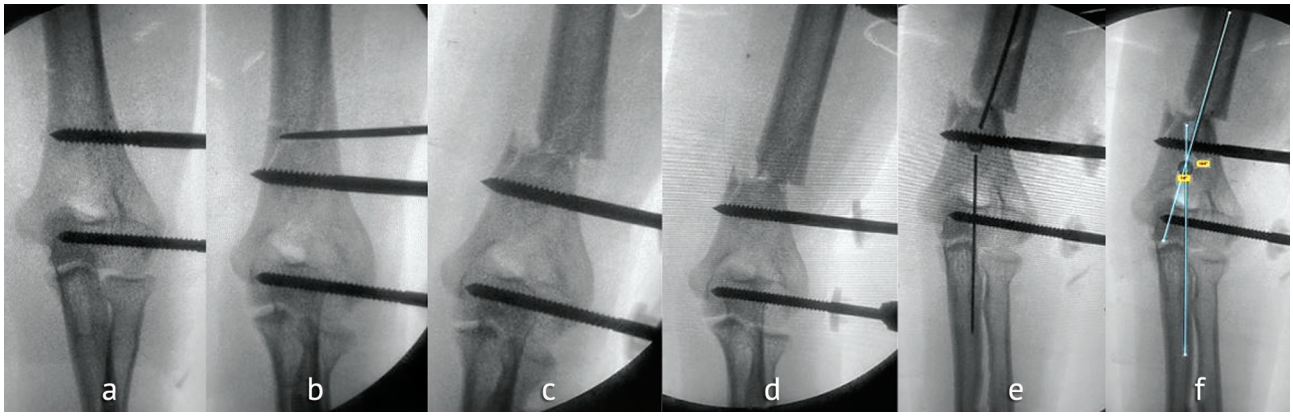

Fig. 4 Mini-Ilizarov frame: (a) with 2 parallel Shanz pins in the distal fragment; (b) multiple drill hole supracondylar osteotomy; (c) medial translation performed first; (d) followed by angulation to the desired degree; (e, f) measurement of the angular correction intra-op, using a radiolucent, sterile goniometer

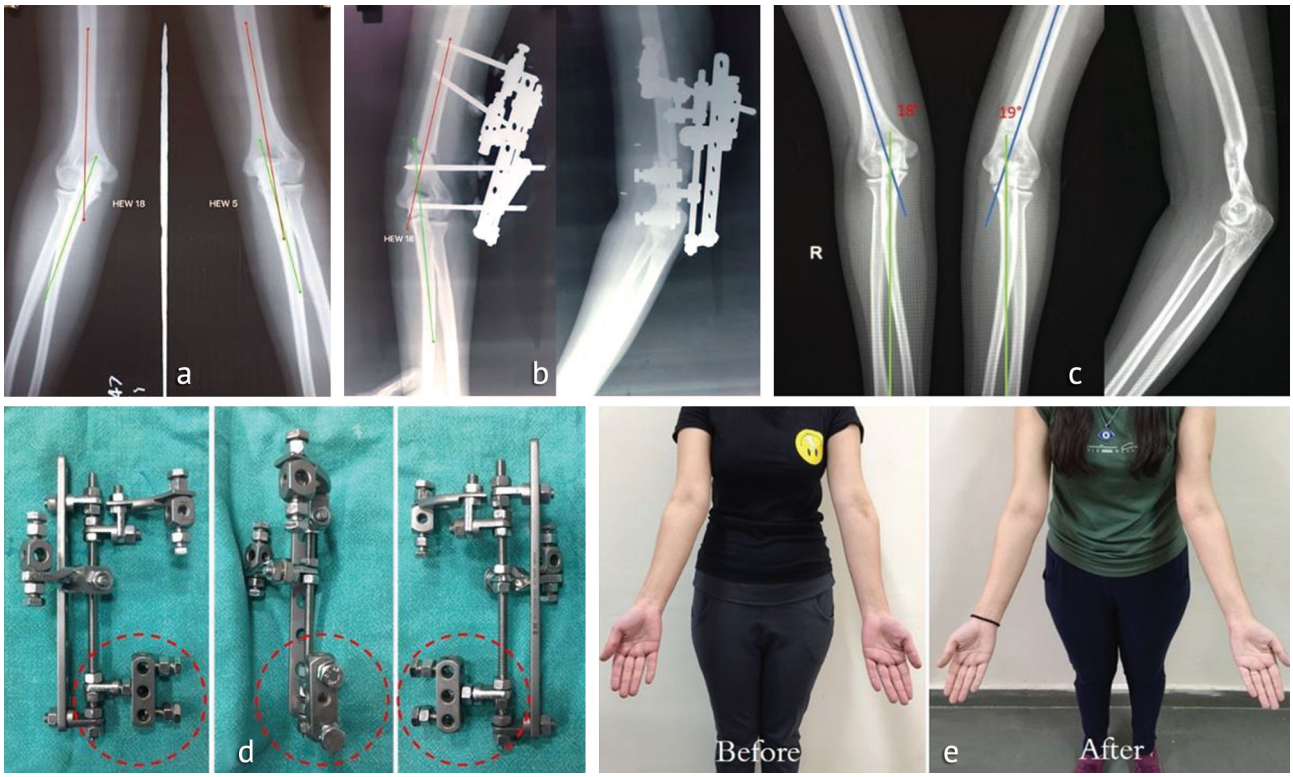

Fig. 5 Case of a 17-year-old girl: (a) pre-operative radiographs of cubitus rectus; (b) post-operative radiographs following mini-Ilizarov correction; (c) final follow-up radiographs showing accurate correction, comparable to contralateral elbow; (d) mini-Ilizarov frame assembly, red circled portion represents the swivel-type Rancho cube for the distal fragment; (e) clinical images before and after correction

Fine adjustments and fastening of all connections was performed under C-arm guidance. Derotation was performed only in one patient who had impaired shoulder function compared to the contralateral side.

Post-operative protocol comprised of assisted joint ROM exercises at the end of week 1, followed by strengthening exercises at 4 weeks. Crutch-assisted walking using the operated upper limb was encouraged in older patients, to simulate weight-bearing in the lower extremity, in order to promote union. Frame removal was done after satisfactory consolidation was seen on orthogonal radiographs. Follow-up was done at 2-week intervals until frame removal, and every 6 month thereafter. The functional outcome was assessed and graded as excellent, good, or poor according Oppenheim's criteria [17]. Statistical analysis was done using Microsoft Excel 2024 (v.16), applying Student's paired t-test, with a *p*-value of < 0.05 considered as significant.

RESULTS

The mean patient's age recorded was 16.2 years. Of the 12 patients, 4 (33.3 %) were males and 8 (66.7 %) were females. The mean time to union was 14.2 weeks (range 11–18 weeks). The average duration of follow-up was 24 months. Functional outcome was graded as excellent in 9 cases (75 %), good in 2 (17 %) and poor in 1 case (8 %) using the grading system of Oppenheim et al. [7, 17]. There was no significant difference between the mean pre- and post-operative arc of motion (*p*-value: 0.16). The cumulative results are summarized in Table 1 and Table 2.

Table 1

Comparison of pre-op and post-op assessment parameters

Parameter	Pre-op ° ± SD	Post-op ° ± SD	*P*-value
Mean HEW* angle			
Cubitus varus	–15.5 ± 4.2	8.2 ± 1.5	< 0.05
Cubitus valgus	28.3 ± 5.3	14.1 ± 3.1	< 0.05
Mean flexion / extension	125 / –5	120 / 0.5	0.16
Mean LPI* (cubitus varus)	2.5 ± 0.5	–1.6 ± 0.2)	< 0.05
Mean MPI*(cubitus valgus)	–8.4 ± 1.3	–3.7 ± 0.4	< 0.05

* HEW — Humerus Elbow Wrist angle; LPI — Lateral prominence index; MPI — Medial prominence Index.

Table 2

Functional results as per Oppenheim's grading

Interpretation	Criteria	No. of cases
Excellent	1. Correction of varus or valgus to within 5°of contralateral elbow	9
	2. Loss of motion ⩽ 5° of pre-op value	
	3. No complications	
Good	1. Correction of varus or valgus to within 6–10°of contralateral elbow OR	2
	2. Loss of motion ⩽ 6–10° of pre-op value OR	
	3. Scarring or a lazy-S deformity	
Poor	1. Residual (uncorrected) varus or valgus differing by >10° of contralateral elbow OR	1
	2. Loss of > 10° in any plane of motion OR	
	3. Any complication	

Cubitus varus (*n* = 9): The mean HEW angle improved significantly from (–15.5 ± 4.2) pre-operatively to (8.2 ± 1.5) post-operatively. The average lateral prominence index pre-operatively was (2.5 ± 0.5), which improved to (–1.6 ± 0.2), negative indicating normal values. We included in our series one patient who had a straight elbow (cubitus rectus), who had esthetic concerns and who underwent correction with a mini-Ilizarov frame yielding gratifying results. Complications encountered included superficial pin-tract infection in one case managed with antibiotics and local dressings, and lateral prominence in one case which was managed conservatively.

Cubitus valgus (*n* = 3): The mean HEW angle was (28.3 ± 5.3) pre-operatively and improved to (14.1 ± 3.1) post-operatively, which was statistically significant. Mean medial prominence index (MPI) was calculated for valgus deformities [7], and found to be (–8.4 ± 1.3) pre-operatively and (–3.7 ± 0.4) post-operatively. One patient who underwent corrective osteotomy with the mini-Ilizarov frame (Fig. 6 and Fig. 7) had a post-operative wrist drop, which was initially managed expectantly, with no improvement for the first 14 weeks. Nerve conduction studies (NCS) suggested complete axonotemesis involving the radial nerve and radiographs showed a consolidated osteotomy with satisfactory limb alignment. The patient underwent radial nerve exploration along with frame removal (Fig. 7). Intra-operatively, one of the Shanz pins had inadvertently damaged a portion of the radial nerve, forming a neuroma in continuity (Fig. 7 c). Using a nerve stimulator, the non-conducting segment of the nerve was excised, and end-to-end epineural repair was performed using 9–0 polypropylene sutures (Fig. 7 d, e). The patient had a complete recovery of his elbow, wrist, and finger movements at the end of around 12 months after the repair (Fig. 8). One patient, with a large valgus deformity of 33° underwent a prophylactic anterior transposition of the ulnar nerve along with the osteotomy.

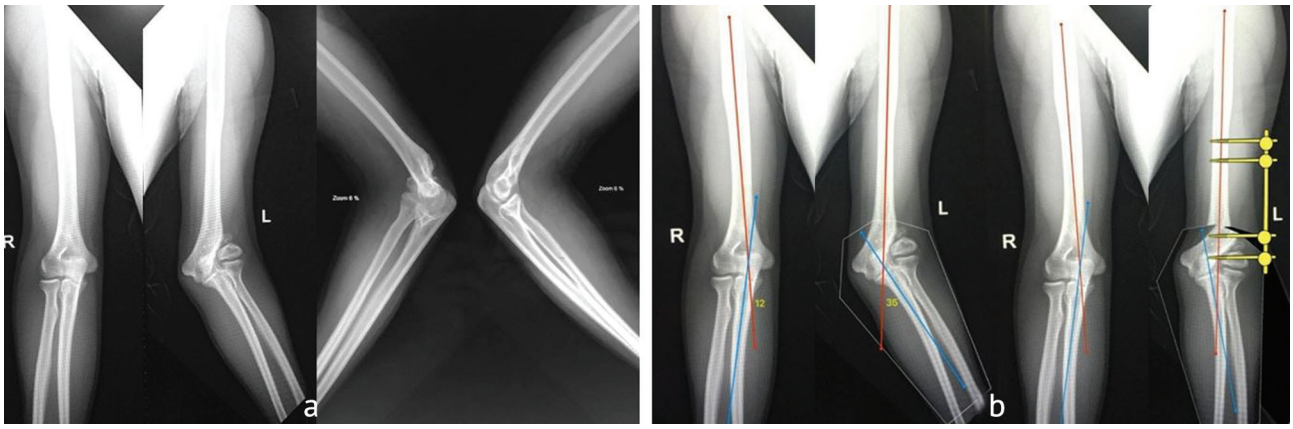

Fig. 6 Case of a 24-year-old male with cubitus valgus: (a) pre-operative radiographs; (b) simulation of correction using the Bone Ninja application

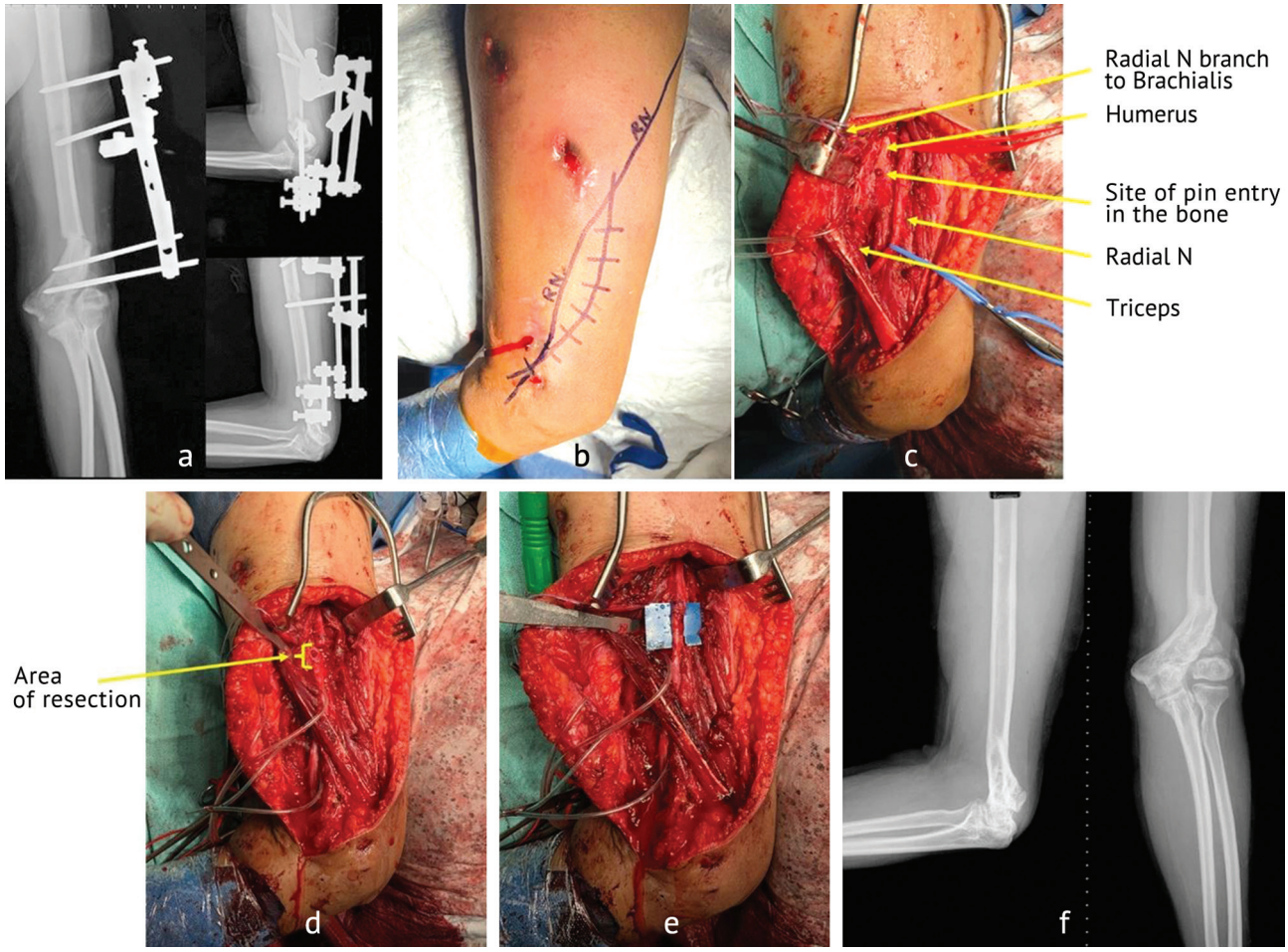

Fig. 7 Case of a 24-year-old male with cubitus valgus: (a) post-operative radiographs following mini-Ilizarov correction; (b) skin marking for radial nerve exploration; (c) intra-operative findings during exploration, showing the pin entry into the bone, immediately adjacent to the neuroma; (d) resected non-conducting segment, as determined by nerve stimulation; (e) end-to-end epineural repair, reinforced with Tisseal® fibrin sealant; (f) final follow-up radiographs showing satisfactory consolidation and limb alignment

Fig. 8 Clinical images of the same individual: (a) before and after correction; (b) functional status post-radial nerve repair

DISCUSSION

Traditional methods of treatment of cubitus varus include the lateral closing wedge osteotomy [18], the medial opening wedge osteotomy (King and Secor) [19], the modified French osteotomy [20], the oblique osteotomy [21], the dome osteotomy [22] and the step-cut osteotomy [23]. Subsequently, many authors described various modifications of the prevailing techniques, such as the penta-lateral osteotomy [24], the 3-dimensional osteotomy [25], the lateral equal-limbs osteotomy [13], the double-dome osteotomy [26], the oblique lateral closing wedge osteotomy [27], and the reverse step-cut osteotomy [28]. Cubitus valgus is most commonly treated with a step-cut translation osteotomy or a rotational dome osteotomy [7]. Despite being successful, a substantial number of complications such as elbow stiffness, nerve injuries, under-correction, recurrence, non-union, osteomyelitis and skin sloughing have been reported with the use of internal fixation following various osteotomies [10, 29]. Furthermore, the mandatory requirement of a relative period of immobilization post-operatively, resulting in stiffness and disuse atrophy, is a deterrent to the use of internal hardware.

External fixation, be it the Ilizarov apparatus, or a standard uniplanar fixator, has gradually gained acceptance and approbation as an effective means of treatment of these deformities. Hasler et al., in their series of 9 patients, reported excellent functional outcomes and cosmetic appearance with the closing wedge osteotomy coupled with a Hoffman (Stryker, USA) external fixator without any major complications [30]. Slongo et al.. described a technique of lateral closing wedge osteotomy, along with a mini-external fixator (DePuy Synthes, USA) application, with reasonable success [31]. However, their technique involved a long surgical incision over the lateral aspect of the elbow, with direct visualisation of the radial nerve. The Ilizarov apparatus, by virtue of its inherent stability, has a definite advantage over other fixators in the fixation of small and unstable fragments [10, 29, 32]. The counter-opposed olive wires provide sufficient stability to resist torsional and bending forces acting on the osteotomized fragment, minimizing the chances of recurrence of the deformity [29]. Another distinctive advantage over conventional methods is the ability to perform residual deformity correction in the post-op phase, with early mobilization and resumption of activities of daily living. Early mobilization leads to better functional rehabilitation and may have an impact on the outcome. Unsightly scars as in traditional approaches are avoided. The internal rotation component of the deformity can be addressed by derotation of the distal ring, if necessary.

Unlike the lateral closing wedge, where the resultant cortical mismatch creates a ‘lazy-S’ deformity, the Ilizarov method, which entails the use of a low-energy osteotomy with careful preservation of the periosteum and gradual distraction through the regenerate, can avert this ugly deformity [33, 34]. Previous studies on the Ilizarov method by Karatosun et al. [32], Piskin et al. [10], and Ozkan et al. [35] described an opening wedge osteotomy along with gradual correction with outstanding results and low rate of complications. A recent study by Agrawal et al. illustrates an angulation-translation osteotomy (rule 2) by using juxta-articular hinges placed at or very near the centre of rotation of angulation (CORA) [29]. The medial translation, achieved thus, minimizes the chances of lateral prominence. In our

study, we have achieved the necessary angulation and translation for both cubitus varus and valgus, by performing acute correction abiding by the osteotomy principles [36], and by measuring the degree of correction achieved under C-arm guidance with a sterile radiolucent goniometer. This, in turn, led to a more accurate correction of the angular deformity, comparable to the contralateral, normal limb. A comparison of our study with similar ones utilizing external fixation is summarized in Table 3. Although we encountered just one major complication [37], it is prudent to mention that the risk of nerve injuries remains substantial, and is best circumvented by careful soft tissue dissection, following safe corridors, and using tissue-protection sleeves while drilling and inserting pins.

Table 3

Summary of similar studies on the use of corrective osteotomies coupled with external fixation for cubitus varus and valgus deformities

Title of study	No. of cases	Technique	Mean follow-up (months)	Functional outcome	Complications and their number#
Karatosun et al. [32]	7	Supracondylar osteotomy + gradual correction	66.7	Excellent outcome in all 7 cases (**Bellemore score**)	Major: Nil Minor: 02
Koch, Exner. [38]	4	Medial opening wedge osteotomy + acute correction	24	Good outcome in all 4 patients. Mean valgus correction of 21.8° was achieved; One patient additional flexion modification was required	Minor: 02
Piskin et al. [10]	24	Medial/lateral open wedge osteotomy + gradual correction	18.3	Excellent outcome in 18 cases; good in 6 (**Bellemore score**)	Major: 03 Minor: 05
Ozkan et al. [35]	5	Medial opening wedge osteotomy + gradual correction	28	Excellent in all 5 cases (**Bellemore score**)	Minor: 01
Agrawal et al. [29]	32	Supracondylar osteotomy (angulation-translation) + gradual correction	48	Excellent in 25 cases (78.12 %), good in 2 (6.25 %) and poor in 5 (15.63 %) (**Oppenheim score**)	Major: 02 Minor: 04
Present study	12	Supracondylar osteotomy (angulation-translation) + acute correction	24	Excellent in 9 cases (75 %), good in 2 (17 %) and poor in 1 case (8 %) (**Oppenheim score**)	Major: 01 Minor: 02

Note: # Major complications include: fracture, lateral prominence, nerve palsy, deep infection; minor complications include: superficial pin-tract infections, loss of motion

CONCLUSION

External fixation with the Ilizarov apparatus is a versatile means of correction of cubitus varus and valgus. It precisely achieves the desired carrying angle and cosmetic appearance of the elbow. Additionally, it facilitates residual adjustments in under/over-corrected scenarios. The stability is indisputable, despite there being only a small area of bony contact. No implant is left after frame removal. Early joint mobilization undeniably leads to an improved functional outcome.

Conflicts of Interest. *None to declare.*

Funding. *This research did not receive any specific grant from funding agencies in the public, commercial, or not-for-profit sectors.*

REFERENCES

1. Rupp M, Schäfer C, Heiss C, Alt V. Pinning of supracondylar fractures in children - Strategies to avoid complications. *Injury*. 2019;50 Suppl 1:S2-S9. doi: 10.1016/j.injury.2019.03.042.
2. Bahk MS, Srikumaran U, Ain MC, et al. Patterns of pediatric supracondylar humerus fractures. *J Pediatr Orthop*. 2008;28(5):493-499. doi: 10.1097/BPO.0b013e31817bb860.
3. Shah M, Agashe MV. Supracondylar Humerus Fractures: Classification Based Treatment Algorithms. *Indian J Orthop*. 2020;55(1):68-80. doi: 10.1007/s43465-020-00285-2.
4. Dowd GS, Hopcroft PW. Varus deformity in supracondylar fractures of the humerus in children. *Injury*. 1979;10(4):297-303. doi: 10.1016/0020-1383(79)90047-0.
5. Labelle H, Bunnell WP, Duhaime M, Poitras B. Cubitus varus deformity following supracondylar fractures of the humerus in children. *J Pediatr Orthop*. 1982;2(5):539-546. doi: 10.1097/01241398-198212000-00014.

6. Kozin SH. Cubitus Valgus. In: Abzug JM, Herman MJ, Kozin S. (eds.) *Pediatric Elbow Fractures: A Clinical Guide to Management*. Berlin: Springer; 2017:217-224. doi: 10.1007/978-3-319-68004-0_16.
7. Kim HT, Lee JS, Yoo CI. Management of cubitus varus and valgus. *J Bone Joint Surg Am*. 2005;87(4):771-780. doi: 10.2106/JBJS.D.01870.
8. Srivastava AK, Srivastava D, Gaur S. Lateral closed wedge osteotomy for cubitus varus deformity. *Indian J Orthop*. 2008;42(4):466-470. doi: 10.4103/0019-5413.43397.
9. Kang HJ, Koh IH, Jeong YC, et al. Efficacy of combined osteotomy and ulnar nerve transposition for cubitus valgus with ulnar nerve palsy in adults. *Clin Orthop Relat Res*. 2013;471(10):3244-3250. doi: 10.1007/s11999-013-3057-9.
10. Piskin A, Tomak Y, Sen C, Tomak L. The management of cubitus varus and valgus using the Ilizarov method. *J Bone Joint Surg Br*. 2007;89(12):1615-1619. doi: 10.1302/0301-620X.89B12.19361.
11. Yamamoto I, Ishii S, Usui M, et al. Cubitus varus deformity following supracondylar fracture of the humerus. A method for measuring rotational deformity. *Clin Orthop Relat Res*. 1985;(201):179-185.
12. Dhillon MS, Gopinathan NR, Kumar V. Misconceptions about the three point bony relationship of the elbow. *Indian J Orthop*. 2014;48(5):453-457. doi: 10.4103/0019-5413.139835.
13. El-Adl W. The equal limbs lateral closing wedge osteotomy for correction of cubitus varus in children. *Acta Orthop Belg*. 2007;73(5):580-587.
14. Kaul R, Akhoon N. Use of the Bone Ninja Mobile Application as a Pre-operative Assessment and Simulation Tool in Patients Undergoing High Tibial Osteotomy. *Rev Bras Ortop (Sao Paulo)*. 2020;57(1):89-95. doi: 10.1055/s-0040-1716761.
15. Frierson M, Ibrahim K, Boles M, Boté H, Ganey T. Distraction osteogenesis. A comparison of corticotomy techniques. *Clin Orthop Relat Res*. 1994;(301):19-24.
16. Paley D, Herzenberg JE, Tetsworth K, et al. Deformity planning for frontal and sagittal plane corrective osteotomies. *Orthop Clin North Am*. 1994;25(3):425-465.
17. Oppenheim WL, Clader TJ, Smith C, Bayer M. Supracondylar humeral osteotomy for traumatic childhood cubitus varus deformity. *Clin Orthop Relat Res*. 1984;(188):34-39.
18. French PR. Varus deformity of the elbow following supracondylar fractures of the humerus in children. *Lancet*. 1959;2(7100):439-441. doi: 10.1016/s0140-6736(59)90422-2.
19. King D, Secor C. Bow elbow (cubitus varus). *J Bone Joint Surg Am*. 1951;33-A(3):572-576.
20. Bellemore MC, Barrett IR, Middleton RW, et al. Supracondylar osteotomy of the humerus for correction of cubitus varus. *J Bone Joint Surg Br*. 1984;66(4):566-572. doi: 10.1302/0301-620X.66B4.6746695.
21. Amspacher JC, Messenbaugh JF Jr. Supracondylar osteotomy of the humerus for correction of rotational and angular deformities of the elbow. *South Med J*. 1964;57:846-850. doi: 10.1097/00007611-196407000-00022.
22. Kanaujia RR, Ikuta Y, Muneshige H, et al. Dome osteotomy for cubitus varus in children. *Acta Orthop Scand*. 1988;59(3):314-317. doi: 10.3109/17453678809149371.
23. DeRosa GP, Graziano GP. A new osteotomy for cubitus varus. *Clin Orthop Relat Res*. 1988;(236):160-165.
24. Laupattarakasem W, Mahaisavariya B, Kowsuwon W, Saengnipanthkul S. Pentalateral osteotomy for cubitus varus. Clinical experiences of a new technique. *J Bone Joint Surg Br*. 1989;71(4):667-670. doi: 10.1302/0301-620X.71B4.2768319.
25. Uchida Y, Ogata K, Sugioka Y. A new three-dimensional osteotomy for cubitus varus deformity after supracondylar fracture of the humerus in children. *J Pediatr Orthop*. 1991;11(3):327-331.
26. Eamsobhana P, Kaewpornsawan K. Double dome osteotomy for the treatment of cubitus varus in children. *Int Orthop*. 2013;37(4):641-846. doi: 10.1007/s00264-013-1815-7.
27. Greenhill DA, Kozin SH, Kwon M, Herman MJ. Oblique Lateral Closing-Wedge Osteotomy for Cubitus Varus in Skeletally Immature Patients. *JBJS Essent Surg Tech*. 2019;9(4):e40.1-8. doi: 10.2106/JBJS.ST.18.00107.
28. Vashisht S, Sudesh P, Gopinathan NR, et al. Results of the modified reverse step-cut osteotomy in paediatric cubitus varus. *Int Orthop*. 2020;44(7):1417-1426. doi: 10.1007/s00264-020-04648-0.
29. Agrawal R, Agrawal RA, Kaul R, et al. Post-traumatic cubitus varus: long-term follow-up of corrective osteotomy using the Ilizarov method of compression distraction osteogenesis. *J Pediatr Orthop B*. 2022;31(1):31-42. doi: 10.1097/BPB.0000000000000845.
30. Hasler CC. Correction of malunion after pediatric supracondylar elbow fractures: closing wedge osteotomy and external fixation. *Eur J Trauma*. 2003; 29:309-315. doi: 10.1007/s00068-003-1325-1.
31. Slongo T. Treatment of posttraumatic cubitus varus in children and adolescents. Supracondylar humeral osteotomy using radial external fixation. *Oper Orthop Traumatol*. 2015;27(3):194-209. (In German.) doi: 10.1007/s00064-015-0403-y.
32. Karatosun V, Alekberov C, Alici E, et al. Treatment of cubitus varus using the Ilizarov technique of distraction osteogenesis. *J Bone Joint Surg Br*. 2000;82(7):1030-1033. doi: 10.1302/0301-620x.82b7.10669.
33. Wong HK, Lee EH, Balasubramaniam P. The lateral condylar prominence. A complication of supracondylar osteotomy for cubitus varus. *J Bone Joint Surg Br*. 1990;72(5):859-761. doi: 10.1302/0301-620X.72B5.2211772.
34. Ilizarov GA. The tension-stress effect on the genesis and growth of tissues. Part I. The influence of stability of fixation and soft-tissue preservation. *Clin Orthop Relat Res*. 1989;(238):249-281.
35. Özkan C, Deveci MA, Tekin M, et al. Treatment of post-traumatic elbow deformities in children with the Ilizarov distraction osteogenesis technique. *Acta Orthop Traumatol Turc*. 2017;51(1):29-33. doi: 10.1016/j.aott.2016.08.019.
36. Paley D. Frontal Plane Mechanical and Anatomic Axis planning. In: Paley D. *Principles of Deformity Correction*. First ed. Berlin: Springer-Verlag; 2002:61-97. doi: 10.1007/978-3-642-59373-4_4.
37. Paley D. Problems, obstacles, and complications of limb lengthening by the Ilizarov technique. *Clin Orthop Relat Res*. 1990;(250):81-104.
38. Koch PP, Exner GU. Supracondylar medial open wedge osteotomy with external fixation for cubitus varus deformity. *Pediatr Orthop B*. 2003;12(2):116-122. doi: 10.1097/01.bpb.0000049571.52224.c8.

The article was submitted 05.03.2025; approved after reviewing 17.03.2025; accepted for publication 31.03.2025.

Information about the authors:

Dr Rajiv Kaul — MS (Orth), DNB (Orth), Associate Professor (Orthopaedics), MRCPS (Glasgow), Diploma SICOT, drrajivkaul@gmail.com, https://orcid.org/0000-0002-6870-9206;

Dr Manish Prasad — DNB (Orth), Professor (Orthopaedics), monu60@gmail.com;

Dr Neha Akhoon — MD (Pharma), MD (Pharmacology), Resident, MD (Dermatology and Venereology), nehakahoon@gmail.com, https://orcid.org/0000-0003-2377-1222.

Original article
https://doi.org/10.18019/1028-4427-2025-31-3-279-286

Ilizarov ring fixator for ankle fusion: a gold standard in managing complex ankle pathologies

M. Dhawan[1], B. Nandan[1], R.K. Guhan[1]✉, S. Dwivedi[1], M. Prasad[2]

[1] Sir Ganga Ram Hospital, New Delhi, India
[2] Armed Forces Medical College, New Delhi, India

Corresponding author: Rayappan Kumaresan Guhan, drguhan1402@gmail.com

Abstract

Introduction Ankle arthrodesis is a surgical procedure for end-stage arthritis and complex ankle pathologies, offering a limb-salvaging alternative to amputation. This study aims to present clinical experience with the Ilizarov apparatus in achieving stable, painless ankle fusion in patients with varied complex ankle pathologies.

Materials and Methods A retrospective study was conducted involving 27 patients who underwent ankle arthrodesis using the Ilizarov fixator between 2014 and 2024. Clinical and radiological evaluations were performed using the ASAMI scoring system. Surgical techniques, patient demographics, and outcomes were analyzed.

Results All 27 patients achieved successful bone union. ASAMI Bone results were rated excellent in 23 and good in 4. Functional outcomes were rated as good in 22 patients and fair in 5. Pin tract infections were effectively managed with antibiotics. The Ilizarov technique demonstrated superior results in achieving stable, pain-free ankles, even in cases with severe osteomyelitis and destroyed ankles with deformities.

Discussion The Ilizarov apparatus provides a minimally invasive, versatile approach for complex ankle pathologies, enabling dynamic axial compression, early weight-bearing, and deformity correction. Despite limitations such as high costs and skill requirements, its success rate surpasses that of internal fixation techniques.

Conclusion The Ilizarov apparatus is the gold standard for ankle arthrodesis, offering stable fusion and addressing comorbidities such as osteomyelitis and limb length discrepancy, with high patient satisfaction and functional recovery.

Keywords: Ankle arthrodesis, Ilizarov apparatus, bone union, limb salvage, complex ankle pathology

For citation: Dhawan M, Nandan B, Guhan RK, Dwivedi S, Prasad M. Ilizarov ring fixator for ankle fusion: a gold standard in managing complex ankle pathologies. *Genij Ortopedii*. 2025;31(3):279-286. doi: 10.18019/1028-4427-2025-31-3-279-286.

INTRODUCTION

Ankle arthrodesis refers to complete fusion of the tibio-talar joint and is recommended for conditions such as secondary painful osteoarthritis, neuromotor disorders, post-septic sequelae, avascular necrosis (AVN) of the talus, Charcot neuroarthropathy, and as a salvage procedure to preserve limb functionality [1]. In patients suffering from end-stage arthritis, where amputation is considered the only option due to complexity of local pathology, ankle arthrodesis serves as the ultimate alternative for limb salvage [2].

Various techniques have been developed over time to achieve ankle fusion, including cross screws at the tibio-talar joint, ankle arthrodesis nail, and external fixators. However, no consensus has been reached regarding the most effective method for achieving good interfragmentary compression under functional weight-bearing conditions, along with sufficient foot functionality [3–7]. Unfortunately, many of the currently used methods are associated with significant complications, including deformities, non-consolidated fractures, and septic arthritis, which may further lead to severe secondary osteoarthritis [8].

In cases where bone quality is good, soft tissue coverage is adequate, and there is no associated shortening, the use of internal plate osteosynthesis for ankle joint fusion can yield good results. However, this technique is linked to a higher risk of chronic osteomyelitis (in some instances tuberculosis osteomyelitis), bone defects, neurological deficits, and soft tissue compromise. Under such circumstances, the Ilizarov apparatus provides a more effective solution for orthopedic surgeons [9, 10].

Compared to the Ilizarov technique, internal fixation methods are less complex and involve a simpler approach. However, the risk of complications such as skin necrosis, severe infections, septic arthritis, lack of fusion, and the necessity for revision arthrodesis remains significant [2, 3, 9].

The Ilizarov apparatus offers a unique advantage by enabling dynamic axial compression and providing 360-degree rigidity. Its minimally invasive approach ensures reliability with significant benefits including immediate weight-bearing and early mobilization of adjacent joints. Moreover, it serves as a definitive fixation technique in a single stage [11]. Beyond compression, the apparatus also enables distraction, allowing for effective correction of bone axis deformities.

Despite its numerous advantages, the Ilizarov apparatus has certain notable limitations including the complexity of the fixator assemblies, the skill required for its application along with temporary patient discomfort with the fixator [1, 2, 9–11].

Patients with severe osteoarthritis of the ankle often endure excruciating pain during routine daily activities. The accompanying functional loss and pain are often the driving factors leading these patients to seek surgical intervention. The success of ankle arthrodesis is highly dependent on patient compliance to postoperative protocols [8, 9, 12]. The most effective treatment outcomes are marked by reduced pain and improved functional capabilities [5, 8, 9, 12, 13].

Aim of the study is to present our clinical experience and the versatility of the Ilizarov apparatus in achieving stable, immobile, and painless ankle fusion in patients with a wide spectrum of ankle joint pathologies.

MATERIALS AND METHODS

The study was conducted at a reputed teaching institution and tertiary care hospital in New Delhi, India. It received approval from the institutional ethics committee. The analysis was based on a retrospective review of 27 patients who underwent ankle arthrodesis using the Ilizarov apparatus between 2014 and 2024, spanning a decade.

The study included all patients who underwent ankle fusion with the Ilizarov fixator. Various parameters such as gender, age, time of injury, fracture type, history of prior surgeries, indications for the procedure, and duration of fixation with the frame on were evaluated. Bone and functional outcomes were evaluated using the ASAMI scoring system [14].

Preoperative radiological assessments were performed based on individual case requirements. Full-length X-rays of the ankle and leg were taken in all patients, while MRI and CT scans were obtained for cases involving osteomyelitis or suspected nonunion to aid in diagnosis.

Medical comorbidities were documented, and any modifiable risk factors were addressed and optimized prior to surgery.

All surgical procedures were carried out by a senior orthopedic surgeon experienced in complex trauma management and an expert in the Ilizarov method.

Surgical technique

All surgeries were performed under general/spinal/epidural anesthesia depending upon the medical condition of the patient, with the patient positioned in supine position with ipsilateral sandbag elevation. Prophylactic intravenous antibiotics were administered at the time of the skin incision in accordance with standard guidelines. The ankle joint was approached laterally, medially, or anteriorly depending on the pathology, with the lateral transfibular (malleolar) approach being the most commonly used due to its advantage of providing wide access to the ankle region.

For the medial approach, a 7-cm skin incision was made starting at the tip of the medial malleolus and curving anteriorly over the distal tibia. The saphenous nerve and vein were carefully protected, and the medial malleolus was osteotomized to access the ankle joint. For the anterior approach, a 10-cm incision was centered midline between both malleoli. Superficial dissection was performed, preserving the superficial peroneal nerve. The extensor digitorum longus and extensor hallucis longus were identified, and a plane was developed between them. Deeper dissection revealed the anterior tibial artery and deep peroneal nerve, which were retracted safely, allowing anterior access to the ankle joint.

In the lateral transfibular approach, a 10-cm incision was made along the subcutaneous border of the distal fibula, with a transverse fibular osteotomy performed 8 cm proximal to the tip of the lateral malleolus. The tibio-talar joint was opened, and the distal tibial articular surface was denuded at the subchondral level, followed by preparation of the talar dome. In cases of infection, thorough debridement of the soft tissue and bone was performed, and culture swabs were taken for postoperative management.

Once fresh metaphyseal bone with the characteristic “paprika sign” was exposed, the tibia and talus were aligned under fluoroscopic guidance and fixed with a tibio-calcaneal 3-mm K-wire. Infected cases underwent meticulous debridement of necrotic tissue before fixation. The Ilizarov frame included proximal tibial rings (R1, R2) and a foot frame with 5/8 rings for the hindfoot and forefoot, if required. The hindfoot ring (R3) was secured with olive wires and half-pins to the calcaneus and connected to the tibial rings (R2) with threaded rods for controlled compression. In some cases, wires were used to secure talus considering having good bone stock in order to get good interfragmentary compression and to put less stress on subtalar joints. Intraoperatively, 1-cm compression was applied between R3 and R2, with corticotomy and distraction performed between R1 and R2 for lengthening when necessary. No primary bone grafting was performed in any of the cases, which is an important observation in this context.

Postoperatively, patients were instructed to perform weight-bearing with walker support after removal of tibio-calcaneal wire at 6 weeks postoperatively. Emphasis was placed on rigorous pin-site care at least twice daily. Follow-ups were conducted thrice monthly initially and transitioned to monthly visits after three months. Radiological evaluations monitored callus formation, alignment, and infection, while clinical assessments focused on skin and pin-tract condition and neurovascular status. Solid union was defined by continuous cortical and trabecular lines on radiographs at the tibiotalar joint, followed by one month of dynamization and CT confirmation before frame removal. Patients used protective bracing for up to six weeks upon frame removal, with the ultimate goal of achieving a pain-free, stable, plantigrade foot and restored gait.

RESULTS

This retrospective study included 27 patients who underwent ankle arthrodesis using the Ilizarov frame, comprising 8 females (29.63 %) and 19 males (70.37 %). The patient's age ranged from 20 to 78 years, with an average of 40 years [SD: 15.48; Median (IQR) is 35 (20–56)]. Among the cases, 12 patients (44.4 %) presented with active osteomyelitis. The Ilizarov frame was used for an average duration of 33 weeks [SD: 13.9; Median (IQR) is 27 (21–43)], earliest frame removal being 19 weeks and longest being 70 weeks. The causes of ankle joint destruction in the study covered a broad spectrum, including post-traumatic cases in 16 patients (59.26 %), post-polio residual deformity in 3 patients (11.11 %), Charcot arthropathy in 6 patients (22.22 %), and cases involving a destroyed or resorbed talus in 2 patients (7.41 %). Adjacent joint arthritis was noted in 6 patients, representing 22.2 % of the sample. All patients exhibited a limb length discrepancy of less than 1.5 cm, which was effectively addressed using appropriately sized shoe lifts.

The study achieved a 100 % bone union rate across all cases. Patients reported significant comfort with the procedure and were able to ambulate independently, pain-free, and without support after frame removal.

The ASAMI scoring system (Association for the Study and Application of the Methods of Ilizarov) was utilized to evaluate bone and functional outcomes. Regarding bone results, 23 patients (85.19 %) demonstrated excellent results, while 4 patients (14.81 %) achieved a good outcome (Table 1). Functional scores revealed that 22 patients (81.48 %) had good results, and 5 patients (18.52 %) had fair results (Table 2). Since functional scoring incorporates ankle dorsiflexion, a "good" functional outcome represents the highest achievable score. In all 27 patients, no primary bone grafting was performed, highlighting that the Ilizarov method is a definitive and less demanding technique for ankle fusion.

A few patients developed pin-tract infection during the treatment period, which was successfully managed with oral and local antibiotics.

Table 1

ASAMI Bone result

Scores	Frequency	Percentage
Excellent	23	85.19 %
Good	4	14.81 %
Total	27	100 %

Abbreviations: ASAMI — Association for the Study and Application of the Methods of Ilizarov; There were no entries in the Fair and Poor scores.

Table 2

ASAMI Functional result

Scores	Frequency	Percentage
Good	22	81.48 %
Fair	5	18.52 %
Total	27	100 %

Abbreviations: ASAMI — Association for the Study and Application of the Methods of Ilizarov; There were no entries in the Excellent and Poor scores.

Cases

Among 27 patients, a 38-year-old male presented with swelling and dull pain in his left ankle. Clinical and radiological assessments confirmed a diagnosis of Charcot arthropathy. The patient had previously undergone multiple unsuccessful corrective fusion surgeries. Following 44 weeks of treatment, a stable and infection-free tibio-calcaneal fusion was achieved. The ASAMI bone results were excellent, and the functional results were good. However, the patient developed a leg length discrepancy (LLD) of approximately 1.5 cm, which was successfully corrected with a customized shoe lift (Fig. 1, 2, 3).

Fig. 1 Pre-op clinical pictures of left ankle with severe septic arthritis (sequelae of Charcot arthropathy): (a) lateral view; (b) medial view; (c) frontal view

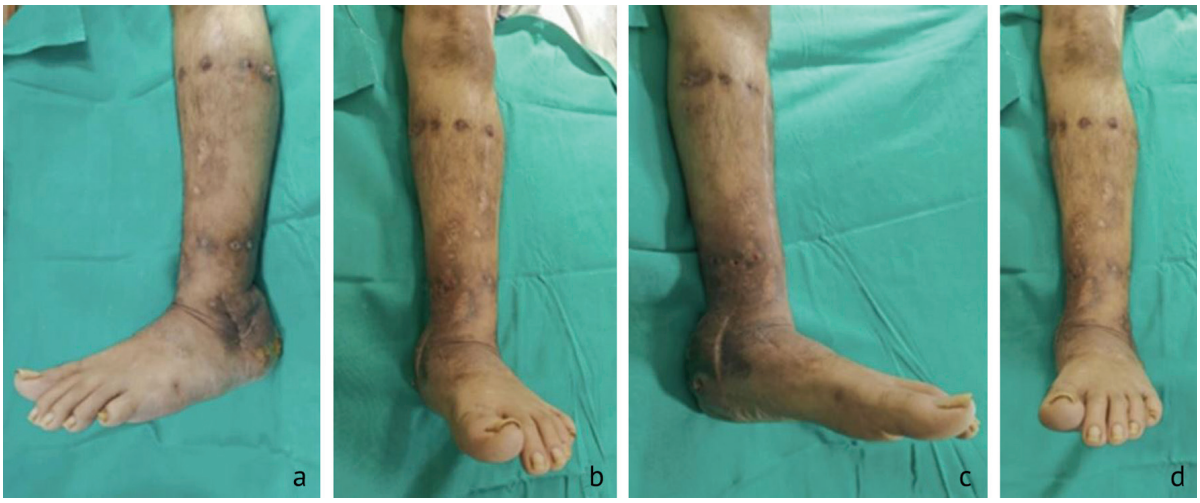

Fig. 2 Clinical picture of stable infection-free painless fused left ankle after frame removal: (a) lateral view; (b) anteromedial view; (c) medial view; (d) frontal view

Fig. 3 Series of left ankle X-Rays during the course of treatment: (a) 3-month pre-op X-ray with broken calcaneal nail; (b) pre-op X-ray at time of surgery

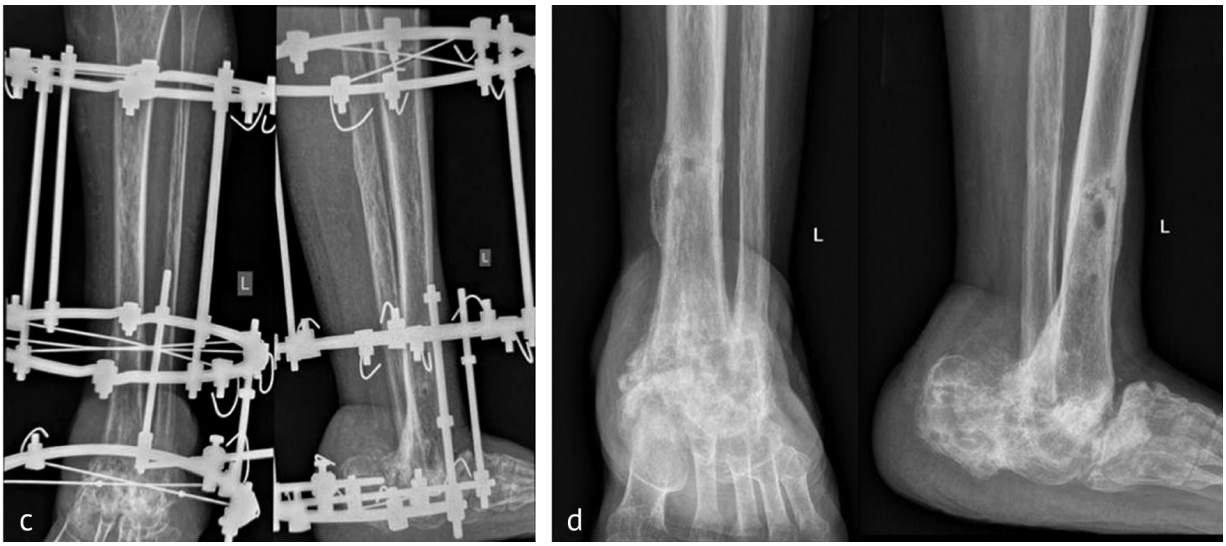

Fig. 3 (continuation) Series of left ankle X-Rays during the course of treatment: (c) at the time of frame removal; *d* 6-month follow-up

DISCUSSION

Ankle arthrodesis is a definitive salvage procedure for addressing severely damaged ankle joints. As it represents patient's final opportunity to achieve a stable and pain-free ankle, careful consideration is essential when selecting an implant for the procedure [15, 16].

The introduction of external fixators for ankle fusion by Charnley marked a significant advancement [1]. Although these devices achieved favorable fusion rates, monoplanar fixators lacked rotational stability. To address this, triangular frames enabling multiplanar compression were developed [17, 18]. Despite these advancements, challenges such as persistent instability at the fusion site remain, particularly in cases with substantial bone loss [7, 12, 19].

For patients with infections, ankle fusion provides absolute stability, thereby minimizing the risk of recurrence [13, 20].

The Ilizarov ring fixator is widely regarded as the most effective system for addressing complex ankle pathologies, outperforming all other fusion techniques [19, 21–26]. Its advantages include dynamic axial fixation, which preserves bone contact without the need for additional grafting. It also offers superior stability against bending, shear, and torsional forces, enabling early weight-bearing and reducing pin-tract infections. Its modular design allows circumferential mechanical control, facilitating postoperative adjustments that are impossible with conventional implants like screws, plates, or nails. Additionally, transfixation wires placed percutaneously provide reliable fixation even in cases with compromised bone and soft-tissue conditions.

Moreover, the Ilizarov method allows ankle arthrodesis to be performed as a single-stage procedure, even in the presence of active infection. Gradual compression at the fusion site promotes biological union, with or without proximal osteotomy and callus distraction. The device also ensures limb length equalization when required [16, 26].

Renowned for its versatility, the Ilizarov device is considered the gold standard for successful ankle arthrodesis. Unlike internal fixation methods, it minimizes damage to soft tissues, vascular structures, and the periosteum, making it suitable for managing complex conditions such as diabetes mellitus, peripheral neuropathy (Charcot), severe osteomyelitis, and peripheral vascular compromise. The Ilizarov system is often the last resort for patients at risk of amputation [16, 27–29].

Among the surgical approaches, the transfibular approach is frequently preferred because it provides access to both the tibiotalar and subtalar joints through a single incision [17, 29]. The choice of approach, however, depends on factors such as deformity type, fixation technique, soft-tissue condition, and surgeon experience [17, 18, 30]. Occasionally, the medial malleolus or anterior

approach may be employed depending on case-specific requirements [18]. Thus, Onodera et al. demonstrated that transfibular ankle arthrodesis using the Ilizarov fixator combined with fibular onlay grafting achieved complete bone union [11]. In contrast, our cases achieved 100 % union without primary bone grafting.

The ASAMI scoring system is used in this study because it provides a standardized, objective, and comprehensive method to evaluate the success of surgical procedure. It allows for a quantitative and qualitative assessment of both bone healing (union, deformity, infection, and limb length) and functional outcomes (pain, mobility, return to daily activities), ensuring a holistic evaluation of patient recovery. Additionally, its widespread use in orthopedic and trauma research enables comparability with existing literature, facilitating evidence-based conclusions and treatment refinements [14].

Consistent with existing literature, our study also demonstrated a 100 % bone union rate using the Ilizarov apparatus for managing complex ankle pathologies. Li et al. concluded that the Ilizarov technique outperforms internal fixation in achieving stable and effective fusion in end-stage ankle arthritis [15].

Similarly, Morasiewicz et al. conducted a radiological comparison and found that the Ilizarov method provided superior outcomes compared to internal fixation. They also reported a higher rate of adjacent joint arthritis with internal fixation, whereas in our study, this was observed in 22.22 % (6 patients), lower than their reported 48 % [4].

Reinke et al. emphasized the reliability of the Ilizarov method for ankle fusion in patients with compromised conditions, highlighting its effectiveness in tibio-calcaneal fusion for severely damaged Charcot arthropathy cases [5]. A case of a tibiocalcaneal fusion for severely destroyed septic arthritis (Charcot arthropathy) is presented in a series of images (Fig. 1, 2, 3). Likewise, our study utilized this technique to achieve stable and functional feet in similar cases.

El-Gafary et al. demonstrated successful outcomes with the Ilizarov fixator in severe joint destruction due to Charcot arthropathy [6]. Similarly, we achieved stable, pain-free ankles in six patients with severe joint damage from Charcot arthropathy. In four patients, simultaneous tibial lengthening and ankle arthrodesis addressed limb length discrepancy (LLD). Sakurakichi et al. similarly reported successful outcomes using this approach [10]. Among our 27 cases, three patients (11.11 %) with post-polio residual paralysis and equinus deformity were successfully managed with this technique. Kirienko et al. reported comparable success in their study involving 27 patients [9]. The most common complication encountered in our cases was pin-tract infection, which was managed effectively with oral antibiotics and, in some cases, local antibiotic injections.

Based on our findings and a review of the literature, the Ilizarov apparatus proves to be an indispensable tool for orthopedic surgeons, providing a comprehensive solution for complex cases in a single definitive procedure.

The primary limitations of this study were the absence of preoperative scoring, a single-centre retrospective study and a small sample size due to irregular follow-ups after frame removal, largely because of patient socio-economic challenges. Conducting a larger, randomized study is necessary to relate the results more effectively to the target population.

For most patients undergoing ankle fusion, their frequent visits to doctors can be frustrating. This frustration can be mitigated through effective encouragement and early weight-bearing mobilization-benefits that are difficult to achieve with internal fixation techniques.

CONCLUSION

The Ilizarov apparatus should be regarded as the gold standard for ankle fusion in cases of complex pathology. Compared to other techniques, it offers superior axial compression for enhanced union and effectively addresses concurrent challenges such as limb length discrepancy, Charcot arthropathy, osteomyelitis, deformities (post-polio), osteoporosis, and failed ankle fusions after multiple prior surgeries. It provides a stable, pain-free ankle, enabling improved mobility.

REFERENCES

1. Charnley J. Compression arthrodesis of the ankle and shoulder. *J Bone Joint Surg Br*. 1951;33B(2):180-191.
2. Rabinovich RV, Haleem AM, Rozbruch SR. Complex ankle arthrodesis: Review of the literature. *World J Orthop*. 2015;6(8):602-613. doi: 10.5312/wjo.v6.i8.602.
3. Ilizarov GA. The tension-stress effect on the genesis and growth of tissues. Part I. The influence of stability of fixation and soft-tissue preservation. *Clin Orthop Relat Res*. 1989 Jan;(238):249-281.
4. Morasiewicz P, Dejnek M, Urbański W, et al. Radiological evaluation of ankle arthrodesis with Ilizarov fixation compared to internal fixation. *Injury*. 2017;48(7):1678-1683. doi:10.1016/j.injury.2017.04.013.
5. Reinke C, Lotzien S, Yilmaz E, et sa'. Tibiocalcaneal arthrodesis using the Ilizarov fixator in compromised hosts: an analysis of 19 patients. *Arch Orthop Trauma Surg*. 2022;142(7):1359-1366. doi: 10.1007/s00402-021-03751-0.
6. El-Gafary KA, Mostafa KM, Al-Adly WY. The management of Charcot joint disease affecting the ankle and foot by arthrodesis controlled by an Ilizarov frame: early results. *J Bone Joint Surg Br*. 2009 Oct;91(10):1322-5. doi: 10.1302/0301-620X.91B10.22431.
7. Pereira VF, Masuda VY, Boatto H, Pereira Junior HC, Fernandes Junior JCF, Mansur NSB. Ankle arthrodesis via a transfibular approach and circular external fixation. *Sci J Foot Ankle* [Internet]. 2019;13(2):104-411. doi: 10.30795/scijfootankle.2019.v13.893.
8. Pierrynowski MR, Smith SB, Mlynarczyk JH. Proficiency of foot care specialists to place the rearfoot at subtalar neutral. *J Am Podiatr Med Assoc*. 1996;86(5):217-23. doi: 10.7547/87507315-86-5-217.
9. Kirienko A, Peccati A, Abdellatif I, et al. Correction of poliomyelitis foot deformities with Ilizarov method. *Strategies Trauma Limb Reconstr*. 2011;6(3):107-120. doi: 10.1007/s11751-011-0111-6.
10. Sakurakichi K, Tsuchiya H, Uehara K, et al. Ankle arthrodesis combined with tibial lengthening using the Ilizarov apparatus. *J Orthop Sci*. 2003;8(1):20-25. doi: 10.1007/s007760300003.
11. Onodera T, Majima T, Kasahara Y, et al. Outcome of transfibular ankle arthrodesis with Ilizarov apparatus. *Foot Ankle Int*. 2012;33(11):964-968. doi: 10.3113/FAI.2012.0964.
12. Ahmed ASA. Ankle fusion by Ilizarov external fixator. *Egypt Orthop J*. 2019;54(2):146-153. doi:10.4103/eoj.eoj_42_19.
13. Salem KH, Kinzl L, Schmelz A. Ankle arthrodesis using Ilizarov ring fixators: a review of 22 cases. *Foot Ankle Int*. 2006;27(10):764-770. doi: 10.1177/107110070602701002.
14. Paley D, Catagni MA, Argnani F, Villa A, Benedetti GB, Cattaneo R. Ilizarov treatment of tibial nonunions with bone loss. *Clin Orthop Relat Res*. 1989;(241):146-165.
15. Li J, Li B, Zhang Z, et al. Ilizarov external fixation versus plate internal fixation in the treatment of end-stage ankle arthritis: decision analysis of clinical parameters. *Sci Rep*. 2017;7(1):16155. doi: 10.1038/s41598-017-16473-4.
16. Sakurakichi K, Tsuchiya H, Uehara K, et al. The relationship between distraction length and treatment indices during distraction osteogenesis. *J Orthop Sci*. 2002;7(3):298-303. doi: 10.1007/s007760200051.
17. Suo H, Fu L, Liang H, et al. End-stage Ankle Arthritis Treated by Ankle Arthrodesis with Screw Fixation Through the Transfibular Approach: A Retrospective Analysis. *Orthop Surg*. 2020;12(4):1108-1119. doi: 10.1111/os.12707.
18. Yasui Y, Hannon CP, Seow D, Kennedy JG. Ankle arthrodesis: A systematic approach and review of the literature. *World J Orthop*. 2016;7(11):700-708. doi: 10.5312/wjo.v7.i11.700.
19. El-Alfy B. Arthrodesis of the ankle joint by Ilizarov external fixator in patients with infection or poor bone stock. *Foot Ankle Surg*. 2010;16(2):96-100. doi: 10.1016/j.fas.2009.06.004.
20. Fragomen AT, Borst E, Schachter L, et al. Complex ankle arthrodesis using the Ilizarov method yields high rate of fusion. *Clin Orthop Relat Res*. 2012;470(10):2864-2873. doi: 10.1007/s11999-012-2470-9.
21. Li J, Li B, Zhang Z, et al. Ilizarov external fixation versus plate internal fixation in the treatment of end-stage ankle arthritis: decision analysis of clinical parameters. *Sci Rep*. 2017;7(1):16155. doi: 10.1038/s41598-017-16473-4.
22. Rozis M, Benetos I, Afrati SR, et al. Results and Outcomes of Combined Cross Screw and Ilizarov External Fixator Frame in Ankle Fusion. *J Foot Ankle Surg*. 2020;59(2):337-342. doi: 10.1053/j.jfas.2019.05.008.
23. Gessmann J, Ozokyay L, Fehmer T, et al. Arthrodesis of the infected ankle joint: results with the Ilizarov external fixator. *Z Orthop Unfall*. 2011;149(2):212-218. (In German). doi: 10.1055/s-0030-1250360.
24. Wheeler J, Sangeorzan A, Crass SM, et al. Locally generated bone slurry accelerated ankle arthrodesis. *Foot Ankle Int*. 2009;30(7):686-689. doi: 10.3113/FAI.2009.0686.
25. Yanuka M, Krasin E, Goldwirth M, et al. Ankle arthrodesis using the Ilizarov apparatus: good results in 6 patients. *Acta Orthop Scand*. 2000;71(3):297-300. doi: 10.1080/000164700317411915.
26. Tellisi N, Fragomen AT, Ilizarov S, Rozbruch SR. Limb salvage reconstruction of the ankle with fusion and simultaneous tibial lengthening using the Ilizarov/Taylor spatial frame. *HSS J*. 2008;4(1):32-42. doi: 10.1007/s11420-007-9073-0.
27. Dimitriou R, Jones E, McGonagle D, Giannoudis PV. Bone regeneration: current concepts and future directions. *BMC Med*. 2011;9:66. doi: 10.1186/1741-7015-9-66.
28. Boc SF, Norem ND. Ankle arthrodesis. *Clin Podiatr Med Surg*. 2012;29(1):103-113. doi: 10.1016/j.cpm.2011.10.005.
29. DeHeer PA, Catoire SM, Taulman J, Borer B. Ankle arthrodesis: a literature review. *Clin Podiatr Med Surg*. 2012;29(4):509-527. doi: 10.1016/j.cpm.2012.07.001.
30. Rabinovich RV, Haleem AM, Rozbruch SR. Complex ankle arthrodesis: Review of the literature. *World J Orthop*. 2015;6(8):602-613. doi: 10.5312/wjo.v6.i8.602.
31. Colman AB, Pomeroy GC. Transfibular ankle arthrodesis with rigid internal fixation: an assessment of outcome. *Foot Ankle Int*. 2007;28(3):303-307. doi: 10.3113/FAI.2007.0303.

The article was submitted 30.01.2025; approved after reviewing 06.02.2025; accepted for publication 31.03.2025.

Information about the authors:

Dr. Manish Dhawan — Professor, Head of the Department, drmanishdhawan@gmail.com;
Dr. Brajesh Nandan — Senior consultant, brajesh.nandan@yahoo.com;
Dr. Rayappan Kumaresan Guhan — Research Fellow, drguhan1402@gmail.com;
Dr. Sahil Dwivedi — Post-graduate student, shl.dwiwedi@gmail.com;
Dr. Manish Prasad — Senior consultant, monu60@gmail.com.

Contribution of the Authors

Manish Dhawan: Development of the concept and design of the study.
Brajesh Nandan: Research coordination interpretation and analysis of the data obtained.
R K Guhan: Collecting and processing the material, conducting research, preparing the text.
Sahil Dwivedi: Collection of material and data pertaining to the research.
Manish Prasad: Analysis, interpretation and editing.

Original article
https://doi.org/10.18019/1028-4427-2025-31-3-287-296

Comparative analysis of the lower leg multiapical deformity correction by various methods of orthopedic hexapods usage

E.S. Golovenkin✉, **L.N. Solomin**

Vreden National Medical Research Center of Traumatology and Orthopedics, St. Petersburg, Russian Federation

Corresponding author: Evgeniy S. Golovenkin, golovenkin_1996@mail.ru

Abstract

Introduction The technique of multiapical deformity correction with orthopaedic hexapods can be accepted as "standard." This requires several software calculations a and lengths changes in the 12–18 struts. The "spring" technique was designed to address these disadvantages.

Purpose To analyze the treatment results of patients with lower leg multiapical deformities corrected by "standard" and "spring" techniques

Methods The data of patient group 1 (standard technique, $n = 17$) and patient group 2 (spring technique, $n = 17$), were used. Correction accuracy, duration of correction, and fixation periods were compared. In patients requiring lengthening, fixation and osteosynthesis indices were additionally analyzed. Quality of life and segment function were assessed using the LEFS questionnaire.

Results There was no statistically significant difference between the groups when comparing each of the parameters studied. When comparing LEFS parameters before external fixation (EF) and 2–3 months after frame removal, a statistically significant difference was observed in patients within each of the first and second groups.

Discussion The correction accuracy in each group was 94.4 %, which, along with the absence of a significant difference in the duration of treatment and data from the LEFS questionnaire, indicates equal clinical effectiveness of both methods. It was noted that treatment with various modifications of circular external fixators is equally uncomfortable for patients. At the same time, the need for only one calculation in a hexapod software instead of 2–3, the ability to change the length of 6 struts instead of 12–18, as well as simpler assembly and less cumbersome construct if there is small (less than 10–12 cm) distance between the rings are advantages of a "spring" technique.

Conclusion Based on the analysis of the criteria used for evaluation, it can be concluded that the “spring” technique for correcting lower leg multiapical deformities is as effective as the “standard” technique. The advantages of the "spring" technique are associated with the greater convenience of its use: both for the orthopedic surgeon and the patient.

Keywords: multiapical deformities, multi-planar deformities, multi-level deformities, lower leg deformities, deformity correction, gradual correction, orthopaedic hexapod, Ortho-SUV frame, «spring» technique, correction accuracy, functional results

For citation: Golovenkin ES, Solomin LN. Comparative analysis of the lower leg multiapical deformity correction by various methods of orthopedic hexapods usage. *Genij Ortopedii*. 2025;31(3):287-296. doi: 10.18019/1028-4427-2025-31-3-287-296.

INTRODUCTION

In recent decades, orthopaedic hexapods have been actively used to correct deformities, including multi-apical deformities. Their main advantage is one-stage correction of all deformity components [1–5]. The method of correction of multi-apical deformities, which can be accepted as standard, is the simultaneous elimination of the deformity at the levels of all apexes using several orthopaedic hexapods, i.e. their number is equal to the number of deformity apexes [2, 6–12] (Fig. 1 a). It is quite difficult to plan the correction, especially if the intermediate fragment is nonlinear, or the second rule of osteotomies must be used at one of the levels. In such a case, the use of the anatomical axis of the intermediate fragment is unacceptable and the so-called assigned axis is necessary for successful implementation of the correction. Moreover, the orthopaedic surgeon must perform several (according to the number of hexapods) independent calculations with computer software, and during correction, change the lengths of 12 (in the presence of two apexes) or 18 (three-apex deformities) strata. The use of several orthopaedic hexapods increases the weight of the frame and worsens patient's comfort during treatment [13].

In order to eliminate these shortcomings, a "spring" technique has been developed and clinically tested [4]. Its implementation requires only one orthopaedic hexapod, which is more convenient for both the surgeon and the patient (Fig. 1 b).

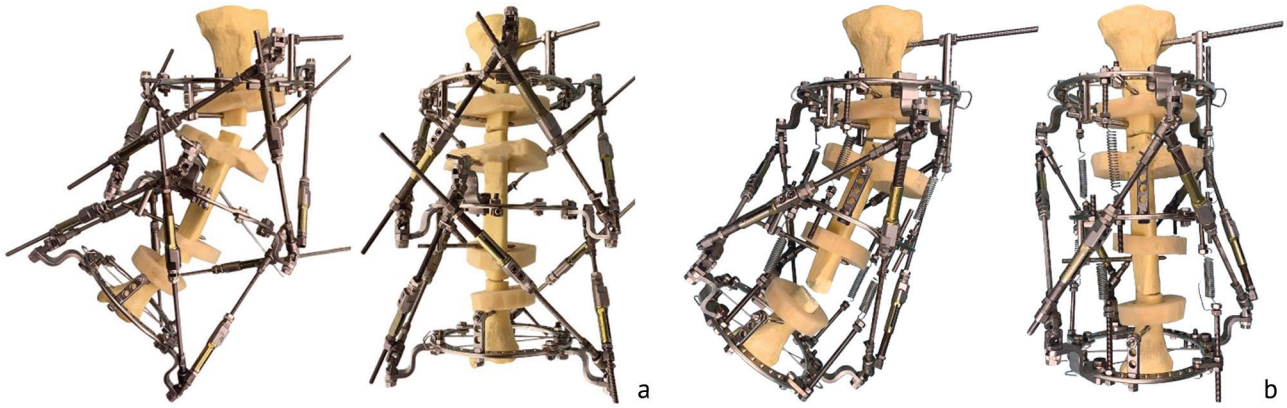

Fig. 1 Diagrams of gradual correction (before and after) of multi-apex deformities of the tibia with orthopaedic hexapods: (a) standard technique; (b) spring technique

However, it is still not known whether the spring technique is as clinically effective as the standard technique.

Purpose To compare treatment results of patients with lower leg multiapical deformities corrected by standard and spring techniques

MATERIAL AND METHODS

The study included patients who were treated at the Vreden National Medical Research Center of Traumatology and Orthopedics from 2012 to 2024. A total of 36 corrections of multi-apical deformity of the lower legs were performed. All patients gave informed consent to participate in the study and subsequent publication of its results.

The control group (Group 1) included 17 patients (18 segments) who were treated with the standard technique (4 retrospective cases, 14 prospective cases). The study group (Group 2) included 17 patients (18 segments), whose deformity correction was performed using the "spring" technique (18 prospective cases). Both groups were comparable in the studied parameters ($p > 0.05$) (Table 1).

Table 1

Patients' data

Parameter	Quantity, Me [Q25; Q75]			
	Group 1 (standard technique), *n* = 17		Group 2 (spring technique), *n* = 17	
	n	%	*n*	%
Total of segments	18	100	18	100
Males	9	50	8	44
Females	9	50	10	56
Congenital etiology	9	50	11	61
Acquired etiology	9	50	7	39
Coronal plane varus	5	28	11	61
Coronal plane valgus	12	67	7	39
Antecurvatum in the sagittal plane	12	67	13	72
Recurvatum in the sagittal plane	2	11	2	11
Lengthening	7	39	5	28
Tosion	7	39	10	56
Number of osteotomies = 2	18	100	17	94
Number of osteotomies = 3	0	0	1	6
Ages, years	39.5 [25;48.8]		36 [26;45.5]	
Angular deformity (coronal plane), °	25 [16.3;33.8]		20 [17.3;23.8]	
Angular deformity (sagittal plane), °	18.5 [1;29.8]		10 [4;12.8]	
Lengthening magnitude, mm	0 [0;25]		0 [0;10.5]	
Value of torsion, °	0 [0;10]		8.5 [0;14.3]	

In both groups, an external fixator (EF) based on three supports was used (35 segments) for two deformity apices or four supports in one patient with three apices. Osteotomies of the tibia and fibula were performed through minimally invasive approaches according to de Bastiani. On postoperative days 5 to 7, the distraction period was initiated at a rate of 1 mm per day in 4 steps. Distraction was performed using two-plane Ilizarov hinge posts and continued until interfragmentary diastases of 4–6 mm were achieved at each osteotomy level. If patients required segment lengthening ($n_1 = 7$; $n_2 = 5$), distraction continued until the required lengthening magnitude was achieved (Group 1: 12–28 mm; Group 2: 12–44 mm). Upon completion of distraction, the EF was readjusted with the installation of several orthopaedic hexapods (Group 1) or one orthopaedic hexapod and springs (Group 2).

For this purpose, when implementing the "spring" technique, the orthopaedic hexapod "Ortho-SUV" struts [1, 3, 11, 14] connected the proximal and distal EF supports. The intermediate supports were attached to the adjacent supports using a spring unit. It included a set of custom manufactured springs in the amount of six for two-apical deformations or nine for three-apical deformities. Each spring was attached to the supports using traction clamps (Fig. 2 a). The parameters required for manufacturing the springs were determined on day 1 or 2 after the operation. The first required parameter was the length of the spring in the working (stretched) state. For this purpose, the minimum distance between the intermediate EF support and one of the osteotomies was measured in the patient's postoperative radiograph. The value of 15 mm which is the thickness of the three nuts required to fix the spring to the traction clamp and the support was subtracted from the resulting measurement.

Next, the transverse restoring force was determined. With the segment in a horizontal position, a multi-turn indicator (Type MIG, GOST 9696-75) was attached to the rear surface, the end of the needle of which touched the intermediate support. Once the two-plane hinges had relaxed under the influence of gravity, the intermediate support shifted, which was recorded by the indicator (Fig. 2 b). Then,

using a dynamometer, a pull was performed in the opposite direction until the indicator arrow was at "0". The dynamometer reading at this point corresponded to the transverse restoring force required to hold the intermediate fragment in a neutral position. The indicators were introduced into an Excel table, which was formed based on the similarity of the force triangle and the transverse displacement triangle (Fig. 2 c). In the calculations, a transverse displacement of the fragment of no more than 1 mm was allowed. Based on the introduced data, the longitudinal (tensile) force of the spring was determined, providing the required restoring force at a given transverse deformation. Based on the available force values, as well as the working length, using a calculator on the manufacturer's website (calculation based on GOST 13765-86), the optimal technical parameters of the springs were determined: diameter and number of spring turns, wire diameter

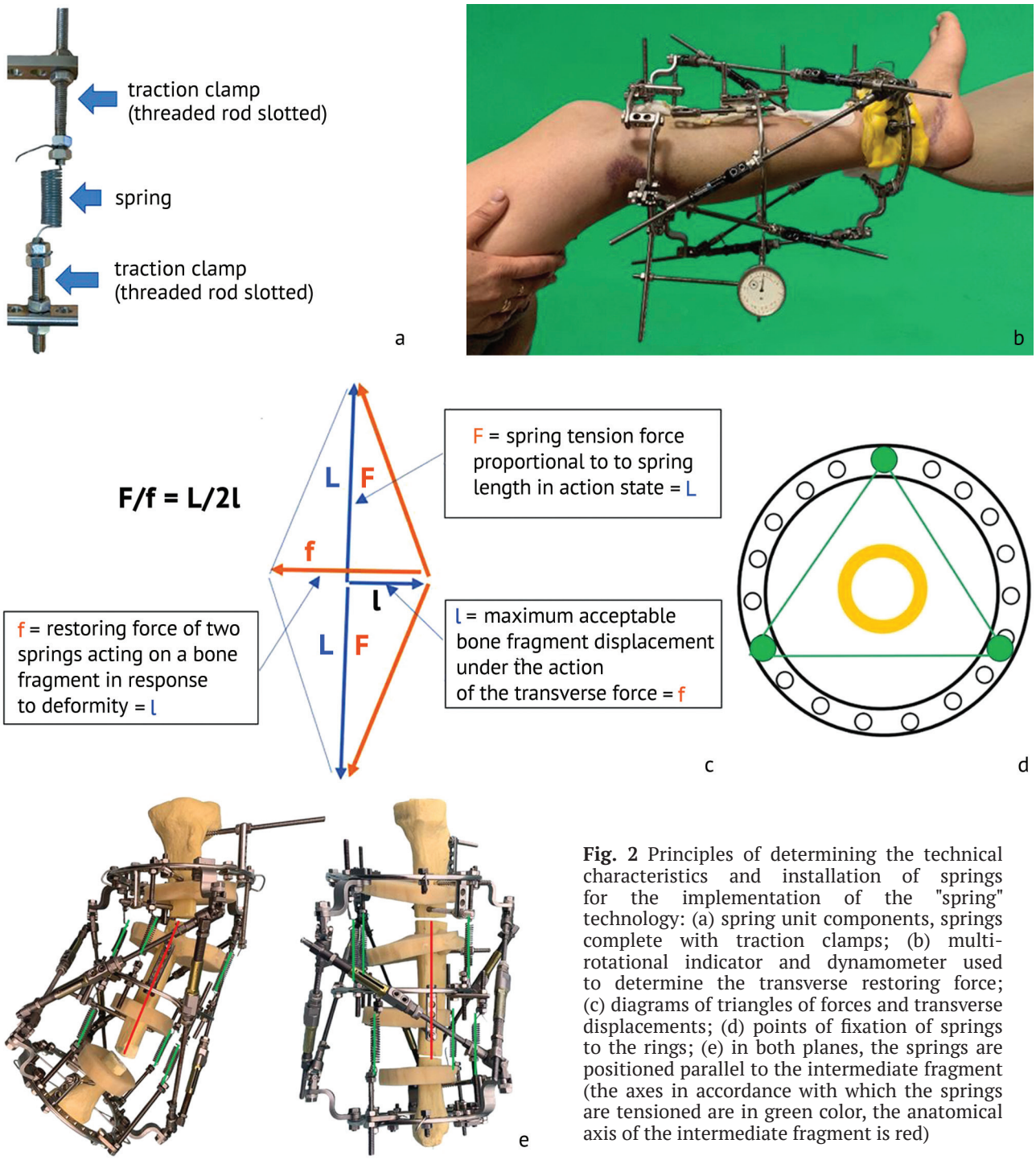

Fig. 2 Principles of determining the technical characteristics and installation of springs for the implementation of the "spring" technology: (a) spring unit components, springs complete with traction clamps; (b) multi-rotational indicator and dynamometer used to determine the transverse restoring force; (c) diagrams of triangles of forces and transverse displacements; (d) points of fixation of springs to the rings; (e) in both planes, the springs are positioned parallel to the intermediate fragment (the axes in accordance with which the springs are tensioned are in green color, the anatomical axis of the intermediate fragment is red)

Orders for the components of the "spring unit" were manufactured by NPP "Slantsevsky Spring Plant", which sells products according to customized designs. Manufacturing of the products took no more than 12 days, which did not affect the duration of the patient's treatment, since it corresponded to the duration of the latent period and the period of primary distraction. During installation, the springs were positioned at the maximum possible equal distance from each other, trying to form an equilateral triangle (Fig. 2 d). Three patients required elimination of the displacement that occurred during the distraction period. In such cases, four springs were used for each apex, positioned in the shape of a square. The springs were fixed to the supports using traction clamps. In this case, the springs were positioned so that they were parallel to the anatomical axis of the intermediate fragment in both planes (Fig. 2 e). The lengths of the springs and the positions of their axes were kept constant during the correction period, and adjustment was performed using traction clamps. Upon completion of correction, the springs and struts of the orthopaedic hexapod were dismantled, and the supports were fixed using two-plane Ilizarov set hinges.

In the comparative analysis, the duration of the correction periods (with and without distraction to achieve the initial diastasis), fixation, and the accuracy of the correction were assessed. In patients who did not undergo segment lengthening (n_1 = 11; n_2 = 13), the duration of the fixation period was calculated. If segment lengthening was necessary (n_1 = 7; n_2 = 5), the following indicators were additionally determined:

— fixation index (FI): the ratio of the number of days of fixation to the value of lengthening in cm;

— osteosynthesis index (fixator period): the ratio of the number of days in the EF to the value of lengthening in cm.

To assess the accuracy of the correction, the values of mechanical (mMPTA, mLDTA) and anatomical (aADTA, aPPTA) angles were assessed before and after the correction.

Complications were evaluated according to the classification of J. Caton [15–19].

The functional outcome and quality of life were assessed by analyzing the LEFS questionnaires completed by patients [17–19]. The questionnaire, consisting of 20 questions, was completed by patients before surgery, at the end of the correction period (before dismantling the struts), before EF removal, and 2.5–3 months after EF removal. A score of less than 19 points was rated as minimal function or no function; 20–39 points as significant limitation of function; 40–59 points as moderate restriction, 60–79 points as minor limitation. A score of 80 points was the maximum and implied full function.

Comparison of frequency characteristics of nominal data (gender, etiology, deformed segment) was performed using the chi-square test (with Yates' correction for small cohorts) and Fisher's exact test. When comparing quantitative parameters (age, RLU values, magnitude of deformation components, duration of treatment and its constituent periods, magnitude of lengthening, IF, IO, etc.), the Mann-Whitney U-test, Student's t-test, and median chi-square were used. The dynamics of the parameters (LEFS questionnaire data) were assessed using the sign test and the Wilcoxon test. Quantitative data were rounded to tenths. Statistical processing was performed using the MO Excel 2016 and Jamovi 2.3.28 software.

RESULTS

Data on the duration of treatment periods for patients in both groups, as well as the values of fixation and osteosynthesis indices assessed in patients requiring segment lengthening, are presented in Tables 2 and 3. No statistically significant difference ($p < 0.05$) was found in any of the assessed indicators.

After correction in each group, the mechanical and anatomical angles were within the reference values in 88.9 % of cases (16 of 18 segments). Two patients (one in each group) had periprosthetic deformity. Since the correction of deformities in those cases had to consider the upcoming

arthroplasty, the target angle values differed from the reference values and were achieved. Thus, the accuracy of correction in both Group1 and Group 2 was 94.4 %. The median values of mechanical angles (in the frontal plane) and anatomical angles (in the sagittal plane), as well as the quartile values, are given in Tables 4 and 5.

Table 2

Duration of separate periods of patients' treatment, Me [Q25;Q75]

Periods	Duration, days		*p*
	Group 1 (standard technique)	Group 2 (spring technique)	
Correction, considering distraction	30.5 [15.8;34.8]	21.5 [18.3;36.5]	> 0.05
Correction without considering distraction	16 [9.3;26.3]	14 [10.3;27.3]	> 0.05
Fixation (among patients who do not need lengthening)	251 [207;272]	239 [196.3;335.5]	> 0.05

Table 3

Additional outcome measures for patients undergoing segment lengthening, Me [Q25;Q75]

Indices	Index value, days/cm		*p*
	Group 1 (standard technique)	Group 2 (spring technique)	
Fixation	98.15 [84.5;128]	107 [91;109.3]	> 0.05
Osteosynthesis	126.55 [102.4;151.4]	119 [80.6;119.5]	> 0.05

Table 4

Accuracy of correction of multi-apical deformities in the frontal plane, Me [Q25;Q75]

Angular deformities	Accuracy of correction of multi-apical deformities, °							
	Group 1 (standard technique)				Group 2 (spring technique)			
	Before correction		After correction		Before correction		After correction	
	mMPTA	mLDTA	mMPTA	mLDTA	mMPTA	mLDTA	mMPTA	mLDTA
Varus	80 [67.3;83]	98 [96.5;99.5]	88 [86.3;89.8]	87.5 [86.3;91]	83 [81;84]	97 [94.5;100]	88 [87;88]	89 [87.5;89.5]
Valgus	95 [91;100]	77.5 [71;84.3]	88 [86;89]	88 [88;90]	95 [94.5;98.5]	76 [68.5;80.5]	88 [87;88]	89 [89;91.5]

Notes: mMPTA — mechanical medial proximal tibial angle; mLDTA mechanical lateral distal tibial angle

Table 5

Accuracy of correction of multi-apical deformities in the sagittal plane, Me [Q25;Q75]

Angular deformities	Accuracy of correction of multi-apical deformities, °							
	Group 1 (standard technique)				Group 2 (spring technique)			
	Before correction		After correction		Before correction		After correction	
	aPPTA	aADTA	aPPTA	aADTA	aPPTA	aADTA	aPPTA	aADTA
Antecurvatum	75 [65;80]	99 [90;103]	80 [79;83.3]	81 [79;82]	79 [76;80.5]	86.5 [84.5;92.5]	80 [78.8;81.3]	81 [80;81.3]
Recurvatum	88 [81;95]	79 [77.5;80.5]	82.5 [82.3;82.8]	80 [79.5;80.5]	80.5 [80.3;80.8]	70.5 [68.3;72.8]	82 [81.5;82.5]	80.5 [79.8;81.3]

Note: aPPTA — anatomical posterior proximal tibial angle; aADTA — anatomical anterior distal tibial angle

The comparison of the LEFS questionnaire data filled in by patients of both groups at different stages of treatment showed no statistically significant difference between the groups (Table 6). The assessment of the dynamics of the indicators before the start of treatment and upon its completion revealed significant difference was in both the control and study groups (Table 7).

All complications that arose during treatment belonged to categories I and II according to Caton (Table 8).

Table 6

Comparison of the indices of subjective assessment of quality of life and segment function according to the LEFS questionnaire at different stages of treatment, Me [Q25;Q75]

Evaluation period	Evaluation score, points		*p*
	Group 1 (standard technique)	Group 2 (spring technique)	
Before surgery	56.5 [43.5;62.5]	55.5 [44.3;65]	> 0.05
Upon correction completion	25.5 [23;29.8]	26.5 [23;31.5]	> 0.05
Before EF removal	38.5 [32;42]	43 [36;45]	> 0.05
2–3 months after EF removal	64 [52;72.3]	65 [56.8;76]	> 0.05

Table 7

Evaluation of the dynamics of the indicators of subjective assessment of the quality of life and segment function according to the LEFS questionnaire before the start of treatment and at its completion, Me [Q25;Q75]

Evaluation period	Evaluation points		*p*
	Group 1 (standard technique)	Group 2 (spring technique)	
Before surgery	56.5 [43.5;62.5]	55.5 [44.3;65]	< 0.05
2–3 after EF removal	64 [52;72.3]	65 [56.8;76]	< 0.05

Table 8

Complications according to J. Caton (1991)

Category J. Caton	Complication	Number of complications			
		Group 1 (standard technique)		Group 2 (spring technique)	
		No	%	No	%
I	Soft-tissue pin-tract infection	8	44.4	7	38.9
	Hypotrophic regenerate	1	5.6	2	11.1
	Neuropathy	1	5.6	1	5.6
	Ankle contracture	1	5.6	1	5.6
	Total	11	61.1	11	61.1
II	Hypotrophic regenerate	2	11.1	3	16.7
	Premature consolidation	1	5.6	0	0
	Transoseous element instability	2	11.1	3	16.7
	Regenerate fracture	2	11.1	0	0
	Total	7	38.9	6	33.3

DISCUSSION

The study revealed that the accuracy of correction in both groups was 94.4 %. The correction period for Group 1 was 16 days (30.5 days with distraction), for Group 2 it was 14 days (21.5 days with distraction). The duration of the fixation period in patients who did not need lengthening was 251 and 239 days, respectively. The difference in all cases was insignificant.

The indicators of quality of life and segment function require separate consideration. This is especially important, since one of the objectives of the "spring" technique development was to ensure greater comfort for the patient during the correction period [4, 13]. However, the analysis of the data of the questionnaire on quality of life and segment function showed no significant difference in the indicators at the end of correction, i.e. before dismantling the strata. Formally, one could conclude that both methods are assessed by patients as equally uncomfortable and equally restricting the function of the segment. However, it should be noted that there was not a single patient in the samples whose treatment was performed in stages using each of the techniques and who could compare the discomfort from both methods from his/her own experience. Therefore, the conclusion can rather be made that the treatment with application of EF modifications (circular ones) is uncomfortable for patients.

Thus, formally, the "spring" technique for correction of multi-apical deformities of the tibia does not have significant advantages over the standard one. However, this statement is based only on the criteria that were considered by the study design. However, it is necessary to indicate other important details. It is known that if the distance between the rings is less than 10–12 cm, the fixator frame is more cumbersome due to the need to use Z-plates and/or "idele" rings, an alternative is to use minimized struts which also has its limitations [20]. The use of the "spring" technique allows us to completely avoid this problem.

Figure 3 shows a case report of a patient with a three-apical deformity. Due to pronounced antecurvatum (75°), the distance between the rings along the posterior surface of the segment was from 68 to 72 mm. The installation of three orthopaedic hexapods would have been technically possible, but it was a difficult task for the orthopaedic surgeon, both in terms of assembling the construct and in the “triple” computer calculation. Such a fixator would have been extremely inconvenient for the patient due to its weight, bulkiness and the need to change the lengths of 18 struts. Therefore, the correction was successfully implemented using the “spring” technique.

The search in the world literature [13] revealed eight studies that discuss the issues of gradual correction of multi-apical deformities of the lower leg using orthopaedic hexapods [2, 4, 6, 8–10, 21, 22]. However, only two of them have the content that allows for a limited comparison of the parameters studied in this work.

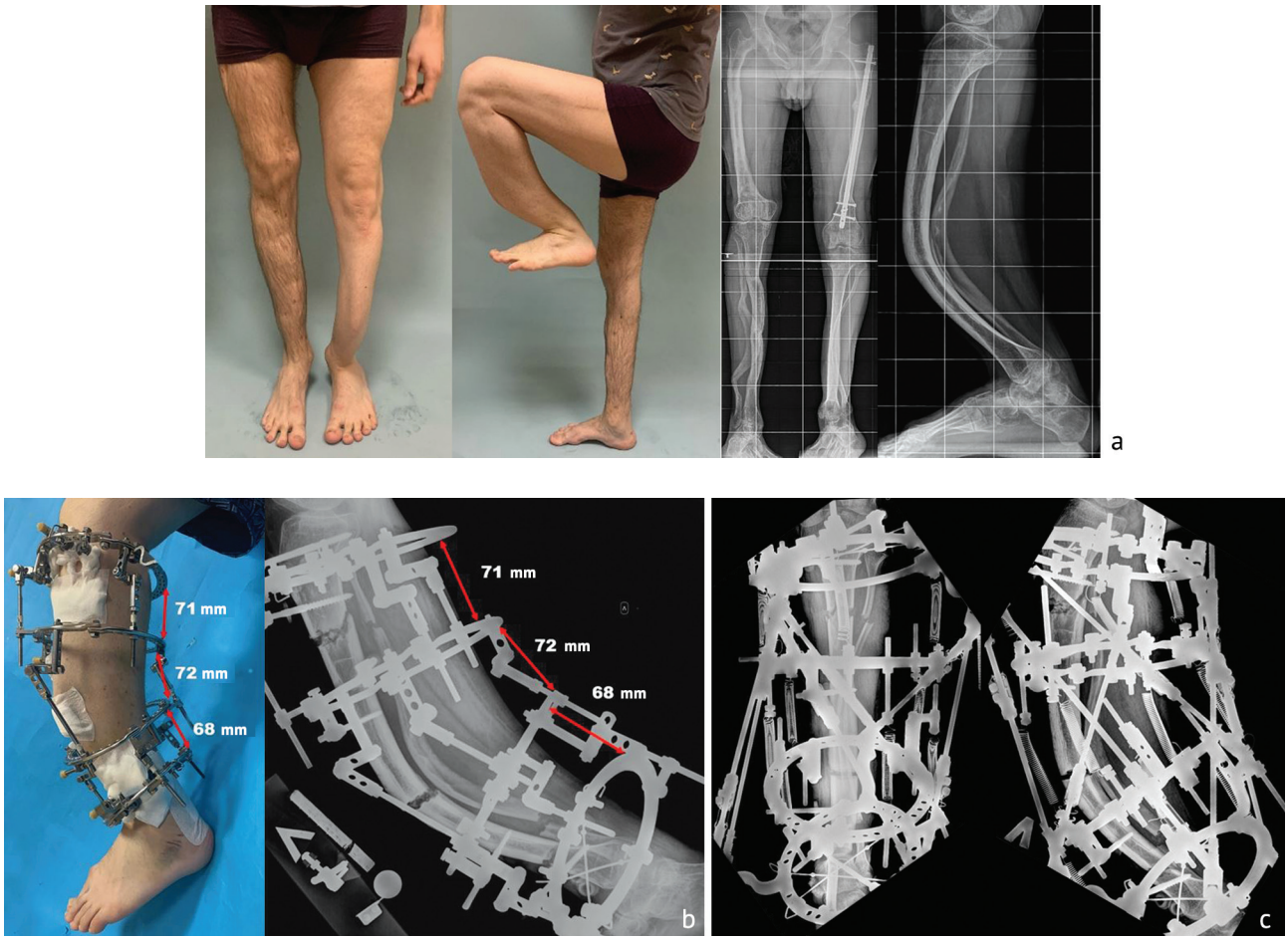

Fig. 3 Clinical case of applying the "spring" technique for tri-apical deformity of the tibia: (a) patient's appearance and radiographs before surgery; (b) at the end of distraction, the distance between the supports along the posterior surface is significantly smaller than the optimal distance for mounting the struts; (c) one orthopaedic hexapod and springs were been successfully mounted and correction began

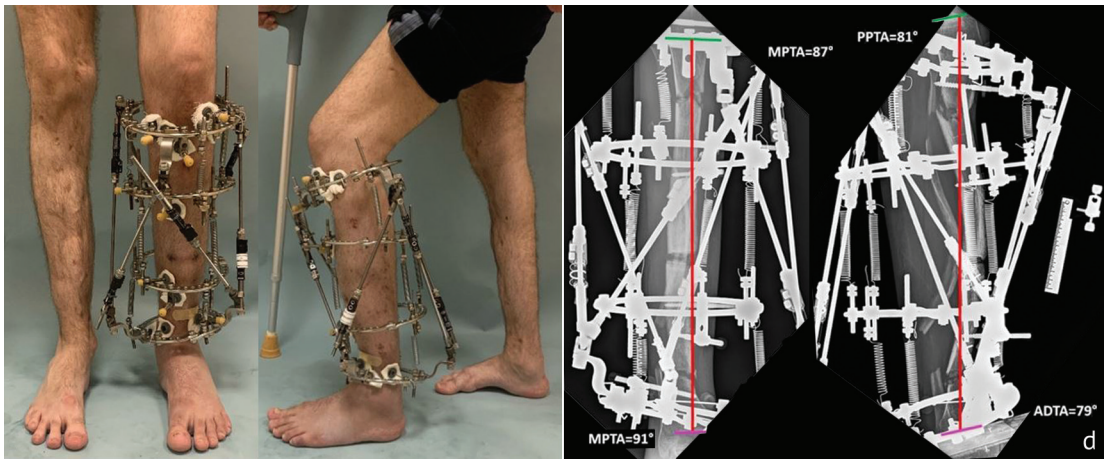

Fig. 3 (continued) Clinical case of applying the "spring" technique for tri-apical deformity of the tibia: (d) photo of the patient and his radiographs at the end of the correction

Among nine patients (13 segments) in the sample of Ray et al. [10], only two patients (three segments) had reached the age of 18 years at the time of treatment and therefore could be considered. To assess the correction accuracy, the authors used the mechanical axis deviation (MAD) which does not allow comparison with the results of our work, since we analyzed the values of mechanical and anatomical angles. The authors of the study assessed consolidation using the angular healing index (AHI). This parameter was the quotient of the number of fixation days divided by distraction regenerate length (cm) in the area where the distance between the bone fragments was the greatest. In adult patients, the average AHI value was 89 days/cm (64–128.3). It can be noted that in comparison with Group 1 of the present study, those data demonstrate better union rates by 9.15 days/cm. However, there is a significant difference in the average age of patients in the samples: 19.7 years (18–21) in Ray et al' s study [10] and 38.8 years (21–65) in our study.

To date, there is only one published paper containing data on the results of clinical application of the "spring" technique. A 2017 article by one of the authors of the present study [4] analyzed four cases of treatment of patients with multi-apical deformities of the lower leg bones. The average value of angular deformity was 34° (11–82). One of the patients also underwent segment lengthening by 30 mm. On average, the correction period was 7 weeks (5–9 weeks), and fixation was 49.5 weeks (41–54). When converted into days (for ease of comparison): 49 days (35–63) for the correction period and 346.5 days (287–441) for the fixation period. The comparison with Group 2 of the present study demonstrates significantly longer correction and fixation periods. However, the average value of angular deformity in the patients of the study was greater, which may partially explain the duration of treatment. It is also necessary to indicate in analyzing the results that the early version of the "spring" technique was used to treat those patients. It differs from the variant described in this paper in the following: the springs were fixed directly to the supports, without traction clamps and positioning the springs parallel to the axis of the intermediate fragment(s). The technical characteristics of the springs also differed: length in the neutral position — 100 mm, wire diameter — 1 mm, coil diameter — 10 mm, number of coils — 42. These factors created conditions for lower rigidity of fixation of the intermediate support. Therefore, it can be assumed that the action of the compression forces of the springs was uneven and multidirectional. The above fact increased the risk of undesired displacement of the intermediate fragment, which, in turn, affected the duration of treatment.

CONCLUSION

Based on the analysis of the criteria used for evaluation, it was found that the "spring" technique for multi-apical deformity correction of the lower-leg bones is as effective as the standard one. The advantages of the "spring" technique are related to its greater convenience of its use for the doctor and more comfort for the patient.

REFERENCES

1. Vilensky VA. *Development of the fundamentals of a new technology for treating patients with diaphyseal injuries of long bones based on a transosseous apparatus with passive computer navigation properties (experimental and clinical study): Autoref. kand. dis*. Saint Petersburg; 2009:31. Available at: https://viewer.rsl.ru/ru/rsl01003482854?page=8&rotate=0&theme=white. Accessed Mar 5, 2025. (In Russ.)
2. Ganger R, Radler C, Speigner B, Grill F. Correction of post-traumatic lower limb deformities using the Taylor spatial frame. *Int Orthop*. 2010;34(5):723-730. doi: 10.1007/s00264-009-0839-5.
3. Vilensky VA, Pozdeev AP, Bukharev EV, et al. Orthopedic hexapods: history, present and prospects. *Pediatric Traumatology, Orthopaedics and Reconstructive Surgery*. 2015;3(1):61-69. (In Russ.) doi: 10.17816/PTORS3161-69.
4. Solomin LN, Shchepkina EA, Korchagin KL, et al. The new method of long bone multilevel deformities correction using the orthopedic hexapod (preliminary report). *Traumatology and Orthopedics of Russia*. 2017;23(3):103-109. (In Russ.) doi: 10.21823/2311-2905-2017-23-3-103-109.
5. Lu Y, Li J, Qiao F, et al. Correction of severe lower extremity deformity with digital hexapod external fixator based on CT data. *Eur J Med Res*. 2022;27(1):252. doi: 10.1186/s40001-022-00887-6.
6. Naqui SZ, Thiryayi W, Foster A, et al. Correction of simple and complex pediatric deformities using the Taylor-Spatial Frame. *J Pediatr Orthop*. 2008;28(6):640-647. doi: 10.1097/BPO.0b013e3181831e99.
7. Keshet D, Eidelman M. Clinical utility of the Taylor spatial frame for limb deformities. *Orthop Res Rev*. 2017;9:51-61. doi: 10.2147/ORR.S113420.
8. Riganti S, Nasto LA, Mannino S, et al. Correction of complex lower limb angular deformities with or without length discrepancy in children using the TL-HEX hexapod system: comparison of clinical and radiographical results. *J Pediatr Orthop B*. 2019;28(3):214-220. doi: 10.1097/BPB.0000000000000573.
9. Vilensky V.A., Zakharyan E.A., Zubairov T.F. et al. Treatment of two-level deformities of lower leg bones: two hexapods or one? *Modern problems of science and education*. 2019;(6). (In Russ.) doi: 10.17513/spno.29352.
10. Ray V, Popkov D, Lascombes P, et al. Simultaneous multisegmental and multifocal corrections of complex lower limb deformities with a hexapod external fixator. *Orthop Traumatol Surg Res*. 2023;109(3):103042. doi: 10.1016/j.otsr.2021.103042.
11. Massobrio M, Mora R. *Hexapod External Fixator Systems: Principles and Current Practice in Orthopaedic Surgery*. Springer International Publishing; 2021:311.
12. Trombetti A, Al-Daghri N, Brandi ML et al. Interdisciplinary management of FGF23-related phosphate wasting syndromes: a Consensus Statement on the evaluation, diagnosis and care of patients with X-linked hypophosphataemia. *Nat Rev Endocrinol*. 2022;18(6):366-384. doi: 10.1038/s41574-022-00662-x.
13. Golovenkin ES, Solomin LN. Correction of Multiapical Deformities of Long Bones of the Lower Extremities: A Review. *Traumatology and Orthopedics of Russia*. 2023;29(4):134-146. doi: 10.17816/2311-2905-11174.
14. Iobst C., Ferreira N., Kold S. A Review and Comparison of Hexapod External Fixators: Current Concept Review. *J Pediatr Orthop Soc North Am*. 2023;5(1):627. doi: 10.55275/JPOSNA-2023-627.
15. Caton J. Bilateral lengthening of lower limbs in short subjects in France. Results of the GEOP survey; our experience: Treatment of inequalities in length of lower limbs and short subjects in children and adolescents: Symposium under the direction of J Caton (Lyon). *Rev Chir Orthop*. 1991;77(1):74-77. (In Fran.)
16. Vilensky VA, Pozdeev AA, Zubairov TF, et al. Treatment of pediatric patients withlower extremity deformities using software-assisted ORTHO-SUV frame: analysis of 213 cases. *Pediatric Traumatology, Orthopaedics and Reconstructive Surgery*. 2016;4(4):21-32. doi: 10.17816/PTORS4421-32.
17. Zakharyan EA. *Complex treatment of lower limb deformities in children with congenital pseudoarthrosis of the tibia: Kand. Dis*. St. Petersburg; 2017:154. Available at: http://dissovet.rniito.ru/ds2/upload/files/zaharian_ea/diss.pdf. Accessed Mar 05, 2025. (In Russ.)
18. Rokhoev S.A. *Justification for the use of an orthopedic hexapod in the treatment of patients with knee joint contractures (anatomical and clinical study): Kand. Dis*. St. Petersburg; 2022:181. Available at: http://dissovet.rniito.ru/ds2/upload/files/rohoev/dissert.pdf. Accessed Mar 05, 2025. (In Russ.)
19. Lebedkov IV. *Comparative evaluation of the effectiveness of combined transosseous and intramedullary osteosynthesis and lengthening according to Ilizarov in restoring the length of the tibia and femur (experimental and clinical study): Kand. Dis*. St. Petersburg; 2023:200. Available at: http://dissovet.rniito.ru/ds2/upload/files/lebedkov/dissert.pdf. Accessed Mar 05, 2025. (In Russ.)
20. Gavrilov DV, Solomin LN. Comparative analysis of the reduction capabilities of orthopedic hexapod Ortho-SUV frame and its minimized (pediatric) version (experimental study). *Genij Ortopedii*. 2023;29(3):270-276. doi: 10.18019/1028-4427-2023-29-3-270-276.
21. Eidelman M, Bialik V, Katzman A. Correction of deformities in children using the Taylor spatial frame. *J Pediatr Orthop B*. 2006;15(6):387-395. doi: 10.1097/01.bpb.0000228380.27239.8a.
22. Koren L, Keren Y, Eidelman M. Multiplanar Deformities Correction Using Taylor Spatial Frame in Skeletally Immature Patients. *Open Orthop J*. 2016;10:71-79. doi: 10.2174/1874325001610010603.

The article was submitted 19.12.2024; approved after reviewing 04.03.2025; accepted for publication 31.03.2025.

Information about the authors:

Evgeniy S. Golovenkin — Clinical Postgraduate Student,
golovenkin_1996@mail.ru, https://orcid.org/0000-0001-7064-5689;

Leonid N. Solomin — Doctor of Medical Sciences, Professor, Leading Researcher,
solomin.leonid@gmail.com, https://orcid.org/0000-0003-3705-3280

Original article
https://doi.org/10.18019/1028-4427-2025-31-3-297-306

Finite element modeling of anatomical constitutional types of the lumbar spine and pelvis (Roussouly) for study of the biomechanical aspects

A.E. Shulga✉, V.Yu. Ulyanov, Yu.Yu. Rozhkova, S.D. Shuvalov

Research Institute of Traumatology, Orthopedics and Neurosurgery
of the Saratov State Medical University named after V.I. Razumovsky, Saratov, Russian Federation

Corresponding author: Alexey E. Shulga, doc.shulga@yandex.ru

Abstract

Introduction Sagittal morphotypes graded by Roussouly are characterized by specific biomechanics of the spinopelvic alignment (SPA) that can be investigated using the finite element (FE) modeling.

The **objective** was to design three-dimensional realistic models simulating anatomical and constitutional types LPA and evaluate deformity and strength of the models under compression.

Materal and methods Lateral standing spondylograms of the skull, pelvis and upper third of the femur were produced for volunteers (n = 169) who agreed to participate in the study. Radiographs were interpreted with Surgimap 2.3.2.1.) and computed tomography (CT) of the SPA was performed for individuals (n = 5) with average sagittal parameters for each of the five Roussouly morphotypes (I, II, III, IIIA, IV). The CT findings were used to simulate (SolidWorks) five parametric finite element models of normal morphotypes of SPA and examine the deformity and strength.

Results The highest von Mises stresses under compression were measured in the bodies and intervertebral discs (IVD) ThX–LI (2.961 MPa), posterior supporting structures LIV–SI (2.515 Mpa) with type I model; vertebral bodies and IVD of the thoracic and lumbar spine, mainly at the ThXII–LI (3.082 MPa) and LIV–LV (3.120 Mpa) levels with type II model; anterior aspects of the bodies and IVD ThXI–LII, posterior thirds of the bodies, pedicles and facet joints LI–SI (1.720 Mpa) with type III model; the bodies and intervertebral discs of the ThIX–LII vertebrae (1.811 MPa), posterior supporting structures of the LI–SI vertebrae (1.650 Mpa) with type IIIA model; in the spinous processes and articular portion of the arches of the LI–SI vertebrae (3.232 MPa) with type IV model.

Discussion The lateral configuration of the SPA has a key effect on the segmental distribution of gravitational force and determines the specificity of the sagittal biomechanics of the spine, its resistance to dynamic loads and tendency to various degenerative pathologies.

Conclusion Types III and IIIA were the most biomechanically balanced types, hypolordotic form (types I and II) was associated with overloaded anterior vertebral structures including intervertebral disc protrusion (IDP) and overloaded posterior supporting structures in case of hyperlordosis (type IV).

Keywords: spine, sagittal balance, Roussouly classification, mathematical modeling, finite element analysis

For citation: Shulga AE, Ulyanov VYu, Rozhkova YuYu, Shuvalov SD. Finite element modeling of anatomical constitutional types of the lumbar spine and pelvis (Roussouly) for study of the biomechanical aspects. *Genij Ortopedii*. 2025;31(3):297-306. doi: 10.18019/1028-4427-2025-31-3-297-306.

INTRODUCTION

The human vertebral column became S-shaped during evolution which is optimal for maintaining an economical orthostatic position [1, 2]. The geometric combination of the physiological curvatures and the pelvis provides a balance chain with the coordination proportionally distributing the trunk weight around the gravitational line minimizing energy expenditures and the need for conscious postural control [3].

In 1992, Duval-Beaupere et al. introduced the concept of sagittal balance and described a number of radiometric parameters of the pelvis, emphasizing the role of morphology in the regulation of postural balance [4]. Studies of the profile geometry of the spinopelvic complex (SPC) revealed significant anatomical variability of the spine in healthy individuals and the impossibility of systematizing the sagittal shape based on average radiometric parameters [5]. In 2005, Roussouly offered to distinguish four morphological types of the SPC in the normal population considering the sacral slope and the sagittal shape of the spine [6]. A hypothesis was proposed about the type-specificity of the distribution of gravitational load on various vertebral structures, which implies the presence of sagittal biomechanics and degeneration of the SPC, being characteristic of each of its morphotypes [7].

The conclusions are mostly based on the analysis of radiometric parameters and are of an inferential nature [8]. Fundamental research is aimed at objectifying the causes of various spinal conditions [9]. Finite element (FE) analysis is one of the most popular methods to simulate a real physical system (geometry and loading conditions) using mathematical approximation [10]. Simple and interacting elements (units) are used with a finite number to be employed for approximation of a real system with an infinite number of unknowns [11]. The FE modeling is widely used in clinical studies due to the reproducibility of its results and low cost of the experiment [12]. FE analysis can be practical for the study of the etiology of degenerative diseases of the spine and for identification of various factors affecting lumbar biomechanics, including the geometric variability of morphotypes of the SPC [13].

Understanding of the sagittal biomechanics of the morphological types of SPC is important for the study of the pathogenesis of degenerative spine diseases to predict outcomes of surgical interventions.

The **objective** was to design three-dimensional realistic models simulating anatomical and constitutional types of SPA and evaluate deformity and strength of the models under compression.

MATERIAL AND METHODS

The FE model of the spine was constructed based on the model proposed by Kolmakova and Rikun [14]. Lordosis and kyphosis are associated with different intervertebral heights anteriorly and posteriorly where the intervertebral disc (IVD) is located. The IVD consists of cartilaginous tissue and is anatomically divided into three parts. The inner part (nucleus pulposus) is a gel-like mass rich in water. The outer portion (fibrous ring) has a hard and fibrous structure. The third part of the disc is a thin layer of hyaline cartilage, which separates the disc from the vertebral body. The geometric model includes the CIII (1) and CIV (2) vertebrae, the intervertebral disc (3), facet joints (4), the interspinous ligament (5), the posterior vertebral arches (6), the spinous (7), transverse (8), and articular (9) processes (Fig. 1 a). Cancellous (10) and compact bone tissue are present in the vertebrae (Fig. 1 b).

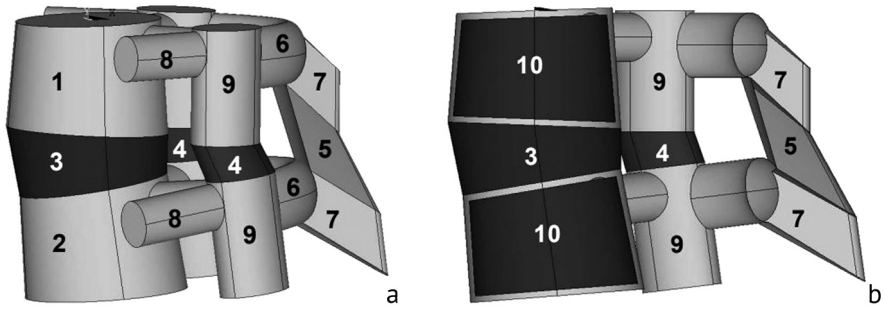

Fig. 1 Geometric model of the CIII–CIV segment of the cervical spine: (a) isometric view; (b) sectioned lateral view [14]

A thin cortical layer covers vertebral bodies. It is assumed that simulated vertebral arches and vertebral processes consist of compact bone tissue. The Z-axis of the coordinate system is directed along the segment axis. The X-axis is directed in the anteroposterior direction of the spinal segment. The presence of lordosis is considered due to a greater anterior IVD height, or kyphosis with a lower anterior height of the disc.

The geometric model of segments with different geometric parameters was used for FE modeling and determination of the stress-strain in the thoracic (ThI–ThXII) and lumbar (LI–LV) spine.

The bone components and intervertebral discs were integrated using first-order hexahedral hybrid solid FEs. The collagen fibers of the annulus and ligaments were represented by flat truss FEs (T2D2). The facet joint surfaces were modeled using frictionless surface-to-surface contact. The nucleus pulposus (NP) and the annular matrix were considered as a virtually incompressible hyperelastic material as described by the Mooney-Rivlin law.

Young's modulus for NP was measured in the range of 0.0045–1.5 MPa ($\nu = 0.45$) and 20 MPa ($\nu = 0.4$) for hyaline plates. The deformed collagen fibers were described by a nonlinear stress-strain function. The contact between the surfaces of the facet joints was assumed to be rigid with a friction coefficient of 0.15. The layers of facet cartilage with an initial gap of 0.5 mm were described as elastically isotropic (Young's modulus 35 MPa).

Cortical and cancellous bone tissues of the vertebral bodies, IVD, facet joints, interspinous ligaments, vertebral arches and processes were considered to be isotropic linearly elastic materials. The mechanical characteristics of the structural components of the segments were set in accordance with the literature data [15, 16] (Table 1).

Table 1

Mechanical properties of the structural components of the vertebral segment

Structural component	Young's modulus of elasticity, MPa	Poisson's ratio
Cortical bone	10000	0.3
Cancellous bone	100	0.2
Facet joints	1,5	0.3
Intervertebral disc	2,5–98	0.45
Interspinous ligament	3,5	0.3

Young's modulus of elasticity and Poisson's ratio for the structural components of the spine were presented in different ranges [6]. The calculations were produced using the ABAQUS software package using the finite element method; the problem was solved using the linear theory of elasticity. Geometric models were constructed in accordance with the actual dimensions of the cervical [17], thoracic, lumbar [18] spine and intervertebral disc [19].

Based on the conducted research, the following sequence of steps was proposed for implementing the algorithm for modeling the stress-strain of the spinal elements:

1) determination of the initial reference body geometry for calculations of the spine (the body relative to which the position of a given body is determined);
2) determination of the displacement of segments for each type of spinal column relative to the position of the segments in the reference body according to the projection of the spine onto the vertical plane;
3) division of the spinal column segment system into sections to be used in the ABAQUS program to form finite superelements used to reduce the amount of calculations in the FE method;
4) Numerical solution for determining the stress-strain of the spinal column in the displacements defined in paragraph 2;
5) determination of additional equivalent stresses in the spinal segments caused by displacements relative to the reference body.

Mesh Convergence Study

A linear hexahedral mesh and eight-node quadratic tetrahedral elements (C3D8) were considered for the cortical bone, cancellous bone, and posterior supporting structures. Collagen fibers of the annulus and ligaments were represented by plane truss elements (T2D2). A mesh convergence test was performed to determine the appropriate mesh resolution of the FE model to confirm the accuracy of the simulation. The mesh density was found to provide good convergence of results with an element side length of approximately 1–1.5 mm. The mesh convergence results showed a difference of less than 5 % in the IVD loads when the number of elements was doubled.

Screening of the healthy population was produced to select individuals with different sagittal morphology of the spine in accordance with the classification revised by Roussouly (2017) [20]. Lateral standing spondylograms of the skull, pelvis and upper third of the femur were produced for volunteers who agreed to participate in the study. Sagittal parameters of the SPC (Surgimap 2.3.2.1.) were interpreted and the subject was assigned to one of the five Roussouly types. Finally, 169 volunteers were rated as type I (n = 20; 11.9 %), type II (n = 42; 24.9 %), type III (n = 50; 29.6 %); type IIIA (n = 25; 14.7 %), type IV (n = 32; 18.9 %). The number of patients in each group was averaged to 20 to improve the proportionality of the data.

The resulting database of 100 individuals allowed us to determine the normal ranges of sagittal parameters (Sacral Slope, SS; Pelvic Incidence, PI; Pelvic Tilt, PT; Global Lumbar Lordosis, GLL; Lordosis Tilt Angle, LTA; Lumbar Lordosis Apex, LLA; Number (verteb) Lumbar Lordosis, NLL) for each of the five morphotypes. The radiographic parameters were subjected to standard statistical analysis, which showed a normal distribution of the variables in the study population. Parametric statistics methods were used for calculations, and quantitative parameters were presented as the arithmetic mean and standard deviation (Table 2). The arithmetic mean values of all radiometric sagittal parameters were measured in each of the five groups characterizing the “reference” lateral shape of the SPC for a specific group, and the standard deviation allowed geometric variations of morphotypes within the designated boundaries. The selected volunteers underwent computed tomography (CT) of the SPC for modeling of parametric FE models.

Table 2

Mean values of sagittal parameters for different Roussouly morphotypes (n = 100), descriptive statistics

Roussouly type	n valid (by list)	Parameters							
		Statistical indicator	age	PI	SS	PT	GLL	LTA	LLA	NLL
I	20	$\bar{X}$	40.70	38.845	29.450	10.110	−50.295	−7.930	5.375	2.650
		σ	6.697	3.6176	2.7907	2.9693	4.2201	2.3595	0.2221	0.4894
II	20	$\bar{X}$	39.40	40.765	30.830	10.270	−48.080	−5.910	4.225	4.075
		σ	6.916	4.3347	2.9631	2.7741	4.3819	1.5697	0.2552	0.5200
III	20	$\bar{X}$	40.30	52.955	39.855	13.080	−59.395	−3.950	4.250	4.100
		σ	7.420	3.5798	2.0028	3.2638	3.6360	2.6106	0.3804	0.5282
IIIA	20	$\bar{X}$	38.85	48.140	45.140	4.140	−64.525	−5.495	4.100	4.775
		σ	8.768	3.0285	4.5217	1.9228	4.3052	2.1852	0.5982	0.2552
IV	20	$\bar{X}$	39.90	62.270	49.850	12.045	−70.555	−1.530	3.175	5.650
		σ	7.752	3.8674	2.8057	4.1461	4.0028	2.1436	0.2447	0.5155

Note: $\bar{X}$ — arithmetic mean; σ — standard deviation.

RESULTS

Parametric FE models were developed in the SolidWorks environment to explore deformation and strength properties of five normal morphotypes of the SPC in accordance with the revised classification of Roussouly. Computer tomograms of five "reference" volunteers selected at the previous stages of the study were used as input data for modeling the spine. The models were constructed in accordance with the determinants of sagittal morphology of the STC, determined by Roussouly for each of the five morphotypes [20], and the radiometric parameters of the “reference” participants.

The simulated three-dimensional model type I (Fig. 2 a) was characterized by low-grade SS (29.4°) and PI (39.4°), had a short (NLL, 3 vertebrae) lumbar hyperlordosis (GLL, (–49.5°)) with a low location of the apex (LLA, IVD LIV–LV) and a negative LTA value (–8.9°). The thoracolumbar spine was characterized by an extended kyphosis, and the PT value (10.3°) corresponded to the average values of the normal range (0–20°).

Type II (Fig. 2 b) was characterized by low-grade values of SS (31.3°) and PI (41.2°). The model was constructed taking into account the hypolordoticity (GLL, (–47.9°)) and hypokyphoticity of the spinal column and in accordance with a higher (than in type I) location of the LLA (the center of the LIV vertebra), a more positive LTA (–6.7°), a larger number of vertebrae in the lordotic arch (NLL, 4 vertebrae) and average PT values (9.8°).

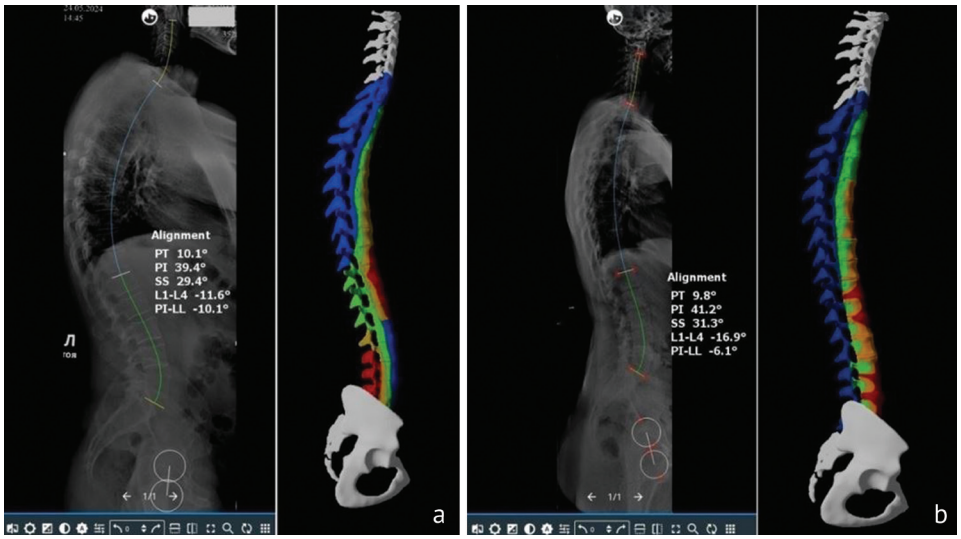

Fig. 2 Sagittal parameters (Surgimap 2.3.2.1.) measured in (a) a volunteer with type I SPC; (b) participants with type II SPC and a 3D model

Three-dimensional modeling of morphotype III (Fig. 3 a) involved the radiometric parameters of the corresponding "reference" participant as SS (39.6°), PI (52.2°), and GLL (–58.8°). This variant of the geometric shape was characterized by a relatively long arc of the lumbar lordosis (NLL, 4.5 vertebrae), high position of the LLA (LPD LIII–LIV), lower LTA values (–4.5°), and average PT values (12.6°).

Some of the parameters used to model type IIIA (Fig. 3 b) were comparable with those used for morphological type III (LTA, –6.1°; LLA, IVD LIII–LIV; NLL, 5 vertebrae), but a number of criteria had differences characteristic of this morphotype. The pelvic anteversion PT (3.9°) specific to type IIIA determined a combination of high SS (45.0°) and GLL (–65.0°) values with low PI parameters (48.9°).

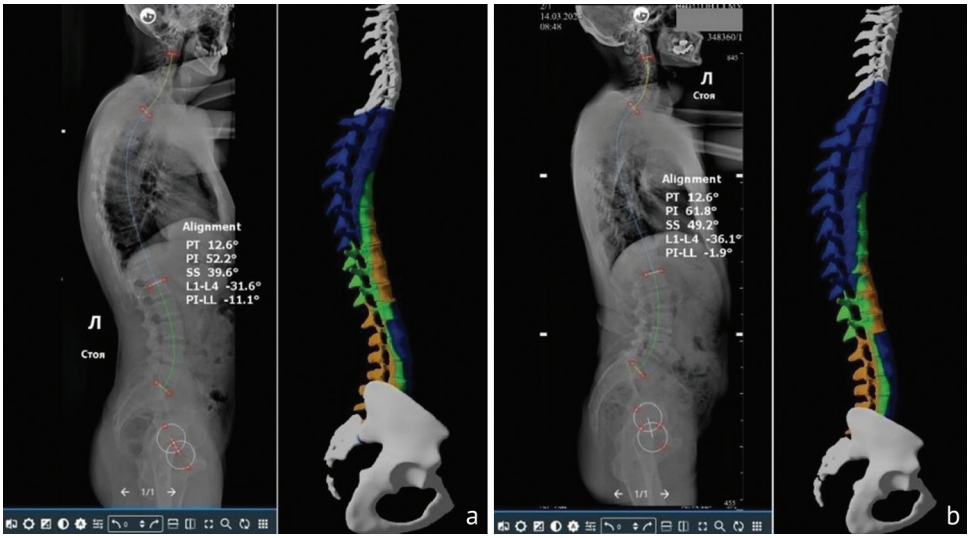

Fig. 3 Sagittal parameters (Surgimap 2.3.2.1.) measured in (a) a volunteer with SPC type III; (b) a volunteer with SPC type IIIA and a 3D model

The three-dimensional model of type IV (Fig. 4) was represented by a harmonious hypercurved SPC with segmental hyperextension of the lumbar spine. The large PI value (61.8°), characteristic of this sagittal morphotype, served as a determinant of a large sacral slope SS (49.2°) and a high-grade GLL (–69.8°), extended LLA (MPD L2–L3; NLL, 5.5 vertebrae) of lumbar lordosis.

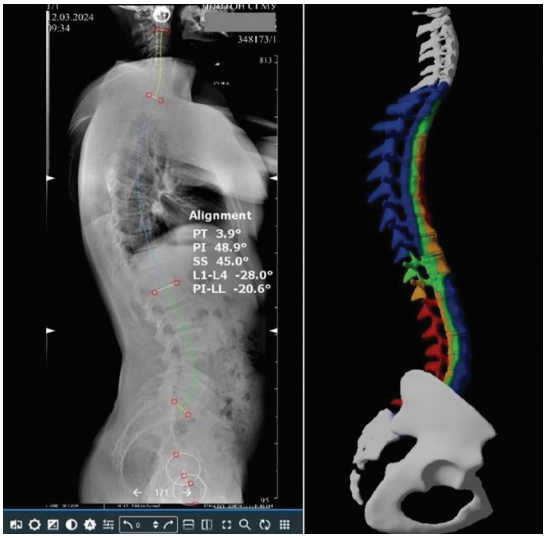

Fig. 4 Sagittal parameters (Surgimap 2.3.2.1.) measured in a volunteer with SPC type IV and a 3D model

LTA (–1.8°) was characterized by values close to 0, and PT (12.6°) was within the average values of the normal range (0–20°).

The FE models of Roussouly five sagittal types of SPC allowed us to explore and characterize the stress-strain state under axial load. All nodes of the lower surface of the FE model of the LV vertebra were fixed as boundary conditions.

Color maps of the stress-strain of five vertebral morphotypes were determined with the FE method. Various zones of the stress-strain of the vertebrae were determined using the results of the method offered to 3D models of the spinal column: the red color corresponded to the zone of the maximum stress; the blue color characterized the minimum vertebral stress; the color transition indicated the stress effect on the adjacent vertebrae.

The type I model showed the highest von Mises equivalent stresses in the thoracolumbar region under axial load (Fig. 2 a). The bodies and IVDs of the ThX–LI vertebrae were the most heavily loaded parts (2.961 MPa). The highest stresses occurred on the posterior supporting structures (spinous processes, articular processes, pedicles) of the lumbar spine and on the dorsal part of the bodies of the lower lumbar vertebrae (LIV–SI) (2.515 Mpa).

The type II model demonstrated the highest equivalent stresses in the anterior supporting structures (vertebral bodies and IVD) of the thoracic and lumbar spine under compression load (Fig. 2 b). The stress field was uneven throughout the specified region, with the highest values noted at the ThXII–LI (3.082 MPa) and LIV–LV (3.120 MPa) levels. The posterior supporting structures of the second type of the spine experienced insignificant loads (0.650 MPa).

The third type, due to its geometric balance, was characterized by biomechanical stability (Fig. 3 a). The most loaded zone was noted in the anterior thoracolumbar vertebrae and IVD (ThXI–LII) and along the lumbar spine (LI–SI): mainly the posterior third of the vertebral bodies, the pedicles and facet joints (1.720 MPa). Nevertheless, the stress level was characterized by significantly lower values compared to Roussouly morphotypes I and II (1.431 Mpa).

The increased stress level in type IIIA had a localization characteristic of type III, but was characterized by a greater extent of boundaries (Fig. 3 b). It covered the area from ThIX to LII vertebrae, and extended to the posterior sections of the bodies of LIII–LV vertebrae. The stresses exceeded those in type III, both in the thoracic (1.811 MPa) and lumbar spine (1.650 Mpa).

The type IV model demonstrated the biomechanics of a hypercurved vertebral column (Fig. 4). In the thoracic region, zones with a moderate level of equivalent stresses (2.743 MPa) were identified along the anterior surface of the bodies (anterior half of the bodies and IVD) of the ThIII–ThXI vertebrae under axial loads. The posterior supporting structures of the LI–SI vertebrae was found to be the most heavily loaded, while the stress values on the spinous processes and articular sections of the arches had values similar to those of type I (3.232 MPa).

DISCUSSION

In recent decades, significant progress has been noted in the study of sagittal morphology and biomechanics of the SPC with assessments becoming a routine procedure in the diagnosis and treatment of various spinal conditions [21]. The variability of the profile geometry of the SPC in healthy individuals was reported by several researchers with the presence of four types (with a fifth subtype in the revised classification) of the normal profile configuration substantiated and the type-specificity of diseases proven. Reproducible and accessible methods for modeling the spinal column are used to objectify the causes of the degenerative pathology [22]. FE modeling is the most common method for studying the spine biomechanics *in silico* [23]. The results of various tests conducted on mathematical models of the spinal column are published to confirm the conclusions of analytical studies [24, 25].

In the present experiment, an attempt was made to explore the mechanical characteristics of parametric FE models of four classical types of SPC and the retroverted variant of morphotype III, constructed on the basis of CT scans of the spine of healthy subjects with average values of sagittal parameters. The findings demonstrated a significant influence of the profile configuration of five SPC models on their sagittal biomechanics, which was manifested by different reactivity of the FE stiffness matrix under axial compression load. The data on the stress-strain of the models confirmed the theoretical patterns formulated earlier in the majority of cases [7]. The hypolordotic lumbar spine was considered as the main predictor of IVD degeneration considering the concept of "contact force" presented by Roussouly. Subsequent clinical studies have repeatedly confirmed the fact that individuals with discogenic pathology are characterized by low PI values corresponding to hypolordosis [26, 27]. The deformation and strength properties of FE models with low PI (types I and II) indicated zones of the greatest equivalent stresses in the vertebral bodies and IVD, mainly in the thoracolumbar (type I, ThX–LI; type II ThXII–LI) and lumbar (type I, LIV–SI; type II LIV–LV) spine. With the vertebral endplates oriented in a plane being closer to the horizontal plane the gravitational load vector has perpendicular impact on them increasing the overload of the IVD. There are significant stresses on the posterior supporting structures (spinous processes, articular processes, pedicles) in the FE model of type I. These features are caused by a short hypercurved lordosis, when the vector of biomechanical axial action is shifted to the posterior supporting column. There are data in the literature that are consistent with our findings. Müller et al. reported complex loads on 28 FE models of the lumbar spine and indicated the compression force had impact primarily on the IVD with a hypolordotic lumbar spine, and on the contrary, the facet joints were more susceptible to its influence with high LL values [28]. The significant impact of gravitational load on the posterior supporting structures of the lumbar spine under hyperlordosis conditions was confirmed by out findings in the study of the stress-strain condition of the FE model of morphotype IV. In addition to that, the region of increased equivalent stresses of this model was determined in the bodies and IVD at the level of thoracic hyperkyphosis (ThIII–ThXI). Roussouly et al. interpreted the biomechanics of local stresses of the hypercurved lumbar spine and noted that the distribution of the KS depended on the PI value [7]. The higher the PI values, the more inclined are the vertebrae that make up the lower arc of the lumbar lordosis, that contributes to the distribution of the gravitational load parallel to the endplates. Under these conditions, the pressure on the IVD decreases, and the facet joints are subject to a combined effect of axial (due to hyperextension) and shear (due to sliding force). The study of FE models of types III and IIIA showed no zones of mechanical overloads equivalent to types I, II and IV, which characterizes their geometric balance and biomechanical harmony. Moderate stress zones in type III and type IIIA were localized in the bodies and IVDs of the thoracolumbar spine, on the posterior supporting structures of the lumbar spine of the FE models. There are similar studies assessing stresses and resulting deformations along the spinal column using geometrically personalized FE models. The authors came to the conclusion that the PI value was closely related to the distribution of load forces: the stress is distributed evenly along the entire spine with the hypolordotic form; the load concentration is observed mainly around the lower part of the spinal column (LIII–LV) with the normal and hyperlordotic configuration [29, 30].

The profile configuration of the SPC has a substantial influence on the segmental distribution of gravitational force and determines the specificity of the sagittal biomechanics of the spine, the resistance to dynamic loads and susceptibility to various degenerative conditions. Type III and type IIIA appeared to be the most balanced types, the anterior vertebral structures including the IVD were overloaded with the hypolordotic form (types I and II), and the posterior supporting structures were overloaded in the case of hyperlordosis (type IV) or local hyperextension (type I).

CONCLUSION

The FE modeling algorithm offered allows *in silico* estimation of the stress-strain condition of various spinal structures with high reproducibility of results. The FE analysis of three-dimensional realistic models of the spinal column, constructed using the geometric parameters of Roussouly five morphological types demonstrated the ambiguity of the sagittal biomechanics. Morphotypes III and IIIA demonstrated the most harmonious distribution of equivalent stresses, whereas hypo- (types I and II) and hyperlordotic (type IV) forms of SPC contributed to type-specific overload of various parts of the spine. Therefore, the anatomical and constitutional features of the spinal column can be considered one of the main factors determining the resistance to dynamic loads and its tendency to different degenerative conditions.

Conflicting Interests *The authors declared no potential conflicts of interest with respect to the authorship and/or publication of this article.*

Informed Consent *Informed consent was obtained from all patients for being included in the study.*

REFERENCES

1. Diebo BG, Varghese JJ, Lafage R, et al. Sagittal alignment of the spine: What do you need to know? *Clin Neurol Neurosurg*. 2015;139:295-301. doi: 10.1016/j.clineuro.2015.10.024.
2. Le Huec JC, Saddiki R, Franke J, et al. Equilibrium of the human body and the gravity line: the basics. *Eur Spine J*. 2011;20(Suppl 5):558-563. doi: 10.1007/s00586-011-1939-7.
3. Hasegawa K, Okamoto M, Hatsushikano S, et al. Standing sagittal alignment of the whole axial skeleton with reference to the gravity line in humans. *J Anat*. 2017;230(5):619-630. doi: 10.1111/joa.12586.
4. Duval-Beaupère G, Schmidt C, Cosson P. A Barycentremetric study of the sagittal shape of spine and pelvis: the conditions required for an economic standing position. *Ann Biomed Eng*. 1992;20(4):451-62. doi: 10.1007/BF02368136.
5. Berthonnaud E, Dimnet J, Roussouly P, Labelle H. Analysis of the sagittal balance of the spine and pelvis using shape and orientation parameters. *J Spinal Disord Tech*. 2005;18(1):40-47. doi: 10.1097/01.bsd.0000117542.88865.77.
6. Roussouly P, Gollogly S, Berthonnaud E, Dimnet J. Classification of the normal variation in the sagittal alignment of the human lumbar spine and pelvis in the standing position. *Spine (Phila Pa 1976)*. 2005;30(3):346-53. doi: 10.1097/01.brs.0000152379.54463.65.
7. Roussouly P, Pinheiro-Franco JL. Biomechanical analysis of the spino-pelvic organization and adaptation in pathology. *Eur Spine J*. 2011;20 Suppl 5(Suppl 5):609-18. doi: 10.1007/s00586-011-1928-x.
8. Naoum S, Vasiliadis AV, Koutserimpas C, et al. Finite Element Method for the Evaluation of the Human Spine: A Literature Overview. *J Funct Biomater*. 2021;12(3):43. doi: 10.3390/jfb12030043.
9. Kossovich LYu, Kharlamov AV, Lysunkina YuV, Shul'ga AE. Mathematical modeling and prediction of the effectiveness of surgical treatment in surgery of the spine and pelvic complex. *J Samara State Tech Univ Ser Phys Math Sci*. 2019;23(4):744-755. doi: https://doi.org/10.14498/vsgtu1702.
10. Zhang S, Bai T, Zhang X, et al. Application of Finite Element Analysis in Biomechanical Research of Degenerative Diseases of Lumbar Spine. *JBM*. 2022;(10):21-33. doi: 10.4236/jbm.2022.103004.
11. Kudo N, Yamada Y, Xiang X, et al. Concept of mathematical modeling of lumbar and thoracic spine based on elastic beam theory. *JBSE*. 2022;17(2):21-00331. doi: 10.1299/jbse.21-00331.
12. Sciortino V, Pasta S, Ingrassia T, Cerniglia D. On the Finite Element Modeling of the Lumbar Spine: A Schematic Review. *Appl Sci*. 2023;13(2):958. doi:10.3390/app13020958.
13. Cho PG, Yoon SJ, Shin DA, Chang MC. Finite Element Analysis of Stress Distribution and Range of Motion in Discogenic Back Pain. *Neurospine*. 2024;21(2):536-543. doi: 10.14245/ns.2347216.608.
14. Kolmakova TV, Rikun YuA. Study of deformation behavior of the intervertebral disc with the slope of cervical spine segment. *Bulletin of the Buryat State University: Mathematics, informatics*. 2017;(2):54-60. (In Russ.)
15. Grigoriev AI, Volozhin AI, Stupakov GP. Mineral metabolism in humans under conditions of altered gravity. In: *Problems of space biology*. Moscow: Nauka Publ.; 1994. 994;74:192-212. (In Russ.)
16. Berezovsky VA, Kolotilov NN. *Biophysical characteristics of human tissues: reference book*. Kiev: Nauk. Dumka; 1990:224. (In Russ.)
17. Chumachenko EN, Logashina IV. Calculation of the stress-strain state of the spinal motor segment under loads. *Aerospace and Environmental Medicine*. 2014;48(5):51-57. (In Russ.)
18. Tan SH, Teo EC, Chua HC. Quantitative three-dimensional anatomy of cervical, thoracic and lumbar vertebrae of Chinese Singaporeans. *Eur Spine J*. 2004;13(2):137-146. doi: 10.1007/s00586-003-0586-z.
19. Berry JL, Moran JM, Berg WS, Steffee AD. A morphometric study of human lumbar and selected thoracic vertebrae. *Spine (Phila Pa 1976)*. 1987;12(4):362-367. doi: 10.1097/00007632-198705000-00010.
20. Laouissat F, Sebaaly A, Gehrchen M, Roussouly P. Classification of normal sagittal spine alignment: refounding the Roussouly classification. *Eur Spine J*. 2018;27(8):2002-2011. doi: 10.1007/s00586-017-5111-x.
21. Abelin-Genevois K. Sagittal balance of the spine. *Orthop Traumatol Surg Res*. 2021;107(1S):102769. doi: 10.1016/j.otsr.2020.102769.
22. Galbusera F, Brayda-Bruno M, Costa F, Wilke HJ. Numerical evaluation of the correlation between the normal variation in the sagittal alignment of the lumbar spine and the spinal loads. *J Orthop Res*. 2014;32(4):537-544. doi: 10.1002/jor.22569.

23. Wang W, Pei B, Wu S, et al. Biomechanical responses of human lumbar spine and pelvis according to the Roussouly classification. *PLoS One*. 2022;17(7):e0266954. doi: 10.1371/journal.pone.0266954.
24. Bassani T, Casaroli G, Galbusera F. Dependence of lumbar loads on spinopelvic sagittal alignment: An evaluation based on musculoskeletal modeling. *PLoS One*. 2019;14(3):e0207997. doi: 10.1371/journal.pone.0207997.
25. Remus R, Selkmann S, Lipphaus A, et al. Muscle-driven forward dynamic active hybrid model of the lumbosacral spine: combined FEM and multibody simulation. *Front Bioeng Biotechnol*. 2023;11:1223007. doi: 10.3389/fbioe.2023.1223007.
26. Cosgun Z, Dagistan E, Dagistan Y. Effects of sagittal balance differences on spondylolisthesis. *Acta Ortop Bras*. 2019;27(2):120-123. doi: 10.1590/1413-785220192702205665.
27. Yüksel S, Özmen E, Barış A, et al. Publication Trends in the Pelvic Parameter Related Literature between 1992 and 2022 : A Bibliometric Review. *J Korean Neurosurg Soc*. 2024;67(1):50-59. doi: 10.3340/jkns.2023.0047.
28. Müller A, Rockenfeller R, Damm N, et al. Load Distribution in the Lumbar Spine During Modeled Compression Depends on Lordosis. *Front Bioeng Biotechnol*. 2021;9:661258. doi: 10.3389/fbioe.2021.661258.
29. Naserkhaki S, Jaremko JL, El-Rich M. Effects of inter-individual lumbar spine geometry variation on load-sharing: Geometrically personalized Finite Element study. *J Biomech*. 2016;49(13):2909-2917. doi: 10.1016/j.jbiomech.2016.06.032.
30. Filardi V, Simona P, Cacciola G, et al. Finite element analysis of sagittal balance in different morphotype: Forces and resulting strain in pelvis and spine. *J Orthop*. 2017;14(2):268-275. doi: 10.1016/j.jor.2017.03.007.

The article was submitted 09.01.2025; approved after reviewing 18.02.2025; accepted for publication 31.03.2025.

Information about authors:

Alexey E. Shulga — Candidate of Medical Sciences, Research Fellow,
doc.shulga@yandex.ru, https://orcid.org/0000-0001-8476-0231;

Vladimir Yu. Ulyanov — Doctor of Medical Sciences, Deputy Director, Assistant Professor,
v.u.ulyanov@gmail.com, https://orcid.org/0000-0002-9466-8348;

Yuliya Yu. Rozhkova — Head of Department, rozhkova280586@gmail.com, https://orcid.org/0000-0001-9506-5234;

Stanislav D. Shuvalov — Neurosurgeon, shuvalov.stan@yandex.ru, https://orcid.org/0000-0002-8095-9398.

Original article
https://doi.org/10.18019/1028-4427-2025-31-3-307-313

Analysis of the microbial landscape in patients with periprosthetic infection of the hip joint

A.M. Ermakov, N.A.Bogdanova, E.L. Matveeva✉, A.G. Gasanova

Ilizarov National Medical Research Centre for Traumatology and Orthopedics, Kurgan, Russian Federation

Corresponding author: Elena L. Matveeva, matveevan@mail.ru

Abstract

Introduction The concept of the pathogenesis of periprosthetic joint infection (PJI) is the ability of pathogenic microorganisms to colonize the surfaces of implants, which are infected during the surgery or by hematogenous dissemination of bacteria. It causes poor results of PJI treatment. Microbiological identification of pathogen species is the gold standard in the diagnosis of PJI.

Purpose To assess the etiology of the infectious process in patients with periprosthetic hip joint infection.

Methods The study analyzed revision interventions (n = 294) for PJI of the hip joint performed within the period from 2010 throughout 2021. A total of 147 patients were operated on: 56 % (n = 82) were men and 4 % (n = 65) were women. At the time of hospitalization, the fistula PJI type was diagnosed in 71 % (n = 105); 20 % (n = 29) had edema and hyperemia of the postoperative suture area, and 9 % (n = 13) of cases had open wounds. The object of the study was bone and soft tissue samples obtained during excision of the infected material, as well as removed implant components. Cultures were grown on dense nutrient media. Bacterial cultures were identified by generally accepted methods using TB Expression (BioMerieux, France) and Walk Away 40 (USA) bacteriological analyzers.

Results The etiology of periprosthetic infection was identified in the majority of patients (93 %), while pathogens could not be detected in the remaining cases. Bacteriological analysis revealed microbial associations in 31 % of patients, gram-positive microflora in 52 % of patients, and gram-negative microflora in 10 %.

Discussion The most common types of microorganisms are gram-positive bacteria with a tendency for resistant strains to grow. Gram-negative bacteria are isolated in joint infection, but less frequently. The results demonstrate isolated gram-negative cultures in 10 % of cases. The second most common cause of periprosthetic joint infection is polymicrobial infection, which was detected in 31 % of cases. Microbial associations occurr in 10–45 % of cases; such a clinical situation at the start of treatment complicates the empirical choice of drugs for antibacterial therapy.

Conclusions Microbiological study allowed identification of the etiology of the infectious process in 93 % of patients. In more than half of the cases (52 %), the cause of implant-associated infection is gram-positive microflora, and in 31 % of cases are microbial associations. Reinfection was noted in 41 % of cases in polymicrobial patients.

Keywords: periprosthetic infection, microflora, inflammation, arthroplasty, revision

For citation: Ermakov AM, Bogdanova NA, Matveeva EL, Gasanova AG. Analysis of the microbial landscape in patients with periprosthetic infection of the hip joint. *Genij Ortopedii*. 2025;31(3):307-313. doi: 10.18019/1028-4427-2025-31-3-307-313.

INTRODUCTION

The concept of the pathogenesis of periprosthetic joint infection (PJI) is based on the dynamic equilibrium of the interaction between the implant and the human immune system [1]. Implants are seeded with pathogenic microorganisms either during surgery or by hematogenous dissemination of bacteria [2–6]. Many bacteria form biofilms on metal and polyethylene surfaces of implant components [2, 7–9]. This ability of microorganisms (the so-called cecil forms) ensures their persistence and survival in the hospital environment. In addition, bacteria resistant to antimicrobial drugs are resistant to them in the biofilms. They become the least vulnerable to the action of antibiotics [10, 11]. Long-term healing of postoperative bone wounds is often associated with the penetration of pathogens and the occurrence of microabscesses in bone tissue, and the colonization of osteoblasts [12–14]. At the same time, there are difficult-to-treat types of PJI pathogens, such as staphylococcal strains resistant to antibacterial drugs of three or more classes, fluoroquinolone-resistant and carbapenem-resistant gram-negative microorganisms, and fungal microflora [2, 15, 16]. All of the above factors reveal the cause of poor results in the PJI treatment and emphasize the need to determine the etiology of the pathological process.

Microbiological diagnosis is carried out by isolating and identifying the pathogen after collecting material from several of the most contaminated affected tissues [17]. To destroy the biofilm, the removed implant components are treated with ultrasound; for the same purpose, a dithiothreitol solution can be used [18–21]. The incubation time of biofilm bacteria is 14–21 days, which leads to their higher survival rate, compared to mono infections, for which the incubation period is 5–14 days [22].

Purpose: to assess the etiology of the microbial landscape in patients with periprosthetic hip joint infection

MATERIAL AND METHODS

The study was conducted on the material obtained from 147 patients (56 % men, 44 % women) after revision surgeries for periprosthetic hip joint infection. The age of the patients was (54.7 ± 12.7) years. The number of study samples was 294. Fistulous PJI type was observed in 105 (71 %) patients, hyperemia and edema in the area of the postoperative suture were noted in 29 (20 %), and open wounds were present in 13 (9 %) cases. In 28 patients (19 %), an acute course of the infectious process duration was on average 21.8 days (Me — 22; 95 % CI from 19.7 to 24.0) and in 119 (81 %) chronic infection continued on average 26.3 months (Me — 13; 95 % CI from 20.5 to 32.3).

In 114 (78 %) cases, purulent inflammatory complications developed after primary arthroplasty and only in 33 (22 %) cases after revision. The treatment process was significantly complicated by severe comorbid conditions of patients according to the ASA (American Society of Anesthesiology) scale, diagnosed in 82 (56 %) patients.

The objects of the study were samples of bone and soft tissues obtained during resection of the infected tissues as well as removed implant components of the patients with hip PJI. Based on the recommended methods, seeding was performed on solid nutrient media (bile-salt agar, Sabouraud agar, Levin medium, Columbia agar and nutrient agar with 5 % sheep blood). The samples were placed in a thermostat and incubated at 37 °C for 24–48 hours. The number of colonies in Petri dishes was calculated; the obtained result was converted to a decimal logarithm, expressed in CFU/ml. To create anaerobic conditions, gas generator bags "Anaerogas" were used, growing fungal flora for 5 days at 30 °C.

Bacterial cultures were studied with conventional methods, as well as using bacteriological analyzers TB Expression (BioMerieux, France) and Walk Away 40 (USA).

Statistical data processing was performed using the Statistica for Windows, v. 13.0 (Stat Soft Inc., USA) and Microsoft Excel (Microsoft, USA) software package. Percentage calculations were performed to characterize the microbiological spectrum. Descriptive statistical results were the mean ± standard error (SE) for quantitative data. Data distribution was analyzed using the Shapiro – Wilk and Kolmogorov – Smirnov normality tests. Comparisons between unrelated samples were performed using the Mann – Whitney test. Differences were considered significant at $p < 0.05$.

RESULTS

In the intra-operatively harvested biological material, 196 strains of pathogenic microorganisms were isolated, the spectrum of which is presented in Figure 1. *Staphylococcus aureus* family was dominant in 64 % of cases, a significant part of the isolated strains also included *Enterobacteria ceae* (10 %), *Enterococcus aureus* (9 %) and Pseudomonas *aureus* (9 %).

MRSA and MRSE were detected in 39 cases (20 %), and in 17 (9 %) cases it was *P. aeruginosa* (Fig. 1).

Identification of microorganisms to verify the taxonomic affiliation of pathogenic bacteria showed that among the isolated and identified bacteria, the main part of the microflora was made up by *Staphylococcaceae* and the dominance of strains *Staphylococcus aureus, Staphylococcus epidermidis* and *Staphylococcus saprophyticus*.

Microflora was identified in 137 patients (93 %), but in 10 patients, pathogens could not be identified. In 76 patients (52 %), isolates of gram-positive microflora were detected, in 15 patients (10 %) it was gram-negative microflora in monoculture. In 46 patients (31 %), the presence of microbial associations was revealed (Fig. 2).

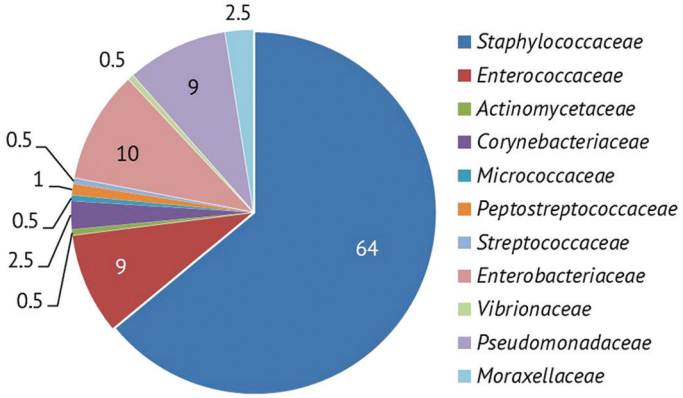

Fig. 1 Spectrum of pathogens causing hip PJI

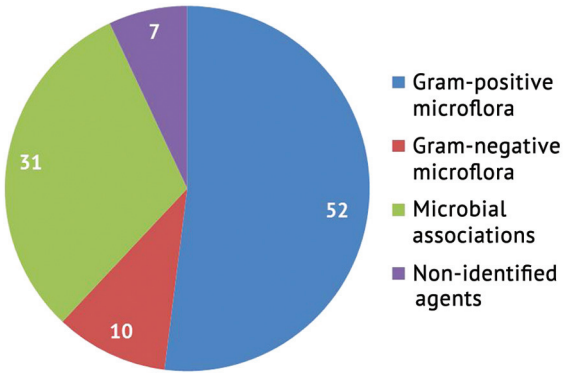

Fig. 2 Identified microflora

It should be noted that in 22 % of cases, or in 17 of 76 patients with isolated gram-positive microflora (dominant strain of *Staphylococcus aureus*, as well as *epidermal Staphylococcus*), recurrence of infection occurred. Repeated suppuration in 15 patients with gram-negative microflora (represented mainly by the strains of *Pseudomonas aeruginosa*) was noted only in two cases (13 %). The most frequently isolated families in the polymicrobial infection were *Staphylococcaceae* (78 %), *Enterobacteriaceae* (28 %), *Enterococcaceae* (26 %), *Pseudomonadaceae* (15 %) and *Moraxellaceae* (6.5 %).

Apparently due to previous therapy with antibacterial drugs, polymicrobial associations are quite common in patients with PJI and occupy the second place after gram-positive microflora. Microbial association of two agents was detected in 34 patients (74 %), of three agents in 11 (24 %). The growth of four microorganisms was revealed in one patient.

The total number of patients with recurrent infection in the presence of microbial associations was 19 (41 %) which was the highest number of complications. In order to stop the inflammatory process, six patients with recurrent infection underwent repeated surgical debridement; eight patients underwent spacer change, and the rest underwent resection arthroplasty.

With an unidentified composition of microflora, two out of 10 patients experienced repeated suppuration during their hospital stay. These patients underwent a two-stage revision intervention.

A comparative assessment of the results of an intraoperative study of the microbiological spectrum of pathogens in patients with acute and chronic forms of implant-associated infection is presented in Fig. 3.

In the structure of surgical interventions for PJI, the manifestation of infection was 22 days (ICI-17 — 27.5 days) in 28 (19 %) patients, and in 119 patients the duration of the purulent process averaged 26 months (8–35 months).

In the structure of the microbial landscape of patients with acute and chronic infection, the contribution of isolated gram-positive (44 % and 55 %) and gram-negative (7 % and 10 %) microflora was comparable (Fig. 3). However, it was noted that microbial associations and MRSE strains were significantly ($p < 0.05$) more common in patients with acute infection. Methicillin-resistant strains of epidermal staphylococcus were the cause of acute infectious process in almost every third case (29 %). In general, re-infection occurred in 7 (25 %) patients with acute and in 39 (33 %) patients with chronic PJI.

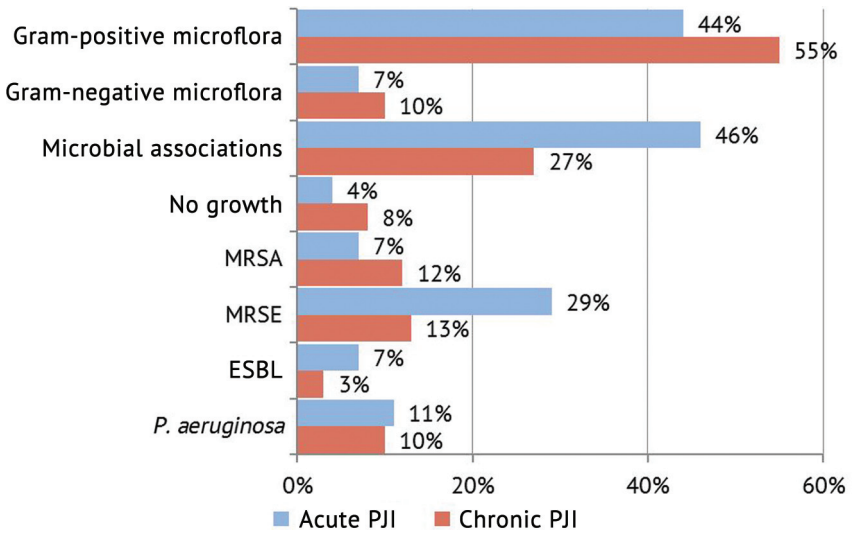

Fig. 3 Microbiological characteristics of the inoculation material of patients with acute and chronic hip joint PJI

DISCUSSION

Assessing the microbial landscape of patients with implant-associated infection, it should be noted that microbial cells, especially in biofilm conditions, acquire increasingly pronounced resistance to antimicrobial drugs. This, in turn, requires new approaches to risk assessment and treatment of the infectious process that developed after hip arthroplasty. The risk of PJI remains during the entire period of presence of an orthopedic implant in the body. The main pathogens are gram-positive bacteria (most often *Staphylococcus aureus* and *Staphylococcus epidermidis*), characterized by the growth of resistant strains [23–26]. The lack of targets for the manifestation of the action of antimicrobial therapy in many gram-positive microorganisms leads to the lack of control over resistant strains, causing legitimate concern among treating physicians, which is reflected in both domestic and foreign publications [27–30].

The second most significant etiologic cause of implant suppuration is polymicrobial infection. The incidence of polymicrobial infection tends to increase; we observed it in 31 % of cases. Polymicrobial infection in our patients is represented by a predictable spectrum: *Staphylococcaceae* — 78 %, *Enterobacteriaceae* — 28 %, *Enterococcaceae* — 26 %, *Pseudomonadaceae* — 15 %, and *Moraxellaceae* — 6.5 %. Such a clinical situation complicates the choice of an adequate antibiotic therapy and often leads to poorer outcomes compared to PJI due to monomicrobial microflora, what has also been stressed in the literature [31, 32]. A number of researchers point out the need to consider the expression of pathogenicity of microorganisms, as well as their ability to form biofilms [33–37]. In this regard, the identification of the spectrum of PJI pathogens is of great importance.

Fungal microflora was not detected in the patients in our study, but foreign literatures reports fungal infections, which occur in 1–4 % of cases. The overwhelming majority (80 %) are *Candida* fungi [38, 39]. This problem is typical for immunocompromised patients [40, 41].

The microbiological study of periprosthetic tissues revealed the etiology of the infection in the overwhelming majority (93 %) of the cases studied. The most common reason for non-identification of the pathogen was obviously the use of antibacterial drugs before the pathogen was detected.

CONCLUSION

The dominant cause of PJI development is gram-positive microflora and microbial associations. Reliable differences in patients with acute and chronic PJI were noted in the level of microbial associations and the presence of MRSE strains with a trend toward dominance in the group with an acute nature of infection.

Conflict of interests *Authors declare no conflicts of interests.*

Funding source *The work was carried out on the base and with the support of the Federal State Budgetary Institution Ilizarov National Medical Research Center of Traumatology and Orthopaedics of the Ministry of Health of the Russian Federation. The authors did not receive financial support from drug manufacturing companies.*

Ethical approval *The study was approved by the Ethics Board of the Federal State Budgetary Institution Ilizarov National Medical Research Center of Traumatology and Orthopedics of the Ministry of Health of the Russian Federation (protocol dated 04/28/2022 No. 1(71)).*

Informed consent *Not applicable.*

REFERENCES

1. Zimmerli W. Infection and musculoskeletal conditions: Prosthetic-joint-associated infections. *Best Pract Res Clin Rheumatol*. 2006;20(6):1045-1063. doi: 10.1016/j.berh.2006.08.003.
2. Sheraliev TU, Fedorov EA, Golnik VN, Pavlov VV. *Periprosthetic infection in hip replacement: features of modern etiology, problems and prospects of diagnosis: monograph*. Krasnoyarsk: Scientific and Innovation Center; 2021:230. (In Russ.) doi: 10.12731/978-5-907208-50-6.
3. Bertani A, Drouin C, Demortière E, et al. A prosthetic joint infection caused by Streptococcus pneumoniae: a case report and review of the literature. *Rev Chir Orthop Reparatrice Appar Mot*. 2006 Oct;92(6):610-614. (In French) doi: 10.1016/s0035-1040(06)75921-9.
4. Zeller V, Lavigne M, Leclerc P, et al. Group B streptococcal prosthetic joint infections: a retrospective study of 30 cases. *Presse Med*. 2009;38(11):1577-1484. doi: 10.1016/j.lpm.2009.02.026.
5. Winkler T, Trampuz A, Renz N, et al. Classification and algorithm for diagnosis and treatment of hip prosthetic joint infection. *Traumatology and Orthopedics of Russia*. 2016;22(1):33-45. (In Russ.) doi: 10.21823/2311-2905-2016-0-1-33-45.
6. Renaud A, Lavigne M, Vendittoli PA. Periprosthetic joint infections at a teaching hospital in 1990-2007. *Can J Surg*. 2012;55(6):394-400. doi: 10.1503/cjs.033610.
7. Afinogenova AG. Darovskaya EN. Microbial biofilms of wounds: status of the issue. *Traumatology and Orthopedics of Russia*. 2011;17(3):119-125. (In Russ.) doi: 10.21823/2311-2905-2011-0-3-119-125.
8. Bozhkova SA. Modern principles of diagnostics and antibacterial therapy of prosthetic joint infection (review). *Traumatology and orthopedics of Russia*. 2011;17(3):126-136. (In Russ.) doi: 10.21823/2311-2905-2011-0-3-126-136.
9. Gristina AG, Naylor P, Myrvik Q. Infections from biomaterials and implants: a race for the surface. *Med Prog Technol*. 1988-1989;14(3-4):205-224.

10. Gonzalez Moreno M, Trampuz A, Di Luca M. Synergistic antibiotic activity against planktonic and biofilm-embedded Streptococcus agalactiae, Streptococcus pyogenes and Streptococcus oralis. *J Antimicrob Chemother*. 2017;72(11):3085-3092. doi: 10.1093/jac/dkx265.
11. Molina-Manso D, del Prado G, Ortiz-Pérez A, et al. In vitro susceptibility to antibiotics of staphylococci in biofilms isolated from orthopaedic infections. *Int J Antimicrob Agents*. 2013;41(6):521-523. doi: 10.1016/j.ijantimicag.2013.02.018.
12. Masters EA, Trombetta RP, de Mesy Bentley KL, et al. Evolving concepts in bone infection: redefining "biofilm", "acute vs. chronic osteomyelitis", "the immune proteome" and "local antibiotic therapy". *Bone Res*. 2019;7:20. doi: 10.1038/s41413-019-0061-z.
13. Garzoni C, Kelley WL. Return of the Trojan horse: intracellular phenotype switching and immune evasion by Staphylococcus aureus. *EMBO Mol Med*. 2011;3(3):115-7. doi: 10.1002/emmm.201100123.
14. Nelson CL, McLaren AC, McLaren SG, et al. Is aseptic loosening truly aseptic? *Clin Orthop Relat Res*. 2005;(437):25-30. doi: 10.1097/01.blo.0000175715.68624.3d.
15. Tikhilov RM, Bozhkova SA, Artyukh VA. Periprosthetic infection in the area of large joints of the extremities. Clinical guidelines. In: Mironov SP. (ed.) *Orthopedics: clinical guidelines*. Moscow: GEOTAR-Media; 2018:719-746. (In Russ.)
16. Livensev VN, Bozhkova AYu, Kochish VN et al. Difficult-To-Treat Periprosthetic Hip Infection: Outcomes of Debridment. *Traumatology and orthopedics of Russia*. 2019;25(4):88-97. doi: 10.21823/2311-2905-2019-25-4-88-97.
17. Gelalis ID, Arnaoutoglou CM, Politis AN, et al. Bacterial wound contamination during simple and complex spinal procedures. A prospective clinical study. *Spine J*. 2011;11(11):1042-1048. doi: 10.1016/j.spinee.2011.10.015.
18. Corvec S, Portillo ME, Pasticci BM, et al. Epidemiology and new developments in the diagnosis of prosthetic joint infection. *Int J Artif Organs*. 2012;35(10):923-934. doi: 10.5301/ijao.5000168.
19. Schmolders J, Hischebeth GT, Friedrich MJ, et al. Evidence of MRSE on a gentamicin and vancomycin impregnated polymethyl-methacrylate (PMMA) bone cement spacer after two-stage exchange arthroplasty due to periprosthetic joint infection of the knee. *BMC Infect Dis*. 2014;14:144. doi: 10.1186/1471-2334-14-144.
20. Holinka J, Bauer L, Hirschl AM, et al. Sonication cultures of explanted components as an add-on test to routinely conducted microbiological diagnostics improve pathogen detection. *J Orthop Res*. 2011;29(4):617-522. doi: 10.1002/jor.21286.
21. Dudareva M, Barrett L, Figtree M, et al. Sonication versus Tissue Sampling for Diagnosis of Prosthetic Joint and Other Orthopedic Device-Related Infections. *J Clin Microbiol*. 2018;56(12):e00688-18. doi: 10.1128/JCM.00688-18.
22. Ji B, Xu E, Cao L, et al. The method and result analyses of pathogenic bacteria culture on chronic periprosthetic joint infection after total knee arthroplasty and total hip arthroplasty. *Zhonghua Wai Ke Za Zhi*. 2015;53(2):130-134. (In Chin).
23. Bozhkova SA, Kasimova AR, Tikhilov RM, et al.Adverse trends in the etiology of orthopedic infection: results of 6-year monitoring of the structure and resistance of leading pathogens. *Traumatology and orthopedics of Russia*. 2018;24(4):20-31. doi: 10.21823/2311-2905-2018-24-4-20-31.
24. Bozhkova SA, Krasnova MV, Polyakova EM, et al. Biofilm Formation by Clinical Isolates of S. aureus and S. epidermidis in Prosthetic Joint Infection. *Clinical microbiology, antimicrobial chemotherapy*. 2014;16(2):149–156. (In Russ.)
25. Font-Vizcarra L, Tornero E, Bori G, et al. Relationship between intraoperative cultures during hip arthroplasty, obesity, and the risk of early prosthetic joint infection: a prospective study of 428 patients. *Int J Artif Organs*. 2011;34(9):870-875. doi: 10.5301/ijao.5000026.
26. Crowe B, Payne A, Evangelista PJ, et al. Risk Factors for Infection Following Total Knee Arthroplasty: A Series of 3836 Cases from One Institution. *J Arthroplasty*. 2015;30(12):2275-2278. doi: 10.1016/j.arth.2015.06.058.
27. Salgado CD, Dash S, Cantey JR, Marculescu CE. Higher risk of failure of methicillin-resistant Staphylococcus aureus prosthetic joint infections. *Clin Orthop Relat Res*. 2007;461:48-53. doi: 10.1097/BLO.0b013e3181123d4e.
28. Spiegl U, Pätzold R, Friederichs J, et al. Risk factors for failed cleansing following periprosthetic delayed hip prosthesis infection. *Orthopade*. 2012 Jun;41(6):459-466. (In German) doi: 10.1007/s00132-012-1936-5.
29. Kurd MF, Ghanem E, Steinbrecher J, Parvizi J. Two-stage exchange knee arthroplasty: does resistance of the infecting organism influence the outcome? *Clin Orthop Relat Res*. 2010;468(8):2060-2066. doi: 10.1007/s11999-010-1296-6.
30. Dieckmann R, Schulz D, Gosheger G, et al. Two-stage hip revision arthroplasty with a hexagonal modular cementless stem in cases of periprosthetic infection. *BMC Musculoskelet Disord*. 2014;15:398. doi: 10.1186/1471-2474-15-398.
31. Marculescu CE, Cantey JR. Polymicrobial prosthetic joint infections: risk factors and outcome. *Clin Orthop Relat Res*. 2008;466(6):1397-1404. doi: 10.1007/s11999-008-0230-7.
32. Tsaras G, Maduka-Ezeh A, Inwards CY, et al. Utility of intraoperative frozen section histopathology in the diagnosis of periprosthetic joint infection: a systematic review and meta-analysis. *J Bone Joint Surg Am*. 2012;94(18):1700-1711. doi: 10.2106/JBJS.J.00756.
33. Garrido-Gómez J, Arrabal-Polo MA, Girón-Prieto MS, et al. Descriptive analysis of the economic costs of periprosthetic joint infection of the knee for the public health system of Andalusia. *J Arthroplasty*. 2013;28(7):1057-1060. doi: 10.1016/j.arth.2013.02.012.
34. Padegimas EM, Maltenfort M, Ramsey ML, et al. Periprosthetic shoulder infection in the United States: incidence and economic burden. *J Shoulder Elbow Surg*. 2015;24(5):741-746. doi: 10.1016/j.jse.2014.11.044.
35. Schwarz EM, Parvizi J, Gehrke T, et al. 2018 International Consensus Meeting on Musculoskeletal Infection: Research Priorities from the General Assembly Questions. *J Orthop Res*. 2019;37(5):997-1006. doi: 10.1002/jor.24293.
36. Niska JA, Meganck JA, Pribaz JR, et al. Monitoring bacterial burden, inflammation and bone damage longitudinally using optical and μCT imaging in an orthopaedic implant infection in mice. *PLoS One*. 2012;7(10):e47397. doi: 10.1371/journal.pone.0047397.

37. Shipicina IV,Osipova EV. Analysis of the qualitative and quantitative community composition of bacteria isolated from the purulent focus in patients with chronic osteomyelitis over a three year period. *Genij Ortopedii*. 2022;28(6):788-793. doi: 10.18019/1028-4427-2022-28-6-788-793.
38. Bori G, McNally MA, Athanasou N. Histopathology in Periprosthetic Joint Infection: When Will the Morphomolecular Diagnosis Be a Reality? *Biomed Res Int*. 2018;2018:1412701. doi: 10.1155/2018/1412701.
39. Wiwattanawarang N. Fungal periprosthetic joint infection after total knee arthroplasty. *J Med Assoc Thai*. 2014 Dec;97(12):1358-1363.
40. Jakobs O, Schoof B, Klatte TO, et al. Fungal periprosthetic joint infection in total knee arthroplasty: a systematic review. *Orthop Rev (Pavia)*. 2015;7(1):5623. doi: 10.4081/or.2015.5623.
41. Sudnicin AS, Klushin NM, Migalkin NS, et ai. Diagnosis of chronic osteomyelitis complicated with mycotic infection. *Genij Ortopedii*. 2019;25(4):528-534. doi: 10.18019/1028-4427-2019-25-4-528-534.

The article was submitted 18.12.2024; approved after reviewing 28.02.2025; accepted for publication 31.03.2025.

Information about the authors:

Artem M. Ermakov — Doctor of Medical Sciences, Head of the Clinic, Researcher,
ema_cab@mail.ru, https://orcid.org/0000-0002-5420-4637, SPIN-code: 9292-8469;

Natalia A. Bogdanova — Head of the Laboratory, mikrona@mail.ru;

Elena L. Matveeva — Doctor of Biological Sciences, Leading Researcher,
matveevan@mail.ru, https://orcid.org/0000-0002-7444-2077, SPIN-code: 8195-5618;

Anna G. Gasanova — Senior Researcher,
gasanova.08@mail.ru, https://orcid.org/0000-0001-7734-2808, SPIN-code: 4629-2875.

Original article
https://doi.org/10.18019/1028-4427-2025-31-3-314-321

Genotype-phenotypic association of heterozygous deletion of the *TBX-6* gene in patients with congenital scoliosis

S.E. Khalchitsky, S.V. Vissarionov, P.A. Pershina✉, K.G. Buslov, Yu.A. Novosad, M.V. Sogoyan, M.S. Asadulaev, M.V. Gretsyk

Turner National Medical Research Center for Children's Traumatology and Orthopedics,
St. Petersburg, Russian Federation

Corresponding author: Polina A. Pershina, polinaiva2772@gmail.com

Abstract

Introduction Congenital scoliosis is a multifactorial disease caused by abnormalities in vertebral development during embryogenesis. The *TBX6* gene, located at locus 16p11.2, plays a key role in somitogenesis, and the heterozygous deletion is associated with the development of specific phenotypes of congenital scoliosis (*TBX6*-associated congenital scoliosis, TACS). Despite numerous studies on the role of *TBX6* in the pathogenesis of congenital scoliosis, there is a paucity of data on the phenotypic manifestations of heterozygous 16p11.2 deletion.

The **objective** was to identify and confirm the TACS phenotype being associated with 16p11.2 deletions in the Russian patients.

Material and methods A single-center retrospective cohort study included 187 patients diagnosed with congenital scoliosis treated at the Turner National Medical Research Center for Pediatric Orthopedics and Traumatology between 2012 and 2021. Heterozygous deletion (16p11.2 region) were verified using MQRT-PCR. The deletion group consisted of 42 patients, and the control group included 145 probands. Clinical and radiological findings were reviewed to identify localization, type and multiplicity of vertebral anomalies and associated malformations. Descriptive statistics and Pearson's correlation coefficient were used for data processing.

Results Heterozygous deletion of *TBX6* was detected in 22.4 % of patients. The thoracic and lumbar spine were common localizations, while involvement of the cervical spine was not identified in the deletion group. Vertebral malformations were the most common anomaly in both study groups, but their prevalence was higher among patients with *TBX6* deletion (50 % vs. 43.4 %). Multiple spinal malformations were more common in the deletion group (50 % vs. 35 %). Associated internal organ defects were less common in patients with deletion (31 % vs. 43.4 %), while rib synostoses and Sprengel's disease were more common.

Discussion TACS is characterized by specific manifestations including multiple vertebral malformations in the thoracic and lumbar spine, rib synostoses and Sprengel's disease, which is consistent with the scientific literature.

Conclusion The findings indicate the need to include genetic testing for *TBX6* deletion in the diagnostic algorithm for congenital scoliosis to facilitate early detection and a personalized approach to treatment of this cohort of patients.

Keywords: congenital scoliosis, TACS, genetics, congenital spinal deformities, children

For citation: Khalchitsky SE, Vissarionov SV, Pershina PA, Buslov KG, Novosad YuA, Sogoyan MV, Asadulaev MS, Gretsyk MV. Genotype-phenotypic association of heterozygous deletion of the *TBX6* gene in patients with congenital scoliosis. *Genij Ortopedii*. 2025;31(3):314-321. doi: 10.18019/1028-4427-2025-31-3-314-321.

INTRODUCTION

Congenital spinal deformities including congenital scoliosis (CS) are a challenge in pediatric orthopedics and are caused by abnormalities in vertebral development during embryogenesis [1]. Teratogenic factors and associated mutational damage to the genome, affecting the formation of the fetus in the first 6–8 weeks of embryogenesis, are considered to be critically significant causes leading to spinal malformations [2]. The incidence of CS, according to epidemiological studies, is 0.5–1 case per 1,000 newborns [3].

Developmental anomalies of the vertebrae, such as hemivertebrae, butterfly vertebrae and segmentation defects, can be the cause of progressive scoliosis and/or kyphosis leading to impaired cardiovascular and respiratory function and neurological deficit [4, 5]. Despite the advances in the diagnosis of the condition in young children, progressive congenital curvatures of the spine require high-tech and timely surgical treatment before the age of three in a significant cohort of patients [6].

Recent advances in molecular genetics allowed for identification of the genes responsible for congenital spinal deformities and congenital scoliosis [7, 8, 9]. The *TBX6* gene is one of the key factors determining the development of the spinal column; it is involved in somitogenesis, regulating the formation of the paraxial mesoderm that gives rise to vertebrae and ribs [10, 11]. Approximately 7.9–10.6 % of cases of congenital scoliosis are associated with *TBX6* mutations and can develop sporadically, with familial cases described in 1–3.4 % of patients [12]. Studies on experimental animal models have confirmed that hypomorphic alleles and deletions of *TBX6* lead to the formation of butterfly vertebrae and hemivertebrae [13]. The target is a heterozygous deletion at the site of chromosome 16p11.2 affecting the region of the short arm (p) of chromosome 16 where *TBX6* gene is located. Deletion is a type of genetic mutation with a particular region of DNA lost [14]. The loss results in changes in the structure of the gene or genes leading to the impaired functions. Homozygous deletion of 16p11.2 is embryonic lethal [15]. In the case of the *TBX6* gene, heterozygous deletion and other genotypes can characterize *TBX6*-associated congenital scoliosis (TACS), described by Liu et al. in 52 Chinese patients [16]. TACS is characterized by specific phenotypes and clinical manifestations including hemivertebrae and butterfly vertebrae, predominantly in the lower thoracic and lumbar spine [16].

Analysis of patient cohorts in China, Japan and the United States has shown that *TBX6* mutations are often associated with simple spinal malformations and are rarely associated with severe segmentation defects or intraspinal abnormalities [17]. The clinical role of the studies includes the development of predictive models, such as TACScore that help identify patients at high risk of having TACS [18]. However, heterozygous *TBX6* deletion and TACS phenotype have not been examined in Russian and European populations.

The **objective** was to identify and confirm the TACS phenotype being associated with 16p11.2 deletions in the Russian patients. Analysis of the findings allows us to identify characteristic phenotypes and determine the frequency of occurrence in the group of patients, and to assess the possible correlation with concomitant anomalies in the development of organs and systems.

MATERIAL AND METHODS

The design was a monocentric cohort retrospective study. The results of molecular genetic and clinical examination of 187 patients treated between 2012 and 2021 at the Turner National Medical Research Center for Pediatric Traumatology and Orthopedics were reviewed.

Inclusion criteria included verified diagnosis of congenital scoliosis based on a comprehensive clinical and radiological examination, absence of a positive genetic history, voluntary informed consent of patients or their legal representatives to participate in the study.

Exclusion criteria included patients whose diagnosis of congenital scoliosis was not confirmed during the examination; verified genetic syndromes in patients and/or their relatives, as well as refusal of the patient or legal representative to participate in the study. The study was performed in two stages. The first stage included molecular genetic testing for genomic DNA isolated from probands' peripheral blood leukocytes and aimed at finding deletions in the region of chromosome 16p11.2. Genomic DNA was isolated using a commercial reagent kit (Synthol, Moscow). A multiplex quantitative real-time polymerase chain reaction (PCR) method (MQRT-PCR) with fluorescently labeled TaqMan hybridization probes was used to detect heterozygous deletion of the TBX-6 gene. PCR was performed in 25 µl mixture containing 1×PCR buffer, 0.5 units of Taq DNA polymerase activity SynTaq (Syntol, Moscow), 3.5 mmol/l MgCl2, 200 µmol/l of each dNTP, 5 % dimethyl sulfoxide, 0.5 % formamide. The reaction mixture also contained 500 nmol/l of each oligonucleotide primer and 200 nmol/l of each fluorescently labeled PCR probe (Eurogen, Moscow). Testing was performed using the Bio-Rad CFX96 system (Bio-Rad, USA).

Clinical data of the selected patients were reviewed to determine the phenotypic manifestations of the disease at the second stage of the study. The probands were divided into two groups depending on the presence of heterozygous deletion. The group with the genotype of heterozygous deletion 16p11.2 consisted of 42 patients and 145 probands constituted the normal group. The analysis included data from medical records, radiography, multispiral computed tomography (MSCT) and magnetic resonance imaging (MRI) findings.

Descriptive statistics methods were used to evaluate the results. The Pearson's contingency coefficient was used to evaluate the significance of correlation.

RESULTS

Multiplex quantitative real-time PCR (MQRT-PCR) performed on 187 genomic DNA samples showed heterozygous deletion of 16p11.2 of the *TBX6* gene (*TBX6*/null genotype) verified in 42 probands. Clinical and instrumentation findings in the groups with heterozygous deletion (n = 42) and without it (norms) (n = 145) were analyzed at the second stage of the study through panoramic radiography of the spine in the supine position, MSCT to verify the localization and type of vertebral anomaly, MRI to rule out intracranial pathology. The average age of patients at the time of examination was (6.00 ± 2.73) years. There were 79 (42 %) male and 108 (57 %) female patients.

Localization of anomalies

The lumbar and thoracic spine were commonly involved segments in both groups among other localizations of spinal anomalies. With the majority of cases suffering from multiple spinal lesions, vertebral malformations the data are presented in absolute numbers. Patients of the normal group (Fig. 1 a) showed 394 maldeveloped vertebrae including 33 (8.5 %) localized in the cervical spine, 288 (73 %) in the thoracic spine and 73 (18.5 %) demonstrated lumbar involvement. The heterozygous deletion group (Fig. 1 b) demonstrated 104 abnormal vertebrae registered with 2 (1.9 %) localized in the cervical spine, 78 (75 %) in the thoracic spine and 24 (23 %) were lumbar involvement. The Pearson's contingency coefficient was used to evaluate the relationship between localization and heterozygous deletion. A positive value obtained (0.09) characterized the tightness of the stochastic relationship of random variables, which confirmed the correlation between the presence of a deletion and the localization of developmental anomalies.

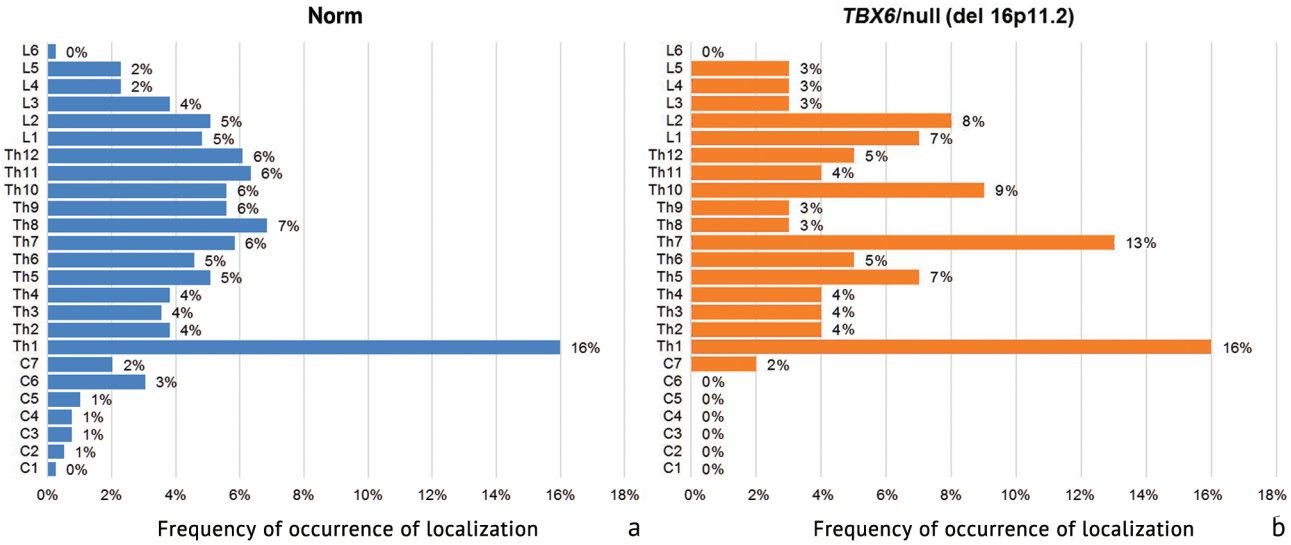

Fig. 1 Distribution of localizations of spinal developmental anomalies: (a) patients in the group without verified deletion (norm); (b) patients in the deletion group (*TBX6*/null)

Typological analysis

Developmental defects are divided into types (grades) in accordance with the generally accepted MacEwan classification that is expanded and supplemented to include defects of vertebral formation (hemivertebrae), impaired vertebral fusion (butterfly vertebrae), vertebral segmentation defects (non-segmented column) and their combinations. Single isolated hemivertebrae were commonly detected in the patients including 63 (43.4 %) in the group without verified deletion and 21 cases (50 %) in the deletion group (Fig. 2). The differences were found in the cohorts of patients with segmentation disorders (isolated non-segmented rods and combinations of non-segmented rods with hemivertebrae and butterfly vertebrae) with a total of 30.9 % in the normal group versus 21.4 % in the group with deletion.

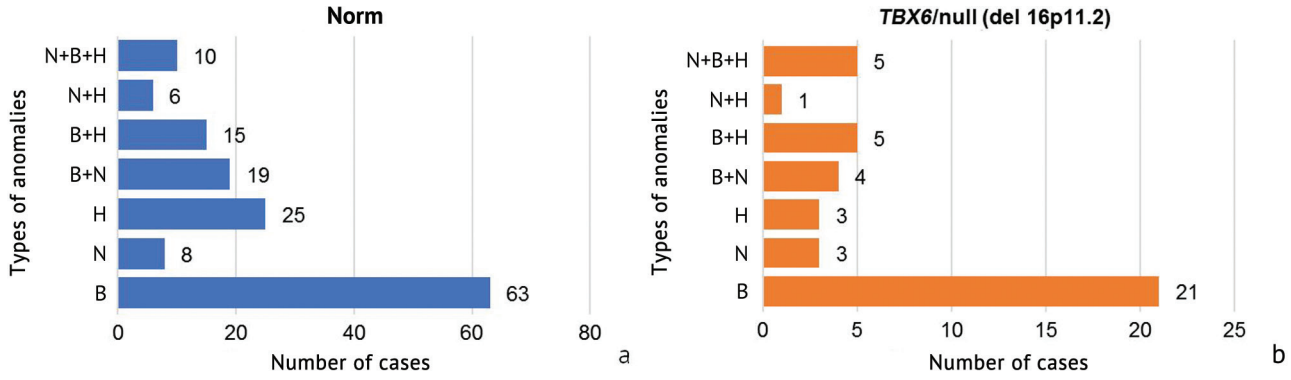

Fig. 2 Distribution of spinal malformations: (a) group without verified deletion (norm); (b) group of heterozygous deletion (*TBX6*/null). B — butterfly vertebra; N — non-segmented rod; H — hemivertebra and their combinations

Multiple spinal malformations were recorded in 51 patients (35 %) of the normal group and in 21 cases (50 %) in the heterozygous deletion group. Considering the proportion of multiple spinal involvement, it can be concluded that this type of developmental anomalies is more common in patients with heterozygous deletion. The Pearson coefficient was greater than the expected value (0.109 > 0.090) suggesting that there was a relationship between the presence of a deletion and the localization of the defect at a significance level of $p = 0.05$.

Associated developmental defects

Pre-admission tests and somatic examination of each patient revealed concomitant congenital spinal deformities, malformations of other organs and systems identified as (Table 1) minor cardiac anomalies, gastrointestinal malformations and urinary anomalies. Orthopedic conditions diagnosed included Sprengel's disease, diastematomyelia, Spina Bifida, tethered spinal cord syndrome, VATER and VACTERL associations, rib synostoses and other malformations (isolated cases of isolated tarsal coalitions, caudal regression syndrome, brachydactyly, aplasia of the fingers, polydactyly, Churg-Strauss syndrome, pituitary dwarfism, high myopia, lipomyeliomeningocele).

Table 1

Specification of associated developmental anomalies in patients

Developmental anomalies	Group			
	Norm		Heterozygous deletion	
	абс.	%	абс.	%
Minor cardiac anomalies (OOO, LVH, autonomic rhythm disturbances)	7	4.8	0	0
Gastrointestinal malformations (anal atresia, esophageal atresia)	5	3.4	0	0
Malformations of the urinary tract (aplasia, duplication, hypoplasia, renal dystopia)	6	4.1	0	0
Sprengel's disease	4	2.8	2	4.7
Diastematomyelia	7	4.8	0	
Spina Bifida	7	4.8	1	0.1
Tethered Cord Syndrome	1	0.6	0	
Synostosis of the ribs	15	10.3	7	16.6
VATER/VACTERL associations	5	3.4	1	2.3
Others	7	4.8	2	4.8
Total number of patients	64	43.8	13	28.5

DISCUSSION

Heterozygous deletion of the *TBX6* gene was detected at locus 16p11.2 in 22.4 % of patients with verified diagnosis of congenital scoliosis. This figure is greater than that reported in the world literature with the frequency of *TBX6*-associated mutations ranging from 7.9 % to 10.6 % in the Chinese, Japanese and North American populations [17]. Chromosomal local deletions and duplications including the 16p11.2 as the cause of congenital scoliosis phenotype was reported by Al-Kateb et al. [19]. Wu et al. [17] suggested that the impact and frequency of *TBX6* mutations determining development of congenital scoliosis vary depending on the population, indicating possible interaction with other genetic and environmental factors. In our opinion, the higher mutation frequency in the Russian cohort can be caused by regional characteristics of the population. Given the data obtained, a more extensive genetic profile of patients in the deletion group is of interest.

Analysis of the localization of spinal malformations revealed predominant lesions of the thoracic and lumbar spine in patients with and without *TBX6* deletion. However, the group with heterozygous deletion showed no anomalies in the cervical spine and anomalies in this localization was 8.4 % in the normal group. This is consistent with the findings reported by Liu et al. with involved lower thoracic and lumbar spine observed with the TACS phenotype [16]. This localization pattern may be related to the function of the *TBX6* gene in somitogenesis, which is critical for the formation of paraxial mesoderm at the spinal levels [20]. Heterozygous deletion of *TBX6* results in decreased

gene expression and impaired segmentation and vertebral formation [21]. White et al. reported a decrease in *TBX6* levels in mice leading to defects in somite formation and correlating with those observed in patients with spinal anomalies [22].

Typological analysis revealed that hemivertebrae were the most common type of skeletal anomalies in patients with *TBX6* deletion (50 %) and without it (43.4 %). The fact is consistent with the findings reported by Liu et al. emphasizing the importance of this morphological feature for determining the treatment strategy of congenital scoliosis and further dynamic observation [23]. Isolated segmentation disorders were not common in the group with a heterozygous deletion (7.2 % versus 17.2 % in the normal group) reflecting the specificity of *TBX6*-associated anomalies reported by Yang et al. The authors suggested that heterozygous *TBX6* mutations led to a decrease in gene expression rather than to the critical level required for the occurrence of complex segmentation defects [24].

Multiple spinal anomalies were detected in 50 % of patients with *TBX6* deletion that was much greater than the similar indicator in the normal group (35 %). This is consistent with the findings reported by Liu et al. [23], Wu et al. [25] and Feng et al. [26] who found multiple spinal defects being more common in patients with *TBX6* mutations. The mechanism emphasizes the more complex nature of the lesions in the cohort of patients and plays a clinical role in predicting the course of the disease and planning surgical treatment [27].

Associated malformations of visceras including cardiovascular, urinary and digestive anomalies were less common in patients with *TBX6* deletion compared to the normal group. These factors partially contradict the data reported by Liu et al. [16] on the high frequency of combined systemic anomalies indicating regional or methodological differences. In addition to that, the findings do not rule out the presence of other mutational injury to the genome in the normal group including microdeletions or polymorphisms of other genes. Powel et al. reported more common cardiac malformations detected in patients with *TBX6* mutations in a systematic review. [28] However, orthopedic anomalies including rib synostoses (16.6 %) and Sprengel's disease (4.7 %) are more characteristic of TACS, and Otomo et al. reported the more frequent cases of synostoses and rib hypoplasia or aplasia in patients with *TBX6* deletions [29]. Panigrahi et al. [30] reported a series of clinical observations of patients with congenital scoliosis and Sprengel's disease and suggested a positive correlation between *TBX6* mutations and the pathological position of the scapula. Yang et al. reported the occurrence of complex forms of congenital scoliosis being associated with developmental abnormalities of other organs and systems and complex oligogenic influence [31].

The study we present has a number of limitations. The patient sample is limited to one clinic reducing the possibility of extrapolating the results to a larger patient sample. The lack of whole-genome sequencing places restriction on the search of etiopathogenetic justifications for other concomitant developmental anomalies in the study groups. A greater cohort of patients is scheduled to be recruited for further investigations to explore regional and ethnic characteristics of patients with TACS. Another study is planned to assess the effect of heterozygous *TBX6* mutations on the occurrence of the dysplastic nature of the course of congenital scoliosis. This will help clarify the mechanisms of pathogenesis and improve approaches to early diagnosis of the pathological condition and treatment of patients with this pathology.

CONCLUSION

The findings obtained suggest that *TBX6*-associated scoliosis is characterized by vertebral malformations localized mainly in the thoracic and lumbar spine, with a predominance of hemivertebrae. The high frequency of rib synostoses and multiple anomalies requires further study to clarify the prognostic value of the manifestations.

Conflict of interest *None.*

Funding *The authors received no financial support for the research and/or authorship of this article.*

Ethical review *The study was approved by the Ethics Committee of the Turner National Medical Research Center of Pediatric Traumatology and Orthopedics of the Ministry of Health of the Russian Federation (Protocol No. 24-9 dated October 22, 2024).*

Informed consent *Written voluntary informed consent was obtained from patients and their legal representatives to participate in the scientific study and process personal data.*

REFERENCES

1. Tikoo A, Kothari MK, Shah K, Nene A. Current Concepts - Congenital Scoliosis. *Open Orthop J*. 2017;11:337-345. doi: 10.2174/1874325001711010337.
2. Mackel CE, Jada A, Samdani AF, et al. A comprehensive review of the diagnosis and management of congenital scoliosis. *Childs Nerv Syst*. 2018;34(11):2155-2171. doi: 10.1007/s00381-018-3915-6.
3. Ulrikh EV, Mushkin AYu, Gubin AV. Congenital spine deformities in children: epidemiological prognosis and management. *Russian Journal of Spine Surgery*. 2009;(2):055-061. (In Russ.) doi: 10.14531/ss2009.2.55-61.
4. Redding G, Song K, Inscore S, et al. Lung function asymmetry in children with congenital and infantile scoliosis. *Spine J*. 2008;8(4):639-644. doi: 10.1016/j.spinee.2007.04.020.
5. Rong T, Jiao Y, Huang Y, et al. Morphological analysis of isolated hemivertebra: radiographic manifestations related to the severity of congenital scoliosis. *BMC Musculoskelet Disord*. 2024;25(1):112. doi: 10.1186/s12891-024-07193-8.
6. Vissarionov S.V., Kokushin D.N., Belyanchikov S.M., Efremov A.M. Surgical treatment of childrenwith congenital deformityof the upper thoracic spine. *Russian Journal of Spine Surgery*. 2011;(2):035-040. (In Russ.) doi: 10.14531/ss2011.2.35-40.
7. Sparrow DB, Chapman G, Smith AJ, et al. A mechanism for gene-environment interaction in the etiology of congenital scoliosis. *Cell*. 2012;149(2):295-306. doi: 10.1016/j.cell.2012.02.054.
8. Giampietro PF. Genetic aspects of congenital and idiopathic scoliosis. Scientifica (Cairo). 2012;2012:152365. doi: 10.6064/2012/152365.
9. Pahys JM, Guille JT. What's New in Congenital Scoliosis? *J Pediatr Orthop*. 2018;38(3):e172-e179. doi: 10.1097/BPO.0000000000000922.
10. Naiche LA, Harrelson Z, Kelly RG, Papaioannou VE. T-box genes in vertebrate development. *Annu Rev Genet*. 2005;39:219-39. doi: 10.1146/annurev.genet.39.073003.105925.
11. Veenvliet JV, Bolondi A, Kretzmer H, et al, Timmermann B, Meissner A, Herrmann BG. Mouse embryonic stem cells self-organize into trunk-like structures with neural tube and somites. *Science*. 2020;370(6522):eaba4937. doi: 10.1126/science.aba4937.
12. Zhang W, Yao Z, Guo R, et al. Molecular identification of T-box transcription factor 6 and prognostic assessment in patients with congenital scoliosis: A single-center study. *Front Med (Lausanne)*. 2022;9:941468. doi: 10.3389/fmed.2022.941468.
13. Ren X, Yang N, Wu N, et al. Increased TBX6 gene dosages induce congenital cervical vertebral malformations in humans and mice. *J Med Genet*. 2020;57(6):371-379. doi: 10.1136/jmedgenet-2019-106333.
14. Wu Y, Zhang L, Lv H, et al. Applying high-throughput sequencing to identify and evaluate foetal chromosomal deletion and duplication. *J Cell Mol Med*. 2020;24(17):9936-9944. doi: 10.1111/jcmm.15593.
15. Blaker-Lee A, Gupta S, McCammon J, et al. Zebrafish homologs of genes within 16p11.2, a genomic region associated with brain disorders, are active during brain development, and include two deletion dosage sensor genes. *Dis Model Mech*. 2012;5(6):834-851. doi: 10.1242/dmm.009944.
16. Liu J, Wu N, Yang N, et al. TBX6-associated congenital scoliosis (TACS) as a clinically distinguishable subtype of congenital scoliosis: further evidence supporting the compound inheritance and TBX6 gene dosage model. *Genet Med*. 2019 Jul;21(7):1548-1558. doi: 10.1038/s41436-018-0377-x.
17. Wu N, Giampietro P, Takeda K. The genetics contributing to disorders involving congenital scoliosis. In: Kusumi K, Dunwoodie S, (eds). *The Genetics and Development of Scoliosis*. Springer, Cham; 2018. doi: 10.1007/978-3-319-90149-7_4.
18. Chen Z, Yan Z, Yu C, et al. Cost-effectiveness analysis of using the TBX6-associated congenital scoliosis risk score (TACScore) in genetic diagnosis of congenital scoliosis. Orphanet *J Rare Dis*. 2020;15(1):250. doi: 10.1186/s13023-020-01537-y.
19. Al-Kateb H, Khanna G, Filges I, et al. S Scoliosis and vertebral anomalies: additional abnormal phenotypes associated with chromosome 16p11.2 rearrangement. *Am J Med Genet A*. 2014;164A(5):1118-1126. doi: 10.1002/ajmg.a.36401.
20. Errichiello E, Arossa A, Iasci A, et al. An additional piece in the TBX6 gene dosage model: A novel nonsense variant in a fetus with severe spondylocostal dysostosis. *Clin Genet*. 2020;98(6):628-629. doi: 10.1111/cge.13854.
21. Lefebvre M, Duffourd Y, Jouan T, et al. Autosomal recessive variations of TBX6, from congenital scoliosis to spondylocostal dysostosis. *Clin Genet*. 2017;91(6):908-912. doi: 10.1111/cge.12918.
22. White PH, Farkas DR, McFadden EE, Chapman DL. Defective somite patterning in mouse embryos with reduced levels of Tbx6. *Development*. 2003;130(8):1681-1690. doi: 10.1242/dev.00367.
23. Liu J, Chen W, Yuan D, et al. Progress and perspective of TBX6 gene in congenital vertebral malformations. *Oncotarget*. 2016;7(35):57430-57441. doi: 10.18632/oncotarget.10619.
24. Yang N, Wu N, Zhang L, et al. TBX6 compound inheritance leads to congenital vertebral malformations in humans and mice. *Hum Mol Genet*. 2019;28(4):539-547. doi: 10.1093/hmg/ddy358.
25. Wu N, Ming X, Xiao J, et al. TBX6 null variants and a common hypomorphic allele in congenital scoliosis. *N Engl J Med*. 2015;372(4):341-50. doi: 10.1056/NEJMoa1406829.
26. Feng X, Cheung JPY, Je JSH, et al. Genetic variants of TBX6 and TBXT identified in patients with congenital scoliosis in Southern China. *J Orthop Res*. 2021;39(5):971-988. doi: 10.1002/jor.24805.

27. Zhao S, Zhang Y, Chen W, et al. Diagnostic yield and clinical impact of exome sequencing in early-onset scoliosis (EOS). *J Med Genet*. 2021;58(1):41-47. doi: 10.1136/jmedgenet-2019-106823.
28. Powel JE, Sham CE, Spiliopoulos M, et al. Genetics of non-isolated hemivertebra: A systematic review of fetal, neonatal, and infant cases. *Clin Genet*. 2022;102(4):262-287. doi: 10.1111/cge.14188.
29. Otomo N, Takeda K, Kawai S, et al. Bi-allelic loss of function variants of TBX6 causes a spectrum of malformation of spine and rib including congenital scoliosis and spondylocostal dysostosis. *J Med Genet*. 2019;56(9):622-628. doi: 10.1136/jmedgenet-2018-105920.
30. Panigrahi I, Angurana SK, Varma H, et al. Phenotypic heterogeneity of kyphoscoliosis with vertebral and rib defects: a case series. *Clin Dysmorphol*. 2019;28(3):103-113. doi: 10.1097/MCD.0000000000000269.
31. Yang Y, Zhao S, Zhang Y, et al. Mutational burden and potential oligogenic model of TBX6-mediated genes in congenital scoliosis. *Mol Genet Genomic Med*. 2020;8(10):e1453. doi: 10.1002/mgg3.1453.

The article was submitted 07.02.2025; approved after reviewing 07.03.2025; accepted for publication 31.03.2025.

Information about the authors:

Sergey E. Khalchitsky — Candidate of Biological Sciences, Head of Laboratory, s_khalchitski@mail.ru, https://orcid.org/0000-0003-1467-8739;

Sergei V. Vissarionov — Doctor of Medical Sciences, Professor, Corresponding Member of the Russian Academy of Sciences, Director, vissarionovs@gmail.com, https://orcid.org/0000-0003-4235-5048;

Polina A. Pershina — Postgraduate Student, polinaiva2772@gmail.com, https://orcid.org/0000-0001-5665-3009;

Konstantin G. Buslov — Candidate of Biological Sciences, Research Associate, kbuslov@yahoo.com;

Yury A. Novosad — research fellow, novosad.yur@yandex.ru, https://orcid.org/0000-0002-6150-374X;

Marina V. Sogoyan — research fellow, sogoyanmarina@mail.ru, https://orcid.org/0000-0001-5723-8851;

Marat S. Asadulaev — Candidate of Medical Sciences, research fellow, marat.asadulaev@yandex.ru, https://orcid.org/0000-0002-1768-2402;

Marina V. Gertsyk — student, mgercyk@mail.ru, https://orcid.org/0009-0006-2138-7541.

Original article
https://doi.org/10.18019/1028-4427-2025-31-3-322-333

Course and medium-term outcomes of implant-associated infection caused by leading gram-negative pathogens

O.S. Tufanova✉, S.A. Bozhkova, E.M. Gordina, V.A. Artyukh

Vreden National Medical Research Center of Traumatology and Orthopedics,
St. Petersburg, Russia

Corresponding author: Olga S. Tufanova, katieva@mail.ru

Abstract

Introduction Implant-associated infection (IAI) caused by gram-negative pathogens is characterized by a more severe, recurrent course and higher mortality than the one caused by gram-positive ones. The main reason is growing antibiotic resistance of these pathogens and the complexity of choosing drugs for inpatient and outpatient therapy.

Purpose To evaluate the influence of various factors and compare the features of the course of implant-associated infection caused by *P. aeruginosa, K. pneumoniae, A. baumannii* in patients with positive and poor treatment outcomes

Methods A retrospective analysis of the medical records of 172 patients treated at the Department of Purulent Osteology between January 1, 2017 and December 31, 2022 for implant-associated infection caused by *P. aeruginosa, K. pneumoniae, A. baumannii* was conducted. Based on the results of a telephone survey or examination, patients were divided into 2 groups: positive and poor treatment outcomes by Delphi criteria. The impact of various factors in the anamnesis, laboratory and microbiological analysis, features of surgical intervention, antibacterial therapy and the course of the early postoperative period on the outcomes was analyzed in the IBM SPSS STATISTICS (version 26).

Results Among patients with IAI caused by gram-negative bacteria, the rate of poor outcomes was 45 %, with fatality rate of 10 %. During the comparative study, a statistically significant effect on the development of a poor outcome was shown by the postoperative level of serum albumin ($p = 0.002$), the sensitivity of the isolated isolate to the tested antibacterial drugs ($p = 0.011$), the isolation of the pathogen from patients' biomaterial in the postoperative period ($p = 0.001$), a more frequent need for intravenous administration of albumin and iron ($p = 0.003$ and $p = 0.056$, respectively) and the need for repeated surgical intervention in the early postoperative period ($p = 0.001$).

Discussion IAI caused by gram-negative bacteria is characterized by a prolonged recurrent course and high mortality, primarily associated with the overall growing antibiotic resistance of pathogens which requires an individual approach to both surgical treatment and drug therapy, as well as the development of new tactical approaches to therapy.

Conclusion The rate of poor outcomes was 45 %. Hypoalbuminemia and antibacterial resistance of isolates of *P. aeruginosa, K. pneumoniae, A. baumannii*, detection of the pathogens in the postoperative material, as well as the need for surgical reoperation in the early postoperative period, are risk factors for poor outcomes.

Keywords: implant-associated infection, periprosthetic joint infection, osteomyelitis, enterobacteria, *K. pneumoniae, P. aeruginosa, A. baumannii*, antibacterial therapy, fluoroquinolones, co-trimoxazole

For citation: Tufanova OS, Bozhkova SA, Gordina EM, Artyukh VA. Course and medium-term outcomes of implant-associated infection caused by leading gram-negative pathogens. *Genij Ortopedii*. 2025;31(3):322-333. doi: 10.18019/1028-4427-2025-31-3-322-333

INTRODUCTION

As the population ages and the incidence of osteoarthritis grows, the number of large joint replacements will increase. By 2040, 2.8 million hip replacements (HRs) and one million knee replacements (KRs) are expected to be performed [1]. Although these interventions are generally successful, joint replacements can be complicated by periprosthetic joint infection (PJI) with a two-year incidence of 1.63 % for HRs and 1.55 % for KRs [2]. The incidence of fracture-associated infection (FAI) ranges from 1.8 % to 27 % and depends on the location and type of fracture [3].

In the majority of cases, implant-associated infection (IAI) develops in the first two years after joint replacement, but thereafter the risk of this complication continues to exist, and its number increases annually by 0.04–0.06 % [4]. Given the widespread growth of primary arthroplasty, the rate of revisions caused by infectious complications has also been growing.

Despite the fact that the leading causative agents of bone and joint infections, including those associated with orthopedic implants, are staphylococci, the participation of Gr(–) pathogens in the etiology, including *K. pneumoniae, P. aeruginosa, A. Baumannii*, is a prognostically unfavorable sign [5, 6]. The rate of Gr(–) bacteria in the structure of causative agents of orthopedic infection varies from 10 % to 23 % [5, 7], but the ever-increasing rate of isolation of strains with resistance to various antibiotics is particularly challenging due to the limited choice of antibacterial drugs, both at the inpatient and outpatient stages of treatment. In this regard, many authors indicate the participation of Gr(–) bacteria in the etiology of IAI as an independent factor in the possible failure of treatment in 50 % of cases of such patients [8, 9].

Currently, there are very few published scientific papers (mainly foreign ones) devoted to the study of treatment outcomes of patients with IAI caused by Gr(–) bacteria. According to researchers, risk factors in the treatment of such patients include, first of all, the wrong choice of the type of surgical intervention [10], and the key error is retention of the infected implant [8, 11, 12]. At the same time, the effectiveness of exclusively conservative therapy is only 10 % [13]. In addition, the factors of poor outcomes include female gender, detection of microbial associations, obesity [11, 12], history of repeated surgical debridements[8, 14], antibiotic resistance of the infectious agent [15], and others.

Due to the relatively small number of publications on the topic of IAI caused by Gr(–) bacteria and the complexity of treating patients with IAI, this problem requires a more detailed study.

Purpose To evaluate the influence of various factors and compare the features of the course of implant-associated infection caused by *P. aeruginosa, K. pneumoniae, A. baumannii* in patients with positive and poor treatment outcomes

MATERIALS AND METHOD

A continuous single-center retrospective study included patients diagnosed with IAI who were treated at the Department of Purulent Osteology from January 1, 2017 to December 31, 2022.

Inclusion criteria:

— Detected IAI;

— Surgical debridement in the infection focus (index surgery);

— Isolation of *P. aeruginosa, K. pneumoniae, A. baumannii* strains (both as isolated strains and in the microbial association) from one or more samples harvested for microbiological study before the intervention and in the intraoperative material (tissue biopsy, removed implant, synovial fluid).

Exclusion criteria:

— reoperation due IAI recurrence caused by *P. aeruginosa, K. pneumoniae, A. baumannii*;

— infection located exclusively within soft tissues;

— spinal IAI;

— amputation (exarticulation) performed during a sanitizing operation,

The exclusion criterion was the lack of information on the two-year outcome (including impossible telephone communication with the patient).

Patients were selected for the study using the Mikrob-2 microbiological monitoring program (2017–2020) and the Across-Engineering LIS (2021–2022) based on the analysis of the results of MBI of the biomaterial of patients treated in 2017–2022 at the Department of Purulent Osteology. Isolation of clinical strains of *P. aeruginosa, K. pneumoniae, A. baumannii* was performed in accordance with international MBI standards (Standards for microbiology investigations, UK SMI). Species identification was carried out on Microlatest panels using iEMS Reader MF (2017–2020), and since 2021 with the MALDI-TOF-MS (Matrix Assisted Laser Desorption Ionization Time of Flight Mass-Spectrometry) method using the FlexControl system. The sensitivity of isolated cultures of Gr(–) bacteria to antibacterial drugs was assessed in accordance with the EUCAST criteria (2017–2022).

After the medical records of patients who met the inclusion criteria (n = 172) had been selected, a telephone survey was conducted, during which patients were asked standard questions about whether they had had clinical or laboratory signs of recurrent infection within two years after the index surgery, and whether repeated debridement operations had been performed. In case of a patient's death, the patient's relatives were interviewed. All included patients were divided into two groups by outcomes according to the Delphi criteria [16]: positive outcome (group 1) and poor outcome (group 2). A positive outcome was absence of clinical and laboratory signs of recurrent infection and debridement surgery within two years from the date of the index surgery.

According to the inclusion and exclusion criteria, 172 individuals were included in the study.

Group 1 comprised 95 subjects (55 %), of whom 37 (22 %) did not undergo surgical interventions either due to the lack of indications or due to dissatisfaction with the quality of life. Surgical interventions, during which no data on infection were found (no growth of microorganisms was obtained during the MBI of the intraoperative material) were performed in 58 patients (34 %).

Group 2 included 78 patients (45 %), of whom 59 patients (34 %) underwent another sanitizing operation due to recurrent infection, both at our Center or at other clinics. In addition, 18 deaths (10 %) were registered in this group.

Based on the medical records and the results of a telephone survey, a database was created, which included:

— anthropometric information (age, gender, body mass index (BMI);

— anamnesis data (infection location, time since the time of the primary surgical intervention or the intervention after which the IAI developed until the manifestation of the infection, duration of the infectious process, number of debridements in the anamnesis, duration since the last debridement until the index operation);

— results of laboratory blood tests at the time of admission and before discharge from the hospital: leukocytes, ESR, CRP level, hemoglobin, total protein, albumin, creatinine;

— results of microbiological investigation (MBI) of biomaterial samples (fistula biopsies, synovial fluid, wound discharge, tissue biopsies, removed implants, hematoma) obtained in the pre-, intra- and postoperative periods;

— type of surgical intervention, its duration, intraoperative blood loss, volume of drained discharge;

— medication therapy at the inpatient (antibacterial therapy (ABT), intravenous infusion of albumin, iron preparations) and outpatient stages;

— re-debridement or its absence in the early postoperative period after the index operation;

— retained implant at the time of discharge from hospital.

The obtained data were recorded in the form of spreadsheets in MS Office Excel, 2007 (Microsoft, USA); the data structure was visualized and analyzed using IBM SPSS STATISTICS (version 26). Quantitative indicators were assessed for compliance with the normal distribution using the Kolmogorov – Smirnov test. In the absence of a normal distribution, quantitative data were described using the median (Me) and the lower and upper quartiles (Q1–Q3). Categorical data were described indicating absolute values and percentages. Comparison of two groups by a quantitative indicator whose distribution differed from normal was performed using the Mann–Whitney U test. To assess the risk in the comparison groups, the odds ratio (OR, 95 % CI) was calculated. Comparison of percentages in the analysis of four-field contingency tables was performed using the Pearson chi-square (χ^2) test (for expected event values greater than 10) or the Fisher exact test (for expected event values less than 10); the relationship was assessed using the Cramer test. Differences in indicators between groups were considered statistically significant at $p < 0.05$.

RESULTS

Anthropometric and anatomical data

The analyzed groups were comparable by gender, age and BMI (Table 1). The dominant IAI location were the joints and bones of the lower limb ($n = 164$, 95 %) in the area of the hip joint ($n = 94$, 55 %) or knee joint ($n = 33$, 19 %). No statistically significant impact of infection location on the outcome of treatment was found ($p = 0.948$).

Table 1

Comparison of groups in gender, age and BMI

Factors	Group 1, $n = 95$	Group 2, $n = 77$	p
Males, n (%)	47 (49)	33 (43)	$p = 0.443$
Age, years, Me [IQR]	63.0 [49.0–68.0]	58.0 [45.0–66.0]	$p = 0.114$
BMI, weight/height W/H^2, Me [IQR]	27.5 [24.2–31.6]	27.8 [23.7–33.0]	$p = 0.838$

Table 2

Comparison of groups in IAI history

Factors	Me [IQR]		p
	Group 1, $n = 95$	Group 2, $n = 77$	
Interval between implant installation* and infection manifestation (days)	153.5 [30–1247]	95 [23–730]	$p = 0,331$
Duration of infection (days)	610 [161–1410]	493 [121–1226]	$p = 0,345$
Interval between previous and index debridement (days)	241 [81–862]	135 [28–455]	$p = 0,095$

Note: * — after primary and revision surgeries

Despite the lack of statistical significance, the manifestation of infection or its relapse developed earlier in group 2 patients, and the duration of the infectious process was shorter than in the comparison group (Table 2).

The proportion of patients with the first debridement intervention was 24 % in group 1 and 14 % in group 2, and two or more debridements in the anamnesis were performed in 40 % and 52 % of patients, respectively ($p = 0.173$). The median number of debridements in the anamnesis was 1 [1.2] in the group with positive outcomes and 2 [1.3] in the comparison group ($p = 0.112$).

Laboratory findings

Table 3

Results of laboratory tests before surgery and before discharge from hospital

Parameter		Me [IQR]		*p*
		Group 1, *n* = 95	Group 2, *n* = 77	
Before surgery	Leucocytes, 10^9/l	7.6 [6.5–9.7]	8.3 [6.0–9.9]	*p* = 0.625
	ESR, mm/h	44 [26–63]	53 [29.5–63]	*p* = 0.430
	CRP, mg/l	25 [10.5–40]	33 [9–75]	*p* = 0.121
	Hemoglobin g/l	117 [104–131]	111 [97.5–132]	*p* = 0.246
	Albumin g/l	**40 [35.5–43]**	**35 [33–43]**	***p* = 0.068**
Before discharge from the hospital	Leucocytes, 10^9/l	6.6 [5.7–8,2]	6.8 [5.2–8.0]	*p* = 0.749
	ESR, mm/h	35 [22–52.5]	39 [22–55.5]	*p* = 0.926
	CRP, mg/l	23.5 [12–42]	25.5 [13–52]	*p* = 0.284
	Hemoglobin g/l	99 [95–114.5]	100 [91–108.5]	*p* = 0.250
	Albumin g/l	**34 [32–41]**	**32 [28–35]**	***p* = 0.002***

On admission, patients in Group 2 tended to have higher levels of inflammation (white blood cell count, CRP, and ESR) and lower levels of hemoglobin and albumin, with no significant differences between the groups (Table 3). Before discharge, laboratory test results were similar in both groups and reflected the normal course of the postoperative period. It is worth noting that there was a statistically significant increase in albuminuria in the patients with poor outcome ($p = 0.002$).

Features of surgical intervention

In the studied cohort of patients, the most common types of surgical intervention were the installation of an antimicrobial spacer ($n = 112$, 65 %), resection arthroplasty with muscle grafting ($n = 16$, 9 %), and revision surgery with implant retention ($n = 11$, 6 %). However the type of surgical intervention did not have a significant impact on the outcome ($p = 0.487$). To fabricate the antimicrobial spacer, gentamicin-containing bone cement was used, which was additionally impregnated with a heat-stable antibacterial drug at a dose of 4 g per 40 g of cement. In this type of surgical intervention, vancomycin was added to the bone cement in 53 % of cases, meropenem in 15 %, and fosfomycin in 10 %. Moreover, only in 23 % of cases was the antibiotic active against the microorganism isolated from the intraoperative material.

The volume of intraoperative blood loss was Me: 600 [400–800] ml, there were no statistically significant differences in the groups for this parameter ($p = 0.133$). In group 1, drainage blood loss was slightly lower than in group 2: 450 [340–600] and 500 [380–750] ml, respectively ($p = 0.091$).

MB findings

According to the MBI results of the biomaterial, K. pneumoniae was isolated in 55 % of cases, *A. baumannii* in 18 % and in 27 % of cases it was *P. aeruginosa*. The distribution of isolated cultures in the compared groups is shown in Fig. 1.

K. pneumoniae in group 2 as the causative agent of IAI was 1.3 times more frequent and *P. aeruginosa* was 1.7 times less frequent but there were no significant differences between the groups ($p = 0.097$).

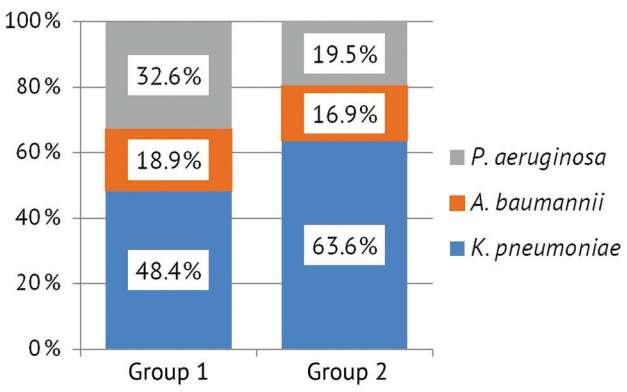

Fig. 1 Distribution of patients in the groups according to the isolated microbes detected

At the preoperative stage, the microbiological study of the biomaterial from the implantation area, monocultures of *K. pneumoniae, A. baumannii* or *P. aeruginosa* were isolated in 58 % of cases. However, no statistically significant impact of the infection etiology, the information about which was obtained at the preoperative stage, on the treatment outcome was found ($p = 0.895$). *K. pneumoniae, A. baumannii* or *P. aeruginosa* were also isolated from other loci in 9.3 % of cases (urine — 7.6 %, blood — 0.6 %, sputum — 0.6 %), which indicates the potential hematogenous spread of the causative IAI agent.

In 94 % of cases ($n = 172$), the pathogen was isolated from intraoperative tissue biopsies. Despite the absence of statistically significant differences between the groups ($p = 0.192$), it is noteworthy that the median number of tissue biopsies from which the microorganism was isolated was 4 [2–5] in group 1 and 5 [3–5] in group 2. *K. pneumoniae, A. baumannii*, or *P. aeruginosa* strains were isolated from the material on the implant surface in 73 % of cases.

The incidence of polymicrobial infection in the compared groups did not differ and was 66 % and 69 %, respectively, in groups 1 and 2 ($p = 0.871$) (Table 4). In both groups, the microbial associations with the leading Gr(–) pathogens also contained Gr(+) bacteria without significant impact of the composition on the treatment outcome ($p = 0.570$).

Table 4

Microbial associations detected in the biomaterial of the patients in the compared groups

Состав микробных ассоциации	Группа 1, $n = 63$		Группа 2, $n = 53$	
	n	%	*n*	%
Contains only Gr(–) bacteria, including *E. coli, Enterobacter spp.* and others	9	14	5	9
Contains only Gr(+) bacteria, including *S. aureus, S. epidermidis* and others	54	86	48	91

The proportion of patients in whom isolated strains of *P. aeruginosa, K. pneumoniae, A. baumannii* were sensitive to fluoroquinolones was 5.25 times higher in group 1 than in group 2, while the proportion of patients with extremely resistant strains, on the contrary, was 1.3 times higher in group 2 (Fig. 2). At the same time, a statistically significant impact of sensitivity to antibacterial drugs on the outcome was observed ($p = 0.011$, Cramer's V = 0.254).

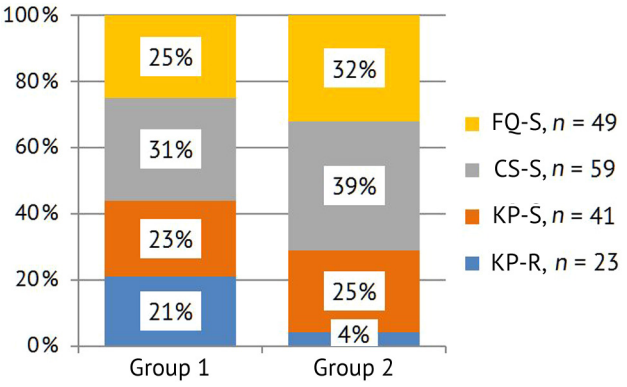

Fig. 2 Analysis of sensitivity of Gr(–) strains to the main antibacterial drugs in comparison groups. Strains:FQ-S—fluoroquinolone-sensitive,CS-S—sensitive to cephalosporins, but resistant to fluoroquinolones, KP-S — sensitive to carbapenems, but resistant to fluoroquinolones and cephalosporins, KP-R — carbapenem-resistant

Postoperative period

Systemic antibacterial therapy was administered to all patients. In 10 % of cases, it was necessary to start antibacterial therapy before the ndex surgery due to either a life-threatening septic condition or a previous sanitizing surgical intervention. Empirical antibacterial therapy with vancomycin and with the fluoroquinolone group agent (cipro- or levofloxacin) from the day of surgery was received by 9 % of patients, and with vancomycin and cefoperazone-sulbactam by 29 %. In the rest of the cases, antibacterial therapy was prescribed based on the results of preoperative cultures. Etiotropic antibacterial therapy from the day of surgery was prescribed to 61 % of patients, while this did not have a statistical impact on the outcome ($p = 0.120$). A tendency towards a shorter inpatient course of antibacterial therapy was noted in the patients of group 1 compared to group 2: 13 [10–15] and 16 [11–24] ($p = 0.096$), respectively.

In 86 % of cases, oral antibacterial drugs were prescribed at the outpatient stage. Among patients with these recommendations, adverse outcomes were somewhat less common (p = 0.077, OR 0.443, 95 % CI: 0.178–1.052). At the outpatient stage, fluoroquinolones were recommended in 55 % of cases, co-trimoxazole in 13 %, and both fluoroquinolones and co-trimoxazole in 9 %. Despite the fact that the very fact of prescribing these drugs did not have a statistically significant impact on the outcome (p = 0.446, p = 0.665 and p = 0.300, respectively), it was confirmed that in the case where the isolated microorganism was sensitive to the drug prescribed at the outpatient stage, the probability of a positive outcome increased significantly (p = 0.001) by 7.87 times (95 % CI: 2.26–27.03).

Patients in group 2, compared to group 1, required the administration of albumin solution infusion (26 % and 2 % of cases, p = 0.003) and iron preparations (27 % and 15 % of cases, p = 0.056) more frequently. Moreover, the duration of prescribed symptomatic therapy in group 2 was also longer (Table 5).

Table 5

Frequency of administration of drugs for symptomatic therapy

Infusion	Me [IQR]		p
	Group 1, n = 63	Group 2, n = 53	
Abumin solution	5.0 [5.0–5.0]	10.0 [5.0–11.0]	p = 0.101
Iron preparations	4.0 [3.0–5.0]	5.0 [5.0–10.0]	p = 0.286

In the postoperative period, 40 patients (23 %) showed a re-growth of the studied pathogens in the intraoperative material, hematoma contents or wound discharge, which increased the risk of an unfavorable outcome in the future by 3.4 times (95 % CI 1.61–7.2; p = 0.001). Revision surgery in the early postoperative period was required in 38 cases (22 %), which increased the likelihood of an unfavorable outcome in the future by 4.86 times (95 % CI 2.18–10.84; p = 0.001), of which postoperative wound debridement was performed in 19 patients (10.9 %), implant removal and muscle grafting in 8 patients (4.6 %), antimicrobial spacer reinsertion in 7 patients (4 %), implant removal in 3 cases (1.7 %) and arthrodesis in one (0.6 %) patient. Finally, at the time of discharge, reimplantation was used in 133 patients (77 %); nowever, the insertion of a new implant did not have a statistically significant impact on the likelihood of a poor outcome (p = 0.101).

DISCUSSION

Gr(–) microorganisms *K. pneumoniae, P. aeruginosa* and *A. baumannii* belong to a group of frequently encountered pathogens that are highly resistant to antibiotics, designated by the Infectious Diseases Society of America as “ESKAPE pathogens”. According to the WHO, the representatives of these species are classified as pathogens with a critically high priority level [17]. *K. pneumoniae, P. aeruginosa* and *A. baumannii* are characterized by the presence of a certain set of pathogenicity and persistence factors, including the ability to form biofilms and internalize into eukaryotic cells, including osteoblasts [18]. As the diversity of resistant strains steadily increases, the frequency of their spread not only among patients but also among the population increases, which causes high alertness among clinicians and the healthcare system [19].

Carbapenem-resistant enterobacterales (CRE) are of particular importance due to their high resistance to antibiotics, including broad-spectrum antibiotics [20]. According to the 2019 report of the Centers for Diseases Control, from 2012 to 2017, 210,500 cases of infections caused by Enterobacterales, producing broad-spectrum beta-lactamase or carbapenemases, were registered in the United States, resulting in 12,900 deaths annually [21]. The global spread of CRE pathogens is rapid, which restricts the choice of antimicrobial drugs during the infectious process to polymyxins, tigecycline, aminoglycosides, and in some cases high doses of carbapenems. However, these drugs

may not be effective enough and cause many adverse reactions [22]. In addition, the resistance ability in these pathogens to beta-lactams and fluoroquinolones makes it impossible to prescribe prolonged etiotropic antibacterial therapy, which is standard for the treatment of bone and joint infections, due to the lack of other oral drugs active against Gr(–) pathogens.

Despite the low rates of IAI caused by Gr(–) pathogens [7], the treatment outcomes of such patients are significantly worse. In addition to rifampicin-resistant staphylococci and fluconazole-resistant *Candida* fungi, Gr(–) microorganisms resistant to fluoroquinolones are also classified as pathogens causing PJI that is difficult-to-treat (DTT), and for which a higher recurrence rate has been proven, requiring repeated sanitizing surgical interventions [23].

The results of a number of studies demonstrate that Gr(–) etiology of IAI is an independent predictor of poor outcome [8, 9, 12]. Thus, Kalbian et al. observed poor treatment results in patients with PJI caused by Gr(–) microorganisms and associations of Gr(–) and Gr(+) bacteria more frequently, compared to infection caused exclusively by Gr(+) pathogens (OR = 2.9, $p < 0.0001$; OR = 2.5, $p = 0.013$, respectively) [24]. And a meta-analysis showed that IAI caused by microbial associations involving Gr(–) bacteria caused treatment failures more frequently compared to monobacterial infection [12]. In our sample, the majority of IAI cases (67 %) were caused by bacterial associations, while the proportion of patients with poor outcomes after a two-year follow-up period was 45 %, which generally confirms global trends. Also, our cohort had a high mortality rate of 10 %, which is significantly higher than among patients with IAI that did not consider the etiology of the infectious process, about 3 % during the first year [25]. Depending on the type of Gr(–) pathogen involved in the IAI etiology, the rate of positive treatment outcome was 65 % for *P. aeruginosa*, 58 % or *A. baumannii* and 48 % for *K. pneumoniae*. No significant effect of the composition of microbial associations on the outcome of complex treatment was found ($p = 0.871$).

In our study, the groups were comparable in terms of gender, age, and BMI regardless of the treatment outcome. The data in scientific publications on this issue vary. Some authors claim that these parameters do not differ in groups with positive and poor outcomes [26], others believe that female gender and obesity are risk factors for failed outcomes [12], and others indicate old age as a predictor of poor outcome [15]. Hsieh et al. conducted a study of 346 patients and compared the influence of various factors on the course of IAI caused by Gr(+) and Gr(–) microorganisms. The authors concluded that patients with IAI caused by Gr(–) microorganisms were older (mean age 68 years versus 59 years; $p < 0.001$), and the period from primary JR to the manifestation of the infectious process was shorter (74 days versus 109 days; $p < 0.001$) [27].

IAI caused by Gr(–) bacteria frequently has a long and wave-like course, combining periods of exacerbations requiring surgical intervention and antibacterial therapy, and remission. In our study, the duration of the infectious process in both groups was more than a year and did not differ significantly. The time interval from the day of surgery to the manifestation of infection and from the last debridement operation to the index operation was slightly shorter in the group of poor outcomes ($p = 0.331$ and $p = 0.095$, respectively). According to a meta-analysis of 11 clinical studies, including 593 patients with PJI caused by Gr(–) pathogens, acute infection had a more unfavorable course compared to chronic infection: the success rate after two-stage treatment was 66 % and 75 %, respectively, at a two-year follow-up [12]. Moreover, it was found that treatment outcomes when the infection was localized in the knee joint were significantly worse than in the hip joint (35 % versus 15 %, $p = 0.002$, respectively). In our study, these indicators did not differ: when the IAI was localized in the hip joint the failure outcome was 37 %, and in the knee joint 39 %.

Pfang et al. concluded that a history of a large number of debridement operations is an independent predictor of an poor outcome of IAI caused by species of the enterobacteria family [8]. Our previous study of the outcomes of IAI caused only by *K. pneumoniae* obtained similar results [14]. In the current

study, no significant intergroup differences ($p = 0.112$) were found in the number of previously performed debridements, while in group 2 there were 30 % more patients with a history of two or more redebridements.

The levels of laboratory markers of inflammation in the studied groups were comparable in the pre- and postoperative periods. However, patients in group 2 showed a tendency toward more pronounced hypoalbuminemia upon admission, the level of which by the time of discharge was significantly different from group 1 ($p = 0.002$), despite the fact that they received albumin solution infusions more often ($p = 0.002$) and for a longer period ($p = 0.101$) after the operation. The obtained results are consistent with the data of Scarcella et al., who found that patients with reduced albumin levels were more likely to develop infection recurrence. The authors believe that a significant role in the development of hypoalbuminemia is played by chronic inflammation resulting in immunosuppression, which, in turn, complicates the elimination of the infectious process itself, closing this vicious circle [28]. In addition, hypoalbuminemia decreases the effectiveness of antibacterial therapy by reducing the amount of transport proteins. As a result, the fraction of the antibiotic unbound to albumin increases in the blood, which increases the risk of adverse reactions due to decreased antibacterial activity of the drug [29]. Thus, both foreign and domestic authors come to the conclusion that hypoalbuminemia increases the risk of infectious complications after orthopedic interventions. This allows us to consider this symptom as an independent predictor of failure of complex IAI treatment [30, 31]. Another possible predictor of failed outcomes in infectious diseases, including IAI, is considered to be anemia [32]. In our study, the need for intravenous iron preparations was also more frequently observed among the patients in group 2 ($p = 0.056$).

We have established a significant ($p = 0.011$, Cramer's V = 0.254) impact of the sensitivity of the isolated microorganisms to the tested antibacterial drugs on the outcome of complex treatment. Among patients in whom the etiology of IAI was strains of Gr(–) microorganisms sensitive to fluoroquinolones, there was the highest rate of successful outcomes — 87 %. And among patients in whom Gr(–) bacteria resistant to fluoroquinolones and cephalosporins and microorganisms with extreme resistance were isolated, the rate of positive outcomes was 49.2 and 49 %, respectively. Similar results were shown by Fantoni et al., whose study reported successful results of treatment in the patients with infection caused by carbapenem-resistant strains of Gr(–) microorganisms in only 50 % of cases [13].

The choice of drugs for ABT, both at the inpatient and outpatient stages, is the cornerstone in the treatment of patients with IAI caused by Gr(–) pathogens. The basis of ABT is considered to be parenteral administration of predominantly bactericidal antibiotics for 7–14 days from the day of surgery, followed by a transition to oral drugs up to 6–8 weeks after each stage of surgical treatment [33] or up to three months after a single-stage intervention [34]. All patients included in our study received systemic ABT with at least two drugs. Therapy was considered etiotropic if the strain of microorganism isolated was sensitive to at least one antibiotic received. Etiotropic ABT from the day of surgery, that considered the results of MBI of preoperative biomaterials, was received by 61 % of patients included in the study. Moreover, the median duration of ABT at the inpatient stage in group 2 was slightly longer than in group 1: 16 [11–24] and 13 [10–15] days, respectively ($p = 0.096$), which was due to a more frequent need to perform revision of the postoperative wound or impossibility of changing to etiotropic oral ABT of patients in group 2.

The small number of oral antibiotics active against the studied pathogens determines the difficulties in carrying out a prolonged etiotropic therapy in specialized patients. The choice of drugs is limited to the fluoroquinolone class and co-trimoxazole. Fluoroquinolones have the advantage of antibiofilm activity, good penetration into bone tissue and relatively good tolerability [35]. In the study by Rodríguez-Pardo et al., which included 242 patients with IAI, the rate of fluoroquinolone-sensitive isolates of Gr(–) bacteria was 81 %, which, when performing revision with implant retention

and prescribing long-term etiotropic oral therapy, arrested infection in 79 % of cases observed at a two-year follow-up [36]. In our study, there was a similar group of patients that had the highest rate of success (87 %), which confirms the significant impact of pathogen sensitivity to antibiotics on treatment outcomes ($p = 0.011$). However, the high level of resistance of Gr(–) microorganisms to antibiotics of this group greatly limits the possibilities of their use [37]. In the sample we studied, 87 % of pathogens were resistant to fluoroquinolones, that, according to scientific publications, affects treatment outcomes for such patients [36].

To date, the question remains open as to whether it is advisable to prescribe fluoroquinolones at the outpatient stage of treatment if the isolates obtained are not sensitive to them. We have not found any studies on the efficacy of fluoroquinolone monotherapy for the treatment of infections caused by strains resistant to them. Grossi et al. showed that additional administration of fluoroquinolones to prolonged beta-lactam infusion throughout the entire treatment period (median 90 days) did not have an effect on the outcome of treatment of patients with IAI caused by strains resistant to fluoroquinolones [26]. In another study, 28 specialized patients received combination therapy with cefepime and fluoroquinolone after debridement. The efficacy over a two-year follow-up was 79 %, but the study did not analyze the effect of each antibiotic separately [38]. In our study, we did not obtain significant differences ($p = 0.446$) in the effectiveness of treatment depending on the presence or absence of a drug from the fluoroquinolone group in the extended antibiotic therapy in case of pathogen resistance to them.

Another drug that is theoretically active against the leading Gr(–) pathogens in orthopedic infection, with the exception of *P. aeruginosa*, which is naturally resistant to the drug, is co-trimoxazole. The antibiotic has a bactericidal effect and is able to penetrate into bone tissue [39]. However, co-trimoxazole does not have antibiofilm activity and about 70 % of *K. pneumoniae* and *A. baumannii* strains are resistant to it [37, 40]. Cisse et al. showed that the use of a combination of fluoroquinolones and co-trimoxazole for 8–12 weeks after surgical debridement in 30 patients with IAI caused by *E. cloacae* was effective in 80 % of cases [41]. The efficacy of co-trimoxazole in IAI caused by other Gr(–) pathogens has not yet been studied. In our study, the administration of co-trimoxazole or fluoroquinolone in the presence of sensitivity to them of isolates isolated from the patient statistically significantly ($p = 0.001$) increased the probability of a favorable outcome by 7.87 times (95 % CI 2.26–27.03), which once again confirms the critical role of antibiotic resistance in predicting the outcome of IAI treatment.

Revision of the surgical intervention area in the early postoperative period was required in every fifth patient, which increased the risk of a poor outcome by 4.86 times (95 % CI 2.18–10.84). Moreover, growth of Gr(–) bacteria in the early postoperative period increased the probability of poor outcomes by 3.4 times (95 % CI 1.61–7.21) (Cramer's V = 0.252). Culture isolation was recorded in 23 % of patients. In most cases, it was isolated from the intraoperative material during revision surgery, less frequently from a hematoma or wound discharge.

It is known that surgery with retention of the infected implant often leads to recurrence of IAI [8, 15]. In our study, in the majority of cases, the index surgery included complete removal or replacement of the infected implant with a new one. In the study sample, 77 % of patients were discharged with exchanged implants, most often antimicrobial spacers. As a result, we did not observe a significant impact of the presence of metal implants on the treatment outcome ($p = 0.101$).

CONCLUSION

Complex treatment of IAI caused by Gr(–) bacteria results in failure in 45 % of cases at a two-year follow-up, including a 10 % mortality rate. The leading gram-negative pathogens in most cases are found in mixed microbial associations with Gr(+) bacteria. IAI of this etiology is characterized by a long

recurrent course. Significant risk factors for poor outcome within two years after the debridement operation are hypoalbuminemia, both initial and in the postoperative period, and early revision of the postoperative wound associated with positive growth of the pathogen from the biomaterial obtained from the surgical intervention area. Moreover, the prognosis in such patients is significantly influenced by the sensitivity of isolated Gr(–) pathogens to antibacterial drugs, which is of particular concern due to widespread growth of antibacterial resistance and requires the development of new tactical approaches to treatment.

Conflict of interests *None*

Funding source *None*

REFERENCES

1. Singh JA, Yu S, Chen L, Cleveland JD. Rates of Total Joint Replacement in the United States: Future Projections to 2020-2040 Using the National Inpatient Sample. *J Rheumatol*. 2019;46(9):1134-1140. doi: 10.3899/jrheum.170990.
2. Tubb CC, Polkowksi GG, Krause B. Diagnosis and Prevention of Periprosthetic Joint Infections. *J Am Acad Orthop Surg*. 2020;28(8):e340-e348. doi: 10.5435/JAAOS-D-19-00405.
3. Birt MC, Anderson DW, Bruce Toby E, Wang J. Osteomyelitis: Recent advances in pathophysiology and therapeutic strategies. *J Orthop*. 2016;14(1):45-52. doi: 10.1016/j.jor.2016.10.004.
4. Liukkonen RJ, Honkanen M, Reito AP, et al. Trends in Revision Hip Arthroplasty for Prosthetic Joint Infection: A Single-Center Study of 423 Hips at a High-Volume Center Between 2008 and 2021. *J Arthroplasty*. 2023;38(6):1151-1159. doi: 10.1016/j.arth.2023.02.061.
5. Kasimova AR, Trufanova OS, Gordina EM, et al. Twelve-year dynamics of leading pathogens spectrum causing orthopedic infection: a retrospective study. *Traumatology and Orthopedics of Russia*. 2024;30(1):66-75. doi: 10.17816/2311-2905-16720.
6. Bozhkova S, Tikhilov R, Labutin D, et al. Failure of the first step of two-stage revision due to polymicrobial prosthetic joint infection of the hip. *J Orthop Traumatol*. 2016;17(4):369-376. doi: 10.1007/s10195-016-0417-8.
7. Tsikopoulos K, Meroni G. Periprosthetic Joint Infection Diagnosis: A Narrative Review. *Antibiotics (Basel)*. 2023;12(10):1485. doi: 10.3390/antibiotics12101485.
8. Pfang BG, García-Cañete J, García-Lasheras J, et al. Orthopedic Implant-Associated Infection by Multidrug Resistant Enterobacteriaceae. *J Clin Med*. 2019;8(2):220. doi: 10.3390/jcm8020220.
9. Zmistowski B, Fedorka CJ, Sheehan E, Deirmengian G, Austin MS, Parvizi J. Prosthetic joint infection caused by gram-negative organisms. *J Arthroplasty*. 2011;26(6 Suppl):104-108. doi: 10.1016/j.arth.2011.03.044.
10. Kochish AA, Bozhkova SA. Modern state of problem for treating patients with recurrent hip periprosthetic joint infection (Literature review). *Department of traumatology and orthopedics*. 2020;(3):11-22. (In Russ.) doi: 10.17238/issn2226-2016.2020.3.11-22.
11. Jernigan JA, Hatfield KM, Wolford H, et al. Multidrug-Resistant Bacterial Infections in U.S. Hospitalized Patients, 2012-2017. *N Engl J Med*. 2020;382(14):1309-1319. doi: 10.1056/NEJMoa1914433.
12. Gonzalez MR, Gonzalez J, Patel RV, et al. Microbiology, treatment, and postoperative outcomes of gram-negative prosthetic joint infections - a systematic review of the literature. *J Am Acad Orthop Surg*. 2024 Sep 5. doi: 10.5435/JAAOS-D-23-01203.
13. Fantoni M, Borrè S, Rostagno R, et al. Epidemiological and clinical features of prosthetic joint infections caused by gram-negative bacteria. *Eur Rev Med Pharmacol Sci*. 2019;23(2 Suppl):187-194. doi: 10.26355/eurrev_201904_17490.
14. Tufanova OS, Kasimova AR, Astakhov DI et al. Factors affecting the course and prognosis of Implant-associated Infection caused by Klebsiella spp. *Traumatology and Orthopedics of Russia*. 2024;30(2):40-53. doi: 10.17816/2311-2905-16719.
15. Papadopoulos A, Ribera A, Mavrogenis AF, et al. Multidrug-resistant and extensively drug-resistant Gram-negative prosthetic joint infections: Role of surgery and impact of colistin administration. *Int J Antimicrob Agents*. 2019;53(3):294-301. doi: 10.1016/j.ijantimicag.2018.10.018.
16. Diaz-Ledezma C, Higuera CA, Parvizi J. Success after treatment of periprosthetic joint infection: a Delphi-based international multidisciplinary consensus. *Clin Orthop Relat Res*. 2013;471(7):2374-2382. doi: 10.1007/s11999-013-2866-1.
17. Abukhalil AD, Barakat SA, Mansour A, et al. ESKAPE Pathogens: antimicrobial resistance patterns, risk factors, and outcomes a retrospective cross-sectional study of hospitalized patients in Palestine. *Infect Drug Resist*. 2024;17:3813-3823. doi: 10.2147/IDR.S471645.
18. Venkateswaran P, Vasudevan S, David H, et al. Revisiting ESKAPE Pathogens: virulence, resistance, and combating strategies focusing on quorum sensing. *Front Cell Infect Microbiol*. 2023;13:1159798. doi: 10.3389/fcimb.2023.1159798.
19. Adar A, Zayyad H, Azrad M, et al. Clinical and demographic characteristics of patients with a new diagnosis of carriage or clinical infection with carbapenemase-producing Enterobacterales: a retrospective study. *Front Public Health*. 2021;9:616793. doi: 10.3389/fpubh.2021.616793.
20. Lasko MJ, Nicolau DP. Carbapenem-resistant Enterobacterales: considerations for treatment in the era of new antimicrobials and evolving enzymology. *Curr Infect Dis Rep*. 2020;22(3):6. doi: 10.1007/s11908-020-0716-3.
21. ohnson A, McEntee L, Farrington N, et al. Pharmacodynamics of cefepime combined with the novel extended-spectrum-β-Lactamase (ESBL) inhibitor enmetazobactam for murine pneumonia caused by ESBL-producing Klebsiella pneumoniae. *Antimicrob Agents Chemother*. 2020;64(6):e00180-20. doi: 10.1128/AAC.00180-20.

22. Sheu CC, Chang YT, Lin SY, et al. Infections caused by carbapenem-resistant Enterobacteriaceae: an update on therapeutic options. *Front Microbiol*. 2019;10:80. doi: 10.3389/fmicb.2019.00080.
23. Wimmer MD, Hischebeth GTR, Randau TM, et al. Difficult-to-treat pathogens significantly reduce infection resolution in periprosthetic joint infections. *Diagn Microbiol Infect Dis*. 2020;98(2):115114. doi: 10.1016/j.diagmicrobio.2020.115114.
24. Kalbian IL, Goswami K, Tan TL, et al. Treatment outcomes and attrition in gram-negative periprosthetic joint infection. *J Arthroplasty*. 2020;35(3):849-854. doi: 10.1016/j.arth.2019.09.044.
25. Artyukh VA, Bozhkova SA, Tikhilov RM, et al. Risk factors for lethal outcomes after surgical treatment of patients with chronic periprosthetic hip joint infection. *Genij Ortopedii*. 2021;27(5):555-561. doi: 10.18019/1028-4427-2021-27-5-555-561.
26. Grossi O, Asseray N, Bourigault C, et al. Gram-negative prosthetic joint infections managed according to a multidisciplinary standardized approach: risk factors for failure and outcome with and without fluoroquinolones. *J Antimicrob Chemother*. 2016;71(9):2593-2597. doi: 10.1093/jac/dkw202.
27. Hsieh PH, Lee MS, Hsu KY, et al. Gram-negative prosthetic joint infections: risk factors and outcome of treatment. *Clin Infect Dis*. 2009;49(7):1036-1043. doi: 10.1086/605593.
28. Scarcella NR, Mills FB, Seidelman JL, Jiranek WA. The effect of nutritional status in the treatment of periprosthetic joint infections in total hip arthroplasty. *J Arthroplasty*. 2024;39(9S1):S225-S228. doi: 10.1016/j.arth.2024.06.040.
29. Ulldemolins M, Roberts JA, Rello J, et al. The effects of hypoalbuminaemia on optimizing antibacterial dosing in critically ill patients. *Clin Pharmacokinet*. 2011;50(2):99-110. doi: 10.2165/11539220-000000000-00000.
30. Bohl DD, Shen MR, Kayupov E, et al. Is hypoalbuminemia associated with septic failure and acute infection after revision total joint arthroplasty? A study of 4517 patients from the national surgical quality improvement program. *J Arthroplasty*. 2016;31(5):963-967. doi: 10.1016/j.arth.2015.11.025.
31. Bozhkova SA, Liventsov VN, Tikhilov RM, et al. Protein-energy malnutrition as a predictor of early recurrent revisions after debridement surgery in patients with difficult-to-treat periprosthetic infection. *Traumatology and Orthopedics of Russia*. 2022;28(1):39-45. doi: 10.17816/2311-2905-1717.
32. Swenson RD, Butterfield JA, Irwin TJ, et al. Preoperative anemia is associated with failure of open debridement polyethylene exchange in acute and acute hematogenous prosthetic joint infection. *J Arthroplasty*. 2018;33(6):1855-1860. doi: 10.1016/j.arth.2018.01.042.
33. Winkler T, Trumpuz A, Renz N, et al. Classification and algorithm for diagnosis and treatment of hip periprosthetic infection. *Traumatology and orthopedics of Russia*. 2016;22(1):33-45. (In Russ.) doi: 10.21823/2311-2905-2016-0-1-33-45.
34. Bernard L, Arvieux C, Brunschweiler B, et al. Antibiotic therapy for 6 or 12 weeks for prosthetic joint infection. *N Engl J Med*. 2021;384(21):1991-2001. doi: 10.1056/NEJMoa2020198.
35. Azamgarhi T, Scarborough M, Peter-Akhigbe V, et al. Fluoroquinolones in orthopaedic infection: balancing risks and rewards. *J Antimicrob Chemother*. 2024;79(10):2413-2416. doi: 10.1093/jac/dkae286.
36. Rodríguez-Pardo D, Pigrau C, Lora-Tamayo J, et al. Gram-negative prosthetic joint infection: outcome of a debridement, antibiotics and implant retention approach. A large multicentre study. *Clin Microbiol Infect*. 2014;20(11):O911-O919. doi: 10.1111/1469-0691.12649.
37. Tsiskarashvili AV, Melikova RE, Novozhilova EA. Analysis of six-year monitoring of common pathogens causing periprosthetic joint infection of major joints and the tendency to resistance. *Genij Ortopedii*. 2022;28(2):179-188. doi: 10.18019/1028-4427-2022-28-2-179-188.
38. Legout L, Senneville E, Stern R, et al. Treatment of bone and joint infections caused by Gram-negative bacilli with a cefepime-fluoroquinolone combination. *Clin Microbiol Infect*. 2006;12(10):1030-1033. doi: 10.1111/j.1469-0691.2006.01523.x.
39. Thabit AK, Fatani DF, Bamakhrama MS, et al. Antibiotic penetration into bone and joints: An updated review. *Int J Infect Dis*. 2019;81:128-136. doi: 10.1016/j.ijid.2019.02.005.
40. Bozhkova SA, Kasimova AR, Tikhilov RM, et al. Adverse trends in the etiology of orthopedic Infection: results of 6-year monitoring of the structure and resistance of leading Pathogens. *Traumatology and orthopedics of Russia*. 2018;24(4):20-31. doi: 10.21823/2311-2905-2018-24-4-20-31.
41. Cisse H, Vernet-Garnier V, Hentzien M, et al. Treatment of bone and joint infections caused by Enterobacter cloacae with a fluoroquinolone-cotrimoxazole combination. Int J Antimicrob Agents. 2019;54(2):245-248. doi: 10.1016/j.ijantimicag.2019.05.010.

The article was submitted 29.01.2025; approved after reviewing 03.02.2025; accepted for publication 31.03.2025.

Information about the authors:

Olga S. Tufanova — Clinical Pharmacologist, katieva@mail.ru, https://orcid.org/0000-0003-4891-4963, SPIN-code: 8704-9195;

Svetlana A. Bozhkova — Doctor of Medical Sciences, Head of the Department, Professor of Department, clinpharm-rniito@yandex.ru, http://orcid.org/0000-0002-2083-2424, SPIN-code: 3086-3694;

Ekaterina M. Gordina — Candidate of Medical Sciences, Senior Researcher, emgordina@win.rniito.ru, http://orcid.org/0000-0003-2326-7413, SPIN-code: 9647-8565;

Vasily A. Artyukh — Doctor of Medical Sciences, Head of the Department, artyukhva@mail.ru, https://orcid.org/0000-0002-5087-6081, SPIN-code: 7412-5114.

Original article
https://doi.org/10.18019/1028-4427-2025-31-3-334-340

Antibacterial action of lysozyme against osteomyelitis agents: S. *aureus* and S. *epidermidis*

I.V. Shipitsyna✉, **E.V. Osipova**

Ilizarov National Medical Research Centre for Traumatology and Orthopedics, Kurgan, Russian Federation

Corresponding author: Irina V. Shipitsyna, ivschimik@mail.ru

ABSTRACT

Introduction The use of lysozyme as a bactericidal agent against the leading pathogens of chronic osteomyelitis can become an alternative or supplement to existing antibacterial drugs.

Purpose To study the antibacterial effect of lysozyme against clinical strains of Staphylococcus *aureus* and Staphylococcus *epidermidis*

Materials and methods Control strains of Staphylococcus aureus (ATCC 25923), Staphylococcus epidermidis (ATCC 14990) and clinical strains (n = 48), including *MRSA* (n = 6) and *MRSE* (n = 6), isolated from wounds and fistulas of patients with chronic osteomyelitis were used as test cultures. The antibacterial effect of lysozyme was assessed using the disk diffusion method.

Results Lysozyme exhibited bactericidal activity against control strains of S. *aureus* and S. *epidermidis*, the growth inhibition zone of bacteria was 11–12 mm. Among clinical strains of S. *aureus*, 87.5 % were sensitive to lysozyme, the growth inhibition zone diameter was 9–13 mm. No bactericidal effect was observed against three strains of S. *aureus*, including two *MRSAs*, and continuous bacterial growth was observed around the disk. Among strains of S. *epidermidis*, the antibacterial activity of lysozyme was observed against 79.2 % of isolates, the growth inhibition diameter was 8–11 mm. Resistance of three *MRSE* strains to lysozyme was noted. Lysozyme enhanced the effect of vancomycin and cefoxitin against methicillin-sensitive staphylococci and norfloxacin and vancomycin against methicillin-resistant staphylococci.

Discussion Despite the inhibitory effect found, the use of lysozyme alone may be limited due to its possible degradation by proteases, as well as some immunogenicity. There are studies on the synergism of the combined action of lysozyme with various antibiotics on gram-positive and gram-negative bacteria. The data obtained in our experiment showed an increased antibacterial effect by the combined action of antibiotics and lysozyme against the leading causative agents of osteomyelitis.

Conclusion It has been established that lysozyme has an antibacterial effect against clinical strains of S. *aureus*, S. *epidermidis*, including *MRSA* and *MRSE*, isolated from wounds of patients with chronic osteomyelitis. An increased antibacterial effect is observed by a combined action of lysozyme with cefotaxime, norfloxacin and vancomycin.

Keywords: chronic osteomyelitis, lysozyme, resistance, antimicrobial peptides, antibiotics

For citation: Shipitsyna IV, Osipova EV. Antibacterial action of lysozyme against osteomyelitis agents: S. *aureus* and S. *epidermidis*. *Genij Ortopedii*. 2025;31(3):334-340. doi: 10.18019/1028-4427-2025-31-3-334-340.

INTRODUCTION

Commonly, osteomyelitis is caused by bacteria of the genus Staphylococcus, mainly S. *aureus* and S. *epidermidis* (including methicillin-resistant strains *MRSA* and *MRSE*), that demonstrate a high degree of resistance to conventional antibiotics. This makes the treatment of patients with osteomyelitis difficult and requires the search for new, more effective drugs [1–4].

As an alternative or addition to existing antibacterial drugs, the use of lysozyme as a bactericidal agent against the leading causative agents of chronic osteomyelitis may be a relevant area. Lysozyme is an antimicrobial enzyme found in various biological fluids, such as saliva, tears, and breast milk [5, 6]. Lysozymes are divided into three main families: chicken type (c-type), goose type (g-type), and invertebrate type (i-type). Phage type, bacterial type, and plant type lysozymes are also known. Chicken and human lysozymes are c-type lysozymes. The chicken one consists of 129 amino acid residues (14.3 kDa), the human one of 130 amino acid residues (14.7 kDa). There is 59 % sequence identity between human and chicken lysozymes, but the antibacterial activity of chicken lysozyme is three times lower than that of the human one. However, its use is limited due to insufficient availability [5, 7, 8].

Since lysozyme is a natural component of the body, it is generally well tolerated and has a low risk of toxicity, so it is used for medical purposes. Lysozyme destroys the peptide glycans that make up the wall of bacterial cells, which leads to osmotic destruction and death of bacteria [8]. The combination of lysozyme with antibacterial drugs may enhance their effect [9, 10]. Lysozyme is also able to modulate the body's immune response [7, 8]. Currently, lysozyme is already used as preservation and antiseptic agent [6, 8]. The prospect of using lysozyme as an antibacterial agent against the leading causative agents of osteomyelitis may expand the scope of its application in medicine.

Purpose To study the antibacterial effect of lysozyme against clinical strains of Staphylococcus *aureus* and Staphylococcus *epidermidis*.

MATERIALS AND METHODS

Control strains of Staphylococcus *aureus* (ATCC 25923), Staphylococcus *epidermidis* (ATCC 14990) and their clinical strains (n = 48), including *MRSA* (n = 6) and *MRSE* (n = 6), isolated from wounds and fistulas of patients with chronic osteomyelitis were used as test cultures.

Bacteria were identified using a BactoScreen bacteriological analyzer (LLC NPF Litekh). The sensitivity of microorganisms to antibacterial drugs was determined with the disk diffusion method. The results were assessed using the EUCAST criteria (2017–2022). Detection of methicillin-resistant staphylococcal genes in the biological material was carried out with a reagent kit for detection and quantitative determination of *MSSA* and *MRSA*, *MSSE* and *MRSE* DNAs by polymerase chain reaction (PCR) with hybridization-fluorescence detection AmpliSens MRSA-screen-titer-FL.

The antibacterial effect of lysozyme was assessed using the disk diffusion method. Discs made of technical filter cardboard (GOST 6722–75) and discs with antibiotics impregnated with lysozyme (CAS–No. 9001-63-2, 20000 U/mg, AppliChem) at a concentration of 30 μg/ml were placed on the surface of a dense nutrient medium (Müller-Hinton agar) seeded with a daily culture of S. *aureus* or S. *epidermidis*. Petri dishes with the seeded cultures were incubated in a thermostat at a temperature of 37 °C. After 24 hours, the results were recorded by measuring the growth inhibition zone around the disc. The action of lysozyme on the control strains was repeated six times.

Bacterial resistance profiles of S. *aureus*, S. *epidermidis* were analyzed to four antimicrobial drugs (AMD): cefoxitin (FOX), gentamicin (GEN), norfloxacin (NOR), vancomycin (VAN).

For statistical processing of the obtained data, the Gnumeric 1.12.17 software and LibreOffice spreadsheets (version: 5.4.1.2) were used. The samples were tested for compliance with a certain distribution law using the Anderson-Darling criterion. Considering that the data in the samples were subject to normal distribution, the Student criterion was used to test the hypothesis of equality of the mean values. The digital data are presented as the arithmetic mean (M) and standard deviation (SD). Differences were considered significant at $p < 0.05$.

Microbiological studies were conducted at the microbiology laboratory of the Ilizarov National Medical Research Center of Traumatology and Orthopaedics.

RESULTS

The control strains of S. *aureus* и S. *epidermidis* were sensitive to the action of lysozyme (Fig. 1). Among the clinical isolates of bacteria, there were strains sensitive and insensitive to lysozyme.

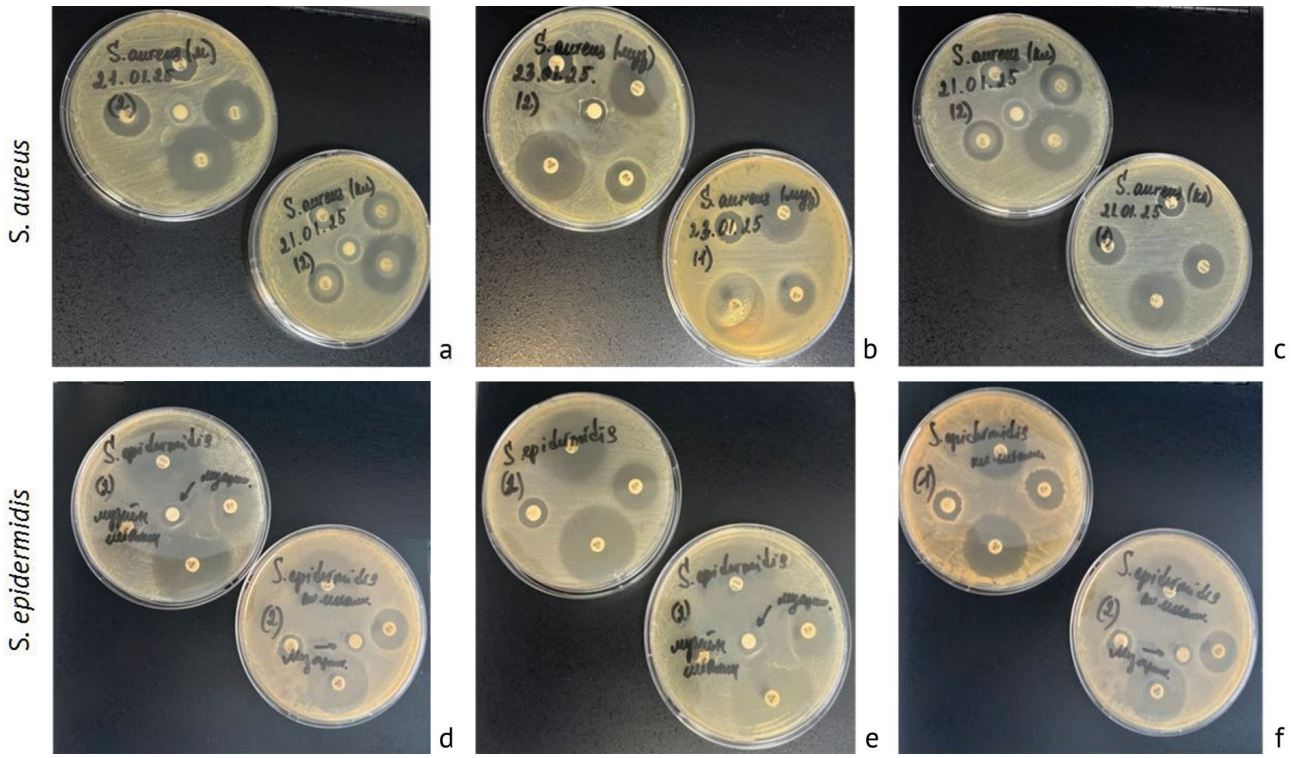

Fig. 1 Antibacterial effect of lysozyme together with and without antibiotics on the control and clinical bacterial strains of S. *aureus*, S. *Epidermidis*: (a, d) — control and clinical stains; (b, e) — control strains; (c, f) — clinical strains

No significant differences in the diameter of growth retardation were observed between the control and clinical strains (Table 1).

Table 1

Growth inhibition of the bacteria S. *aureus* and S. *epidermidis* after action of lysozyme (30 mcg/ml)

Miscroorganism	Diameter of growth inhibition zone, mm
S. *aureus* ATCC 25923 (*n* = 6)	11.3 ± 0. 47
S. *aureus* (*n* = 24)	11.2 ± 1.10
S. *epidermidis* ATCC 12228 (*n* = 6)	10.0± 0.43
S. *epidermidis* (*n* = 24)	10.5 ± 1.05

Lysozyme alone at a concentration of 30 μg/ml showed a bactericidal effect on the control strains of S. *aureus* and S. *epidermidis*, the zone of bacterial growth inhibition was 11–12 mm. Among the clinical strains of S. *aureus*, sensitivity to lysozyme was detected in 87.5 %, the diameter

of the growth inhibition zone was 9–13 mm. In relation with three strains of S. *aureus*, including two *MRSA*, no bactericidal effect was noted, continuous bacterial growth was observed around the disk.

Among S. *epidermidis* strains, antibacterial action of lysozyme was noted against 79.2 % of isolates, growth inhibition diameter was 8–11 mm. Three *MRSE* strains were found to be resistant to lysozyme.

S. *aureus* (*n* = 18) and S. *epidermidis* (*n* = 18) strains were sensitive to the action of the antibacterial drugs tested. Lysozyme enhanced the action of antibiotics, which was expressed in an increased zone of bacterial growth inhibition around the disks. Significant differences were observed for vancomycin and cefoxitin (Table 2).

Lysozyme did not enhance the effect of cefoxitin and gentamicin against methicillin-resistant staphylococci. Significant differences were observed only for norfloxacin and vancomycin (Table 3).

Table 2

Zone of growth inhibition of methicillin-sensitive staphylococci isolated from wounds of patients with chronic osteomyelitis under lysozyme action

Drug (mcg)	Diameter of growth inhibition zone, mm			
	MSSA, (*n* = 18)		*MSSE*, (*n* = 18)	
	–	+ lysozyme (30)	–	+ lysozyme (30)
Cefoxitin (30)	23.3± 0.47	26.5 ± 0.81* *p* = 0.02476	33.3 ± 2.10	35.7 ± 1.90
Norfloxacin (10)	29.0 ± 0.82	30.0 ± 0.79	31.3 ± 0.83	32.0 ± 1.40
Gentamicin (10)	19.0 ± 1.40	19.7 ±1.24	20.8 ± 6.60	22.3 ± 1.80
Vancomycin (5)	13.7 ± 0.94	15.8 ± 0.47* *p* = 0.0404	15.0 ± 0.51	17.3 ± 1.10* *p* = 0.0216

Note: * — level of significance of differences between groups, $p < 0.05$

Table 3

Zone of growth inhibition of methicillin-resistant staphylococci isolated from wounds of patients with chronic osteomyelitis under lysozyme action

Drug (mcg)	Diameter of growth inhibition zone, mm			
	MSSA, (*n* = 18)		*MSSE*, (*n* = 18)	
	–	+ lysozyme (30)	–	+ lysozyme (30)
Cefoxitin (30)	20.3 ± 0.84	20.0 ± 0.82	19.5 ± 1.10	20.0 ±0.80
Norfloxacin (10)	27.3 ± 1.25	30.2 ± 0.61* *p* = 0.0248	29.8 ± 1.03	32.2 ±0.62* *p* = 0.0242
Gentamicin (10)	18.8 ± 0.24	18.5 ± 0.20	10.7 ±0.94	12.0 ± 0.41
Vancomycin (5)	14.3 ± 0.47	14.2 ± 0.62	14.7 ±0.47	17.5 ± 0.72* *p* = 0.025

Note: * — level of significance of differences between groups, $p < 0.05$

DISCUSSION

S. *aureus* is considered a clinically significant pathogen in chronic osteomyelitis, which, interacting with the body's cells through the small colony variant (SCV), biofilm formation and toxin secretion, induces an inflammatory response, causing cell death by apoptosis and necrosis [1]. S. *epidermidis* bacteria also play an important role in the development of infections in chronic osteomyelitis [3, 11]. In the last decade, there has been an increase in the number of bacteria with multidrug resistance, which leads to the ineffectiveness of traditional approaches to the treatment of patients with chronic osteomyelitis and determines the need to search for new drugs [2, 4].

A promising direction is considered to be the use of antimicrobial peptides of the innate immune system [12]. It is known that peptides obtained as a result of lysozyme cleavage exhibit antimicrobial activity, primarily against gram-positive bacteria [13]. They can act directly (lytic effect) or indirectly (modulate the immune system). The antibacterial mechanism of lysozyme is due to its muramidase activity, which hydrolyzes the β-l.4-glycosidic bond of peptide glycans, the ability to bind to nucleic acids of microorganisms and cause mutation or decay of bacterial genetic material [5, 14, 15].

Due to differences in the mechanisms of bacterial resistance to antibiotics and antimicrobial peptides, clinical use of lysozyme has a lower risk of developing resistance in microorganisms. It is believed that resistance to peptide-degrading enzymes in bacteria develops rarely, resulting from horizontal transfer of resistance determinants rather than de novo mutation [16].

The available literature reports on an inhibitory effect of lysozyme obtained from egg white on drug-resistant bacteria, including *MRSA* [17]. In our study, 87.5 % of *MSSA*, 79.2 % of *MSSE*, and 50 % of *MRSA* and *MRSE* strains were sensitive to the action of lysozyme.

The use of lysozyme alone may be limited by the possibility of its degradation by proteases present in body fluids, as well as some immunogenicity, which may cause immune reactions when used repeatedly [18, 19]. The issue of lysozyme as an allergen remains controversial. Some researchers believe that lysozyme, being a component of the human immune system, does not cause an allergic reaction [20]. Other studies have shown that it acts as a weak allergen [21, 22]. Moreover, being applied directly on the wound surface, lysozyme can be easily washed off by exudate. In this regard, new methods for delivering lysozyme to the site of infection are being developed to increase the effectiveness of its action and reduce side effects [23]. Those include hydrogels, nanofilms, fibrous membranes and composite systems with modified lysozyme, which could improve the stability of lysozyme and reduce its immunogenicity [24, 25].

One of the alternative uses of peptides is their combination with traditional antibiotics to treat patients with osteomyelitis [26]. The data obtained in our experiment showed an increased effect of antibiotics on all sensitive microorganisms, but significant differences were found for the combination of lysozyme with vancomycin and cefoxitin. In relation to methicillin-resistant staphylococci, an increase in antimicrobial activity was noted only for the combination of lysozyme with vancomycin and norfloxacin.

The study of the combined action of lysozyme obtained from egg white with various antibiotics (gentamicin, ofloxacin, oxacillin, rifampicin, polymyxin B, vancomycin, ciprofloxacin and tetracycline) on gram-positive and gram-negative bacteria, including drug-sensitive and drug-resistant strains, a synergistic mechanism of action was established that reduces the resistance of microbes [9, 26, 27]. Antibacterial peptides change the permeability of the cell membrane, allowing more antibiotic to penetrate the cell and bind to intracellular targets, enhancing its action and reducing the side effects of high concentrations [9, 10].

Researchers have shown that the bactericidal effect of the combined action of lysozyme and antibiotics against planktonic cells and biofilms obtained *in vitro* is more pronounced compared to the use of the drugs separately [28].

At the same time, it is necessary to consider the fact that all bacteria have both general and specific mechanisms of protection against innate immunity factors. The resistance mechanisms used by gram-positive bacteria, including S. *aureus*, include changes in the charge and composition of the cell wall. The sensitivity of gram-positive bacteria to antimicrobial peptides depends on: the content of negatively charged teichoic acids in the cell wall which bind lysozymes and reduce

their enzymatic activity [8, 19]; inactivation of peptides due to their binding to surface or secreted proteins and polysaccharides; cleavage of antimicrobial peptides by bacterial proteases; adaptation of bacteria to the effects of antimicrobial peptides; displacement of antimicrobial peptides by efflux pumps and transport systems [16, 29, 30].

CONCLUSION

It has been established that lysozyme has an antibacterial effect against clinical strains of S. *aureus*, S. *epidermidis*, including *MRSA* and *MRSE*, isolated from wounds of patients with chronic osteomyelitis. An increased antibacterial effect is observed by a combined action of lysozyme with cefotaxime, norfloxacin and vancomycin.

Conflict of interest *Not declared.*

Funding *Not declared.*

REFERENCES

1. Nasser A, Azimi T, Ostadmohammadi S, Ostadmohammadi S. A comprehensive review of bacterial osteomyelitis with emphasis on Staphylococcus aureus. *Microb Pathog*. 2020;148:104431. doi: 10.1016/j.micpath.2020.104431.
2. Shipitsyna IV, Osipova EV. Monitoring of the leading gram-positive microflora and its antibiotic sensitivity in individuals with chronic osteomyelitis over a three-year period. *Genij ortopedii*. 2022;28(2):189-193. doi: 10.18019/1028-4427-2022-28-2-189-193.
3. Mironov SP, Tsiskarashvili AV, Gorbatyuk DS. Chronic post-traumatic osteomyelitis as a problem of modern traumatology and orthopedics (literature review). *Genij ortopedii*. 2019;25(4):610-621. doi: 10.18019/1028-4427-2019-25-4-610-621.
4. Besal R, Adamič P, Beović B, Papst L. Systemic Antimicrobial Treatment of Chronic Osteomyelitis in Adults: A Narrative Review. *Antibiotics (Basel)*. 2023;12(6):944. doi: 10.3390/antibiotics12060944.
5. Ovsyannikov VG, Toropkina YuE, Kraskevich VV, et al. Lysozyme — the boundaries of the possible. *Modern problems of science and education*. 2020;(3). (In Russ.) doi: 10.17513/spno.29903.
6. Potapov MI. Functions, properties and uses of lysozyme. *Trends in the development of science and education*. 2022;(84):120-124. (In Russ.) doi: 10.18411/trnio-04-2022-80.
7. Kalyuzhin OV. Antibacterial, antifungal, antiviral and immunomodulatory effects of lysozyme: from mechanisms to pharmacological use. *Effective pharmacotherapy*. 2018;(14):6-12. (In Russ.) Available at: https://umedp.ru/upload/iblock/645/Lizobakt.pdf. Accessed Mar 13, 2025.
8. Ferraboschi P, Ciceri S, Grisenti P. Applications of Lysozyme, an Innate Immune Defense Factor, as an Alternative Antibiotic. *Antibiotics (Basel)*. 2021;10(12):1534. doi: 10.3390/antibiotics10121534.
9. Zharkova MS, Orlov DS, Golubeva OY, et al. Application of antimicrobial peptides of the innate immune system in combination with conventional antibiotics-a novel way to combat antibiotic resistance? *Front Cell Infect Microbiol*. 2019;9:128. doi: 10.3389/fcimb.2019.00128.
10. Wang X, Zhang M, Zhu T, et al. Flourishing antibacterial strategies for osteomyelitis therapy. *Adv Sci (Weinh)*. 2023;10(11):e2206154. doi: 10.1002/advs.202206154.
11. Shipitsyna IV, Osipova EV. Antibiotic resistance of S. epidermidis isolated from wounds of patients with purulent infection of bones and joints. Experim*ental and Clinical Pharmacology*. 2023;86(9):43-48. (In Russ.) doi: 10.30906/0869-2092-2023-86-9-43-4814.
12. Shamova OV, Zharkova MS, Chernov AN, et al. Antimicrobial peptides of innate immunity as prototypes of new agents to fight antibiotic-resistant bacteria. *Russian Journal for Personalized Medicine*. 2021;1(1):146-172. (In Russ.)
13. Carrillo W, Lucio A, Gaibor J, et al. Isolation of Antibacterial Hydrolysates from Hen Egg White Lysozyme and Identification of Antibacterial Peptides. *J Med Food*. 2018;21(8):808-818. doi: 10.1089/jmf.2017.0134.
14. Wu T, Jiang Q, Wu D, et al. What is new in lysozyme research and its application in food industry? A review. *Food Chem*. 2019;274:698-709. doi: 10.1016/j.foodchem.2018.09.017.
15. Primo ED, Otero LH, Ruiz F, et al. The disruptive effect of lysozyme on the bacterial cell wall explored by an in-silico structural outlook. *Biochem Mol Biol Educ*. 2018;46(1):83-90. doi: 10.1002/bmb.21092.
16. Grishin AV, Karyagina AS, Vasina DV, et al. Resistance to peptidoglycan-degrading enzymes. *Crit Rev Microbiol*. 2020;46(6):703-726. doi: 10.1080/1040841X.2020.1825333.
17. Chen LL, Shi WP, Zhang TD, et al. Antibacterial activity of lysozyme-loaded cream against MRSA and promotion of scalded wound healing. *Int J Pharm*. 2022;627:122200. doi: 10.1016/j.ijpharm.2022.122200.
18. Zou L, Xiong X, Liu H, et al. Effects of dietary lysozyme levels on growth performance, intestinal morphology, immunity response and microbiota community of growing pigs. *J Sci Food Agric*. 2019;99(4):1643-1650. doi: 10.1002/jsfa.9348.
19. Ragland SA, Criss AK. From bacterial killing to immune modulation: Recent insights into the functions of lysozyme. *PLoS Pathog*. 2017;13(9):e1006512. doi: 10.1371/journal.ppat.1006512.
20. Taylor TM, Johnson EA, Larson AE. Lysozyme. In: Davidson PM, Taylor TM, David JRD. (eds.). *Antimicrobials in Food*. Boca Raton: CRC Press; 2020:445-474. doi: 10.1201/9780429058196.

21. Brasca M, Morandi S, Silvetti T, et al. Different analytical approaches in assessing antibacterial activity and the purity of commercial lysozyme preparations for dairy application. *Molecules*. 2013;18(5):6008-6020. doi: 10.3390/molecules18056008.
22. Silvetti T, Morandi S, Hintersteiner M, Brasca M. Use of hen egg white lysozyme in the food industry. In: Hester PY. (ed.). *Egg Innovations and Strategies for Improvements*. San Diego, CA: Academic Press; 2017:233-242. doi:10.1016/B978-0-12-800879-9.00022-6.
23. Wu T, Huang J, Jiang Y, et al. Formation of hydrogels based on chitosan/alginate for the delivery of lysozyme and their antibacterial activity. *Food Chem*. 2018;240:361-369. doi: 10.1016/j.foodchem.2017.07.052.
24. Gong W, Huang HB, Wang XC, et al. Construction of a sustained-release hydrogel using gallic acid and lysozyme with antimicrobial properties for wound treatment. *Biomater Sci*. 2022;10(23):6836-6849. doi: 10.1039/d2bm00658h.
25. Zhao M, Huang M, Li Z. Exploring the therapeutic potential of recombinant human lysozyme: a review on wound management system with antibacterial. *Front Bioeng Biotechnol*. 2023;11:1292149. doi: 10.3389/fbioe.2023.1292149.
26. Wu CL, Peng KL, Yip BS, et al. Boosting Synergistic Effects of Short Antimicrobial Peptides With Conventional Antibiotics Against Resistant Bacteria. *Front Microbiol*. 2021;12:747760. doi: 10.3389/fmicb.2021.747760.
27. Moravej H, Moravej Z, Yazdanparast M, et al. Antimicrobial Peptides: Features, Action, and Their Resistance Mechanisms in Bacteria. *Microb Drug Resist*. 2018;24(6):747-767. doi: 10.1089/mdr.2017.0392.
28. Thellin O, Zorzi W, Zorzi D, et al. Lysozyme as a cotreatment during antibiotics use against vaginal infections: An in vitro study on Gardnerella vaginalis biofilm models. *Int Microbiol*. 2016;19(2):101-107. doi: 10.2436/20.1501.01.268.
29. Assoni L, Milani B, Carvalho MR, et al. Resistance Mechanisms to Antimicrobial Peptides in Gram-Positive Bacteria. *Front Microbiol*. 2020;11:593215. doi: 10.3389/fmicb.2020.593215.
30. Gordina EM, Horowitz ES, Lemkina LM, Pospelova SV. The study of the stability of lysozyme to the bacteria of the genus Staphylococcus. *Diary of Kazan Medical School*. 2018;(1):12-14. (In Russ.)

The article was submitted 19.02.2025; approved after reviewing 11.03.2025; accepted for publication 31.03.2025.

Information about the authors:

Irina V. Shipitsyna — Candidate of Biological Sciences, Leading Researcher,
ivschimik@mail.ru, https://orcid.org/0000-0003-2012-3115;

Elena V. Osipova — Candidate of Biological Sciences, Senior Researcher,
E-V-OsipovA@mail.ru, http://orcid.org/0000-0003-2408-4352.

Original article
https://doi.org/10.18019/1028-4427-2025-31-3-341-349

Remodeling of articular cartilage and subchondral zone of the tibia in exo-prosthetics of the limb

T.A. Stupina[1]✉, A.A. Emanov[1], V.P. Kuznetsov[1,2], E.N. Ovchinnikov[1]

[1] Ilizarov National Medical Research Centre for Traumatology and Orthopedics, Kurgan, Russian Federation
[2] Ural Federal University named after the First President of Russia B.N. Yeltsin, Ekaterinburg, Russian Federation

Abstract

Introduction Exo-prosthetics of limbs through osseointegration opens up new possibilities in prosthetics. Modern prostheses are becoming more high-tech, which requires deep understanding of the anatomical and functional features of the bone-joint system.

Aim To identify features of structural reorganization of articular cartilage and subchondral zone of the tibia in lower leg prosthetics using an implant with calcium phosphate coating and an implant without additional coating.

Materials and methods The study was performed on 5 intact (control) and 6 experimental dogs (age 1.8 ± 0.5 years, weight 19 ± 1.2 kg). A tibial stump was modeled in the animals at the border of the middle and upper third of the diaphysis. After 2.5 months a PressFit type implant was installed. Depending on the Press-Fit type, the animals were divided into groups: group 1 made of Ti6Al4V alloy (n = 3); group 2 of Ti6Al4V alloy with calcium phosphate coating (n = 3). Duration of the experiment was 180 days after prosthesis fitting. Histomorphometric study of the articular cartilage and subchondral zone was performed on paraffin sections using an AxioScope.A1 microscope supplied with AxioCam camera and Zenblue software (CarlZeissMicroImagingGmbH, Germany).

Results Bone tissue remodeling was expressed by thinning of the subchondral bone plate, osteolysis, changes in the architecture of bone trabeculae in the subchondral trabecular bone, and a decrease in bone tissue mineralization. These signs were more intense in group 1. Signs of reparative osteogenesis with osteoblasts on the surface of bone trabeculae were noted in group 2. Subchondral bone plate thickness reduced twofold in group 1, and by 1.5 times in group 2 relative to the control. The values of the parameter of trabecular area were reduced in group 1 by 17 % and in group 2 by 10 %. Statistically significant decrease in the values of articular cartilage thickness was recorded in group 1 and was accompanied by a higher (by 1.8 times) frequency of vessels been found in the deep zone of cartilage compared to group 2.

Discussion The identified changes in the subchondral zone corresponded to stage 0 (according to the O-M classification. Aho et al., 2017): very early signs of osteoarthritis, when subchondral sclerosis is not pronounced, the subchondral bone plate is thin. Structural changes in articular cartilage corresponded to grade 0–1 according to the histological classification of the International Society for the Study of Osteoarthritis OARSI.

Conclusion Histomorphometric changes in the osteochondral component of the tibial plateau during lower leg prosthetics (thinning of the subchondral bone plate, rarefaction of the subchondral trabecular bone, penetration of vessels into non-calcified cartilage) are predictors of arthrosis. The use of implants made of Ti6Al4V alloy coated with a calcium phosphate provides reduction of bone resoption intensity and activates reparative osteogenesis.

Keywords: exo-prosthetics, titanium implant, calcium phosphate coating, articular cartilage, subchondral bone, histomorphometry

For citation: Stupina TA, Emanov AA, Kuznetsov VP, Ovchinnikov EN. Remodeling of articular cartilage and subchondral zone of the tibia in exo-prosthetics of the limb. *Genij Ortopedii*. 2025;31(3):341-349. doi: 10.18019/1028-4427-2025-31-3-341-349.

INTRODUCTION

Exoprosthetics of limbs via osseointegration provides physiological weight-bearing, osteoperceptual sensory feedback, improved range of motion in the proximal joint, which contributes to the creation of a fully functional artificial limb and opens up new possibilities for prosthetics [1–3]. Modern prostheses are becoming increasingly complex and high-tech, requiring a deep understanding of the anatomical and functional features of the musculoskeletal system [4–6]. The study of the structural reorganization of the main elements of the adjacent joint due to prosthetics is of great importance for the development of rehabilitation programs aimed at improving the quality of life of patients.

Previous studies on a single-stage technology for lower leg prosthetics showed stability and survival of the Press-Fit implant and bone formation along the entire length [7], while structural changes in the femoral condyles in the area of contact between the hyaline cartilage and the subchondral bone were detected in the adjacent joint [8]. Numerous recent studies demonstrated increasing evidence of pathological changes in the subchondral bone during the development of arthrosis [9–11]. Today, there is an urgent need to develop methods for visualization and histological quantitative assessment of the processes of subchondral bone remodeling [12, 13].

The study of the processes of implant osseointegration is aimed at improving the contact between bone tissue and the implant by acting on the composition of the implant and the microstructure of its surface [14, 15], the bone tissue regenerating on the surface of the implant [16], and also by applying medicinal and biologically active substances to the surface of the implant [17, 18].

Studies of the structural reorganization of the articular cartilage of the adjacent joint in prosthetic care are few in number; the features of the reorganization of the subchondral bone and histological predictors of arthrosis have not been studied. These facts determined the purpose of the study.

The **purpose** of the study was to identify features of structural reorganization of articular cartilage and subchondral bone of the tibia in lower leg prosthetic fitting using a calcium-phosphate coated implant and an implant without any coating.

MATERIALS AND METHODS

Study design

The study was conducted on six mongrel male dogs (age: (1.8 ± 0.5) g; body weight: (19.0 ± 1.2) kg). A tibial stump was modeled at the border of the middle and upper thirds of the diaphysis.

After 2.5 months, a Press-Fit implant was installed in the animals [19]. Then the implant was fixed and a compression load on the bone $F_н$ = 20 N was performed using a special device (Fig. 1) [20] for 35 days, followed by an exoprosthesis attachment. The animals were divided into two equal groups depending on the implant material: group 1 with an implant made of Ti6Al4V alloy (n = 3); group 2 with an implant made of Ti6Al4V alloy coated with calcium (n = 3). The experiment period was 180 days after prosthesis fitting.

Object of study: articular cartilage and subchondral plate of the tibia

As a control, the articular cartilage and subchondral bone of the tibia of three intact dogs were examined.

Ethical approval

The study was conducted in accordance with the principles of the European Convention ETS No. 123 for the Protection of Vertebrate Animals used for Experimental and other Scientific Purposes (with the

appendix of 15.06.2006, Strasbourg) and the rules of good laboratory practice (GOST 33044-2014). The protocol of the institutional ethics committee dated 29.11.2024 No. 1 (76).

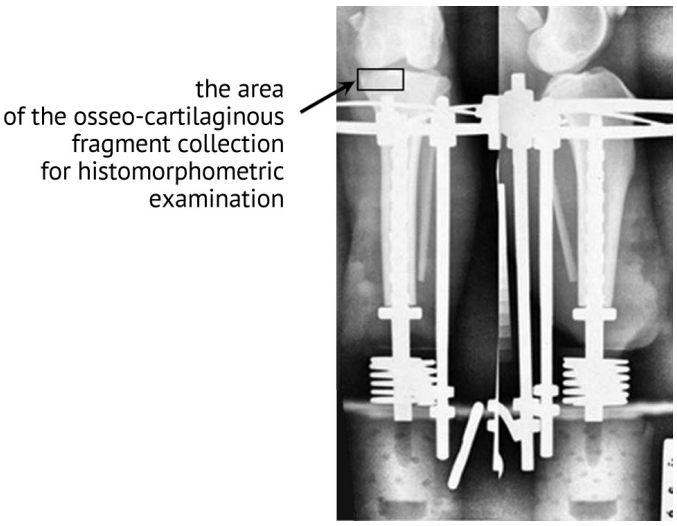

Fig. 1 Radiographs of the tibia with a prosthetic fitting using a Press-Fit implant and the installation of a compression device; the rectangle shows

Euthanasia

The animals were withdrawn from the experiment after muscle relaxation with a solution of 1 diphenhydramine (0.02 mg/kg) and 2 rometar (5 mg/kg), followed by a lethal dose of barbiturates.

Histomorphometric study

For histomorphometric study, the articular end of the tibia was exposed; soft tissues were removed, and the bone-cartilage fragments were fixed in a 10 solution of neutral formalin (pH 7.4). Then the bone-cartilage fragments were placed in a decalcifying solution consisting of a mixture of formic and hydrochloric acid solutions. After the decalcification stage, the material was washed in running water and subjected to histological processing, including the stages of dehydration, impregnation, and embedding in paraffin.

By embedding, the pieces were oriented considering the zonal structure of the articular cartilage; paraffin sections of adequate thickness [21] were used perpendicular to the articular surface and were prepared using a Thermo Scientific HM 450 microtome (USA). The main method of staining histological preparations was used: hematoxylin and eosin staining and a special method of three-color staining according to Masson with aniline blue.

Light-optical study of the preparations and digitalization of the images were performed on an AxioScope.A1 microscope with an AxioCam digital camera (CarlZeissMicroImagingGmbH, Germany). Describing the subchondral bone based on the definition of its two structural units: the subchondral bone plate and the subchondral trabecular bone [9].

For the quantitative study, Zenblue software (CarlZeissMicroImagingGmbH, Germany) was used. The following parameters were measured: thickness of non-calcified cartilage ($h_{uncal.cr}$, mm), thickness of calcified cartilage ($h_{cal.cr}$, μm), thickness of subchondral bone plate ($h_{s.b.pl}$, μm). In the subchondral trabecular bone, the area of bone trabeculae (S_{Tr}, %,) and their thickness (h_{Tr}, μm) were calculated. In the deep zone of the cartilage, the frequency of vessel was determined; this parameter was calculated as the sum of vessels in the visual fields divided by the number of all visual fields studied (an average of 20 fields were analyzed in each animal at 400-fold magnification).

Statistical methods

Quantitative data were processed in Microsoft Excel spreadsheets. Samples were assessed for normal distribution using the Kolmogorov criterion. The measure of the central tendency of morphometric parameters was presented as a median and quartiles, minimum and maximum values (*Me* (p25–p75) [min–max]) and as the mean and error of the mean (M ± m). The Mann – Whitney criterion was used to assess differences in the compared groups, and the Barnard criterion for the frequency indicator; differences were considered significant at $p < 0.05$.

RESULTS

Articular cartilage histopathology

The light-optical study of histological preparations showed that the articular cartilage of the lateral condyle of the tibia in the experimental and control groups retained its zonal structure (Fig. 2).

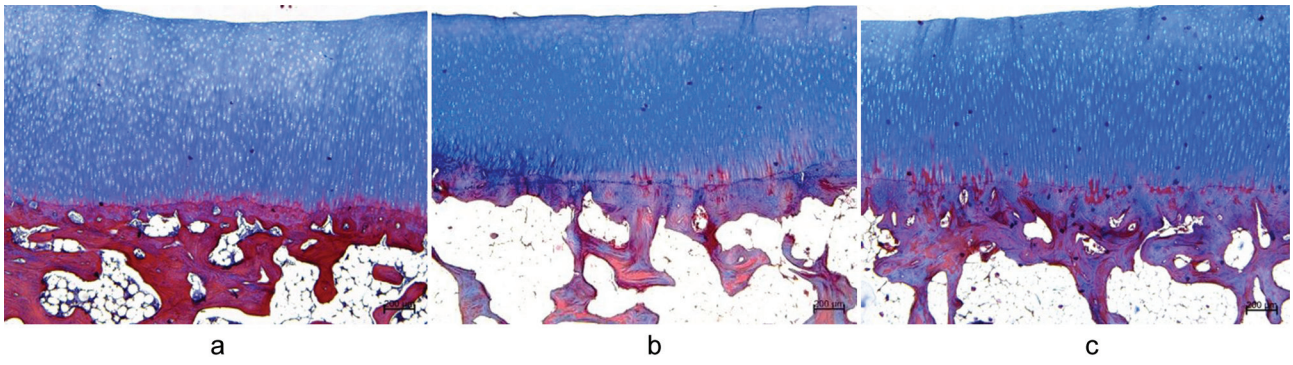

Fig. 2 Articular lining of the lateral condyle of the tibia: (a) control (intact norm); (b) group 1; (c) group 2. Paraffin sections, stained with the three-color method according to Masson, ×40

In most experimental cases, there was no tangential arrangement of cells in the superficial zone; empty cellular lacunae and acellular fields were noted; the intercellular substance of the superficial zone was unevenly stained (Fig. 3 a); difibering foci were not detected; in group 1, synovial pannus was noted in one case (Fig. 3 c).

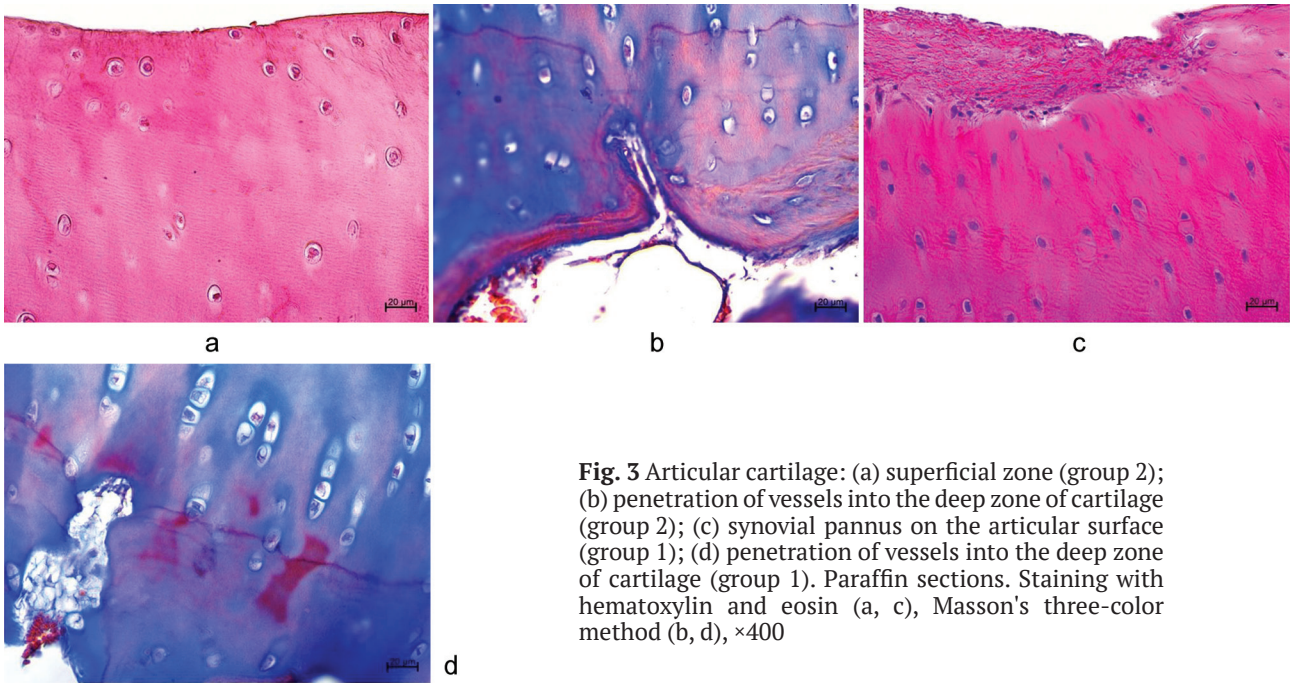

Fig. 3 Articular cartilage: (a) superficial zone (group 2); (b) penetration of vessels into the deep zone of cartilage (group 2); (c) synovial pannus on the articular surface (group 1); (d) penetration of vessels into the deep zone of cartilage (group 1). Paraffin sections. Staining with hematoxylin and eosin (a, c), Masson's three-color method (b, d), ×400

In the intermediate zone, chondrocytes were located more solely and in the form of isogenic groups consisting of two cells. In the deep zone, there was a columnar arrangement of cartilaginous cells; hypertrophied chondrocytes prevailed, some cells had signs of chondroptosis.

In both groups, areas of basophilic line disruption, penetration of vessels and bone marrow pannus into the deep zone of non-calcified cartilage were revealed (Fig. 3 b, d).

The frequency of vessels in the deep zone in group 1 was (0.65 ± 0.06), which is statistically significantly (p = 0.0148) higher than in group 2 (0.35 ± 0.02).

The thickness of non-calcified cartilage in group 1 was statistically significantly lower than in the controls; in group 2 it was comparable to the controls; the differences between the groups are statistically significant (Table 1). The values of the parameter “calcified cartilage thickness” in groups 1 and 2 are comparable with the controls (Table 1).

Table 1

Quantitative characteristics of articular cartilage and subchondral zone of the tibia in experimental groups and in controls

Groups		Parameters				
		$h_{uncal.cr}$, (mm)	$h_{cal.cr.}$(μm)	$h_{s.b.pl}$ (μm)	h_{Tr} (μm)	S_{Tr} (%)
Control	*Me*	1,28	125,93	144,11	156,47	45,21
	(Q1; Q3)	(1,21; 1,33)	(104,68; 135,66)	(87,55; 205,31)	(81,95; 234,91)	(24,73; 49,15)
	[min–max]	[1,16–1,66]	[95,98–173,84]	[60,92–223,87]	[28,23–281,94]	[20,31–51,01]
Group 1	*Me*	1,09	132,64	67,95	107,93	30,81
	(Q1; Q3)	(1,06; 1,13)	(79,92; 154,41)	(87,55; 205,31)	(59,05; 124,93)	(20,11; 35,49)
	[min–max]	[1,01–1,15]	[60,14–194,82]	[40,02–203,86]	[21,06–293,71]	[11,79–38,51]
	p	0,0001	0,3263	0,0218	0,0071	0,0102
Group 2	*Me*	1,24	120,34	97,44	112,91	37,04
	(Q1; Q3)	(1,18; 1,32)	(105,43; 129,24)	(87,97; 172,96)	(70,35; 140,54)	(28,72; 37,69)
	[min–max]	[1,15–1,79]	[75,36–189,76]	[60,92–167,86]	[56,82–195,12]	[18,28–49,01]
	p	0,5823	0,9081	0,0105	0,2801	0,0126
	p^1	0,0124	0,9528	0,001	0,0129	0,0268

Note: p level of difference as compared with the controls; p^1 level of significance of differences between groups according to the Mann-Whitney criterion, at $p \leqslant 0.05$

Subchondral bone plate histopathology

The subchondral bone plate in the control group was of uneven thickness and continuous throughout (Fig. 4 a). In the experimental groups, the subchondral bone plate was thinned; in group 1 it was absent in some places (Fig. 4 b); in group 2, areas lined with osteoblasts were seen (Fig. 4 c). The values of the parameter "thickness of the subchondral bone plate" in both groups were statistically significantly lower than the norm; the minimum values were recorded in group 1 (Table 1).

Staining histological sections with the three-color method according to Masson showed that the subchondral bone plate in the control was stained mainly red; in group 2 a decrease in the proportion of fuchsinophilic structures was noted, and in group 1, anilinophilic structures predominated (Fig. 4), which indirectly indicated a decrease in bone matrix mineralization.

In the experimental groups, rarefaction of the subchondral trabecular bone was revealed; the most pronounced signs of resorption were noted in group 1 (Fig. 5 a, b). Histomorphometric study revealed a statistically significant decrease in the values of the parameters of the area and thickness of the trabeculae in group 1 relative to the controls (Table 1), in group 2 the parameter "thickness of the trabeculae" did not have statistically significant differences with the controls, the differences between the groups were statistically significant (Table 1).

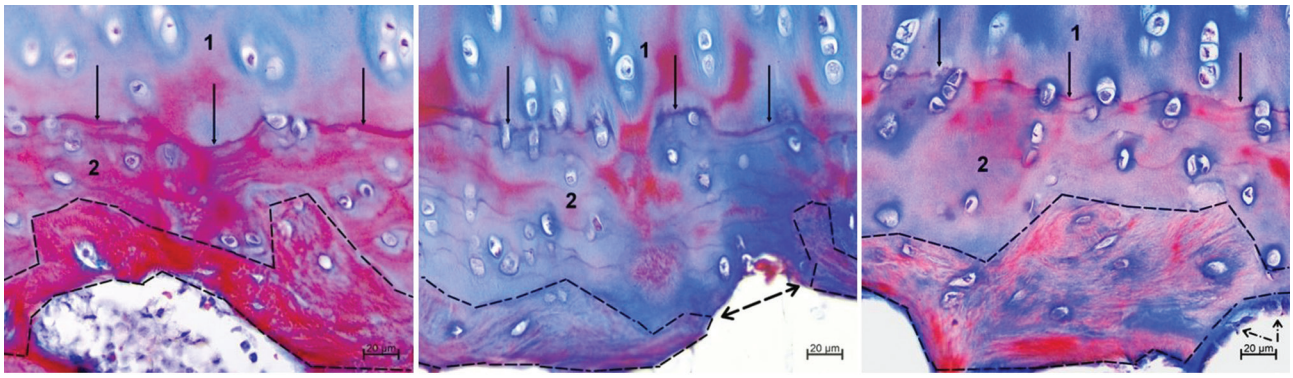

Fig. 4 Contact of the articular cartilage and subchondral bone: (a) control; (b) group 1; (c) group 2. Designations: 1 — deep zone of articular cartilage; 2 — zone of calcified cartilage; solid arrows — basophilic line; dotted line — borders of subchondral bone plate; double-edged dotted arrow — subchondral bone plate is absent; dotted arrows — osteoblasts lining the subchondral bone plate. Paraffin sections. Staining by Masson's three-color method, ×400

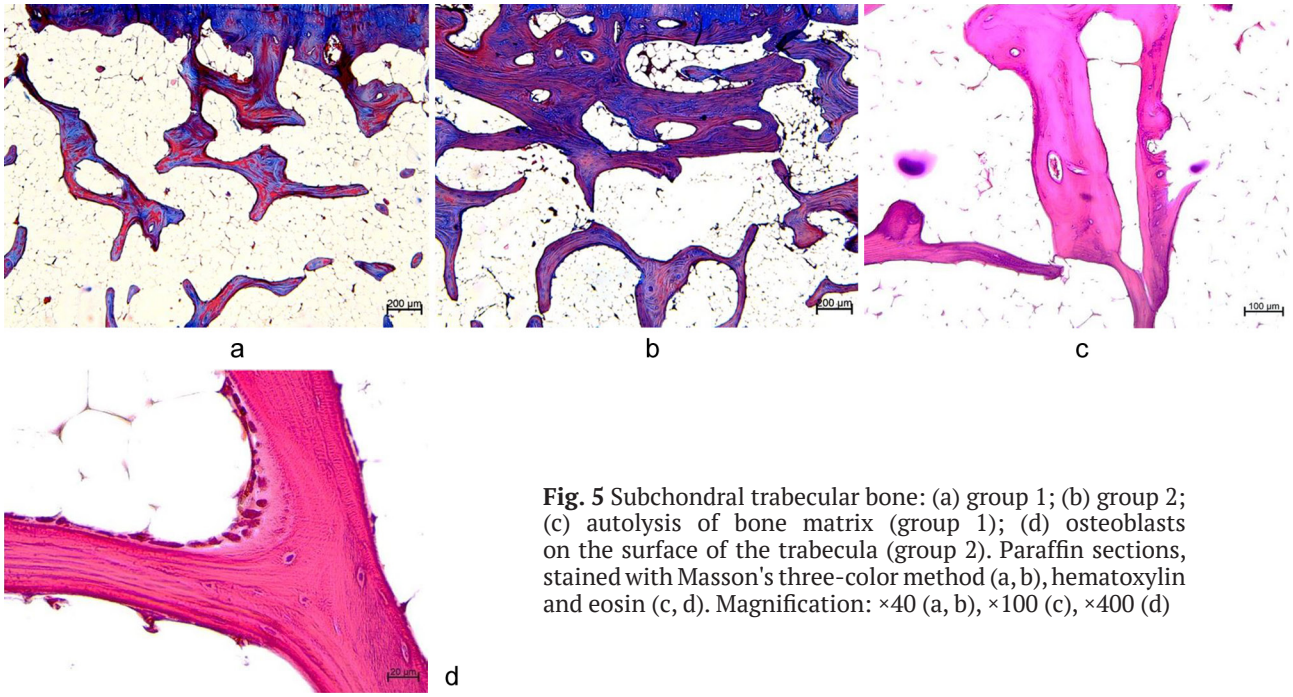

Fig. 5 Subchondral trabecular bone: (a) group 1; (b) group 2; (c) autolysis of bone matrix (group 1); (d) osteoblasts on the surface of the trabecula (group 2). Paraffin sections, stained with Masson's three-color method (a, b), hematoxylin and eosin (c, d). Magnification: ×40 (a, b), ×100 (c), ×400 (d)

In group 1, osteolytic phenomena were more frequent: autolysis of the bone matrix, splitting of the basic substance of the trabeculae along the adhesion lines (Fig. 5 c); the surfaces of the bone trabeculae did not contain cells. In group 2, there were trabecular surfaces lined with active osteoblasts producing the basic substance (Fig. 5 d).

DISCUSSION

The condition of the adjacent joint is of great importance for the restoration of the function of the prosthetic limb. Prosthetics of the lower limbs in both children and adult patients may result in contractures and deforming arthrosis in the joints located above [22]. It is known that surgical intervention on bone structures is accompanied by compensatory changes in bone tissue metabolism, the development of stress remodeling, which ensures the adaptive restructuring of bone tissue after surgery [23]. Thereby, destructive changes in the articular cartilage are noted in the adjacent joint [24, 25].

In this study, the features of subchondral zone remodeling in the tibia during exoprosthetics of the limb were studied for the first time on an experimental model using histomorphometry methods. The processes of bone tissue remodeling include thinning of the subchondral bone plate, osteolysis and changes in the architectonics of bone trabeculae in the subchondral trabecular bone, a decrease in bone tissue mineralization that was more intensely expressed in group 1, and signs of reparative osteogenesis expressed by active osteoblasts lining the surfaces of bone trabeculae in group 2. Histomorphometrically, a twofold decrease in the values of the parameter "thickness of the subchondral bone plate" in group 1 and by 1.5 times in group 2, compared to the controls, can be attributed to the processes of bone tissue remodeling. The values of the parameter “trabecular area” were reduced on average by 17 in group 1, by 10 in group 2, and the minimum values of the parameter “trabecular thickness” were recorded in group 1.

According to the classification of Aho et al. [26], the changes in the subchondral zone observed in our study corresponded to stage 0 (very early signs of osteoarthritis), when subchondral sclerosis is not expressed but the subchondral bone plate is thin.

The initiating role of the subchondral bone in the degradation of the articular cartilage was confirmed by numerous studies [27–29]. The subchondral bone, together with the articular cartilage, forms an “osteochondral” functional unit and is a mechanical basis for the articular cartilage, supporting its structure and trophism, protecting it from excessive loads [30–32].

The pathological changes in the contact zone between cartilage and subchondral bone provoke significant structural changes in the entire joint. Thinning of the subchondral bone plate and rarefaction of the subchondral trabecular bone lead to an increased load on the articular cartilage and disruption of its structure [29]. Remodeling of subchondral bone tissue is accompanied by vascular invasion into the area of calcified cartilage. The combination of vascular invasion into the articular cartilage and an increased influx of catabolic factors without inhibition of metalloproteinases ensures the progression of cartilage tissue destruction [33, 34].

The observed structural changes in the articular cartilage of the tibial plateau in lower leg prosthetic applicatoion (thinning, death of some chondrocytes in the superficial zone, uneven staining of the intercellular matrix) corresponded to grade 0–1 according to the histological classification of the International Osteoarthritis Society OARSI [35].

A statistically significant decrease in the articular cartilage thickness was observed in group 1 and was accompanied by a higher (1.8 times) of occurrence of vessels in the deep zone of non-calcified cartilage compared to group 2. The use of group 2 implants contributed to less pronounced changes in the subchondral zone.

The knowledge gained about the features of structural reorganization of the articular cartilage and the subchondral zone of the adjacent joint in the conditions of limb prosthetics is of great importance. Therapeutic strategies aimed at stimulating reparative osteogenesis can prevent joint destruction.

CONCLUSION

Histomorphometric changes in the osteochondral component of the tibial plateau in lower leg prosthetic care (thinning of the subchondral bone plate, rarefaction of the subchondral trabecular bone, penetration of vessels into non-calcified cartilage) are predictors of arthrosis. The use of implants made of Ti6Al4V alloy coated with a calcium phosphate provides reduction of bone resoption intensity and activates reparative osteogenesis.

Conflict of interests *Not declared.*

Funding source *The work was supported by the program of the Ministry of Health of the Russian Federation within the framework of the state assignment to the Federal State Budgetary Institution Ilizarov National Medical Research Center of Traumatology and Orthopedics for the implementation of research in 2024-2026.*

Ethical approval *The study was conducted in accordance with the principles of the European Convention ETS No. 123 for the Protection of Vertebrate Animals used for Experimental and other Scientific Purposes (with the appendix of 15.06.2006, Strasbourg) and the rules of good laboratory practice (GOST 33044-2014). Protocol of the institutional ethics board dated 29.11.2024 No. 1 (76).*

REFERENCES

1. Li Y, Lindeque B. Percutaneous Osseointegrated Prostheses for Transfemoral Amputations. *Orthopedics*. 2018;41(2):75-80. doi: 10.3928/01477447-20180227-03.
2. Ontario Health (Quality). Osseointegrated Prosthetic Implants for People With Lower-Limb Amputation: A Health Technology Assessment. *Ont Health Technol Assess Ser*. 2019;19(7):1-126.
3. Hoellwarth JS, Tetsworth K, Rozbruch SR, et al. Osseointegration for Amputees: Current Implants, Techniques, and Future Directions. *JBJS Rev*. 2020;8(3):e0043. doi: 10.2106/JBJS.RVW.19.00043.
4. Bates TJ, Fergason JR, Pierrie SN. Technological Advances in Prosthesis Design and Rehabilitation Following Upper Extremity Limb Loss. *Curr Rev Musculoskelet Med*. 2020;13(4):485-493. doi: 10.1007/s12178-020-09656-6.
5. Raschke SU. Limb Prostheses: Industry 1.0 to 4.0: Perspectives on Technological Advances in Prosthetic Care. *Front Rehabil Sci*. 2022;3:854404. doi: 10.3389/fresc.2022.854404.
6. Varaganti P, Seo S. Recent Advances in Biomimetics for the Development of Bio-Inspired Prosthetic Limbs. *Biomimetics (Basel)*. 2024;9(5):273. doi: 10.3390/biomimetics9050273.
7. Kuznetsov VP, Emanov AA, Gorbach EN, Gorgots VG. Implants for one-stage osteointegration with mechanobiological stimulation of bone formation. *Materials. Technologies. Design*. 2021;3(5):23-30. (In Russ.) doi: 10.54708/26587572_2021_33523.
8. Stupina TA, Emanov AA, Kuznetsov VP, Ovchinnikov EN. Assessment of knee osteoarthritis risk following canine tibial prosthetics (pilot experimental morphological study). *Genij Ortopedii*. 2021;27(6):795-799. doi: 10.18019/1028-4427-2021-27-6-795-799.
9. Li G, Yin J, Gao J, et al. Subchondral bone in osteoarthritis: insight into risk factors and microstructural changes. *Arthritis Res Ther*. 2013;15:223. doi: 10.1186/ar4405.
10. Stupina TA, Stepanov MA, Teplen'kii MP. Role of subchondral bone in the restoration of articular cartilage. *Bulletin of Experimental Biology and Medicine*. 2015;158(6): 820-823. doi: 10.1007/s10517-015-2870-4.
11. Kotelnikov GP, Lartsev YV, Kudashev DS, et al. Pathogenetic and clinical aspects of osteoarthritis and osteoarthritis-associated defects of the cartilage of the knee joint from the standpoint of understanding the role of the subchondral bone. *N.N. Priorov Journal of Traumatology and Orthopedics*. 2023;30(2):219-231. doi: 10.17816/vto346679.
12. Nagira K, Ikuta Y, Shinohara M, et al. Histological scoring system for subchondral bone changes in murine models of joint aging and osteoarthritis. *Sci Rep*. 2020;10(1):10077. doi: 10.1038/s41598-020-66979-7.
13. Dudaric L, Dumic-Cule I, Divjak E, et al. Bone Remodeling in Osteoarthritis-Biological and Radiological Aspects. *Medicina (Kaunas)*. 2023;59(9):1613. doi: 10.3390/medicina59091613.
14. Zhang YY, Zhu Y, Lu DZ, et al. Evaluation of osteogenic and antibacterial properties of strontium/silver-containing porous TiO_2 coatings prepared by micro-arc oxidation. *J Biomed Mater Res B Appl Biomater*. 2021;109(4):505-516. doi: 10.1002/jbm.b.34719.
15. Wang YR, Yang NY, Sun H, et al. The effect of strontium content on physicochemical and osteogenic property of Sr/Ag-containing TiO_2 microporous coatings. *J Biomed Mater Res B Appl Biomater*. 2023;111(4):846-857. doi: 10.1002/jbm.b.35195.
16. Drevet R, Fauré J, Benhayoune H. Bioactive calcium phosphate coatings for bone implant applications: a review. *Coatings*. 2023;13(6):1091. doi: 10.3390/coatings13061091.
17. Stogov MV, Emanov AA, Kuznetsov VP, et al. The effect of zinc-containing calcium phosphate coating on the osseointegration of transcutaneous implants for limb prosthetics. *Genij Ortopedii*. 2024;30(5):677-686. doi: 10.18019/1028-4427-2024-30-5-677-686.
18. Ivashenka SV, Astapovich AA, Jamal A. Experimental substantiation of the use of drug magnetophoresis to improve the osseointegration of dental implants. *Modern dentistry*. 2021;1:27-31. (In Russ.)
19. Kuznetsov VP, Gorgots VG, Anikeev AV, et al. *Tubular bone stump implant*. Patent RF, no. 194912, 2019. Available at: https://www.fips.ru/registers-doc-view/fips_servlet?DB=RUPM&DocNumber=194912&TypeFile=html. Accessed May 28, 2025. (In Russ.)
20. Kuznetsov VP, Gubin AV, Gorgots VG, et al. *Device for osseointegration of the implant into the bone of the stump of the lower limb*. Patent RF, no. 185647, 2018. Available at: https://www.fips.ru/registers-doc-view/fips_servlet?DB=RUPM&DocNumber=185647&TypeFile=html. Accessed May 28, 2025. (In Russ.)
21. Stupina TA, Chtchoudlo MM. A technique for quantitative evaluation of articular cartilage condition at different levels of structural organization. *Genij Ortopedii*. 2009;(1):55-57. (In Russ.)
22. Susliaev VG, Shcherbina KK, Smirnova LM, et al. Early prosthetic and orthopedic assistance in medical rehabilitation of children with congenital and amputation defects of the lower limbs. *Genij Ortopedii*. 2020;26(2):198-205. doi: 10.18019/1028-4427-2020-26-2-198-205.
23. Makarov MA, Makarov SA, Pavlov VP, Vardikova GN. Stress bone remodeling after endoprosthetic replacement of large joints and its conservative correction. *Modern Rheumatology Journal*. 2009;3(1):62-67. (In Russ.) doi: 10.14412/1996-7012-2009-526.

24. Emanov AA, Stupina TA, Borzunov DYu, Shastov AL. The features of structural reorganization of the knee articular cartilage and synovial membrane in the process of filling a postresection defect of leg bones under transosseous osteosynthesis with the Ilizarov fixator experimentally. *International Journal of Applied and Fundamental Research*. 2015;12(7):1228-1232. (In Russ.)
25. Stupina TA, Emanov AA, Antonov NI. Bone union and structural changes in the articular cartilage of the knee joint after immediate and delayed antegrade locked intramedullary nailing of femoral shaft fractures. Experimental findings. *Genij Ortopedii*. 2016;(4):76-80. doi: 10.18019/1028-4427-2016-4-76-80.
26. Aho O-M, Finnila M, Thevenot J, et al. Subchondral bone histology and grading in osteoarthritis. *PLoS One*. 2017;12(3):e0173726. doi: 10.1371/journal.pone.0173726.
27. Klementeva VI, Chernisheva TV, Korochina KV, Korochina IE. Laboratory and instrumntal study of knee joints in patients with early gonarthrosis: search for relationship. *Medical academic journal*. 2020;20(3):99-106. (In Russ.) doi: 10.17816/MAJ43455.
28. Burr DB, Gallant MA. Bone remodelling in osteoarthritis. *Nat Rev Rheumatol*. 2012;8(11):665-673. doi: 10.1038/nrrheum.2012.130.
29. Hu Y, Chen X, Wang S, Jing Y, Su J. Subchondral bone microenvironment in osteoarthritis and pain. *Bone Res*. 2021;9(1):20. doi: 10.1038/s41413-021-00147-z.
30. Pavlova VN, Pavlov GG, Shostak NA, Slutsky LI. *Joint: Morphology, clinic, diagnosis, treatment*. Moscow: Medical Information Agency Publ.; 2011:552. (In Russ.).
31. Madry H, Orth P, Cucchiarini M. Role of the Subchondral Bone in Articular Cartilage Degeneration and Repair. *J Am Acad Orthop Surg*. 2016;24(4):e45-e46. doi: 10.5435/JAAOS-D-16-00096.
32. Imhof H, Sulzbacher I, Grampp S, et al. Subchondral bone and cartilage disease: a rediscovered functional unit. *Invest Radiol*. 2000;35(10):581-588. doi: 10.1097/00004424-200010000-00004.
33. Bäuerle T, Roemer FW. Dynamic contrast-enhanced MRI for assessment of subchondral bone marrow vascularization in an experimental osteoarthritis model: a major step towards clinical translation? *Osteoarthritis Cartilage*. 2021;29(5):603-606. doi: 10.1016/j.joca.2021.03.001.
34. Dorraki M, Muratovic D, Fouladzadeh A, et al. Hip osteoarthritis: A novel network analysis of subchondral trabecular bone structures. *PNAS Nexus*. 2022;1(5):pgac258. doi: 10.1093/pnasnexus/pgac258.
35. Pritzker KP, Gay S, Jimenez SA, et al. Osteoarthritis cartilage histopathology: grading and staging. *Osteoarthritis Cartilage*. 2006;14(1):13-29. doi: 10.1016/j.joca.2005.07.014.

The article was submitted 04.02.2025; approved after reviewing 28.02.2025; accepted for publication 31.03.2025.

Information about the authors:

Tatyana A. Stupina — Doctor of Biological Sciences, Leading Researcher,
StupinaSTA@mail.ru, https://orcid.org/0000-0003-3434-0372;

Andrey A. Emanov — Candidate of Veterinary Sciences, Leading Researcher,
a_eman@list.ru, https://orcid.org/0000-0003-2890-3597;

Viktor P. Kuznetsov — Doctor of Technical Sciences, Professor, Head of Laboratory,
wpkuzn@mail.ru, https://orcid.org/0000-0001-8949-6345;

Evgenij N. Ovchinnikov — Candidate of Biological Sciences, Deputy Director for Research,
omu00@list.ru, https://orcid.org/0000-0002-5595-1706.

Original article
https://doi.org/10.18019/1028-4427-2025-31-3-350-360

Biocompatibility and osteointegrative characteristics of zirconium ceramic implants for diaphyseal defect filling

E.A. Volokitina[1]✉, M.V. Saushkin[1], I.P. Antropova[1], S.M. Kutepov[1], S.A. Brilliant[2]

[1] Urals State Medical University, Ekaterinburg, Russian Federation

[2] Institute of Immunology and Physiology Ural Branch of the Russian Academy of Sciences, Ekaterinburg, Russian Federation

Corresponding author: Elena A. Volokitina, volokitina_elena@rambler.ru

Abstract

Introduction The development of new ceramic materials with high osteointegrative characteristics and experimental substantiation of their application is an important issue in traumatology. The purpose of the work was to study the biological compatibility and osteointegrative characteristics of implants made of zirconium ceramics stabilized with yttrium, ytterbium and gadolinium for filling diaphyseal bone defects in an experiment.

Material and methods The study was performed on 18 male Chinchilla rabbits. Diaphyseal defects with intramedullary implantation of a rod made of a new ceramic porous (PC), non-porous (NPC) material and titanium alloy (TA) were modelled. The animals were divided into 3 groups based on the rod used: PC, NPC and TA (n = 6 in each). Hematological parameters were studied one day before and 8 weeks after the operation. Withdrawal of animals from the experiment, X-ray control and tissue sampling with subsequent histological and morphometric examination were performed at 8 weeks after the operation. Statistical data processing was performed using the Statistica 10 software. The Kruskal – Wallis test with subsequent intergroup analysis was used to compare the study groups. The Wilcoxon criterion was used to assess changes in dynamics in individual groups. The results are presented as median and interquartile range.

Results Eight weeks after the surgery, in the PC group compared to the NPC and TA groups the levels of leukocytes, monocytes and granulocytes were significantly lower (p = 0.025; p = 0.022; p = 0.005, respectively); no significant differences were found in other hematological parameters. The results of histomorphological studies showed that better integration of implants was observed when using PC rods compared to TA and NPC implants. The thickness of the bone trabecula in the implantation area was significantly higher in the PC group compared to the TA and NPC groups (86.2 [55.8; 109.9], 56.0 [47.2; 75.9] and 33.1 [19.0; 84.5], respectively, in both cases p < 0.001).

Discussion We studied the biocompatibility and osteointegrative properties of implants made of a new ceramic material in two versions, nonporous and porous (pore size of 10–50 μm), and compared them with titanium alloy implants. It was previously proven that alloyed ceramic materials are attractive for tissue regeneration due to their functional properties, biological activity, and therapeutic effects provided by the introduced ions. The results of our histological and morphometric studies confirmed the better biocompatibility and osteointegration of implants made of porous zirconium ceramics (PC) containing yttrium, ytterbium, and gadolinium ions, compared to implants made of NPC and TA.

Conclusion A new zirconium-based ceramic demonstrates biological compatibility. Implants with pore sizes of 10–50 μm have good osteointegrative characteristics which determine their possible use in the treatment of bone defects.

Keywords: diaphysis, bone defect, implant, zirconium ceramics, biological compatibility, osseointegration, experiment

For citation: Volokitina EA, Saushkin MV, Antropova IP, Kutepov SM, Brilliant SA. Biocompatibility and osteointegrative characteristics of zirconium ceramic implants for diaphyseal defect filling. *Genij Ortopedii*. 2025;31(3):350-360. doi: 10.18019/1028-4427-2025-31-3-350-360.

INTRODUCTION

In 2020, in peacetime, more than 11 million fractures resulting from accidents were registered in Russia. Bone injuries to the upper limbs in the structure of injuries, poisoning and other consequences of external causes amounted to 34.6 %, the lower limbs to 33.2 %, malignant neoplasms of bone tissue to 4.2 % of all oncological diseases [1]. The rate of limb injuries during military conflicts of the last decade exceeds 60–70 % and does not tend to decrease, while injuries to the lower limbs with disruption of bone integrity and weight-bearing function occur twice as often as to the upper limbs [2]. The presence of a bone defect is the cause of long-term, sometimes failed treatment, and can lead to persistent disability [3]. To compensate diaphyseal defects, various methods of auto- and alloplasty are used in combination with closed intramedullary osteosynthesis with a titanium nail or transosseous distraction osteosynthesis, as well as a combination of bone grafting technologies according to Ilizarov and Masquelet [4].

An orthopedic traumatologist must have a sufficient number of implants/augmentations of various designs, as well as a diverse arsenal of osteoplastic and bone substituting materials to treat a pathological orthopedic symptom complex and critical bone tissue defects resulting from high-energy and gunshot trauma. Autobone, allografts and demineralized matrix as bone substituting materials are often not applicable for extensive defects; there are risks of donor bed inflammation, immune reaction of recipients and rejection of a foreign implant [5]. Special bioinert durable materials and structures made of ceramics and titanium with high osteointegrative characteristics are required, which will allow not only recovery of the shape of the lost bone fragment, but also restoration of the supporting function of the limb as a whole [6, 7].

The use of artificial bone substitute biomaterials has advantages due to their compatibility with autologous bone, ease of modeling and the possibility of their use in large volumes [8]. Bioceramics have found wide application in surgical traumatology and orthopedics [6]. In Russia and abroad, various types of ceramics based on calcium phosphate are successfully used, being the closest materials in their composition and structure to human bone tissue [9], as well as zirconium ceramics due to their inertness to body tissues and good mechanical characteristics [10]. Moreover, a positive effect of zirconium on osteoblasts has been shown [11]. Research has been conducted on the modification of the chemical structure of bone substituting materials to optimize their biointegration and physical characteristics [12]. In particular, the introduction of rare earth elements into zirconium ceramics has a significant effect on the corrosion resistance of composites [13] and on the inhibition of the expression of genes specific to osteoclasts [14].

Due to the fact that the development of new ceramic materials with high osteointegrative features and experimental trials of their use for diaphyseal defects is a relevant problem in modern traumatology, the Mikroakustika LLC has developed a new ceramic material, zirconium ceramics stabilized with yttrium, ytterbium and gadolinium Zr9Y5Yb5Gd (TU-20.12.19.001-20883295-2020). The ceramic material has corrosion and erosion resistance, wear resistance, is resistant to oxidation and high-temperature sterilization.

The **purpose** of the work was to study the biological compatibility and osteointegrative characteristics of implants made of zirconium ceramics stabilized with yttrium, ytterbium and gadolinium for filling diaphyseal bone defects in experimental conditions.

MATERIALS AND METHODS

Samples for tests

A new ceramic material was studied: zirconium ceramics stabilized with yttrium, ytterbium and gadolinium. The samples were made by cold pressing followed by sintering in an atmospheric furnace. After sintering, final mechanical treatment was performed. Samples of the ceramic material of two types were prepared: non-porous and porous (pore size 10–50 μm). Rods for fracture

osteosynthesis (intramedullary implantation) 50 mm long with a round cross-section of 5 mm were fabricated from porous and non-porous materials. Rods of a similar size were made of a medical titanium-based alloy.

Experimental animals

The study was performed on 18 male Chinchilla rabbits weighing 3–3.5 kg. The animals were kept in identical feeding and housing conditions (at the vivarium of the Ural State Medical University). All animals had a veterinary certificate of quality and health. The protocol for the use and care of animals complied with the "Methodological recommendations for the maintenance of laboratory animals in vivariums of research institutes and educational institutions" RD-APK 3.10.07.02-09 and "Directive 2010/63/EU of the European Parliament and of the Council of the European Union on the protection of animals". The study was approved by the local ethics board of the Ural State Medical University, protocol dated 05.20.2020 No. 5.

Diaphyseal defect modelling and intramedullary implantation of the rod

All animals underwent bilateral modeling of the diaphyseal defect of the femurs and bilateral intramedullary osteosynthesis with rods. In accordance with the study design, the animals were divided into three groups (six in each). Non-porous ceramic (NPC) rods were implanted into the right and left femurs in the first group, porous ceramic rods (PC) were implanted in the second group, and titanium alloy (TA) rods were implanted in the third group.

Under intravenous anesthesia, the medullary canal of the femur in the intercondylar region was retrogradely drilled, and a rod made of bone substituting material was installed in the canal. Then, a linear incision of the skin and fascia was made along the lateral surface of the thigh, and access to the diaphysis of the femur was achieved layer by layer between the muscles. At the border of the middle and lower thirds of the femur, a cylindrical 10-mm long bone defect of the diaphysis was formed by double circular osteotomy which was crossed with a rod made of bone substituting materials that had been retrogradely installed in the medullary canal at the first stage of the surgical intervention. The wound was sutured layer by layer. The animals were withdrawn from the experiment; radiography of the hind limbs and tissue harvesting were performed eight weeks after the operation.

Hematological study

Blood samples were collected from the marginal vein of the rabbits' ears into standard laboratory test tubes one day before surgery and eight weeks after surgery before the animals were withdrawn from the experiment. Hematological parameters were determined using an automatic hematological analyzer Cell-70 (Biocode-Hygel, France). The study was performed according to the protocol recommended by the manufacturer.

Histological study of peri-implant bone tissue

Each sample of laboratory animal femurs, cleared of soft tissue, was fixed by immersion in 10 % buffered formaldehyde at room temperature for at least seven days. After fixation, the samples were decalcified for 48 hours in a solution of hydrochloric (11.5 ± 0.5 %) and formic (5.8 ± 0.3 %) acids, which was changed every 24 hours. Decalcified samples with partially dissolved and removed ceramic specimens, as well as with removed titanium implants, were cut to form two 2- to 4-mm-thick plates at the diaphysis level. The resulting plates were dehydrated in graded ethanol and embedded in paraffin to form blocks. Paraffin blocks were sectioned to a thickness of 3 to 4 μm, and the material was stained with hematoxylin and eosin. Histological and morphometric studies were performed using an Olympus CX-41 microscope and a Levenhuk M1000 PLUS camera. Measurements were taken using the Phenix Phmias 3.0.6731 software. Histomorphological determination of bone trabecular thickness was performed in the peri-implant area (10 measurements per sample, 60 measurements

per study group). The length of the bone trabecular surface (LBTS) formed in the implant area, the total length of the osteoblast surface (TLObS) and the total length of the osteoclast surface (TLOcS) located on the surface of these trabeculae were measured in micrometers (μm) on digital images of histological preparations captured at a total magnification of 400× (eyepiece — 10×, lens — 40×). Measurements were taken in at least 20 fields of view for one case. Next, we calculated relative indicators: the percentage of the length of each of the designated cell types. The length of the trabecula was taken as 100 %. The calculation was carried out using the formulas:

%TLObS = TLObS (μm) × 100 % / LBTS(μm);

%TLOcS = TLOcS (μm) × 100 % / LBTS (μm).

Statistical processing of the findings was performed using the methods of variation statistics in Statistica 10. The Kruskal – Wallis test with subsequent intergroup analysis was used to compare the study groups. To assess changes in dynamics (before surgery and eight weeks after surgery) in the groups, the Wilcoxon test for comparing two related (dependent) samples was used. The level of $p < 0.05$ was considered significant. The data are presented as median [interquartile range].

RESULTS

Eight weeks after the implantation of the test materials, radiography of the pelvis and both hind limbs of the experimental animals was taken (Fig. 1). Radiography showed that the area of the diaphyseal defect was bridged by a ceramic implant installed intramedullary and tightly fitted the bone tissue in certain areas. Osteotomy lines were not traced, the cortical plates in the area of the previously formed bone defect were closed. The integrity of the femur was restored.

Fig. 1 Frontal X-ray of the pelvis and both hind limbs of a rabbit with implanted ceramic rods (porous ceramics) eight weeks after surgery

Results of hematological counts of rabbits' blood samples before surgery and eight weeks after surgery are presented in Table 1. Before surgery, no significant differences were found between the groups in any of the studied indicators.

Eight weeks after the surgery, the level of leukocytes, monocytes and granulocytes was significantly lower in the PC group. It was noted that in the NPC group two months after the surgery the level of leukocytes and granulocytes demonstrated a significant increase relative to the initial level while in the PC group a significant decrease in these indicators was observed. No significant differences were found between the groups in the level of lymphocytes, although there was a tendency towards lower values in the PC group for this indicator. No significant differences were found between the studied groups in the number of erythrocytes, hemoglobin level, and volume of erythrocytes. No significant differences were found between the groups in the platelet count of the blood either. At the same time, a significant increase in the number of platelets and plateletcrit relative to the initial level was observed in the TA and NPC groups, which was apparently due to moderate reactive thrombocytosis. In the PC group, the number of platelets did not differ from the preoperative level.

Table 1

Hematological parameters of rabbits before and after surgery

Parameter	Term	Hematological indicators in the studied groups			
		Titanium (TA)	Non-porous ceramics (NPC)	Porous ceramics (PC)	*p*1
Leucocytes, ×10⁹/l	1	9.4 [8.0; 11.1]	9.9 [8.0; 10.7]	9.4 [8.0; 12.4]	0.932
	2	11.8 [10.2; 13.00]	11.7 [11.1; 12.4]	7.6 [6.9; 8.1]	**0.021**
*p*2		0.138	**0.028**	**0.028**	
Lymphocytes, ×10⁹/l	1	5.3 [4.8; 5.6]	5.7 [5.1; 7.1]	4.9 [4.1; 6.5]	0.301
	2	6.8 [6.3; 8.3]	6.60[5.9; 6.8]	4.6 [4.5; 7.2]	0.103
*p*2		**0.043**	0.686	0.675	
Monocytes, ×10⁹/l	1	0.3 [0.2; 0.3]	0.3 [0.2; 0.3]	0.3 [0.2; 0.4]	0.888
	2	0.4 [0.2; 0.5]	0.3 [0.3; 0.3]	0.2 [0.2; 0.2]	**0.043**
*p*2		0.361	0.068	0.285	
Granulocytes, ×10⁹/l	1	3.8 [3.0; 5.4]	4.0 [2.8; 3.5]	4.7 [3.9; 5.4]	0.243
	2	4.2 [4.0; 4.7]	5.2 [4.2; 5.4]	2.7 [2.4; 3.4]	**0.005**
*p*2		0.686	**0.028**	**0.028**	
Erythrocytes, ×10¹²/l	1	6.68 [6.39; 6.93]	6.90 [6.69; 7.17]	6.67 [6.42; 6.78]	0.368
	2	6.83 [6.75; 7.69]	6.82 [6.55; 7.05]	6.94 [6.52; 7.74]	0.816
*p*2		0.345	0.463	0.345	
Hemoglobin, g/l	1	144 [142; 148]	147 [144; 150]	145 [140; 148]	0.526
	2	150 [141; 152]	146 [134; 149]	148 [147; 152]	0.684
*p*2		0.686	0.295	0.281	
Hematocrit, %	1	41.8 [40.5; 41.9]	42.4 [41.3; 42.8]	41.3 [40.9; 42.8]	0.613
	2	43.7 [43.2; 44.0]	42.5 [41.0; 43.6]	42.9 [41.6; 43.1]	0.459
*p*2		0.225	0.917	0.116	
MPV, fl	1	63.2 [62.7; 63.6]	63.2 [61.9; 66.4]	63.3 [62.5; 63.8]	0.927
	2	63.1 [62.4; 64.0]	62.1 [61.0; 62.6]	63.2 [61.2; 64.0]	0.479
*p*2		0.178	0.116	0.463	
Thrombocytes, ×10⁹/L	1	372 [341; 429]	491 [473; 575]	429 [392; 508]	0.150
	2	647 [433; 700]	636 [473; 836]	496 [393; 593]	0.264
*p*2		**0.043**	**0.046**	0.249	
MPV, fl	1	5.2 [4.8; 5.5]	5.5 [5.1; 6.0]	5.5 [5.2; 5.8]	0.498
	2	5.1 [5.1; 5.4]	5.3 [4.9; 6.0]	5.2 [5.0; 5.9]	0.963
*p*2		0.500	0.465	0.753	
Plateletcrit, %	1	0.19 [0.18; 0.24]	0.27 [0.23; 0.35]	0.24 [0.22; 0.25]	0.095
	2	0.32 [0.23; 0.36]	0.32 [0.28; 0.50]	0.29 [0.21; 0.30]	0.610
*p*2		**0.043**	**0.028**	0.249	

Note: 1 — before surgery; 2 — eight weeks after surgery; *p*1 — Kruskal – Wallis test; *p*2 — Wilcoxon test

Histomorphometric evaluation of osteointegrative features of implants

Osseointegration studies in the TA group showed that a continuous band of trabecular bone, represented by both lamellar and reticulofibrous bone tissue, was formed around the implant (Fig. 2 a). Active and resting osteoblasts were visualized on the internal side of the trabeculae facing the implant (Fig. 2 c). In some small areas. loose fibrous connective tissue with moderately dilated microvessels filled with erythrocytes was found (Fig. 2 b). Particles of implantation material measuring from one to 7 μm and isolated areas with an increased accumulation of monocyte-macrophage differon cells with signs of phagocytosis were visualized (Fig. 2 c). Local inflammatory infiltrates were detected. A few resorption cavities with osteoclasts were found on the surface of the bone tissue; active osteogenesis and osteoblasts with amorphous bone substance around them were noted in some cavities. Hematopoietic fatty bone marrow occupied a significant place between the bone layer around the implant and the compact plate. The microcirculatory bed in the bone

marrow area was represented mainly by dilated thin-walled sinusoidal capillaries with signs of erythrostasis. Moderate reactive changes were noted in the compact plate. It was characterized by thickening of the adhesion lines. expansion of the Haversian canals of osteons (Fig. 2 a). In most Haversian and Volkmann canals, blood microvessels with dilated lumens surrounded by a layer of loose fibrous connective tissue were found (Fig. 2 d). Small layers of partially compacted spongy bone substance were determined on the endosteal and periosteal surfaces of the plate. Vascularized loose connective tissue was found in the intertrabecular spaces (Fig. 2 a). Osteoclastic resorption was weak. There were signs of reactive reparative restructuring of the maternal bone against the background of sluggish chronic aseptic inflammation due to mild metallosis in the peri-implant zone. The relative extent of the osteoblast surface was 57.47 %, the relative extent of the osteoclast surface was 4.5 %. In general, osseointegration of the implant was noted, the material used did not cause a pronounced negative impact on the tissues of the compact plate and bone marrow.

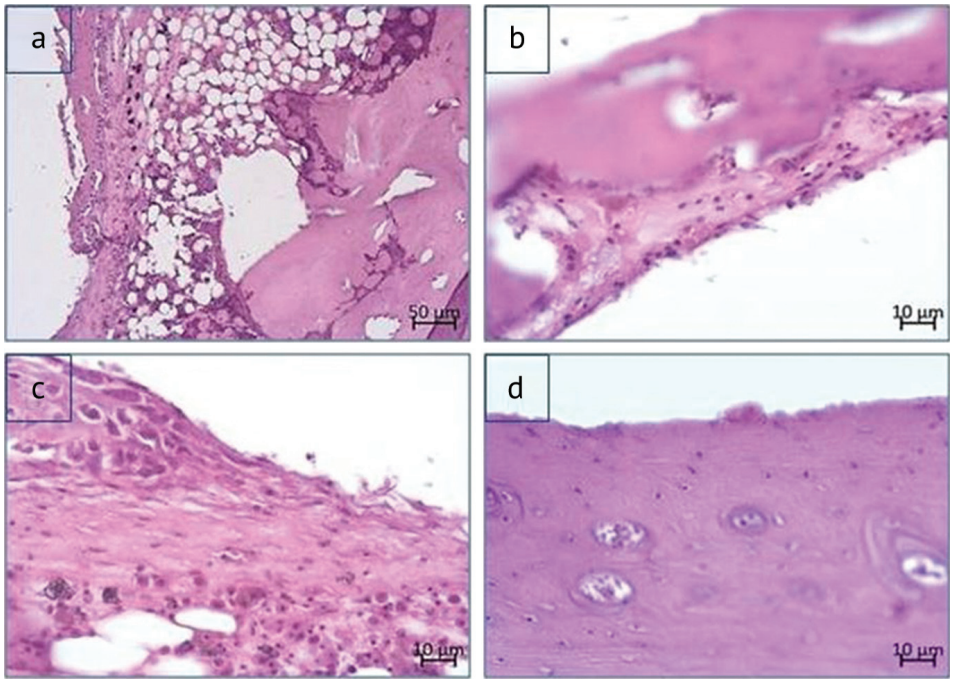

Fig. 2 Histological structure of tissues in the area of TA implantation: (a) formation of a bone "sleeve" of trabecular structure around the implant; (b) fibrous connective tissue on the surface of the trabecular bone on the side adjacent to the implant, osteoclasts are visible on the surface of the bone trabeculae; (c) area of loose fibrous connective tissue in the intertrabecular zone with signs of imbibition of the implantation material and a local focus of inflammation; (d) a compact plate with dilated Haversian canals and dilated full-blooded microvessels. Paraffin section. Stained with hematoxylin and eosin. Magnification 100 (a), magnification 400 (b–d)

In the NPC group, the histomorphological study revealed the formation of fibrous tissue with a layer of bone trabeculae on the outside at the border with the implant along its perimeter (Fig. 3 a). The connective tissue showed scarce cellularity, represented by a few fibroblastic differon cells and clusters of inflammatory cells (leukocytes, lymphocytes, plasma cells, monocyte-macrophage differon cells). Closer to the compact plate, fibrosing bone marrow with foci of inflammatory infiltrates was noted. Microvessels were few in number, mostly with fibrosed walls and obliterated lumens (Fig. 3 a). Imbibition of particles of the implantation material in the tissue of the peri-implantation area was noted (Fig. 3 b). Bone trabeculae of lamellar structure on the surface of the connective tissue sleeve had signs of chronic inflammation (Fig. 3 c). Haversian canals of the compact plate were unevenly expanded, mostly empty or filled with fibrous tissue (Fig. 3 d). Expressed osteoclastic resorption was not observed, the histological picture was probably associated with impaired bone

microcirculation and the state of the chronic inflammatory process. According to the results of the morphometric study, the relative extent of the osteoblast surface was 57.2 %, the relative extent of the osteoclast surface was 1.7 %.

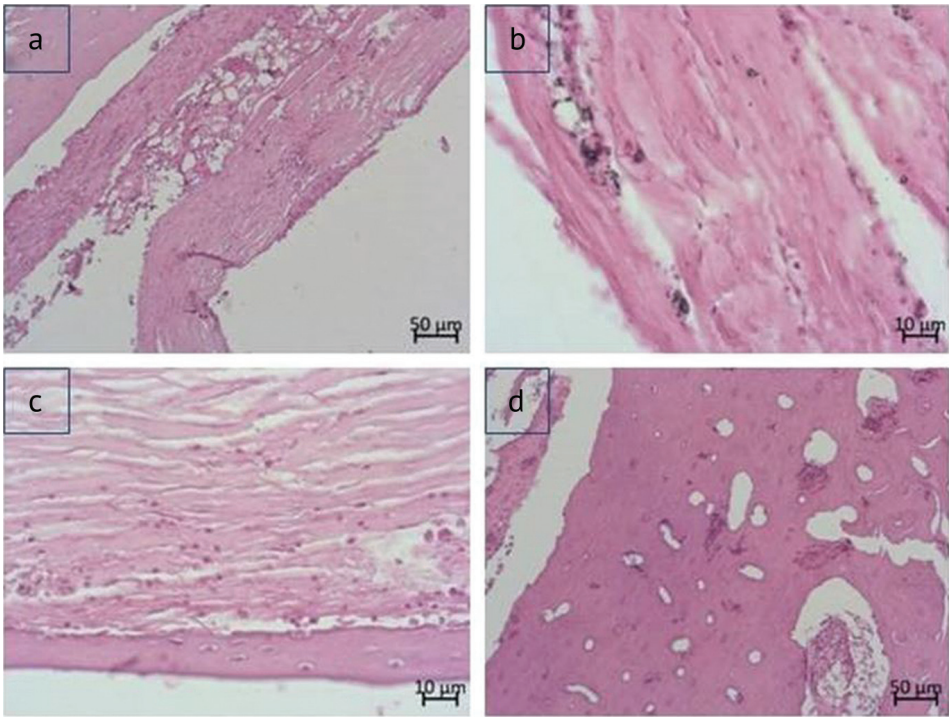

Fig. 3 Histological structure of tissues in the area of implantation of the NPC rod made: (a) formation of a fibrous sleeve with a thin trabecular layer outside around the implant, the bone marrow is fibrotic with foci of inflammatory infiltrate; (b) fibrous, poorly vascularized tissue adjacent to the implant, particles of the implantation material integrated into the connective tissue are visible; (c) bone trabeculae of a lamellar structure on the surface of the connective tissue case with signs of chronic inflammation; (d) compact plate with unevenly expanded, deserted, fibrotic Haversian canals. Paraffin section. Stained with hematoxylin and eosin. Magnification 100 (a, d); magnification 400 (b, c)

In the PC group, the results of histomorphological studies of implant osseointegration revealed that a layer of trabecular bone tissue was formed around the implant; its bone trabeculae were represented by reticulofibrous bone tissue, but closer to the compact plate the bone tissue had a lamellar structure;imbibition of material particles in the tissue of the peri-implantation area was revealed (Fig. 4 a, b). Between the compact plate and the bone tissue formed on the surface of the implant, gelatinous bone marrow with fatty inclusions and areas of hematopoiesis, or hematopoietic fatty bone marrow, were visualized. The bone marrow vessels had thin walls, were dilated and filled with blood cells and plasma, unevenly distributed in the vessel bed. On the surface of the bone trabeculae, consisting of lamellar bone tissue, functionally active osteoblasts located in a single row were more often visualized (Fig. 4 c). An active process of osteogenesis was noted on the surface and in the outer areas of the reticulofibrous bone trabeculae. Osteoclasts were rare and were often not attached to the surface of the trabeculae. However, resorption lacunae were found, filled with loose fibrous connective tissue with foci of osteogenesis or bone cells with newly formed amorphous bone substance in the pericellular space. The compact plate was characterized by widening of the lumens of some Haversian canals. On the periosteum side, foci of osteoclastic resorption were noted (Fig. 4 d). Morphometry showed that the relative extent of the osteoblast surface was 62.3 %, the relative extent of the osteoclast surface was 2.9 %. Thus, the new porous zirconium-based ceramics showed good osseointegration of the implant; the material used did not cause a pronounced negative impact on the tissues of the compact plate and bone marrow.

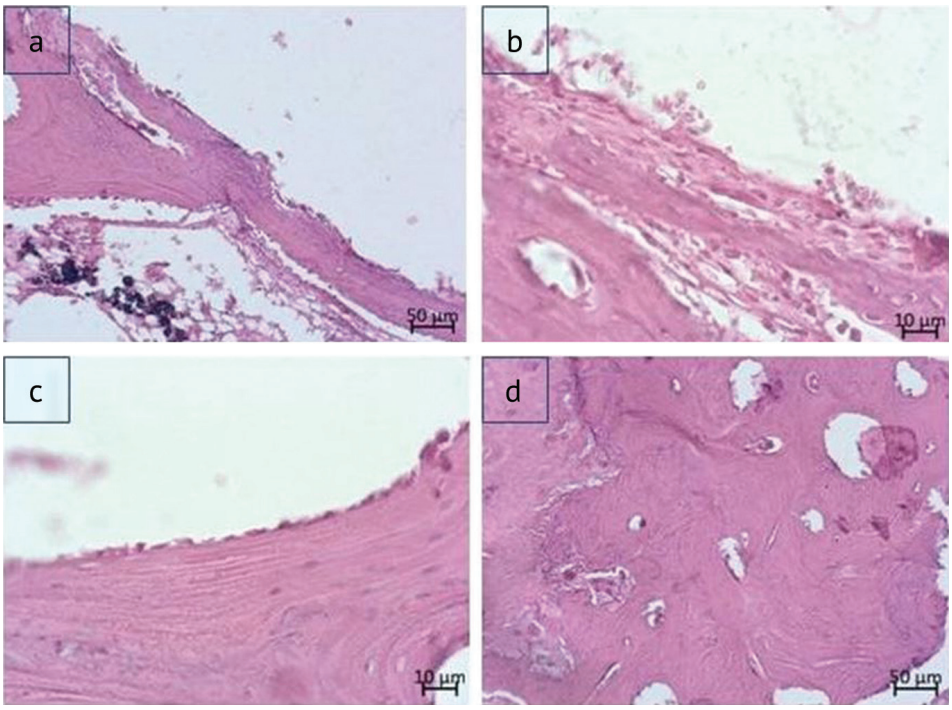

Fig. 4 Peculiarities of the histological structure of tissues in the area of implantation of a PC rod: (a) formation of a bone "sleeve" of trabecular structure around the implant, the space between newly formed bone trabeculae and the compact plate of the maternal bone is filled with hematopoietic fatty bone marrow with small areas of loose fibrous connective tissue; accumulations of particles of implanted material were found on the surface of bone trabeculae and in the intertrabecular spaces; (b) trabeculae of reticulo-fibrous bone tissue on the surface of the implant; (c) a layer of cuboid-shaped active osteoblasts on the surface of the bone trabeculae adjacent to the implant; (d) a compact plate with widened Haversian canals, enhanced adhesion lines and resorption from the periosteum. Paraffin section. Stained with hematoxylin and eosin. Magnification: 100 (a, d), magnification: 400 (b, c)

The results of histomorphological studies to determine the thickness of bone trabeculae in the implantation area in the TA, NPC and PC groups are presented in Figure 5. This indicator for the implanted porous ceramic rod was significantly higher not only compared to a titanium alloy implant ($p < 0.001$), but also compared to a non-porous ceramic implant ($p < 0.001$): 86.2 [55.8; 109.9] µm, 56.0 [47.2; 75.9] µm and 33.1 [19.0; 84.5] µm, respectively.

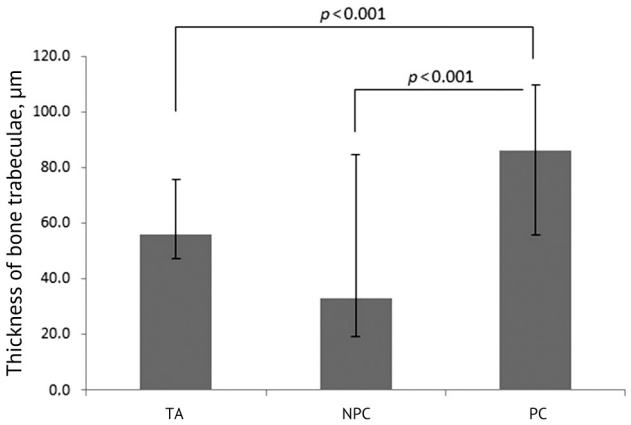

Fig. 5 Thickness of bone trabeculae in the area of implantation: titanium alloy (TA) rod, non-porous new ceramic material (NPC) and porous new ceramic material (PC) in rabbits

DISCUSSION

Due to the increase in human life expectancy and the aging of the population, the development of new materials and technologies for the functional replacement of a part of an organ or system is one of the key areas of scientific and technological strategy in the Russian Federation (Decree

of the President of the Russian Federation No. 642). Special durable materials and structures with high osteointegrative characteristics are required, which will allow not only to recover the shape of the lost bone fragment, but also to restore the supporting function of the limb as a whole [15]. Ceramic materials as bone substitutes occupy a special place due to their unique combination of properties. High strength, wear resistance, low friction coefficient allow the use of such material under high loads, and compatibility with human tissues reduces the risk of inflammation and adverse reactions [16]. Moreover, the composition of the ceramic material can be adapted to improve specific properties [17]. To improve the biological and physical efficiency of multifunctional biomaterials, metal ions are used [18]; in particular, research is being conducted on alloying ceramics with rare earth elements [19]. Such alloy ceramic materials are attractive for tissue regeneration due to their functional properties, biological activity and therapeutic effects provided by the introduced ions [20].

In our experimental study, we investigated the biocompatibility and osseointegration of implants made of a new ceramic material based on zirconium oxide containing yttrium, ytterbium, and gadolinium ions. It has been previously proven that the introduction of zirconium into the composition of ceramics significantly improves the mechanical properties of materials [21]. At the same time, the presence of zirconium in composites does not have a cytotoxic effect on pre-osteoblasts [22], improves the reaction of osteoblasts in vitro [11], and does not affect the dynamics of hematological parameters [23]. Good results were obtained in clinical studies on the use of zirconium oxide implants [24]. The introduction of yttrium into zirconium dioxide-based ceramics provides exceptional mechanical properties; such a material demonstrates cytocompatibility and does not cause cytotoxic side-effects or allergic reactions in surrounding tissues [25]. The inclusion of ytterbium and gadolinium in the ceramic material promotes the proliferation and differentiation of mesenchymal stem cells of the bone marrow, stimulates the deposition of newly formed bone and collagen, and increases the durability of the ceramics [26, 27].

We conducted a study of the reaction of the experimental animal organism to the implantation of a new ceramic material based on zirconium oxide containing ions of yttrium, ytterbium, and gadolinium. We obtained the main hematological indices in this experiment to fill diaphyseal bone tissue defects. Our study showed a similar reaction of the animal organism to the new material and the titanium alloy.

It is known that by changing the nature of the surface and porosity of the implant, its functional properties can be significantly changed. Thus, smaller pore sizes can increase molecular transport and removal of cellular metabolic waste. Conversely, large pore sizes promote cell movement [28, 29]. In our study, implants made of a new ceramic material are presented in two versions, non-porous and porous (with a pore size of 10–50 μm). It was determined that in the case of using non-porous ceramic samples and titanium alloy implants, the parameters of the leukocyte, erythrocyte and platelet blood components in the postoperative period do not have significant differences. Whereas in porous ceramics application, the level of leukocytes, the number of granulocytes and monocytes was lower than in the other two groups, which may indicate a less pronounced inflammatory process in response to the implantation of an artificial bone substitution material.

The results of previous studies prove that new bone actively forms in contact with zirconium ceramic surfaces; secreting osteoblasts are found peri-implant in large quantities [30]. Comparative studies have established that zirconium dioxide implants and titanium-based implants demonstrate similar results in terms of osseointegration indices [31, 32]. The results of our histomorphological studies have shown that the implanted rods made of porous zirconium ceramics show better integration compared to the titanium implants and the implants made of non-porous zirconium ceramics.

Titanium and non-porous ceramic rods showed moderate or insignificant osseointegration. Moreover, signs of chronic inflammation were noted, which indicated a worse survival rate of these implants.

CONCLUSION

The development of new bioceramics based on zirconium oxide and containing ions of yttrium, ytterbium, gadolinium for compensation of bone and osteoarticular critical size defects is grounded on the physical and chemical stability, high mechanical strength of the material, the possibility of demonstrating not only osteoconductive, but also osteoinductive properties. The biological compatibility of the new ceramic material for filling diaphyseal defects of bone tissue was established in an experiment on animals. Implants with pore sizes of 10–50 μm have good osteointegrative characteristics, which determines the possibility and necessity of conducting clinical trials (with the permission of Roszdravnadzor).

Conflict of interests *None.*

Ethical approval *The study was approved by the institutional ethics board of the Ural State Medical University, protocol dated 05.20.2020 No. 5.*

REFERENCES

1. *Healthcare in Russia. 2021: Stat.sb./Rosstat*. Moscow; 2021:171. Available at: https://youthlib.mirea.ru/ru/reader/1357. Accessed Mar 18, 2025. (In Russ.)
2. Krivenko SN, Shpachenko NN, Popov SV. Emergency medical care at the prehospital stage and outcome prediction for concomitant injuries with spine-and-spinal cord trauma as their component. *Genij Ortopedii*. 2015;(3):22-25. (In Russ.) https://doi.org/10.18019/1028-4427-2015-3-22-25.
3. Tsiskarashvili AV, Zhadin AV, Kuzmenkov KA, et al. Biomechanically validated transosseus fixation in patients with femur pseudarthrosis complicated by chronic osteomyelitis. *N.N. Priorov Journal of Traumatology and Orthopedics*. 2018;(3-4):71-78. (In Russ.) doi: 10.17116/vto201803-04171.
4. Borzunov DYu, Mokhovikov DS, Kolchin SN, et al. Problems and successes in the combined application of the Ilizarov and Masquelet technologies. *Genij Ortopedii*, 2022;28(5):652-658. doi: 10.18019/1028-4427-2022-28-5-652-658.
5. Mukhametov UF, Lyulin SV, Borzunov DY, et al. Alloplastic and Implant Materials for Bone Grafting: a Literature Review. *Creative surgery and oncology*. 2021;11(4):343-353. (In Russ.) doi: 10.24060/2076-3093-2021-11-4-343-353.
6. Volokitina EA, Antropova IP, Timofeev KA, Trufanenko RA. Current state and perspectives on the use of zirconium ceramic implants in traumatology and orthopaedics. *Genij Ortopedii*. 2024;30(1):114-123. doi: 10.18019/1028-4427-2024-30-1-114-123.
7. Archunan MW, Petronis S. Bone Grafts in Trauma and Orthopaedics. *Cureus*. 2021;13(9):e17705. doi: 10.7759/cureus.17705.
8. Rodríguez-Merchán EC. Bone Healing Materials in the Treatment of Recalcitrant Nonunions and Bone Defects. *Int J Mol Sci*. 2022;23(6):3352. doi: 10.3390/ijms23063352.
9. Bohner M, Santoni BLG, Döbelin N. β-tricalcium phosphate for bone substitution: Synthesis and properties. *Acta Biomater*. 2020;113:23-41. doi: 10.1016/j.actbio.2020.06.022.
10. Padhye NM, Calciolari E, Zuercher AN, et al. Survival and success of zirconia compared with titanium implants: a systematic review and meta-analysis. *Clin Oral Investig*. 2023;27(11):6279-6290. doi: 10.1007/s00784-023-05242-5.
11. Chen Y, Roohani-Esfahani SI, Lu Z, et al. Zirconium ions up-regulate the BMP/SMAD signaling pathway and promote the proliferation and differentiation of human osteoblasts. *PLoS One*. 2015;10(1):e0113426. doi: 10.1371/journal.pone.0113426.
12. Tarasova N, Galisheva A, Belova K, et al. Ceramic materials based on lanthanum zirconate for the bone augmentation purposes: materials science approach. *Chimica Techno Acta*. 2022;9(2):09. doi: 10.15826/chimtech.2022.9.2.09.
13. Willbold E, Gu X, Albert D, et al. Effect of the addition of low rare earth elements (lanthanum, neodymium, cerium) on the biodegradation and biocompatibility of magnesium. *Acta Biomater*. 2015;11:554-562. doi: 10.1016/j.actbio.2014.09.041.
14. Jiang C, Shang J, Li Z, et al. Lanthanum Chloride Attenuates Osteoclast Formation and Function Via the Downregulation of Rankl-Induced Nf-κb and Nfatc1 Activities. *J Cell Physiol*. 2016;231(1):142-151. doi: 10.1002/jcp.25065.
15. Niu Y, Du T, Liu Y. Biomechanical Characteristics and Analysis Approaches of Bone and Bone Substitute Materials. *J Funct Biomater*. 2023;14(4):212. doi: 10.3390/jfb14040212.
16. Kaur G, Kumar V, Baino F, et al. Mechanical properties of bioactive glasses, ceramics, glass-ceramics and composites: State-of-the-art review and future challenges. *Mater Sci Eng C Mater Biol Appl*. 2019;104:109895. doi: 10.1016/j.msec.2019.109895.
17. Vaiani L, Boccaccio A, Uva AE, et al. Ceramic Materials for Biomedical Applications: An Overview on Properties and Fabrication Processes. *J Funct Biomater*. 2023;14(3):146. doi: 10.3390/jfb14030146.
18. Bai L, Song P, Su J. Bioactive elements manipulate bone regeneration. *Biomater Transl*. 2023;4(4):248-269. doi: 10.12336/biomatertransl.2023.04.005.

19. Chen Z, Zhou X, Mo M, et al. Systematic review of the osteogenic effect of rare earth nanomaterials and the underlying mechanisms. *J Nanobiotechnology*. 2024;22(1):185. doi: 10.1186/s12951-024-02442-3.
20. Li H, Xia P, Pan S, et al. The Advances of Ceria Nanoparticles for Biomedical Applications in Orthopaedics. *Int J Nanomedicine*. 2020;15:7199-7214. doi: 10.2147/IJN.S270229.
21. Izmodenova MYu, Gilev MV, Ananyev MV, et al. Bone Tissue Properties after Lanthanum Zirconate Ceramics Implantation: Experimental Study. *Traumatology and Orthopedics of Russia*. 2020;26(3):130-140. doi: 10.21823/2311-2905-2020-26-3-130-140.
22. Bhowmick A, Pramanik N, Jana P, et al. Development of bone-like zirconium oxide nanoceramic modified chitosan based porous nanocomposites for biomedical application. *Int J Biol Macromol*. 2017;95:348-356. doi: 10.1016/j.ijbiomac.2016.11.052.
23. Antropova IP, Volokitina EA, Udintseva MYu, et al. Effect of Lanthanum Zirconate Ceramic on the Dynamics of Hematological Parameters and the Bone Remodeling Markers:Experimental Study. *Traumatology and Orthopedics of Russia*. 2022;28(1):79-88. (In Russ.). doi: 10.17816/2311-2905-1704.
24. Mohseni P, Soufi A, Chrcanovic BR. Clinical outcomes of zirconia implants: a systematic review and meta-analysis. *Clin Oral Investig*. 2023;28(1):15. doi: 10.1007/s00784-023-05401-8.
25. Pantulap U, Arango-Ospina M, Boccaccini AR. Bioactive glasses incorporating less-common ions to improve biological and physical properties. *J Mater Sci Mater Med*. 2021;33(1):3. doi: 10.1007/s10856-021-06626-3.
26. Liao F, Peng XY, Yang F, et al. Gadolinium-doped mesoporous calcium silicate/chitosan scaffolds enhanced bone regeneration ability. *Mater Sci Eng C Mater Biol Appl*. 2019;104:109999. doi: 10.1016/j.msec.2019.109999.
27. Zhu DY, Lu B, Yin JH, et al. Gadolinium-doped bioglass scaffolds promote osteogenic differentiation of hBMSC via the Akt/GSK3β pathway and facilitate bone repair in vivo. *Int J Nanomedicine*. 2019;14:1085-1100. doi: 10.2147/IJN.S193576.
28. Wang Z, Zhang M, Liu Z, et al. Biomimetic design strategy of complex porous structure based on 3D printing Ti-6Al-4V scaffolds for enhanced osseointegration. *Mater. Des*. 2022;218:110721. doi: 10.1016/j.matdes.2022.110721.
29. Jin HW, Noumbissi S, Wiedemann TG. Comparison of Zirconia Implant Surface Modifications for Optimal Osseointegration. *J Funct Biomater*. 2024;15(4):91. doi: 10.3390/jfb15040091.
30. Scarano A, Di Carlo F, Quaranta M, Piattelli A. Bone response to zirconia ceramic implants: an experimental study in rabbits. *J Oral Implantol*. 2003;29(1):8-12. doi: 10.1563/1548-1336(2003)029<0008:BRTZCI>2.3.CO;2.
31. Gahlert M, Roehling S, Sprecher CM, et al. In vivo performance of zirconia and titanium implants: a histomorphometric study in mini pig maxillae. *Clin Oral Implants Res*. 2012;23(3):281-286. doi: 10.1111/j.1600-0501.2011.02157.x.
32. Kohal RJ, Weng D, Bächle M, Strub JR. Loaded custom-made zirconia and titanium implants show similar osseointegration: an animal experiment. *J Periodontol*. 2004;75(9):1262-1268. doi: 10.1902/jop.2004.75.9.1262.

The article was submitted 18.02.2025; approved after reviewing 14.03.2025; accepted for publication 31.03.2025.

Information about the authors:

Elena A. Volokitina — Doctor of Medical Sciences, Professor, Head of the Department, volokitina_elena@rambler.ru, https://orcid.org/0000-0001-5994-8558;

Maksim V. Saushkin — assistant, saushkin66@mail.ru;

Irina P. Antropova — Doctor of Biological Sciences, Leading Researcher, aip.hemolab@mail.ru, https://orcid.org/0000-0002-9957-2505;

Sergey M. Kutepov — Corresponding Member of the Russian Academy of Sciences, Doctor of Medical Sciences, Professor, Chief Researcher, kcm@usma.ru, https://orcid.org/0000-0002-3069-8150;

Svetlana A. Brilliant — Candidate of Biological Sciences, Researcher, svetlana.brilliant@bk.ru, https://orcid.org/0000-0001-8640-6674.

Original article
https://doi.org/10.18019/1028-4427-2025-31-3-361-371

Experimental study of impregnation conditions for sustained antimicrobial activity of the original osteoplastic material based on cancellous bone allograft

A.P. Antipov✉, S.A. Bozhkova, E.M. Gordina, M.Sh. Gadzhimagomedov, A.A. Kochish

Vreden National Medical Research Center of Traumatology and Orthopedics, St. Petersburg, Russian Federation

Corresponding author: Alexander P. Antipov, a.p.antipov@yandex.ru

Abstract

Introduction Local antibiotic therapy is used to prevent and treat periprosthetic joint infection, but the available antibiotic delivery systems have some limitations.

The **objective** was to determine optimal parameters of pressure, exposure time and type of solvent to ensure prolonged elution of vancomycin from the original osteosubstituting material based on cancellous allograft bone using an *in vitro* experiment.

Material and methods Seven impregnation techniques with different combinations of parameters were examined including pressure: from atmospheric to reduced (7–10 hPa), time: from 5 minutes to 24 hours, solvent (distilled water, 50 % ethanol solution, a combination of 50 % ethanol and 5 % polyvinylpyrrolidone (PVP)). The efficacy was assessed by changes in the diameter of the *S. aureus* ATCC 43300 inhibition zone using the bacteriological method and the dynamics of vancomycin concentration in the eluate and high-performance liquid chromatography (HPLC). Statistical analysis was performed using the ANOVA method, Tukey's post-hoc test, Spearman's rank correlation and calculation of the area under the pharmacokinetic curve.

Results The best efficiency was demonstrated by the method employing reduced pressure, 60-minute exposure and an alcohol solution with PVP, which provided prolonged release of vancomycin for 14 days with the maximum area under the elution curve (301364.70) and a high correlation between the concentration of the antibiotic and the growth inhibition zone ($r = 0.908$, $p < 0.001$). The pressure was found to be the most significant factor ($F = 19.9916$, $p < 0.0001$), followed by solvent type ($F = 7.7485$, $p = 0.0006$) and impregnation time ($F = 6.8084$, $p = 0.0014$).

Discussion The technique with use of reduced pressure and an alcohol solution with PVP provides prolonged release of vancomycin for 14 days as opposed to conventional local antibiotic therapy with limited effectiveness of 3 to 7 days. The advantage of the approach includes uniform elution kinetics compared to polymethyl methacrylate and biodegradable carriers, which demonstrate a sharp initial release of the antibiotic. The complementary use of the microbiological method and HPLC indicated antimicrobial activity of vancomycin maintained after impregnation being essential for the therapeutic effect.

Conclusion It has been experimentally established that reduced pressure (7–10 hPa), an exposure time of 60 min and the use of 50 % ethanol with 5 % PVP as a solvent appeared to be the optimal parameters for ensuring prolonged elution of vancomycin from an osteosubstituting material based on cancellous allograft bone.

Keywords: bone-substituting material, impregnation, vancomycin, local antibiotic therapy, antibiotic elution, periprosthetic joint infection, MRSA

For citation: Antipov AP, Bozhkova SA, Gordina EM, Gadzhimagomedov MSh, Kochish AA. Experimental study of impregnation conditions for sustained antimicrobial activity of the original osteoplastic material based on cancellous bone allograft. *Genij Ortopedii*. 2025;31(3):361-371. doi: 10.18019/1028-4427-2025-31-3-361-371.

INTRODUCTION

Osteosubstitute materials (bone grafts, calcium phosphate materials, bioactive glasses, biopolymers, composite materials) are used to fill defects formed during total joint replacement, spinal arthrodesis, after radical treatment of chronic osteomyelitis and in orthopedic oncology [1]. With modern antiseptic and antibacterial agents used intra- and postoperatively infection is one of the most serious and devastating complications following orthopedic surgery [2].

Staphylococcus aureus is the most common causative agent of periprosthetic joint infection [2, 3]. The infectious process caused by this microorganism passes through several stages: penetration into the body, evasion of immune system factors, adhesion to the implant surface and formation of a biofilm [4, 5]. Cell wall components, enzymes and exotoxins of *S. aureus* contribute to the virulence by ensuring invasion and stable persistence of the pathogen in the bone [1]. Moreover, staphylococcal cells in biofilms demonstrate reduced sensitivity to antibiotics [4, 6] which leads to chronic infection, repeated surgical interventions and long-term etiotropic antibacterial therapy [7].

Systemic antibacterial therapy to be administered in the perioperative period as a standard of medical care during the interventions is used to prevent infections during implantation of a significant volume of allogeneic osteosubstituting materials which is the [8]. However, systemic antibiotic therapy can be ineffective due to insufficient blood supply at the site of the replaced defect [9]. Physical adsorption of antibiotics on the surface of osteoplastic materials is a promising method of local antibiotic therapy in the treatment of infections. Key factors of therapeutic effectiveness are to be identified in the development of osteosubstituting materials with antibacterial properties. The ability to ensure stable maintenance of a local antibiotic concentration exceeding the minimum inhibitory concentration (MIC) over a long period of time is the fundamental criterion to be considered. This condition is necessary to achieve an antibiofilm effect and prevent the selection of resistant strains of microorganisms [10]. The uniformity of antibiotic release from the osteosubstituting material is an important parameter. Previous studies have shown that a significant portion of the antibiotic elutes during the first day after implantation, which reduces the effectiveness of antibacterial therapy [11].

The **objective** was to determine optimal parameters of pressure, exposure time and type of solvent to ensure prolonged elution of vancomycin from the original osteosubstituting material based on cancellous allograft bone using an in vitro experiment.

MATERIAL AND METHODS

The biological material was obtained from the femoral heads resected during primary hip arthroplasty and immediately placed in a three-layer sterile package. The patients were examined preoperatively for antibodies to human immunodeficiency viruses HIV-1 and HIV-2, hepatitis B and C, total IgM/IgG antibodies to *Treponema pallidum* (ELISA) in the blood and signed informed voluntary consent for intraoperative bone collection. The material was frozen at –80 °C, a standard temperature for long-term storage of biological tissues to slow down protein and other molecules degradation.

Freshly frozen femoral heads were manually cleaned off the cartilage and cortical bone under sterile conditions. The remaining cancellous bone was sawn into 5×5×5 mm blocks (n = 21) to standardize the samples and facilitate placement in 10 ml test tubes. A combination of chemical and physical effects was used to delipidize and purify the material according to the method described in patent RU 2722266 C1 “Lyophilized biological biodegradable mineralized bone-plastic material and the manufacturing method” (Fig. 1).

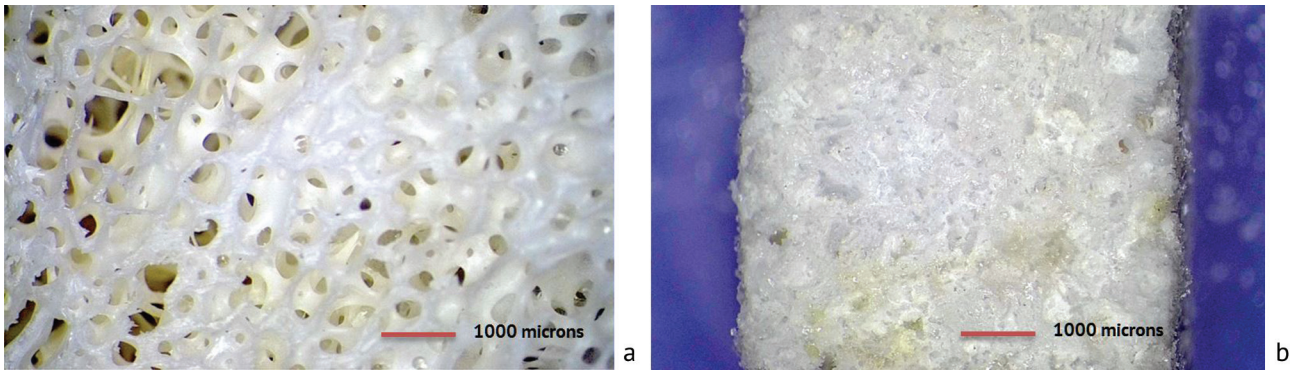

Fig. 1 Stereomicroscopic image of purified delipidized bone material prior to block cutting (a) and after block cutting and impregnation with AB vancomycin (b). Magnification 2× (Lomo, Russia)

Pressure, impregnation time and type of solvent as the three key parameters were explored to optimize impregnation of osteosubstituting material with vancomycin (Vancobact, Pharmasyntez JSC, Russia).

The pressure during impregnation varied from atmospheric (≈ 1013 hPa) to reduced (7–10 hPa) at a solution temperature of +2 °C to +8 °C. The pressure allowed for conditions under which the water was in a pre-boiling state to ensure the best penetration of the antibiotic into the porous structure of the material and the effective impregnation.

The impregnation time period ranged from 5 min to 24 h. Short impregnation periods (5 and 60 min) were used to assess the possibility of rapid saturation of the material with antibiotic, which is important for the practical application of the method and the potential reduction in the overall manufacturing time of the final product. Long-term exposure (24 hours) allowed us to estimate the maximum possible degree of material saturation under various conditions.

The following solvents were used:

1) distilled water (H_2O) as a base solvent;

2) 50 % ethanol solution with better penetrating ability due to lower surface tension;

3) a combination of 50 % ethanol with 5 % polyvinylpyrrolidone (PVP), where the polymer additive was supposed to provide better stabilization and retention of the antibiotic in the transplant structure.

The volume of the solution depends on the calculated density of the solvents, based on the need to achieve a mass percentage of the antibiotic of 5 %. The aqueous solution has a density of approximately 1 g/ml, while a 50 % alcohol solution has a lower density (~0.93 g/ml) and the density of the solution slightly increases (~0.94 g/ml) with use of a 50 % alcohol solution with the addition of PVP. Three cancellous bone samples were used for each method. A comparative analysis of the methods was produced by sequential changing of one parameter with fixed values of the others (Table 1).

Table 1

Methods of impregnation of samples of original osteosubstituting material with vancomycin

No	Solvent	V of the solution, mL	Pressure, hPa	Impregnation time
1	H_2O	20	≈1013	60 min.
2	H_2O	20	≈1013	24 h
3	H_2O	20	7–10	5 min.
4	H_2O	20	7–10	60 min.
5	H_2O	20	7–10	24 h
6	Ethanol 50 %	21.5	7–10	60 min.
7	Ethanol 50 % + PVP 5 %	21.2	7–10	60 min.

For a comparative study of the duration of antibacterial activity, each impregnated sample was placed in a separate sterile tube containing 3 ml of physiological solution. A sample without vancomycin was used as a negative control. Incubated at 37 °C for 18–24 hours. The samples were transferred to fresh saline after 24 hours and continued to be incubated under the same conditions. A suspension of the test isolates with an optical density of 0.5 by McF was prepared, applied with a cotton swab to Mueller-Hinton agar and distributed over the surface. Reference strains of *S. aureus* ATCC 43300 (MRSA) with a vancomycin MIC of 1.5 mg/ml were used as test strains. A suspension of the daily bacterial culture (0.5 McF) was distributed over the surface of Mueller-Hinton agar. After each day of incubation, 10 µl of the incubation solution with samples were applied to the bacterial lawn in three replicates and incubated for 24 hours at 37 °C. The formation of a growth inhibition zone at the site of application of a drop of supernatant was assessed as the presence of a sufficient concentration of vancomycin to inhibit bacterial growth. The dynamics of vancomycin elution were assessed visually by the presence and size (diameter, mm) of the MRSA growth inhibition zone (Fig. 2). The physiological solution was replaced daily and fresh saline was added to the sample tube. The procedure was repeated until there was no visible growth inhibition zone in the Petri dishes.

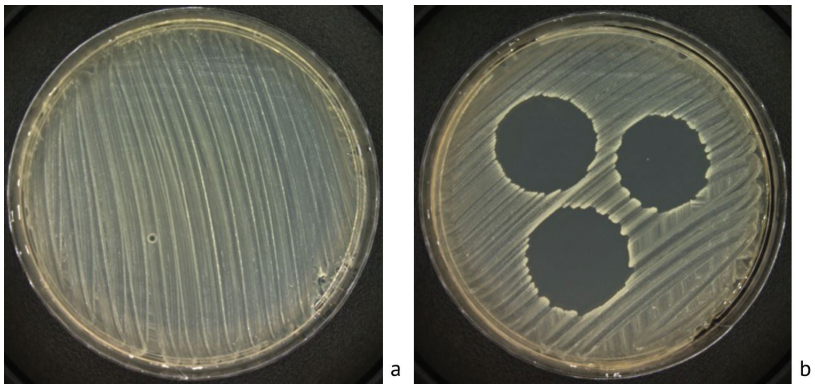

Fig. 2 Petri dishes with *S. aureus* ATCC 43300 (MRSA) culture 10 days after the start of the experiment: (a) no growth inhibition zone, method 1; (b) growth inhibition zone at the site of drop application, method 7

The concentration of vancomycin in the incubation solution was determined by high-performance liquid chromatography (HPLC) on a SHIMADZU device, Shim-pac HR-ODS column (Japan). From test tubes with samples, 1 ml of the daily incubation solution was transferred to Eppendorf tubes and centrifuged for 5 min., 13,000 rpm. Then the supernatant was transferred to a vial and placed in the chromatograph. The volume of the injected sample was 100 µl. Flow rate was 0.45 ml/min. The test lasted for 25 min. The vancomycin retention time on the chromatogram was 8.5 min. During the first 7 days, the incubation solution was diluted 1000 times, and the concentrations were multiplied by the dilution factor. Standard vancomycin solutions in concentrations from 0.1 to 10 mg/ml were used for HPLC calibration. The calibration curve was plotted based on the peak area corresponding to the vancomycin retention time (8.5 min). Chromatographic analysis was performed in LabSolutions software, ensuring accuracy and reproducibility of measurements by performing triplet analyses of each sample.

Statistical analysis was used to process the data in order to determine significant differences between vancomycin impregnation methods. Primary data were recorded in Microsoft Excel 2019, Version 16.72. The normality of distribution was tested using the Shapiro – Wilk test as the most powerful for small and medium-sized samples ($n < 50$). All quantitative indicators demonstrated normal distribution ($p > 0.05$). Quantitative data were presented as mean ± SD. One-way analysis of variance (ANOVA) was used to compare means between groups, followed by Tukey's post-hoc test to detect pairwise comparisons because:

— all groups had equal sample size;

— pairwise comparisons between all groups were needed;

— Tukey's test provided good control of Type I error maintaining sufficient statistical power.

The area under the pharmacokinetic curve (AUC, Area Under Curve) was calculated as an integral pharmacokinetic indicator of vancomycin elution during the observation period using the trapezoid method. The calculation was produced using GraphPad Prism 9.0 software (GraphPad Software, USA) based on the experimentally obtained drug concentrations at various time points (from 1 to 14 days). The Spearman correlation coefficient was used to assess correlation between vancomycin concentration and the zone of growth inhibition. The significance threshold was set at $p < 0.05$. The determination coefficient (R^2) was used to assess the degree of compliance of the experimental data with the exponential model. All statistical analyses were performed using Microsoft Excel 2019, Version 16.72, IBM SPSS Statistics, Version 23.0.0.0 (USA), MacOS, Monterey 12.2.1.

RESULTS

Analysis of the antibacterial activity of various impregnation methods for *S. aureus* (MRSA) demonstrated comparable efficiency with growth inhibition zones in the range of 20.7–24.7 mm (Table 2) on the first day of observation. Some groups of samples reduced the activity after two days.

Table 2

Dynamics in the diameter of MRSA growth inhibition zones in groups of samples impregnated with different methods

Day	Diameters of MRSA growth inhibition zones using different methods, M ± SD, mm						
	Method 1	Method 2	Method 3	Method 4	Method 5	Method 6	Method 7
1	22.0 ± 0.0	21.7 ± 0.6	24.0 ± 0.0	23.3 ± 1.6	24.7 ± 0.6	20.7 ± 0.6	22.3 ± 1.2
2	16.7 ± 2.3	18.3 ± 0.6	20.0 ± 0.0	20.7 ± 0.6	20.7 ± 0.6	20.7 ± 0.6	22.3 ± 1.2
3	15.3 ± 0.6	16.0 ± 1.7	16.3 ± 1.2	16.7 ± 0.6	15.3 ± 1.5	15.3 ± 0.6	22.0 ± 0.6
4	9.0 ± 0.0	12.7 ± 1.2	14.0 ± 3.5	14.0 ± 3.6	16.7 ± 1.5	15.7 ± 2.5	16.7 ± 1.5
7	b/d*	b/d	12.0 ± 0.0	13.3 ± 1.2	15.3 ± 1.2	15.3 ± 1.2	16.0 ± 0.0
8	b/d	b/d	8.0 ± 0.0	8.7 ± 0.6	13.3 ± 1.2	13.7 ± 0.6	15.0 ± 1.0
9	b/d	b/d	b/d	8.0 ± 0.0	9.3 ± 2.3	11.7 ± 2.5	13.0 ± 13.0
10	b/d	b/d	b/d	b/d	9.0 ± 0.0	8.7 ± 0.6	10.7 ± 2.3
11	b/d	b/d	b/d	b/d	b/d	5.3 ± 4.6	8.0 ± 0.0
14	b/d	b/d	b/d	b/d	b/d	b/d	8.0 ± 0.0

Note: b/d — values below the detection limit of the method (0.0 ± 0.0); data are presented as mean ± standard deviation (M ± SD), $n = 3$ for each group.

Statistical analysis of the results revealed significant differences in the effectiveness of the antimicrobial treatment methods. One-way analysis of variance (ANOVA) showed statistically significant differences in the dynamics of the diameter of MRSA growth zone suppression in samples impregnated with different methods ($F = 4.8192$, $p = 0.0001$). Impregnation in an aqueous solution of antibiotic at atmospheric pressure was the least effective, and increasing the time from 60 min to 24 h had no impact on the duration of antimicrobial activity (AMA) of samples impregnated by methods 1 and 2. Saturation of samples in an aqueous solution of antibiotic under negative pressure did not lead to a significant prolongation of the antistaphylococcal activity. The use of an alcohol solution for impregnation under vacuum conditions was the most effective in comparison with methods 1 and 2 ($p = 0.0283$ and 0.05). The impregnation of 5 min., 60 min. and 24 hours showed no significant effect of time on the duration of AMA of samples groups 5, 6 and 7, respectively (p from 0.9476 to 1.0 in pairwise comparisons). Statistical analysis of the dynamics in the diameters of the MRSA growth inhibition zones using the Tukey post-hoc test showed that this parameter for samples impregnated with methods 5, 6 and 7 was statistically significantly higher than the indicator for method 1; in addition, the indicators for method 7 were significantly better

than those for method 2 ($p = 0.0023$) (Fig. 3). A detailed study of the influence of impregnation parameters on the duration of antimicrobial activity showed that pressure was the most significant factor ($F = 19.9916$, $p < 0.0001$), followed by the type of solvent used ($F = 7.7485$, $p = 0.0006$) and impregnation time ($F = 6.8084$, $p = 0.0014$). All the parameters showed a statistically significant influence on the efficiency of the impregnation process.

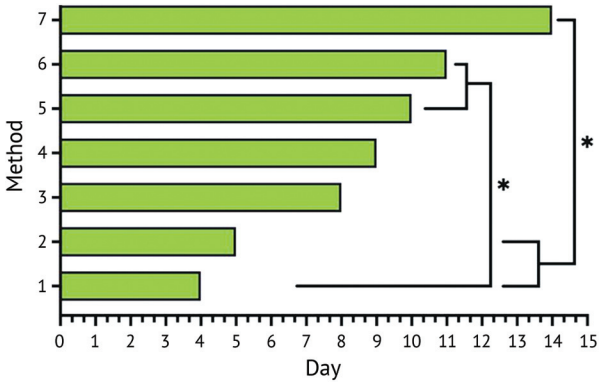

Fig. 3 Duration of in vitro antimicrobial activity of samples with different impregnation methods; * — $p < 0.05$

Analysis of the results of vancomycin elution evaluated by HPLC showed significant differences between the impregnation methods (Table 3). The duration of effective elution ranged from 4 to 14 days, with the least total amount of vancomycin isolated from samples impregnated according to Method 1 using an aqueous solution and atmospheric pressure and the largest amount was isolated from samples saturated in an alcohol solution with a polymer under vacuum conditions (method 7).

Table 3

Dynamics of vancomycin concentration in incubation solution with samples impregnated in different ways

Day	Vancomycin concentration, M ± SD, μg/ml						
	1	2	3	4	5	6	7
1	23658 ± 1183	18747 ± 938	21551 ± 1078	25001 ± 1250	65258 ± 3263	44679 ± 2234	82755 ± 2069
2	258 ± 13	3234 ± 162	4287 ± 215	7839 ± 392	17894 ± 895	17516 ± 876	99578 ± 4979
3	574 ± 29	1234 ± 62	1852 ± 92	2816 ± 141	4648 ± 233	5791 ± 287	92877 ± 4644
4	447 ± 3	246 ± 13	1554 ± 75	1755 ± 88	3780 ± 189	5260 ± 263	45621 ± 2281
5	b/d*	36 ± 2	1354 ± 68	489 ± 25	1957 ± 98	3649 ± 183	9658 ± 483
6	b/d	b/d	823 ± 41	546 ± 28	933 ± 47	2846 ± 143	5710 ± 286
7	b/d	b/d	450 ± 23	480 ± 24	784 ± 39	1120 ± 56	3903 ± 195
8	b/d	b/d	129 ± 7	238 ± 12	417 ± 21	490 ± 25	1244 ± 62
9	b/d	b/d	b/d	38.1 ± 2.0	236.1 ± 12.0	166.9 ± 8.0	987 ± 50
10	b/d	b/d	b/d	b/d	45.0 ± 2.3	69.0 ± 3.5	259 ± 13
11	b/d	b/d	b/d	b/d	b/d	43.0 ± 3.4	54.1 ± 2.7
14	b/d	b/d	b/d	b/d	b/d	b/d	27.9 ± 1.4
Total release	24937 ± 1183.5	23497 ± 954.8	32000 ± 1112.6	39202.1 ± 1314.8	95952.1 ± 3384.9	81629.9 ± 2414.8	342674 ± 7507.3

Note: b/d — values below the detection limit of the method (0.0 ± 0.0); data are presented as mean ± standard deviation (M ± SD), $n = 3$ for each group; total release calculated as the sum of the average values for the observation period, μg/ml.

It was found that increasing the impregnation time in an aqueous solution of the antibiotic at atmospheric pressure from 60 min. to 24 h statistically increased the concentration of vancomycin in the incubation solution throughout the observation period ($p < 0.05$). The most pronounced differences were observed after two and four days ($p = 0.0000$).

Increasing the saturation time of the samples in an aqueous solution under vacuum from 5 to 60 min showed no significant differences in the concentration of the antibiotic isolated on the first day ($p > 0.05$), and the concentration of vancomycin eluted from the samples in method 4 was 1.4–1.8 times higher than in method 3 after 2 to 3 days ($p = 0.0001$). A similar trend was revealed when analyzing the effect of pressure on the intensity of the antibiotic release. A similar trend was revealed when analyzing the effect of pressure on the intensity of antibiotic release. Samples inoculated with methods 1 and 4 showed no significant differences in vancomycin release on the first day ($p = 0.2479$), however, differences in the concentration of the antibiotic in the incubation

solution were statistically significant after two days ($p = 0.0000$). Increasing the impregnation time of samples in an aqueous solution in a vacuum to 24 hours (method 5) showed the highest saturation efficiency of all the methods using distilled water, both in terms of the duration of vancomycin elution and the concentration ($p < 0.05$).

A 60-min impregnation in an alcoholic antibiotic solution (method 6) under vacuum conditions was comparable to 24-h saturation in an aqueous solution (method 5) ($p > 0.05$) in terms of the duration of vancomycin elution and the total mass of antibiotic released. Addition of the polymer to the alcoholic antibiotic solution (method 7) provided the longest elution time (14 days) and the highest amount of released antibiotic among the methods.

The area under the elution curve (AUC) demonstrated significant variability between groups. The minimum value was recorded with method 1 (13108.00), then a consistent increase in the indicator was observed: method 2 (14123.50), method 3 (21224.50), method 4 (26701.60), method 5 (63323.10), method 6 (59333.40). The maximum AUC value was achieved with method 7 (301364.70), which exceeded the indicator by more than 23 times for method 1 and by 5 times for method 6.

The results indicated a significant influence of both impregnation time and pressure on the elution characteristics, with the greatest efficiency achieved when using a combined solvent with the addition of PVP.

Assessment of the correlation between the concentration of vancomycin in the incubation fluid and the zones of inhibition of microorganism growth (Fig. 4) indicated the strongest correlation for samples of group 7 ($r = 0.908$; $p < 0.001$), which indicated a high degree of linear dependence between the parameters. Methods 4, 5 and 6 demonstrated statistically significant correlations ($p < 0.05$), with correlation coefficients of 0.809, 0.822 and 0.723, respectively. Method 3 showed borderline statistical significance ($r = 0.796$; $p = 0.058$), while Methods 1 and 2 did not reach the level of statistical significance ($p > 0.05$) despite high correlation coefficients (0.777 and 0.870, respectively).

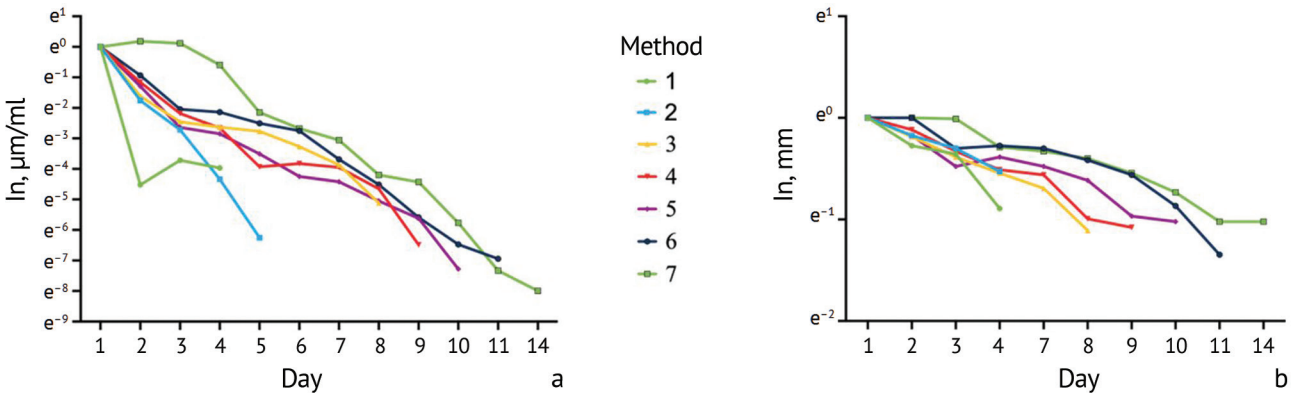

Fig. 4 Dynamics: (a) of vancomycin elution from samples impregnated with different methods; (b) of changes in growth inhibition zones of *S. aureus* (MRSA)

The exponential decay analysis revealed a high degree of confomity of the exponential model for most groups, as confirmed by the values of the coefficient of determination (R^2). Group 2 showed an almost perfect conformity ($R^2 = 0.990$) and the steepest slope of the exponent (–1.509) indicating the fastest decrease in indicators in this group. Groups 3–7 showed similar exponential decay characteristics with $R^2 > 0.91$ and flatter slopes ranging from –0.591 to –0.778. Notably, Group 1 showed the lowest conformity to the exponential model ($R^2 = 0.484$) with a relatively steep slope (–1.111).

The exponential dependence of the antibiotic release kinetics demonstrated the importance of a comprehensive assessment of several key parameters: the duration of antimicrobial activity, the total dose of the released antibiotic and the area under the pharmacokinetic curve (AUC), which together determine the therapeutic efficacy of local antibiotic therapy.

DISCUSSION

Local antibiotic therapy in modern orthopedic surgery demonstrates high efficiency in the prevention and treatment of infectious complications after operations (arthroplasty, vertebrology, maxillofacial surgery, oncology, purulent osteology) [12–15]. Literature analysis indicates significant progress in the development and implementation of various systems for local delivery of antibacterial drugs [16–18].

Polymethyl methacrylate (PMMA), as a traditional material for local antibiotic therapy, provides stable, but not prolonged release of the antibiotic when mixed with vancomycin lasting from 1 to 9 days and up to 14 days in exceptional cases [19–21]. In addition to disadvantages of bone cement including re-intervention [16, 22] and the risk of bacterial colonization with the formation of primary biofilms on the PMMA surface in the first 18 hours [23, 24], only 7 % of the total amount of antibiotic used is eluted into the surrounding tissue [25]. Increased local concentration of the antibiotic through increased mass of the added drug (more than 6 g per 40 g of PMMA) reduces the mechanical strength of the cement, which does not meet ISO standards [26].

As an alternative for creating a local depot, biodegradable carriers (calcium sulfate, biodegradable polyurethane, polyethyl acetate, polylactide-coglycolide and polylactide) are reported [12, 27] with local concentrations being approximately ten times higher than with PMMA but remained below reported cell toxicity thresholds[28]. However, complete resorption of the implants after 6 weeks (range 30–60 days), outpacing the rate of bone formation can lead to the formation of bone cavities, fractures and recurrent infection [29]. The kinetics of antibiotic release from all carriers is characterized by an initial peak release after 48 hours: (9862 ± 1782) ng/ml for PMMA spacers; (38394 ± 7071) ng/ml for PMMA beads, with a subsequent gradual decrease in local concentration [30]. Biodegradable materials demonstrate a faster and more complete release of antibiotics compared to PMMA (CaSO4 during the first three days) [22]. In our series Method 7 demonstrated a smoother exponential decrease ($R^2 > 0.91$, slope from –.591 to –0.778).

Other methods of local antibiotic therapy include direct sprinkling of the wound with antibiotic during surgical treatment or intra-articular administration of antibiotic solutions, which allows for the short-term creation of therapeutic concentrations at the site of surgical intervention (up to 24 hours) without a significant increase in systemic levels of the antibiotic [31, 32].

Allografts impregnated with antibiotics is an alternative method for creating local concentrations of antibiotics, devoid of the above-described disadvantages. The available methods can be divided into several categories depending on the technology of saturating the material with antibacterial drugs. Allograft bone mixed manually in antibiotic solution followed by drying is the simplest and most common method. Impregnation time can vary from a short period of 30–60 min to prolonged 120–180 min. Antibiotic release is uneven, with the maximum concentration in the first 24–48 hours with 40–60 % of the total amount of impregnated antibiotic being released [33–36]. Coraça-Huber et al. reported some of the antibiotic concentrations exceeding the MIC for staphylococci for up to 7 days *in vitro* and for up to 3 days *in vivo* with the allograft immersed in an antibiotic solution [36].

Iontophoresis is an effective method for providing high initial concentrations of antibiotics and maintaining antimicrobial activity for up to 2 weeks [37]. However, the method is characterized by significant variability of results and requires additional studies of the effect on bone structure.

Our study offered an optimized method for impregnating osteosubstituting material as an approach to local antibiotic therapy. As opposed to conventional methods demonstrating limited effectiveness (3–7 days of antimicrobial action), the method provided prolonged release of vancomycin for up to 14 days while maintaining therapeutically significant concentrations using a combination of reduced pressure (7–10 hPa) and an alcohol solution with the addition of PVP. Statistical analysis revealed that the factors explored in the study had impact on the impregnation efficiency.

In our series, we used a complementary approach, combining the microbiological method and HPLC, which allowed us to obtain a more complete picture of the efficiency of the impregnation method developed.

Microbiological analysis plays a role and allows confirmation of the preserved vancomycin AMA after exposure to various physical and chemical factors during the impregnation process.

The presence of zones of inhibition of MRSA growth throughout the observation period suggests that the antibiotic retains its biological activity despite potential structural changes under the influence of pressure, temperature and chemical agents. High correlation between the size of inhibition zones and antibiotic concentration ($r = 0.908$; $p < 0.001$) confirms the release of the active form of the drug from the samples.

HPLC provides a quantitative assessment of the kinetics of vancomycin elution and allows us to determine the exact concentrations of the drug at different time points. This enables detailed pharmacokinetic profiles to be constructed, release uniformity to be assessed and the total antibiotic release to be determined. Analysis of AUC and exponential decay patterns ($R^2 > 0.91$) demonstrates the benefits of the optimized impregnation technique for sustained drug delivery. The osteosubstituting material used in the study is characterized by an optimal porous structure comparable to other materials used in bone grafting. Autografts and allografts have a porosity of 50–90 % with a pore size of 100–500 μm. Synthetic materials demonstrate the following parameters: hydroxyapatite, porosity of 30–90 % with pores of 100–400 μm; tricalcium phosphate, porosity of 35–80 % with pores of 100–400 μm; bioactive glasses, porosity of 20–60 % with pores of 100–500 μm. Biopolymers, such as collagen matrices (porosity of 85–95 %, pores of 50–350 μm) and PLLA scaffolds (porosity of 60–90 %, pores of 100–500 μm) have a developed porous structure [38, 39]. The material architecture provides a large surface area for interaction with antibiotics, which is confirmed by examples of impregnation of synthetic osteosubstituting materials [40–42]. The spongy structure of such a product allows for a high degree of antibiotic adsorption, which ensures stable and controlled release of the drug in combination with optimal impregnation conditions (pressure, solvent, time).

Despite the high local concentrations of the antibiotic achieved during elution, the use of vancomycin remains safe in the context of potential toxicity. At concentrations up to 1000 μg/ml, vancomycin does not have a significant cytotoxic effect on osteoblasts, confirming its safety for bone tissue when applied locally [43]. With high local concentrations of the antibiotic (up to 1400 μg/ml) laboratory tests demonstrate minimal systemic vancomycin levels (less than 1.5 mg/ml) and the absence of nephrotoxicity, confirmed by the absence of statistically significant changes in creatinine and urea levels after surgery ($p > 0.05$) [15]. The exponential nature of the antibiotic release ($R^2 > 0.91$ for methods 3–7) ensures a gradual decrease in local concentrations and increases the material safety.

A longer period of antibiotic release can be expected in clinical scenario when the impregnated allograft is impacted in the bone bed. This is due to the fact that the compression of the material creates additional diffusion barriers that slow down the elution of the drug. This assumption requires further study *in vivo*, but the results obtained allow us to predict a sufficient duration of the antimicrobial effect for the prevention and treatment of peri-implant infection.

The study allowed us to identify the optimal parameters of impregnation of osteosubstituting material based on spongy allobone with vancomycin to ensure prolonged elution of the antibiotic. The obtained results open up prospects for the creation of new protocols of local antibiotic therapy in orthopedic surgery. The method can be used to obtain material for osteosubstitution in infected cases to form a local depot of an antibiotic with controlled release to be employed in the complex treatment of patients with peri-implant infection.

CONCLUSION

Pressure followed by the type of solvent and exposure time were shown to hav the greatest influence on the impregnation efficiency. The combination of reduced pressure, an alcohol solution with the addition of polyvinylpyrrolidone and an optimal exposure time provided the best results being superior to those obtained with conventional methods. The technique allows for a more uniform release of the antibiotic with a gentle slope of the exponential elution curve and ensures the maintenance of therapeutically significant concentrations of vancomycin for two weeks. This exceeds the indicators of standard methods of local antibiotic therapy and creates prerequisites for effective prevention and treatment of peri-implant infection. High correlation between the concentration of the antibiotic and the zones of MRSA growth inhibition confirms the preservation of the biological activity of vancomycin after impregnation, which is essential for clinical use.

Conflict of interest *Not declared.*

Funding *The work was funded within the framework of State Assignment No. 056-00030-24 "Improving the treatment of patients with osteomyelitis and peri-implant infection using original lyophilized osteoplastic material with prolonged antimicrobial activity."*

REFERENCES

1. Masters EA, Ricciardi BF, Bentley KLM, et al. Skeletal infections: microbial pathogenesis, immunity and clinical management. *Nat Rev Microbiol*. 2022;20(7):385-400. doi: 10.1038/s41579-022-00686-0.
2. Kasimova AR, Tufanova OS, Gordina EM, et al. Twelve-Year Dynamics of Leading Pathogens Spectrum Causing Orthopedic Infection: A Retrospective Study. *Traumatology and Orthopedics of Russia*. 2024:30(1):66-75. doi: 10.17816/2311-2905-16720.
3. Garcia-Moreno M, Jordan PM, Günther K, et al. Osteocytes Serve as a Reservoir for Intracellular Persisting Staphylococcus aureus Due to the Lack of Defense Mechanisms. *Front Microbiol*. 2022;13:937466. doi: 10.3389/fmicb.2022.937466.
4. Trouillet-Assant S, Lelievre L, Martins-Simoes P, et al. Adaptive processes of Staphylococcus aureus isolates during the progression from acute to chronic bone and joint infections in patients. *Cell Microbiol*. 2016;18(10):1405-1414. doi: 10.1111/cmi.12582.
5. Ricciardi BF, Muthukrishnan G, Masters E, et al. Staphylococcus aureus Evasion of Host Immunity in the Setting of Prosthetic Joint Infection: Biofilm and Beyond. *Curr Rev Musculoskelet Med*. 2018;11(3):389-400. doi: 10.1007/s12178-018-9501-4.
6. Paharik AE, Horswill AR. The Staphylococcal Biofilm: Adhesins, Regulation, and Host Response. *Microbiol Spectr*. 2016;4(2):10.1128/microbiolspec.VMBF-0022-2015. doi: 10.1128/microbiolspec.VMBF-0022-2015.
7. Coraca-Huber DC, Fille M, Hausdorfer J, et al. Staphylococcus aureus biofilm formation and antibiotic susceptibility tests on polystyrene and metal surfaces. *J Appl Microbiol*. 2012;112(6):1235-1243. doi: 10.1111/j.1365-2672.2012.05288.x.
8. Mankin HJ, Hornicek FJ, Raskin KA. Infection in massive bone allografts. *Clin Orthop Relat Res*. 2005;(432):210-216. doi: 10.1097/01.blo.0000150371.77314.52.
9. Michalak KA, Khoo PP, Yates PJ, et al. Iontophoresed segmental allografts in revision arthroplasty for infection. *J Bone Joint Surg Br*. 2006;88(11):1430-1437. doi: 10.1302/0301-620X.88B11.18335.
10. Elawady R, Aboulela AG, Gaballah A, et al. Antimicrobial Sub-MIC induces Staphylococcus aureus biofilm formation without affecting the bacterial count. *BMC Infect Dis*. 2024;24(1):1065. doi: 10.1186/s12879-024-09790-3.
11. Witsø E, Persen L, Løseth K, Bergh K. Adsorption and release of antibiotics from morselized cancellous bone. In vitro studies of 8 antibiotics. *Acta Orthop Scand*. 1999;70(3):298-304. doi: 10.3109/17453679908997812.
12. Mader JT, Calhoun J, Cobos J. In vitro evaluation of antibiotic diffusion from antibiotic-impregnated biodegradable beads and polymethylmethacrylate beads. *Antimicrob Agents Chemother*. 1997;41(2):415-418. doi: 10.1128/AAC.41.2.415.
13. Buttaro MA, Morandi A, Rivello HG, Piccaluga F. Histology of vancomycin-supplemented impacted bone allografts in revision total hip arthroplasty. *J Bone Joint Surg Br*. 2005;87(12):1684-1687. doi: 10.1302/0301-620X.87B12.16781.
14. Buttaro MA, Pusso R, Piccaluga F. Vancomycin-supplemented impacted bone allografts in infected hip arthroplasty. Two-stage revision results. *J Bone Joint Surg Br*. 2005;87(3):314-319. doi: 10.1302/0301-620x.87b3.14788.
15. Buttaro MA, Gimenez MI, Greco G, et al. High active local levels of vancomycin without nephrotoxicity released from impacted bone allografts in 20 revision hip arthroplasties. *Acta Orthop*. 2005;76(3):336-340.
16. Inzana JA, Schwarz EM, Kates SL, Awad HA. Biomaterials approaches to treating implant-associated osteomyelitis. *Biomaterials*. 2016;81:58-71. doi: 10.1016/j.biomaterials.2015.12.012.
17. Markov PA, Eremin PS, Berezkina ES, et al. Osteoplastic biomaterials from organic and mineral components of the bone matrix: a literature review. *Bulletin of Rehabilitation Medicine*. 2024;23(5):97-107. (In Russ.) doi: 10.38025/2078-1962-2024-23-5-97-107.
18. Mukhametov UF, Lyulin SV, Borzunov DY, et al. Alloplastic and implant materials for bone grafting: a literature review. *Creative surgery and oncology*. 2021;11(4):344. (In Russ.) doi: 10.24060/2076-3093-2021-11-4-343-353.
19. Bozhkova SA, Gordina EM, Markov MA, et al. The Effect of Vancomycin and Silver Combination on the Duration of Antibacterial Activity of Bone Cement and Methicillin-Resistant Staphylococcus aureusBiofilm Formation. *Traumatology and Orthopedics of Russia*. (In Russ.) 2021;27(2):54-64. doi: 10.21823/2311-2905-2021-27-2-54-64.
20. Melikova RE, Tsiskarashvili AV, Artyukhov AA, Sokorova NV. IIn vitro study of the dynamics in elution of antibacterial drugs impregnated into matrices based on polymer hydrogel. *Genij Ortopedii*. 2023;29(1):64-70. doi: 10.18019/1028-4427-2023-29-1-64-70.
21. Stogov MV, Shastov AL, Kireeva EA, Tushina NV. Release of antibiotics from the materials for postosteomyelitic bone defect filling. *Genij Ortopedii*. 2024;30(6):873-880. doi: 10.18019/1028-4427-2024-30-6-873-880.

22. McConoughey SJ, Howlin RP, Wiseman J, et al. Comparing PMMA and calcium sulfate as carriers for the local delivery of antibiotics to infected surgical sites. *J Biomed Mater Res B Appl Biomater*. 2015;103(4):870-877. doi: 10.1002/jbm.b.33247.
23. Janssen DMC, Willems P, Geurts J, Arts CJJ. Antibiotic release from PMMA spacers and PMMA beads measured with ELISA: Assessment of in vitro samples and drain fluid samples of patients. *J Orthop Res*. 2023;41(8):1831-1839. doi: 10.1002/jor.25510.
24. Bertazzoni Minelli E, Della Bora T, Benini A. Different microbial biofilm formation on polymethylmethacrylate (PMMA) bone cement loaded with gentamicin and vancomycin. *Anaerobe*. 2011;17(6):380-383. doi: 10.1016/j.anaerobe.2011.03.013.
25. Miclau T, Dahners LE, Lindsey RW. In vitro pharmacokinetics of antibiotic release from locally implantable materials. *J Orthop Res*. 1993;11(5):627-632. doi: 10.1002/jor.1100110503.
26. Kwong JW, Abramowicz M, Kühn KD, et al. High and Low Dosage of Vancomycin in Polymethylmethacrylate Cements: Efficacy and Mechanical Properties. *Antibiotics (Basel)*. 2024;13(9):818. doi: 10.3390/antibiotics13090818.
27. Tsiskarashvili AV, Melikova RE, Volkov AV, et al. In vivo effectiveness of polymer hydrogels impregnated with an antibacterial drug in chronic osteomyelitis. *Genij Ortopedii*. 2023;29(5):535-545. doi: 10.18019/1028-4427-2023-29-5-535-545.
28. Wahl P, Guidi M, Benninger E, et al. The levels of vancomycin in the blood and the wound after the local treatment of bone and soft-tissue infection with antibiotic-loaded calcium sulphate as carrier material. *Bone Joint J*. 2017;99-B(11):1537-1544. doi: 10.1302/0301-620X.99B11.BJJ-2016-0298.R3.
29. Luo S, Jiang T, Yang Y, et al. Combination therapy with vancomycin-loaded calcium sulfate and vancomycin-loaded PMMA in the treatment of chronic osteomyelitis. *BMC Musculoskelet Disord*. 2016;17(1):502. doi: 10.1186/s12891-016-1352-9.
30. Giavaresi G, Bertazzoni Minelli E, Sartori M, et al. New PMMA-based composites for preparing spacer devices in prosthetic infections. *J Mater Sci Mater Med*. 2012;23(5):1247-1257. doi: 10.1007/s10856-012-4585-7.
31. Kang DG, Holekamp TF, Wagner SC, Lehman RA Jr. Intrasite vancomycin powder for the prevention of surgical site infection in spine surgery: a systematic literature review. *Spine J*. 2015;15(4):762-770. doi: 10.1016/j.spinee.2015.01.030.
32. Lawrie CM, Kazarian GS, Barrack T, et al. Intra-articular administration of vancomycin and tobramycin during primary cementless total knee arthroplasty : determination of intra-articular and serum elution profiles. *Bone Joint J*. 2021;103-B(11):1702-1708. doi: 10.1302/0301-620X.103B11.BJJ-2020-2453.R1.
33. Kamra P, Lamba AK, Faraz F, Tandon S. Effect of antibiotic impregnation time on the release of gentamicin from cryopreserved allograft bone chips: an in vitro study. *Cell Tissue Bank*. 2019;20(2):267-273. doi: 10.1007/s10561-019-09765-8.
34. Berglund B, Wezenberg D, Nilsson M, et al. Bone allograft impregnated with tobramycin and vancomycin delivers antibiotics in high concentrations for prophylaxis against bacteria commonly associated with prosthetic joint infections. *Microbiol Spectr*. 2024;12(12):e0041424. doi: 10.1128/spectrum.00414-24.
35. Coraça-Huber DC, Ammann CG, Nogler M, et al. Lyophilized allogeneic bone tissue as an antibiotic carrier. *Cell Tissue Bank*. 2016;17(4):629-642. doi: 10.1007/s10561-016-9582-5.
36. Coraça-Huber DC, Steixner SJM, Najman S, et al. L Lyophilized Human Bone Allograft as an Antibiotic Carrier: An In Vitro and In Vivo Study. *Antibiotics (Basel)*. 2022;11(7):969. doi: 10.3390/antibiotics11070969.
37. Edmondson MC, Day R, Wood D. Vancomycin iontophoresis of allograft bone. *Bone Joint Res*. 2014;3(4):101-7. doi: 10.1302/2046-3758.34.2000223.
38. Karageorgiou V, Kaplan D. Porosity of 3D biomaterial scaffolds and osteogenesis. *Biomaterials*. 2005;26(27):5474-91. doi: 10.1016/j.biomaterials.2005.02.002.
39. Ketonis C, Barr S, Adams CS, et al. Bacterial colonization of bone allografts: establishment and effects of antibiotics. *Clin Orthop Relat Res*. 2010;468(8):2113-2121. doi: 10.1007/s11999-010-1322-8.
40. Dolete G, Purcăreanu B, Mihaiescu DE, et al. Comparative Loading and Release Study of Vancomycin from a Green Mesoporous Silica. *Molecules*. 2022;27(17):5589. doi: 10.3390/molecules27175589.
41. Kato A. Atmospheric impregnation behavior of calcium phosphate materials for antibiotic therapy in neurotrauma surgery. *PLoS One*. 2020;15(3):e0230533. doi: 10.1371/journal.pone.0230533.
42. Kato A. Antibiotic Impregnation, Release, Activity, and Interaction With Porous Hydroxyapatite for Infectious Control in Neurotrauma Surgery. *J Pharm Sci*. 2022;111(8):2389-2396. doi: 10.1016/j.xphs.2022.04.017.
43. Edin ML, Miclau T, Lester GE, et al. Effect of cefazolin and vancomycin on osteoblasts in vitro. *Clin Orthop Relat Res*. 1996;(333):245-251.

The article was submitted 09.01.2025; approved after reviewing 14.03.2025; accepted for publication 31.03.2025.

Information about the authors:

Alexander P. Antipov — orthopedic surgeon,
a.p.antipov@yandex.ru, https://orcid.org/0000-0002-9004-5952;

Svetlana A. Bozhkova — Doctor of Medical Sciences, Head of the Department, Professor of the Department,
clinpharm-rniito@yandex.ru, https://orcid.org/0000-0002-2083-2424;

Ekaterina M. Gordina — Candidate of Medical Sciences, senior researcher,
emgordina@win.rniito.ru, https://orcid.org/0000-0003-2326-7413;

Magomed Sh. Gadzhimagomedov — postgraduate student, orthopaedic surgeon,
orthopedist8805@yandex.ru, https://orcid.org/0009-0001-6113-0277;

Andrey A. Kochish — Candidate of Medical Sciences, orthopaedic surgeon,
kochishman@gmail.com, https://orcid.org/0000-0001-8573-1096

Original article
https://doi.org/10.18019/1028-4427-2025-31-3-372-379

Testing the effectiveness of a new type of spacers for local antibiotic therapy

I.F. Akhtyamov[1,2,3]✉, O.A. Sachenkov[1], R.A. Shafigulin[1,2,3], A.E. Galyautdinova[1,2], N.V. Kharin[1], I.A. Bespalov[3], S.V. Boychuk[1,2]

[1] Kazan (Volga Region) Federal University, Kazan, Russian Federation
[2] Kazan State Medical University, Kazan, Russian Federation
[3] Republican Clinical Hospital, Kazan, Russian Federation

Corresponding author: Ildar F. Akhtyamov, yalta60@mail.ru

Abstract

Introduction The established treatments for purulent infection in the bone and joint involve one- or two-stage local effect on the biofilm with use of bone cement and an active substance including an antibiotic in addition to systemic therapy.

The **objective** was to evaluate experimental qualitative and quantitative antibiotic release from bone cement introduced into a new type of lattice-structured spacer.

Material and methods A new type of lattice-structured implant/spacer manufactured using additive technologies and a comparison sample simulating a traditional reinforced spacer made of bone cement + antibiotic were used. Vancomycin release was measured by spectrophotometry for periods of 30 days. A regression line was used to plot calibration curves based on data obtained from mother solutions.

Results An effective profile of antibiotic release from bone cement was obtained in the first days of the experiment, followed by a decrease at the end of the first week and an exit to a uniform plateau. The amount of fixed antibiotic in solutions did not exceed 1 % of the total mass of bone cement and active substance. The amount of antibiotic released from the lattice-structured samples was higher than that in the comparison samples.

Discussion Antibiotic release is a superficial process and is not dependent on the total volume of bone cement. A possible increase in the volume of the medicinal composition does not lead to a proportional increase in the amount of the active substance released. The findings showed that the antibiotic release is more intense even with a smaller volume of material in the lattice structures compared to the control samples, which emphasizes the importance of optimizing the geometry and structure of the material to achieve maximum efficiency of the release of active substances.

Conclusion The lattice structure of implants quantitatively affects the release of antibiotic from bone cement into the environment.

Keywords: bone infection, bone cement, implant, antibiotic elution, additive technologies

For citation: Akhtyamov IF, Sachenkov OA, Shafigulin RA, Galyautdinova AE, Kharin NV, Bespalov IA, Boychuk SV. Testing the effectiveness of a new type of spacers for local antibiotic therapy. *Genij Ortopedii*. 2025;31(3):372-379. doi: 10.18019/1028-4427-2025-31-3-372-379.

INTRODUCTION

Purulent infection is one of the most formidable complications in surgery of the musculoskeletal system [1–3]. Conventional systemic therapy is effectively accompanied by a local effect on the pathological focus [4–7]. Infection can be arrested with a two-stage revision surgery: placement of a spacer made of bone cement (BC) with an active substance (selected antibiotic) followed by implantation of a revision construct. The technique can be applied to joint and long bone conditions [8].

Many technologies have been developed to increase the time and amount of antibiotic release into the environment. It is a known fact that the elution of the active substance occurs from the superficial layer of the spacer (within 2–3 mm). This predetermines the possibility of increasing the degree of elution by increasing the contact area of the therapeutic composite layer (bone cement + antibiotic) and the environment [9]. The antibiotic (AB) effect on the surrounding tissue extends to a maximum of 20–25 mm. Technologically, the distribution of the therapeutic composite layer (TCL) over the surface of the spacer is limited by the location of the infectious focus and is costly in terms of the use and redistribution of large volumes of AB [10]. The strength characteristics of the formed spacer are supposed to facilitate functional capabilities of the patient and serve as the basis for osteosynthesis if needed [11, 12].

The use of lattice structures in the manufacture of basic implants could increase the contact area of the composite layer and the environment and improve the elution of AB from the BC. Preliminary calculation of strength characteristics allows to minimize changes in the implant design specified by the manufacturer. The combination of a volumetric lattice structure with TCL forms the so-called metamaterial, which could become one of the options for solving the problem [13]. A volumetric lattice structure as part of an implant/spacer is produced using additive technologies. This is achieved with the design of elementary cells that fill the volume of the product. The distribution of the elementary cell has an impact on the strength of the structure [14]. Topological or structural optimization is another method to be used. N. Kladovasilakis et al. [15] optimized the designs for hip implants achieving 50% porosity and maintaining strength requirements. Lattice-based implants can act as a preformed base with predetermined parameters to reduce or eliminate the need for handicraft production of reinforced spacers.

The **objective** was to evaluate experimental qualitative and quantitative antibiotic release from bone cement introduced into a new type of lattice-structured spacer.

MATERIAL AND METHODS

A lattice-structured cylinder (Fig. 1 a) was selected as a base for antibiotic loaded bone cement, copying a fragment of the proposed implant number I and comparison sample II (Fig. 1 b), that is, a fragment of a pin with a 2 mm mantle of BC applied on the surface as a continuous layer.

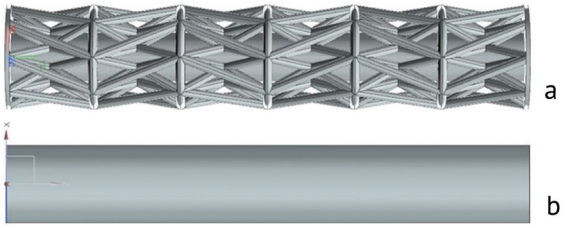

Fig. 1 Types of the samples: (a) lattice-structured implant I; (b) comparison sample II

Sample I is a composition of an inner rod with a diameter of 6 mm and a layer of outer ribs at an angle of 45° with an outer diameter of 12 mm. A cylinder with an outer diameter of 8 mm serves as a comparison sample. The characteristics of the samples are presented in Table 1.

Table 1

Comparative parameters of the samples

№	Diameter, mm	Length, mm	Diameter of the pin, mm	Diameter of the rib, mm	Porosity, %	Cement volume, mm^3	Surface area, mm^2
I	12	60	6	1	61.9	3702	2261
II	8	60	–	–	0	3769	2261

The study samples

The antibiotic release from the TCL was explored using four samples of each structure produced with laser stereolithography and strengthened using ultraviolet light. A photopolymer printer with photopolymer resin was selected for the sample production. Synycem bone cement (France) was used for the study. TCL of each test sample was prepared with 4.0 g of the dry bone cement and 0.2 g of Vancomycin. AB was chosen with regard to the thermal stability, active use in clinical practice and research on the problem. The powdered component of the BC was homogeneously mixed with the antibiotic, then 2 ml of monomer was added to the mixture, and homogeneously mixed to a plastic condition. The TCL was applied to the samples using a disposable 5 ml syringe and an internal diameter of 12 mm which served as a mold. The samples are shown in Fig. 2.

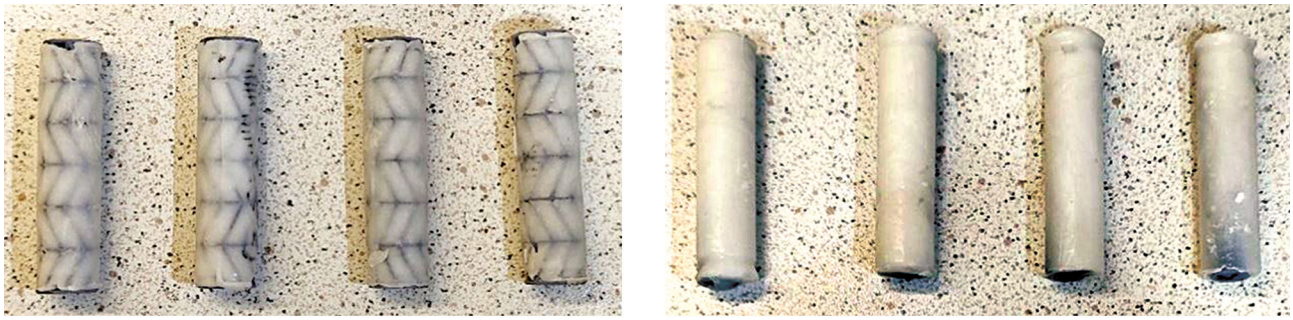

a b

Fig. 2 Appearance of the manufactured samples: (a) samples I; (b) samples II

The lattice structures were coated with TCL so that it did not protrude beyond the ends o the sample. The outer diameter of the samples was 12 mm. Each sample was placed in a Falcon tube filled with 30 mL of Dulbecco's phosphate-buffered saline (DPBS) without Ca^{2+} and Mg2+ at 37 °C. The samples were immersed to ensure complete contact with DPBS.

Evaluation of antibiotic release from the medicinal composite

Quantification of the antibiotic in solutions was produced using the spectrophotometric method and a BioMate 3S UV-Visible spectrophotometer (USA) to identify the dependence of the optical density of solutions and the concentration of the AB. Measurements were performed in the wavelength range from 190 to 230 nm. The peak of measurements corresponding to the antibiotic was assessed in the spectra. Several stock solutions of AB were used as calibration standards: Vancomycin at concentrations of 0, 0.00005, 0.0001, 0.00025, 0.0005, 0.00075, 0.001, 0.002, 0.003, 0.004 mg/ml. The sample volume in the cuvette measured was 1000 µl. Vancomycin in a volume of 0.5 g was dissolved in 5 ml of DPBS to obtain a concentration of 1 mg/ml.

To construct calibration curves, a regression line was used based on data obtained from mother solutions. The nonparametric Mann – Whitney test was used to assess the reliability of differences in AB release between the structures and compare two independent samples and determine statistically significant differences between them.

Table 2

Concentration calculated for constructing Vancomycin calibration curves using stock solutions

Amount of stock solution, µl	Amount of DPBS, µl	Concentration, mg/ml
400 from a concentration of 0.01	600	0.004
300 from a concentration of 0.01	700	0.003
200 from a concentration of 0.01	800	0.002
500 from a concentration of 0.01	4500	0.001
750 from a concentration of 0.001	250	0.00075
500 from a concentration of 0.001	500	0.0005
250 from a concentration of 0.001	750	0.00025
200 from a concentration of 0.001	1800	0.0001
500 from a concentration of 0.0001	500	0.00005

Measurement of antibiotic elution kinetics

The AB elution was measureed after 1, 3, 7, 15 and 29 days, respectively. The total amount of Vancomycin in the solution was determined at each measurement point according to the schedule. For each day, the concentration was estimated using the following formula:

$$C_a(d) = \frac{p(d)}{k} \cdot c(d),$$

where p is the spectrometer value in the sample taken on a given day, k is the regression coefficient, c is the coefficient associated with the dilution of the sample in the cuvette, d is the exposure length in days.

The coefficient associated with sample dilution in the cuvette depended on the day of measurement. This was due to the fact that the concentration increased over time. To determine the kinetics of the antibiotic, the time derivative was used and the rate of the antibiotic release was calculated with the formula:

$$U(d_i) = \frac{C_a(d_i) - C_a(d_{i-1})}{d_i - d_{i-1}},$$

where d_i is the exposure duration of the i-th shot.

The mass of the extracted antibiotic at a given exposure time (d) was calculated by multiplying the corresponding concentration of the antibiotic in the sample by the total volume in the vial V:

$$m_a(d) = C_a(d) \cdot V.$$

RESULTS

Analysis of the peaks for the absorption spectra showed that the wavelength for Vancomycin was 271–280 nm, which is consistent with the drug's pharmacopoeia data.

The regression coefficient was measured and the regression curve plotted (0). The value of the regression coefficient k was 405.9 for Vancomycin. The linear dependence for AB showed a high determination coefficient $R^2 \geqslant 0.986$ (Fig. 3). Based on the concentration measured within one day of shooting, the average values were calculated for both structures. The average elution values for the experimental sample I were higher than those for the comparison sample II at all stages of exposure (Fig. 4). The pairwise reliability of differences in mean values was assessed.

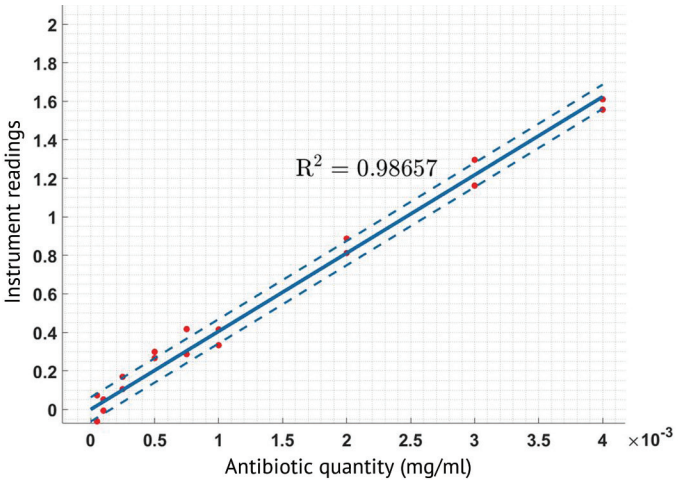

Fig. 3 Vancomycin regression curve: solid line is the regression curve, dash-dotted line is the confidence interval, red dots are the spectrophotometer values

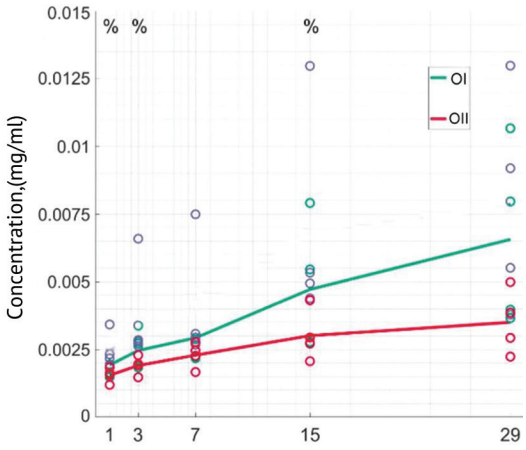

Fig. 4 Comparative curve of antibiotic concentration

No significant difference in the average values of Vancomycin concentration was found between the samples. Control sample II showed the lowest rate of antibiotic release and the smallest spread (Fig. 5). The total mass of the isolated AB Vancomycin was calculated separately and measured 0.1969 mg in sample I and 0.1051 mg in sample II, respectively (Fig. 6). The average value of AB release in experimental sample II was 97% better than in the control.

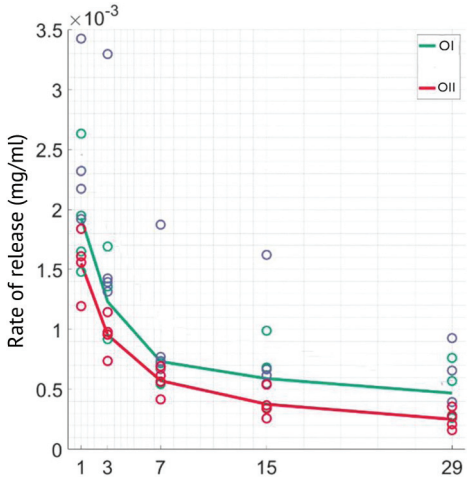

Fig. 5 Kinetics of Vancomycin

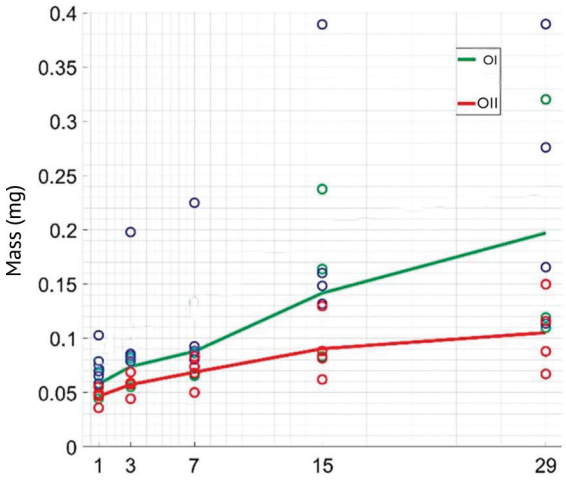

Fig. 6 Mass of isolated antibiotic

The results of a multi-day experiment showed changes in the mass of the isolated AB obtained depending on the control periods (Table 3).

Table 3

Antibiotic release from TCL

No	Amount of Vancomycin, mcg				
	1	3	7	15	29
I	57.8 ± 15.2	73.8 ± 21.9	87.8 ± 31.6	141.5 ± 74.4	196.9 ± 101
II	46.5 ± 8.0	57.2 ± 10.0	68.6 ± 13.9	90.3 ± 28.4	105.1 ± 35.8

A coefficient was introduced as the ratio of the free surface of the sample to the volume of the TCL to describe the comparative characteristics of the samples. The parameter allowed us to evaluate the efficiency of AB release depending on the geometric features of each sample. The percentage of the released AB to the initially set was calculated to quantitatively evaluate the elution process (Table 4).

The introduced coefficient as the ratio of the free surface of the sample to the volume of the BC showed the dependence on the released amount of AB.

Table 6

Relative characteristics of samples

No	Area / Volume	Vancomycin, %
I	0.61	0.07 ± 0.05
II	0.6	0.05 ± 0.0179

DISCUSSION

The study was conducted to determine the effect of a lattice structure on the antibiotic eluted from the drug composite layer, i.e. antibiotic-loaded bone cement. A characteristic profile of AB elution from the BC was obtained in all samples with a significant release in the first days of the experiment, followed by fading after seven days and reaching a uniform plateau after 15 days, which is consistent with the results of similar studies [16–20]. The amount of released AB measured to a maximum of 1% of the mass of the impregnated preparation.

A significant difference in the amount of isolated Vancomycin was noted between the samples. Lattice-structured samples showed higher amount of AB isolated despite the relatively higher initial content of TCL in the comparison samples.

The main part of the antibiotic is eluted from micropores and cracks of the surface layer of bone cement [21–25], which is confirmed by our results. The higher level of Vancomycin release can be explained by the presence of lattice-structured ribs. The single TCL structure divided into small areas increases the contact zone with the washing solution and increases the diffusion of AB compared to the control sample. This phenomenon is important for local antibiotic therapy with controlled and prolonged release of active substances being a key factor in the effectiveness [26].

The antibiotic release is considered as a surface process and does not depend on the total volume of the BC [27, 28]. A possible increase in the volume of the TCL does not lead to a proportional increase in the amount of AB released. In this series, this is confirmed by the fact that even with a smaller volume of material in the lattice structures, the release of the antibiotic is more intense compared to the control samples. Optimizing the geometry and structure of the material is essential for achieving maximum efficiency in the release of active substances [29, 30].

The limitation of the study include investigation of one type of a common antibiotic only. A comparative analysis of combinations of active substances eluted from the TCL, lattice variants, studies on metal samples, that is, a large volume of experiments, is required.

CONCLUSION

The study showed that the use of lattice structures for the fabrication of spacer implants allowed for an increase in the rate and amount of AB eluted from the TCL compared to conventional reinforcement with bone cement.

Conflict of interest *The authors declare that there is no conflict of interest.*

Funding *The study was carried out within the framework of the grant of the Federal State Budgetary Institution of Higher Education Kazan State Medical University of the Ministry of Health of the Russian Federation, with the financial support of the State Program "Priority-2030".*

Ethical review *Not applicable.*

Informed consent for publication *Not required.*

REFERENCES

1. Morcos MW, Kooner P, Marsh J, et al. The economic impact of periprosthetic infection in total knee arthroplasty. *Can J Surg*. 2021;64(2):E144-E148. doi: 10.1503/cjs.012519.
2. Murylev VYu, Rudnev AI, Kukovenko GA, et al. Diagnosis of Deep Periprosthetic Infection of the Hip. *Traumatology and Orthopedics of Russia*. 2022;28(3):123-135. (In Russ.) doi: 10.17816/2311-2905-1797.
3. Bozhkova SA, Kasimova FR, Tikhilov RM, et al. Adverse trends in the etiology of orthopedic Infection: Results of 6-year monitoring of the structure and resistance of leading pathogens. *Traumatology and Orthopedics of Russia*. 2018;24(4):20-31. doI: 10.21823/2311-2905-2018-24-4-20-31.
4. Afinogenova AG, Darovskaya EN. Microbial biofilms of wounds: status of the issuea. *Traumatology and Orthopedics of Russia*. 2011;17(3):119-125. (In Russ.) doi: 10.21823/2311-2905-2011-0-3-119-125.
5. Adams K, Couch L, Cierny G, et al. In vitro and in vivo evaluation of antibiotic diffusion from antibiotic-impregnated polymethylmethacrylate beads. *Clin Orthop Relat Res*. 1992;(278):244-252.
6. Ermakov AM, Kliushin NM, Ababkov IV, et al. Efficiency of two-stage revision arthroplasty in management of periprosthetic knee and hip joint infection. *Genij Ortopedii*. 2018;24(3):321-326. doi: 10.18019/1028-4427-2018-24-3-321-326.
7. Ermakov A., Kliushin N., Ababkov I., et al. One-stage revision arthroplasty for management of periprosthetic hip infection. *Genij Ortopedii*. 2019;25(2):172-179. doi: 10.18019/1028-4427-2019-25-2-172-179.
8. Sereda AP, Bogdan VN, Andrianova MA, Berenstein M. Treatment of Periprosthetic Infection: Where and Who? *Traumatology and Orthopedics of Russia*. 2019;25(4):33-55. (In Russ.) doi: 10.21823/2311-2905-2019-25-4-33-55.
9. Bozhkova SA, Novokshonova AA, Konev VA. Current trends in loCal antibaCterial therapy of periprosthetic infection and osteomyelitis. *Traumatology and Orthopedics of Russia*. 2015; (3):92-107. (In Russ.) doi: 10.21823/2311-2905-2015-0-3-92-107.
10. Murylev VYu, Parvizi J, Rudnev AI, et al. Results of the intraoperative alpha defensin lateral flow test in the second stage of revision hip arthroplasty. *Genij Ortopedii*. 2024;30(6):811-821. doi: 10.18019/1028-4427-2024-30-6-811-821.
11. Williams DF, Rouf R. *Implants in surgery* [Russian translation]. Moscow: Medicina; 1978:552. (In Russ.)
12. Prokhorenko VM, Pavlov VV. *Infectious complication in hip joint endoprosthetics*. Novosibirsk: Nauka; 2010:179. (In Russ.)
13. Abdullah NN, Abdullah H, Ramlee MH. Current trend of lattice structures designed and analysis for porous hip implants: A short review. *Materials Today Proceedings*. 2023. doi: 10.1016/j.matpr.2023.09.199.
14. Kharin N, Bolshakov P, Kuchumov AG. Numerical and Experimental Study of a Lattice Structure for Orthopedic Applications. *Materials (Basel)*. 2023;16(2):744. doi: 10.3390/ma16020744.
15. Kladovasilakis N, Tsongas K, Tzetzis D. Finite Element Analysis of Orthopedic Hip Implant with Functionally Graded Bioinspired Lattice Structures. *Biomimetics (Basel)*. 2020;5(3):44. doi: 10.3390/biomimetics5030044.
16. Luo S, Jiang T, Long L, et al. A dual PMMA/calcium sulfate carrier of vancomycin is more effective than PMMA-vancomycin at inhibiting Staphylococcus aureus growth in vitro. *FEBS Open Bio*. 2020;10(4):552-560. doi: 10.1002/2211-5463.12809.
17. Wall V, Nguyen TH, Nguyen N, Tran PA. Controlling Antibiotic Release from Polymethylmethacrylate Bone Cement. *Biomedicines*. 2021;9(1):26. doi: 10.3390/biomedicines9010026.
18. Mensah LM, Love BJ. A meta-analysis of bone cement mediated antibiotic release: Overkill, but a viable approach to eradicate osteomyelitis and other infections tied to open procedures. *Mater Sci Eng C Mater Biol Appl*. 2021;123:111999. doi: 10.1016/j.msec.2021.111999.
19. Paz E, Sanz-Ruiz P, Abenojar J, et al. Evaluation of Elution and Mechanical Properties of High-Dose Antibiotic-Loaded Bone Cement: Comparative "In Vitro" Study of the Influence of Vancomycin and Cefazolin. *J Arthroplasty*. 2015;30(8):1423-1429. doi: 10.1016/j.arth.2015.02.040.
20. Melikova RE, Tsiskarashvili AV, Artyukhov AA, Sokorova NV. In vitro study of the dynamics in elution of antibacterial drugs impregnated into matrices based on polymer hydrogel. *Genij Ortopedii*. 2023;29(1):64-70. doi: 10.18019/1028-4427-2023-29-1-64-70.
21. Miller R, McLaren A, Leon C, McLemore R. Mixing method affects elution and strength of high-dose ALBC: a pilot study. *Clin Orthop Relat Res*. 2012;470(10):2677-2683. doi: 10.1007/s11999-012-2351-2.
22. Samelis PV, Papagrigorakis E, Sameli E, et al. Current Concepts on the Application, Pharmacokinetics and Complications of Antibiotic-Loaded Cement Spacers in the Treatment of Prosthetic Joint Infections. *Cureus*. 2022;14(1):e20968. doi: 10.7759/cureus.20968.
23. Wu K, Chen YC, Hsu YM, Chang CH. Enhancing Drug Release From Antibiotic-loaded Bone Cement Using Porogens. *J Am Acad Orthop Surg*. 2016;24(3):188-195. doi: 10.5435/JAAOS-D-15-00469.
24. Shi M, Kretlow JD, Spicer PP, et al. Antibiotic-releasing porous polymethylmethacrylate/gelatin/antibiotic constructs for craniofacial tissue engineering. *J Control Release*. 2011;152(1):196-205. doi: 10.1016/j.jconrel.2011.01.029.
25. Spicer PP, Shah SR, Henslee AM, et al. Evaluation of antibiotic releasing porous polymethylmethacrylate space maintainers in an infected composite tissue defect model. *Acta Biomater*. 2013;9(11):8832-8839. doi: 10.1016/j.actbio.2013.07.018.

26. Mironov SP, Tsiskarashvili AV, Gorbatiuk DS. Chronic post-traumatic osteomyelitis as a problem of contemporary traumatology and orthopedics (literature review). *Genij Ortopedii*. 2019;25(4):610-621. doi: 10.18019/1028-4427-2019-25-4-610-621.
27. Samelis PV, Papagrigorakis E, Sameli E, et al. Current Concepts on the Application, Pharmacokinetics and Complications of Antibiotic-Loaded Cement Spacers in the Treatment of Prosthetic Joint Infections. *Cureus*. 2022;14(1):e20968. doi: 10.7759/cureus.20968.
28. Perry NPJ, Tucker NJ, Hadeed MM, et al. The Antibiotic Cement Bead Rouleaux: A Technical Trick to Maximize the Surface Area to Volume Ratio of Cement Beads to Improve the Elution of Antibiotics. *J Orthop Trauma*. 2022;36(9):369-373. doi: 10.1097/BOT.0000000000002335.
29. Kuropatkin GV, Akhtiamov IF. *Bone cement in traumotology and orthopaedic*. Kazan: Tagraf Publ.; 2014:188. (In Russ.)
30. 30. Stogov MV, Shastov AL, Kireeva EA, Tushina NV. Release of antibiotics from the materials for postosteomyelitic bone defect filling. *Genij Ortopedii*. 2024;30(6):873-880 doi: 10.18019/1028-4427-2024-30-6-873-880.

The article was submitted 31.01.2025; approved after reviewing 18.02.2025; accepted for publication 31.03.2025.

Information about the authors:

Ildar F. Akhtyamov — Doctor of Medical Sciences, Professor, Leading Researcher, Head of Department, Chief Researcher, yalta60@mail.ru, https://orcid.org/0000-0002-4910-8835;

Oskar A. Sachenkov — Candidate of Medical Sciences, Senior Researcher, Associate Professor, 4works@bk.ru, https://orcid.org/0000-0002-8554-2938, SPIN-code: 2926-2436;

Rashid A. Shafigulin — Candidate of Medical Sciences, Senior Researcher, Assistant Professor, orthopaedic surgeon, rashid221@yandex.ru, https://orcid.org/0009-0008-6146-4470, SPIN-code: 1458-1630;

Alina E. Galyautdinova — Research Assistant, wiiskas15@gmail.com, https://orcid.org/0009-0003-0885-5994, SPIN-code: 1458-1630;

Nikita V. Kharin — Research Fellow, nik1314@mail.ru, https://orcid.org/0000-0003-4850-143X, SPIN-code: 3574-8161;

Igor A. Bespalov — Research Assistant, bespalovigora@gmail.com, https://orcid.org/0009-0008-8062-8733, SPIN-code: 3574-8161;

Sergey V. Boychuk — Doctor of Medical Sciences, Professor, Leading Researcher, Head of Department, boichuksergei@mail.ru, https://orcid.org/0000-0003-2415-1084, SPIN-code: 8058-6246.

Clinical case
https://doi.org/10.18019/1028-4427-2025-31-3-380-387

A series of clinical observations of the treatment of patients with atrophic nonunion and defects of the clavicle midshaft managed with free fibular autografting, the Ilizarov mini-fixator and an intramedullary wire

S.N. Kolchin✉, D.S. Mokhovikov, T.A. Malkova

Ilizarov National Medical Research Centre for Traumatology and Orthopedics, Kurgan, Russian Federation

Corresponding author: Sergey N. Kolchin, sergei.kolchin@gmail.com

Abstract

Introduction Atrophic nonunion and defects is a rare complication of clavicle fractures. Therefore questions arise when choosing the optimal method of their treatment.

Purpose We aimed to retrospectively assess the effectiveness of treating atrophic clavicle midshaft nonunion and defects with a free fibular autologous graft fixed with the Ilizarov mini-fixator in combination with an intrameduallary wire.

Materials and methods A retrospective study of 14 patients (11 females, 3 males) in the mean age of 34.1 ± 2.8 years with atrophic nonunion and defects of the clavicle was carried out. Eleven patients had post-traumatic nonunion after failures of its surgical treatment including seven cases of multiple surgeries, and three cases were congenital nonunion. Pain in the clavicle area was the main complaint in 13 patients. Five had minor restrictions in the shoulder joint function, and two had a pronounced adduction contracture of the shoulder joint. Surgical treatment included debridement, resection of the ends of the fragments to the paprika sign, defect plasty with a free autologous fibular graft followed by combined fixation with an intramedullary wire and the Ilizarov mini-fixator. Supportive compression of 1 mm every two weeks was produced at the junction of the fragments in order to stimulate repair. The mini-fixator was removed after radiographic confirmation of a continuous union of the graft with the fragments.

Results and discussion The post-resection defect averaged 3.1 ± 0.2 cm. Union was achieved in 11 cases. The average period in the mini-fixator was 159.9 ± 11.9 days. In all cases, after dismantling the device, the range of motion in the shoulder joint retained preoperative parameters. The complications were one graft migration, soft-tissue inflammation and deep infection (two cases). Soft-tissue inflammation was treated with antibiotics while deep infection required prompt debridement. Long-term results were followed in 13 patients. There were no problems with the donor site in the long term. The Ilizarov mini-fixator assisted by an intramedullary wire provides stable fixation and allows compression at the junction of bone fragments with a fibular autograft to stimulate bone formation and union in clavicle midshaft nonunion and defects.

Conclusion The combination of three technical components (autologous grafting, Ilizarov mini-fixator, intramedullary wire) yields positive results in the management of large post-resection defects of the clavicle midshaft. Upon graft consolidation, the clavicle acquires a near-to-normal radiographic bone structure.

Keywords: clavicle midshaft, nonunion, bone defect, free fibular grafting, mini-Ilizarov apparatus, intramedullary fixation

For citation: Kolchin SN, Mokhovikov DS, Malkova TA. A series of clinical observations of the treatment of patients with atrophic nonunion and defects of the clavicle midshaft managed with free fibular autografting, the Ilizarov mini-fixator and an intramedullary wire. *Genij Ortopedii*. 2025;31(3):380-387. doi: 10.18019/1028-4427-2025-31-3-380-387.

INTRODUCTION

Clavicle fractures account for 2 to 5 % and up to 10 % of fractures in adult and paediatric population, respectively, and therefore are a frequent practice for an orthopaedic surgeon [1]. The middle third of the clavicle is affected in 80 %. It can be effectively treated conservatively [1–3]. However, non- or mal-union of the clavicle were reported in up to 15 % of conservatively treated displaced fractures [2–5]. Therefore, unstable and open clavicle fractures, displaced fractures and with pronounced shortening or threat of skin perforation continue to require surgical treatment [3–5]. Currently, the main surgical techniques for clavicle fracture repair are plating and intramedullary osteosynthesis, resulting in nonunion rates ranging from 2.6 to 5.9 % [4–8]. It is difficult to assess a direct relationship between surgery and incidence of nonunion. However, it is obvious that inaccurate reduction and instability of fixation can be considered as factors provoking nonunion.

Autologous iliac crest grafting in combination with either plating or nailing are the most common surgical methods for clavicle nonunion [9, 10]. Fragment end layer and the need for a wide dissection of tissues in clavicle nonunion are undoubted problems for achieving union with these techniques. Donor site morbidity after collection of a tricortical graft is a negative consequence. External fixation in the treatment of clavicle nonunion is not a unified approach, and has not been used for extended defects [6, 11–14]. Vascularized grafting, as reported, requires precision techniques, experienced plastic surgeons, and is very traumatic for the donor site [14, 15].

Treatment failure is always a challenging problem that encourages surgeons to search for the most appropriate way of treating clavicle nonunion, including recalcitrant cases [14]. To date, the approach to surgical treatment of clavicle nonunion and defects is not standardized but external fixation has been discussed both for fractures and hyper- /hypotrophic nonunion of the clavicle [6, 16].

We **aimed** to retrospectively assess the effectiveness of treating atrophic clavicle midshaft nonunion and defects with a free fibular autologous graft fixed with the Ilizarov mini-fixator in combination with an intrameduallary wire.

MATERIAL AND METHODS

From 2011 to 2022, fourteen patients (11 females, 3 males) with clavicle nonunion and defects were treated with free autologous fibular grafting and combined fixation with the Ilizarov mini-fixator and an intramedullary wire (Table 1). Their mean age was 34.1 ± 2.8 years (range, 12–53 years). All patients had been previously treated surgically at other hospitals with various methods. The nonunion was post-traumatic after operations for closed fractures in 11 patients. The disease duration ranged from one to 24 years. Three youngest patients had presumably congenital pseudarthrosis of the clavicle diagnosed at the age of over 10 years. They started feeling pain or deformity while growing but their medical records had no history of trauma. Seven patients had more than one intervention for nonunion. One patient had a history of deep infection with remission for more than one year (Table 1, P7) but active signs of inflammation were not diagnosed at admission both by clinical examination and laboratory tests.

Pain of varying intensity was the main complaint in 13 patients. Preoperative examination assessed the range of motion (ROM) in the shoulder joint and radiographic views in two projections. ROM was full in seven patients. Five had a slight restriction in shoulder abduction (up to 30 degrees of total ROM), and two had a pronounced joint motion limitation.

Table 1

Patient data

Patients	P1	P2	P3	P4	P 5	P 6	P7	P 8	P9	P10	P11	P 12	P13	P 14	Means or %
Age	12	20	49	19	16	30	38	53	36	39	51	44	39	44	34.1 ± 2.8 years
Gender	F	F	F	F	F	M	F	F	F	F	M	M	F	F	76.8 % F
Etiology	CP	IF	IF	CP	CP	IF	MVA	MVA	MVA	IF	IF	MVA	MVA	IF	
Duration of the disease (years)	12	2	2	6	9	3	1	1	1	1	24	1	4	9	5.4 ± 1.2
Previous surgery	IW	PL IW	PL IW EF	EF	EF	PL IW	PL PL+ BG	PL PL+ BG	EF	PL	2 PL PL+ BG	PL PL+ BG	IW	IW	7 recalcitrant
Bone defect (cm)	2	2	1.5	2	2.5	4	2.5	4.5	3.5	3.5	3.5	3.5	3	5	3.1 ± 0.2
Surgery time (min)	205	180	180	120	245	175	105	100	145	125	130	100	180	185	155.4 ± 10.0
Consolidation	+	+	–	–	+	+	–	+	+	+	+	+	+	+	78.6 %
Duration of fixation (days)	144	216	183	123	124	168	183	105	121	166	178	163	147	175	159.9 ± 11.9
Follow-up (years)	1	1	1	1	1	1	0.5	1.5	1	1	1	1	5	9	Long-term 92.9 %
Complications	–	BGM	PI	PTI	PTDI	–	DI	–	–	–	–	–	–	DSP	35.7 %

Notes: P — patient; MVA — motor vehicle accident; IF — isolated fracture; CP — congenital pseudarthrosis; IW — intramedullary wire; PL — plating; BG — bone grafting; EF — external fixator; BGM — bone graft migration; PI — pin instability; PTI — pin tract infection; PTDI — pin tract deep infection; DI — deep infection; DSP — donor site pain

The size of the defect was measured in frontal and axial radiographs, the hypotrophy of the fragments was assessed, and the resection of the endplates was planned (Fig. 1 a).

Surgical technique and postoperative care

An anterior approach to the clavicle was used with a patient lying in the supine position. After the removal of foreign bodies and debridement of the interfragmentary gap, resection of nonunion endplates was performed to the bleeding bone (paprika sign) and the fragment ends were shaped for a side-to-side contact with the graft. The length of the defect was measured. The wound was tamponed.

The ipsilateral lower limb was chosen for graft harvesting, what facilitated the work of the surgical team. The fibula was approached in the middle third, retreating proximally at least 10 cm from the ankle joint gap, and a vibrating saw was used for cutting the graft. After hemostasis, the wound was sutured. Primary co-aptation of the graft was assisted by inserting a 1.8-mm intramedullary wire. Depending on the anatomical features of the fragments (defects caused by metal implants), the wire exited from the acromial or sternal end of the clavicle. The wound was sutured.

Three 1.5-mm cantilever wires were inserted in each fragment of the clavicle (Fig. 1 b). The wires passed through both cortical plates. The moment of exit from the cortex was felt as a "fall"; therefore, the pressure on the drill was weakened when passing the second cortical plate. The penetration of the wire into the soft tissues outside the second cortex was no more than 1 to 2 mm. The topography of the neurovascular bundle was necessarily considered. The wires were held at an angle of 90–100° to each other, depending on the soft tissues. The external part of the wires was bent using a wire holder and mounted on the threaded rod of the Ilizarov mini-apparatus. The rod was positioned along the axis of the clavicle and along the projection of the intramedullary wire. Proximally, washers could be used in order to maximize the stability of the support. The distal support was attached to a connection plate in order to enable axial compression (Fig. 1 b).

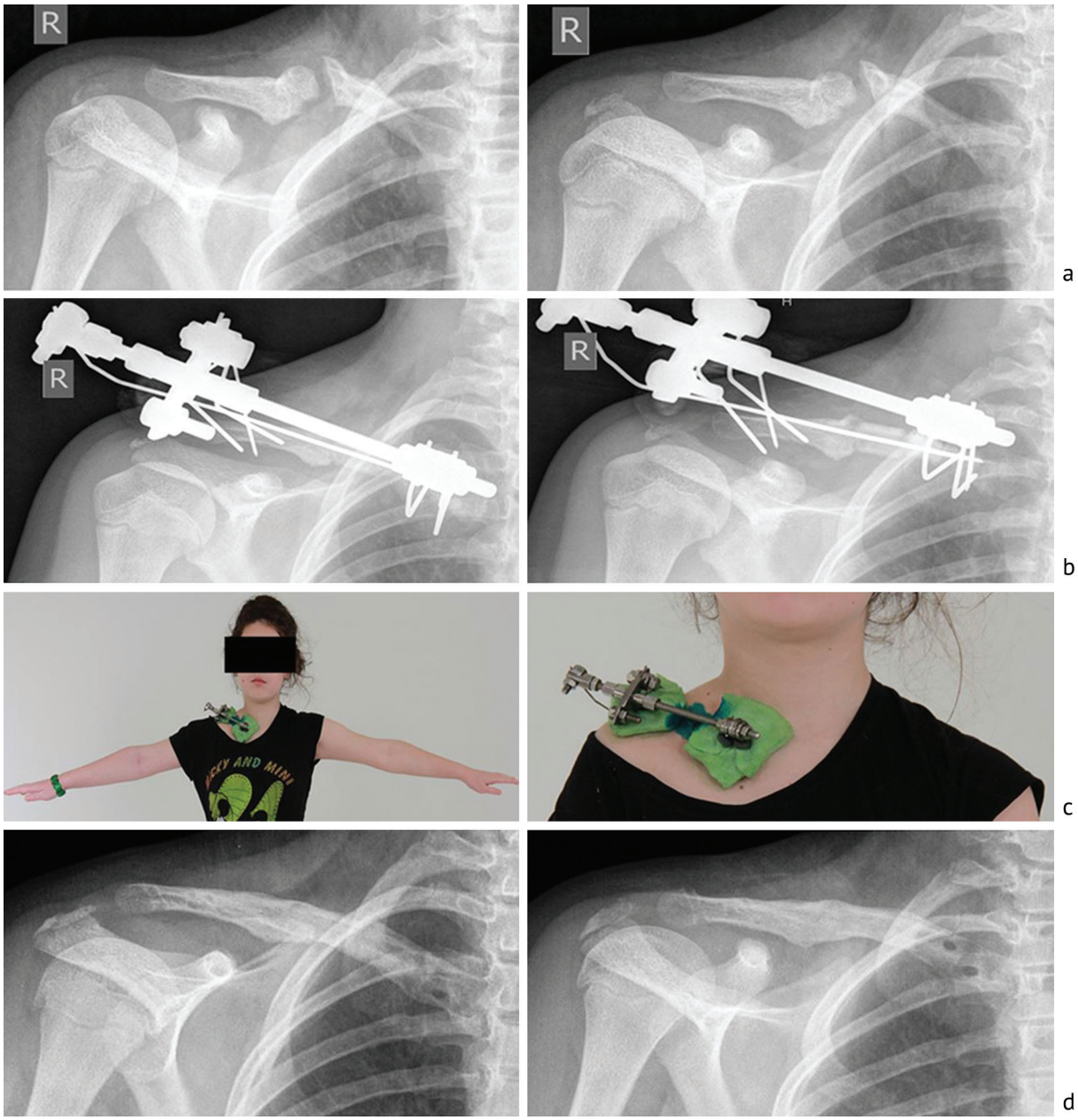

Fig. 1 X-rays and photo of P1 (Table 1) with hypotrophic nonunion of the clavicle with a 5-mm gap and incongruent sclerotic ends of the fragments (a); defect repair and deformity correction upon mini-fixator placement and tight contact of the graft with the fragments (b); photo of the patient showing the shoulder function which is slightly restricted due to the placed mini-fixator (c); union and graft remodeling after 1-year (d)

In the postoperative period, dressings were changed if required. Supportive compression of 1 mm was produced every two weeks. Radiographic checks were taken after 2 and 4 months, further radiographic assessment was recommended based on the consolidation dynamics after 5 and 6 months post-surgery. In the case of the radiographic signs of graft lysis in the contact area, acute compression up to 2–3 mm was performed for tighter contact of the fragments. Exercise therapy was initiated on the first postoperative day with the upper limb fixed in a scarf bandage that was prescribed for at least three months after the operation (Fig. 1 c).

RESULTS

The size of the defects varied from 1.5 to 5 cm and averaged 3.1 ± 0.2 cm after resection. Union was achieved in 11 cases (78.6%) and an average consolidation time was somewhat over 4 months (Table 1). Failures in union were patients 3, 4 and 7. In patient 3, union of the graft was achieved

with only the proximal fragment. The device was removed due to wire instability. Re-osteosynthesis was recommended, but the patient was lost for further treatment. Patient 4 had the device removed due to pin-tract infection; a second osteosynthesis procedure was proposed after infection arrest but the patient was lost for repeated treatment due to a change in his residence place. In patient 5, pin-tract infection developed into deep infection with the need for surgical debridement, after which it was arrested and nonunion healed. Case 7 had a history of chronic infection and this was one of the reasons for infection recurrence. After three months, a fistula opened in the projection of the graft; there were radiographic signs of sequestration, what required surgical debridement but the patient rejected further surgical treatment.

Among other complications was graft migration in patient 2 as instability of the intramedullary wire developed due to marginal defects and bedsores from the previous metal implant. Migration was diagnosed in the early postoperative period while producing compression. This required revision intervention with changing the intramedullary wire. Pain at the donor site was observed in patient 14. The patient fell with her foot twisted on the 7th day after surgery. Pain persisted in the area of the ankle joint but radiography did not reveal any ankle fracture. In the long-term follow-up period, the patient did not complain, radiological signs of ankle joint osteoarthritis were not detected.

In all cases, after fixator removal, the passive ROM in the shoulder joint was within the preoperative ROM and the patients were referred for physiotherapy rehabilitation.

DISCUSSION

Despite the severity of the condition, it is difficult to consider clavicle nonunion and defects a common pathology as the nonunion rate following clavicle fractures is not high [1–7]. Pain, shortening, deformity and limitation of shoulder ROM that accompany nonunion and defects of the clavicle make surgical treatment mandatory. The success rate after primary treatment of nonunion with various methods of osteosynthesis is quite high [6, 9, 10]. Therefore, there is not much experience in treating its failures, and comparative and prospective studies on the topic are unlikely in the future. Our study was a retrospective series of 14 cases collected within a relatively long period of eleven years due to the rarity of the pathology. Moreover, the cases were failures of nonunion treatment with common methods at other facilities. Therefore, based on our retrospective experience of clavicle surgery for nonunion treatment failures, we are inclined to opine that the tactics of treating clavicle nonunion and defects should choose the method of autologous grafting and a fixator that is capable of maintaining stability over a long period of time required for graft remodeling [10, 11].

The Ilizarov mini-fixator that was designed for small bones is capable to produce stable bone fixation, compression and distraction [12, 17, 18]. While planning a revision operation, it is also necessary to consider such negative factors as a history of polytrauma, unstable fixation, multiple interventions, and blood supply disorders at the ends of fragments.

Intramedullary nailing has been successfully used for treating clavicle nonunion. However, the optimal category for this kind of intervention is patients who had no previous surgical treatment [10]. The lack of rotational stability of this fixation method, in our opinion, is a significant drawback. On the other hand, nailing seems more reasonable than plating due to a complex three-dimensional anatomy of the clavicle. It was the reason for the use of an intramedullary reinforcement wire in the technique described by us.

Undoubtedly, bone plating has sufficient fixation capability. However, the surgeon may encounter difficulties in positioning the screws as previous implants leave their tracts in the clavicle. Moreover, compression in the area of the junction with the fragments could be produced once only

during the intervention to install the plate. There were also problems with postoperative wound healing by using wave plating [9]. AO plates used as external fixators cannot allow compression in the postoperative period [11]. The removal of the plate will always require additional surgical intervention and this intervention is associated with the risk of refracture if a structural graft is used. Good results were obtained with double plating [19], but the sample was relatively small. Unfortunately, our study also features this limitation.

It was assumed that external fixation appears to be a reasonable treatment option in hypertrophic nonunion of the clavicle but not in the atrophic one [6]. In our series of atrophic nonunion, an important merit of the Ilizarov mini-fixator was utilized which its ability to produce supportive compression. The technique seems reasonable for marginal aseptic lysis of the graft in the areas of contact with the clavicle fragments, diagnosed by radiographic checking. Thus, additional surgical plasty with bone chips would not be required. To produce compression would be enough to approximate the fragments to the graft. The intramedullary wire in our technique allows such compression without the risk of secondary displacement of the graft. For cortical defects in the fragments caused by previous implants, we recommend paying close attention to stable insertion of the intramedullary wire as it should provide necessary fixation of the graft. The cantilever wires do not pass through the graft and do not hinder its periosteal blood supply. As wide dissection of soft tissues to insert the wires into the fragments is not required, their periosteal blood flow remains preserved and certainly has a positive effect on achieving union [9, 10, 20]. The variability of Ilizarov mini-fixator assemblies allows the inclusion of half-pins, as in AO mini-fixators [13]. Therefore, this external fixator can be used in adult patients with increased body weight. On the other hand, the technology can be used in children and adolescents with small clavicle sizes as insertion of 1.5–1.8-mm wires will not splinter the bone. Given the lack of consensus on the treatment of congenital nonunion of the clavicle [21, 22], the described technique, in our opinion, has shown its possible application in children despite the difficulties with the wire and mini-fixator care in terms of their compliance with asepsis. Other advantages of the Ilizarov mini-fixator include the ease of its dismantling and the possibility to start physiotherapy exercises early [12].

Undoubtedly, cancellous bone from the iliac crest can be considered the "gold standard" of bone grafting. Its use for cases of a small interfragmentary gap, marginal defects in the fragments, or combined with osteoperiosteal decortication leads to good outcomes [9, 11, 19]. However, the iliac crest is a spongy graft, and the closure of a segmental defect of the tubular bone with it requires samples with 2–3 cortical plates and its harvesting may result in donor site pain. On the contrary, the diameter of the fibular graft is close to the diameter of the clavicle and its adaptation in the zone of contact of fragments does not require additional time or complex techniques. The advantages of a fibular graft include its reinforcing properties due to the cortical structure and a medullary canal, which facilitates the insertion of an intramedullary wire. Pain at the donor site level occurred only in one of our cases and was associated with a concomitant injury of the ankle joint ligaments in the early postoperative period. Conservative treatment proved to be effective and the patient had no complaints in the long term.

Moreover, our technique does not require precision equipment, is relatively simple and affordable in contrast to vascularized bone grafting [14, 15]. Moreover, the technique is sufficiently safe. There were no cases of neurovascular problems, brachialgia or injury to the pleura in our clinical cases, similar to other studies with the application of mini-fixators to manage clavicle nonunion [12, 13]. There were two patients who developed deep infection, including the one with its history. It was recently reported that revision surgery after failed surgical treatment of midshaft clavicle fractures is often associated with positive detection of bacteria but without signs of infection [23, 24].

One could judge our technique being a complex procedure due to its three-component structure and possible wire-tract infection. Other techniques that ensured union in recalcitrant cases with resection defect within 1.5 cm are also complex and took longer time to heal [24]. We developed our technology that provides stability and compression mainly for failures of clavicle nonunion treatment accompanied by larger defects or for congenital cases, being aware of the atrophic condition of the fragments ends. Finally, only two cases after multiple previous surgeries did not heal.

Randomized controlled trials would be a valuable contribution to the problem but unfortunately their implementation could hardly be realized.

CONCLUSION

The combination of three technical components (autologous free fibular grafting, Ilizarov mini-fixator, intramedullary wire) provides control of the graft by mechanical compression and consolidation in the management of large postresection defects of the clavicle midshaft. Upon graft consolidation, the clavicle acquires a near-to-normal radiographic bone structure. The upper limb recovers its functionality.

Conflict of interest *The authors have no potential conflicts of interest regarding this manuscript.*

Funding *The authors received no financial support for the preparation, research, and publication of this manuscript.*

Ethical approval *is not required for the presentation of a case series.*

Informed consent *There is no information in the presented work that could be used to identify patients.*

REFERENCES

1. Morgan C, Bennett-Brown K, Stebbings A, et al. Clavicle fractures. Br J Hosp Med (Lond). 2020;81(7):1-7. doi: 10.12968/hmed.2020.0158.
2. Burnham JM, Kim DC, Kamineni S. Midshaft Clavicle Fractures: A Critical Review. Orthopedics. 2016;39(5):e814-21. doi: 10.3928/01477447-20160517-06.
3. Gordienko II, Sakovich AV, Tsap NA, et al. Treatment tactics in pediatric clavicle fractures. Genij Ortopedii. 2021;27(1):13-16. doi: 10.18019/1028-4427-2021-27-1-13-16.
4. Naimark M, Dufka FL, Han R, et al. Plate fixation of midshaft clavicular fractures: patient-reported outcomes and hardware-related complications. J Shoulder Elbow Surg. 2016;25(5):739-46. doi: 10.1016/j.jse.2015.09.029.
5. Eisenstein ED, Misenhimer JJ, Kotb A, et al. Management of displaced midshaft clavicle fractures in adolescent patients using intramedullary flexible nails: A case series. J Clin Orthop Trauma. 2018;9(Suppl 1):S97-S102. doi: 10.1016/j.jcot.2017.06.019.
6. Barlow T, Upadhyay P, Barlow D. External fixators in the treatment of midshaft clavicle non-unions: a systematic review. Eur J Orthop Surg Traumatol. 2014;24(2):143-148. doi: 10.1007/s00590-013-1173-6.
7. Leroux T, Wasserstein D, Henry P, et al. Rate of and Risk Factors for Reoperations After Open Reduction and Internal Fixation of Midshaft Clavicle Fractures: A Population-Based Study in Ontario, Canada. J Bone Joint Surg Am. 2014;96(13):1119-1125. doi: 10.2106/JBJS.M.00607.
8. Zlowodzki M, Zelle BA, Cole PA, et al. Treatment of acute midshaft clavicle fractures: systematic review of 2144 fractures: on behalf of the Evidence-Based Orthopaedic Trauma Working Group. J Orthop Trauma. 2005;19(7):504-507. doi: 10.1097/01.bot.0000172287.44278.ef.
9. Marti RK, Nolte PA, Kerkhoffs GM, et al. Operative treatment of mid-shaft clavicular non-union. Int Orthop. 2003;27(3):131-135. doi:10.1007/s00264-002-0424-7.
10. Wu CC, Shih CH, Chen WJ, Tai CL. Treatment of clavicular aseptic nonunion: comparison of plating and intramedullary nailing techniques. J Trauma. 1998;45(3):512-516. doi: 10.1097/00005373-199809000-00014.
11. Kerkhoffs GM, Kuipers MM, Marti RK, Van der Werken C. External fixation with standard AO-plates: technique, indications, and results in 31 cases. J Orthop Trauma. 2003;17(1):61-64. doi: 10.1097/00005131-200301000-00010.
12. Demiralp B, Atesalp AS, Sehirlioglu A, et al. Preliminary results of the use of Ilizarov fixation in clavicular non-union. Arch Orthop Trauma Surg. 2006;126(6):401-5. doi: 10.1007/s00402-006-0137-2.
13. Lodhi IA, Russell R, Sharp DJ, Shah KY. The treatment of non-union of the clavicle with the AO mini external fixator. Surgeon. 2007;5(6):335-338. doi: 10.1016/s1479-666x(07)80085-0.
14. Jaloux C, Bettex Q, Levadoux M, et al. Free vascularized medial femoral condyle corticoperiosteal flap with non-vascularized iliac crest graft for the treatment of recalcitrant clavicle non-union. J Plast Reconstr Aesthet Surg. 2020 Jul;73(7):1232-1238. doi: 10.1016/j.bjps.2020.03.018.
15. Lenoir H, Williams T, Kerfant N, et al. Free vascularized fibular graft as a salvage procedure for large clavicular defect: a two cases report. Orthop Traumatol Surg Res. 2013;99(7):859-863. doi: 10.1016/j.otsr.2013.06.004.
16. Özkul B, Saygılı MS, Dinçel YM, et al. Comparative Results of External Fixation, Plating, or Nonoperative Management for Diaphyseal Clavicle Fractures. Med Princ Pract. 2017;26(5):458-463. doi: 10.1159/000481865.
17. Kolchin SN, Mokhovikov DS. Method of replacing a clavicle defect. Patent RF, no. 2807898, 2023. Available at: https://www.fips.ru/registers-doc-view/fips_servlet?DB=RUPAT&rn=6788&DocNumber=2807898&TypeFile=html. Accessed Jan 24, 2025.

18. Zhang J, Yin P, Han B, et al. The treatment of the atrophic clavicular nonunion by double-plate fixation with autogenous cancellous bone graft: a prospective study. J Orthop Surg Res. 2021;16(1):22. doi: 10.1186/s13018-020-02154-y.
19. Tomori Y, Nanno M, Sonoki K, Majima T. Minimally Invasive Corrective Osteotomy with the Ilizarov Mini-Fixator for Malunited Fractures of the Phalanges: Technical Note. J Nippon Med Sch. 2021;88(3):262-266. doi: 10.1272/jnms.JNMS.2021_88-314.
20. Tomić S, Bumbasirevic M, Lesić A, Bumbasirević V. Modification of the Ilizarov external fixator for aseptic hypertrophic nonunion of the clavicle: an option for treatment. J Orthop Trauma. 2006;20(2):122-128. doi: 10.1097/01.bot.0000197548.84296.2f.
21. Borzunov DY, Mitrofanov AI, Kolchev OV. Treatment of clavicular pseudoarthroses. Genij Ortopedii. 2006;(2):74-77. (In Russ.).
22. Der Tavitian J, Davison JN, Dias JJ. Clavicular fracture non-union surgical outcome and complications. Injury. 2002;33(2):135-143. doi: 10.1016/s0020-1383(01)00069-9.
23. Depaoli A, Zarantonello P, Gallone G, et al. Congenital Pseudarthrosis of the Clavicle in Children: A Systematic Review. Children (Basel). 2022;9(2):147. doi: 10.3390/children9020147.
24. Assouto C, Bertoncelli CM, Gauci MO, et al. Congenital pseudarthrosis of the clavicle: a systematic review. Int Orthop. 2022;46(11):2577-2583. doi: 10.1007/s00264-022-05470-6.
25. Hemmann P, Brunner J, Histing T, Körner D. Revision surgery after failed surgical treatment of midshaft clavicle fractures is often associated with positive detection of bacteria. Arch Orthop Trauma Surg. 2023;143(7):4133-4139. doi: 10.1007/s00402-022-04669-x.
26. Grewal S, Baltes TP, Wiegerinck E, Kloen P. Treatment of a Recalcitrant Non-union of the Clavicle. Strategies Trauma Limb Reconstr. 2022;17(1):1-6. doi: 10.5005/jp-journals-10080-1544.

The article was submitted 27.12.2024; approved after reviewing 21.01.2025; accepted for publication 31.03.2025.

Information about the authors:

Sergey N. Kolchin — Candidate of Medical Sciences, orthopaedic surgeon,
sergei.kolchin@gmail.com, https://orcid.org/0000-0001-9049-5710;

Denis S. Mokhovikov — Candidate of Medical Sciences, orthopaedic surgeon, Head of Department,
https://orcid.org/0000-0001-8728-8948;

Tatiana A. Malkova — Leading Translator, https://orcid.org/0000-0002-4301-9161.

Review article
https://doi.org/10.18019/1028-4427-2025-31-3-388-398

Smart orthopedic implants: the future of personalized joint replacement and monitoring

E. Kirolos

Faculty of Medicine and Surgery, Helwan University, Egypt

kiroloss.eskandar@gmail.com

Abstract

Introduction Smart orthopedic implants integrate advanced sensor technologies to revolutionize joint replacement and orthopedic care. These implants enable real-time monitoring of key parameters such as wear, load distribution, and infection indicators, facilitating early intervention and personalized treatment.

This review **aims** to evaluate the current advancements, clinical applications, challenges, and future directions of smart orthopedic implants.

Methods A systematic literature review was conducted following PRISMA guidelines, analyzing peer-reviewed studies published between February 2015 and January 2025. Sources were retrieved from PubMed, Scopus, Web of Science, and Google Scholar. Inclusion criteria focused on technological innovations, clinical applications, and regulatory considerations.

Results & Discussion Technological advancements in materials, sensor integration, wireless communication, and artificial intelligence have optimized implant functionality. Smart implants enhance postoperative monitoring, predict implant wear, and personalize rehabilitation. Despite their benefits, challenges such as biocompatibility, data security, battery life, and regulatory approval hinder widespread adoption. Addressing these issues through interdisciplinary research is critical for future developments.

Conclusion Smart orthopedic implants have the potential to transform musculoskeletal healthcare by enabling real-time patient monitoring and personalized treatment strategies. Continued innovation in materials, AI-driven analytics, and regulatory frameworks will be crucial for overcoming current limitations and ensuring their widespread clinical adoption.

Keywords: Smart orthopedic implants, Spinal implants, Trauma fixation, Sports medicine implants, Joint replacement, Integrated sensors, Real-time patient monitoring, Personalized healthcare

For citation: Kirolos E. Smart orthopedic implants: the future of personalized joint replacement and monitoring. *Genij Ortopedii*. 2025;31(3):388-398. doi: 10.18019/1028-4427-2025-31-3-388-398.

INTRODUCTION

Smart orthopedic implants represent a significant advancement in medical technology, combining therapeutic functions with diagnostic capabilities to enhance patient care. These implants are designed to monitor various physiological parameters in real-time, providing valuable data that can inform treatment decisions and improve outcomes [1]. By integrating sensors and communication technologies, smart implants can detect changes in pressure, force, strain, displacement, proximity, and temperature within the body, offering insights that were previously unattainable through traditional methods [2].

The evolution of orthopedic implants has been marked by a transition from purely mechanical devices to sophisticated systems capable of interactive functions. Traditional implants primarily served structural roles, such as replacing or supporting damaged bones and joints [3]. However, advancements in materials science, sensor technology, and wireless communication have enabled the development of smart implants that not only fulfill structural requirements but also monitor the biological environment. For instance, modern smart implants can measure mechanical loads and stresses, providing data on how the implant interacts with the surrounding tissues during different activities [4]. This information is crucial for assessing implant performance and longevity.

Beyond joint replacement, smart orthopedic implants are being explored for applications in spine surgery, trauma fixation, and sports medicine. Personalization in joint replacement has become increasingly important as it allows for treatments tailored to individual patient needs. Smart implants facilitate this by providing continuous, patient-specific data that can guide personalized rehabilitation protocols and postoperative care [5]. For example, sensors within the implant can monitor the healing process and detect early signs of complications, such as infection or implant loosening, enabling timely interventions. This personalized approach not only enhances patient outcomes but also contributes to more efficient healthcare delivery by reducing the incidence of complications and the need for revision surgeries [6].

To ensure a comprehensive evaluation, this review follows a systematic methodology, incorporating studies from a diverse range of orthopedic specialties. By analyzing the latest technological advancements, clinical applications, and emerging challenges, this review provides a holistic overview of the role of smart orthopedic implants in modern medicine.

This review **aims** to evaluate the current advancements, clinical applications, challenges, and future directions of smart orthopedic implants.

METHODOLOGY

To conduct this comprehensive literature review on smart orthopedic implants, a systematic and structured approach was employed to ensure thorough and unbiased coverage of relevant research. The methodology adhered to the Preferred Reporting Items for Systematic Reviews and Meta-Analyses (PRISMA) guidelines to enhance transparency and reproducibility. The steps of the methodology are detailed below:

Literature Search Strategy

- A comprehensive search was conducted across multiple reputable scientific databases, including PubMed, Scopus, Web of Science, and Google Scholar.
- Search queries incorporated relevant keywords and Boolean operators to ensure a wide but precise retrieval of literature. The primary search terms included:
  - "Smart orthopedic implants";
  - "Joint replacement";
  - "Integrated sensors";
  - "Real-time patient monitoring";
  - "Personalized healthcare".
- Synonyms and related terms were also included, such as "intelligent implants", "biomechanical sensors" and "orthopedic innovations".

Inclusion and Exclusion Criteria

- Inclusion criteria were applied to identify studies relevant to the scope of the review:
  - — Studies published in English;
  - — Peer-reviewed articles, conference papers, and systematic reviews;
  - — Publications focused specifically on smart orthopedic implants and their applications in joint replacement or patient monitoring;
  - — Studies discussing technological innovations, clinical applications, or challenges associated with smart implants.
- Exclusion criteria were employed to refine the selection further:
  - — Articles not available in full text;
  - — Non-peer-reviewed sources, editorials, and opinion pieces;
  - — Publications focusing solely on traditional orthopedic implants without integrating smart technologies.

Study Selection Process

- — The initial database search yielded 164 articles;
- — After removing duplicate entries, 116 articles remained;
- — Titles and abstracts were screened independently by two reviewers to assess relevance. A total of 84 articles were selected for full-text review;
- — The full-text evaluation led to the final inclusion of 66 studies based on their alignment with the inclusion criteria and their contribution to the objectives of the review.

Data Extraction and Management

- A standardized data extraction form was developed to ensure consistency across studies. Key data points included:
  - — Publication details (authors, year, journal);
  - — Study type (e.g., experimental, observational, or review);
  - — Focus of the study (e.g., sensor technology, clinical outcomes, biocompatibility);
  - — Key findings and conclusions.
- Extracted data were systematically organized into tables to facilitate synthesis and analysis.

Quality Assessment

- The quality of included studies was assessed using established tools tailored to the study type. For example:
  - — Experimental studies were evaluated using the Cochrane risk-of-bias tool;
  - — Observational studies were assessed with the Newcastle-Ottawa Scale (NOS);
- Studies with significant methodological limitations were noted but retained if they provided valuable insights.

Synthesis of Findings

- A narrative synthesis approach was adopted to summarize findings across diverse studies;
- Data were categorized into key themes, including technological innovations, clinical applications, real-time monitoring, and challenges associated with smart implants;
- Visual aids, such as the PRISMA flow diagram and summary tables, were employed to enhance clarity and presentation of the findings.

A PRISMA flow diagram (Fig. 1) was used to illustrate the study selection process, including the number of records identified, screened, assessed for eligibility, and included in the final review. Reasons for exclusion at each stage were clearly documented.

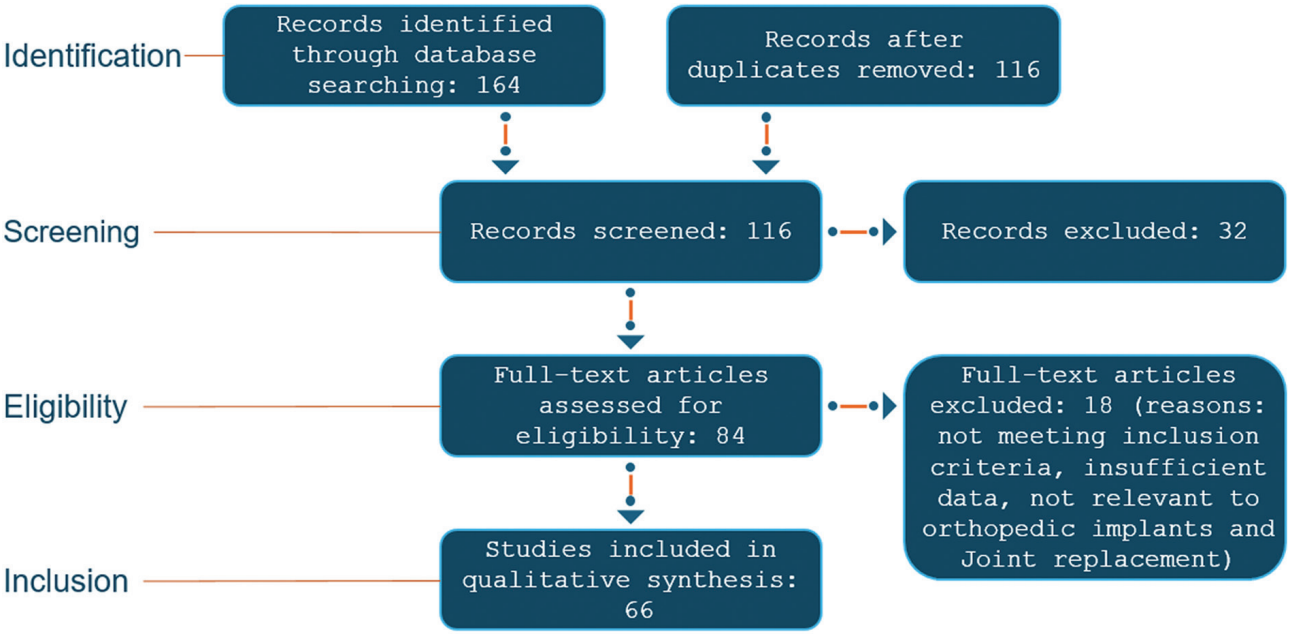

Fig. 1 Illustrates the PRISMA flow diagram

RESULTS AND DISCUSSION

Technological Innovations in Smart Implants

Smart orthopedic implants have undergone significant technological advancements, particularly in the integration of various sensor types, material selection, design considerations, and wireless communication technologies [7]. These innovations aim to enhance the functionality and efficacy of implants in monitoring patient health and improving clinical outcomes.

A variety of sensors have been incorporated into smart implants to monitor physiological and mechanical parameters. Strain gauges are commonly used to measure mechanical load and stress on the implant, providing data on pressure applied during different activities [8]. Temperature sensors monitor local temperature around the implant to detect signs of inflammation or infection. Accelerometers track patient movements and activity levels, ensuring proper usage and adherence to rehabilitation protocols. pH sensors detect changes in pH levels, indicating infection or tissue response to the implant [2]. Additional developments include biosensors capable of detecting biochemical markers that signal early complications, such as osteolysis or metallosis, further improving diagnostic precision (Table 1).

Table 1

Comparison of Smart Implant Technologies Based on Functionality, Application, and Advantages

Technology	Function	Application	Advantages
Strain Gauges	Measure stress/load	Joint replacements	Early detection of implant wear
Temperature Sensors	Detect infection	Trauma fixation	Timely intervention for inflammation
Accelerometers	Monitor movement	Spinal implants	Optimize rehabilitation adherence
Biosensors	Detect biomarkers	Various implants	Advanced infection diagnostics
5G/IoMT	Wireless communication	All smart implants	Faster, real-time data transmission

The selection of materials and design of smart implants are critical to their performance and biocompatibility. Implants are typically made from materials such as titanium, stainless steel, and various polymers designed to integrate well with bone and tissue. These materials are chosen for their strength, durability, and compatibility with the human body to minimize the risk of rejection and complications [9]. Recent advances have introduced bioactive coatings that promote osseointegration, further enhancing the longevity and stability of implants. The design must also accommodate the integration of sensors and electronic components without compromising the structural integrity of the implant. Advancements in microelectronics and nanotechnology have enabled the development of smaller, more efficient sensors and power sources, making smart implants less intrusive and more comfortable for patients [10].

Wireless communication and data transmission technologies are integral to the functionality of smart implants, enabling real-time monitoring and data collection. Smart implants are equipped with wireless communication capabilities, such as Bluetooth or Near Field Communication (NFC), allowing them to transmit data to external devices like smartphones, tablets, or computers [11]. This facilitates remote monitoring by healthcare providers, enabling timely adjustments to treatment plans without the need for frequent in-person visits. Emerging communication technologies, such as 5G and Internet of Medical Things (IoMT), offer faster, more secure data transfer, enhancing real-time decision-making in orthopedic care. Some implants also have onboard data storage, allowing them to store information locally until it can be downloaded during a follow-up appointment. Advanced algorithms and software can analyze this data to detect patterns, predict potential issues, and provide recommendations for personalized care [12].

Real-Time Monitoring Capabilities

Smart orthopedic implants have significantly advanced real-time monitoring capabilities, offering detailed insights into implant wear, early infection detection, and the measurement of load distribution and stress. These functionalities are pivotal in enhancing patient outcomes and extending implant longevity [7].

One of the primary advantages of smart implants is their ability to monitor wear and tear in real-time. By integrating strain gauges and other sensors, these implants can detect minute deformations and stresses that occur during daily activities [1]. This continuous monitoring allows for the early identification of potential issues, such as implant loosening or material degradation, enabling timely medical interventions to prevent further complications [13]. AI-powered predictive modeling is now being employed to analyze wear trends, allowing for proactive maintenance and early intervention strategies.

Early detection of infections is another critical function of smart implants. Infections can lead to severe complications if not promptly addressed. Smart implants equipped with temperature and pH sensors can monitor the local environment around the implant site [1]. Elevations in temperature or shifts in pH levels can indicate the onset of an infection, allowing healthcare providers to initiate treatment before the condition worsens [14]. Advanced biosensors capable of detecting inflammatory cytokines and bacterial activity are now being explored, offering a more precise and earlier detection of infections.

Measuring load distribution and stress on implants is essential for assessing their performance and ensuring patient safety. Smart implants utilize embedded sensors to capture data on the forces exerted during various physical activities [15]. This information is invaluable for understanding how different movements affect the implant and surrounding tissues. For instance, in joint replacements, monitoring load distribution can inform personalized rehabilitation protocols, ensuring that patients engage in activities that promote healing without overloading the implant [16]. Real-time biomechanical feedback allows for dynamic adjustments in patient rehabilitation plans, further enhancing recovery outcomes.

The integration of these monitoring capabilities into orthopedic implants represents a significant advancement in personalized medicine [17]. By providing continuous, real-time data, smart implants enable healthcare providers to tailor treatments to individual patient needs, promptly address

complications, and optimize rehabilitation strategies. This proactive approach not only enhances patient outcomes but also contributes to the longevity and success of the implants [5]. As these technologies continue to evolve, integration with cloud-based analytics and AI-driven diagnostics will further refine personalized patient care.

Data-Driven Optimization of Patient Outcomes

The integration of artificial intelligence (AI) and machine learning (ML) into smart orthopedic implants has ushered in a new era of data-driven optimization in patient care. These technologies enable the analysis of real-time data, facilitating personalized treatment strategies and enhancing clinical outcomes [18].

AI and ML algorithms are adept at processing vast amounts of data generated by smart implants, identifying patterns, and predicting potential complications [19]. For instance, by analyzing sensor data on joint movement and load distribution, AI can detect anomalies indicative of implant wear or misalignment, facilitating early interventions. This predictive capability enhances patient outcomes by preventing issues before they become clinically significant [20].

Personalized rehabilitation plans are another significant benefit of AI integration. Data from smart implants inform tailored rehabilitation protocols, adjusting exercises based on real-time feedback [21]. This approach ensures that patients engage in activities that promote optimal recovery while avoiding movements that could jeopardize implant integrity. Such individualized care accelerates healing and improves overall patient satisfaction [22].

Integrating implant data with electronic health records (EHRs) creates a comprehensive patient profile, enhancing clinical decision-making. This amalgamation allows healthcare providers to monitor patient progress remotely, adjust treatment plans in real-time, and maintain detailed records of implant performance [23]. Moreover, the continuous data flow from smart implants to EHRs facilitates large-scale analyses, contributing to improved implant designs and personalized treatment strategies [24].

The integration of AI and ML into smart orthopedic implants represents a significant advancement in personalized medicine. By providing continuous, real-time data, smart implants enable healthcare providers to tailor treatments to individual patient needs, promptly address complications, and optimize rehabilitation strategies [25]. This proactive approach not only enhances patient outcomes but also contributes to the longevity and success of the implants.

Applications in Specific Orthopedic Conditions

Smart orthopedic implants represent a significant advancement in the treatment of various musculoskeletal conditions, offering real-time data and personalized therapeutic interventions. Their applications are particularly notable in knee and hip replacements, spinal implants, and the management of trauma and sports-related injuries [26].

In knee arthroplasty, the advent of smart implants has transformed postoperative care. Devices such as the Persona IQ® have been developed to function similarly to standard knee replacements but with integrated sensor technology. These sensors are embedded within the tibial stem and are capable of measuring a range of parameters, including range of motion, step count, and walking speed [27]. The collected data is wirelessly transmitted to healthcare providers, enabling continuous remote monitoring of the patient's progress. This real-time feedback allows for the timely identification of any deviations from expected recovery patterns, facilitating prompt interventions when necessary [28]. Moreover, the personalized data supports the customization of rehabilitation protocols, ensuring that exercises are tailored to the individual's specific needs and capabilities, thereby promoting optimal recovery outcomes [29].

Similarly, in hip arthroplasty, smart implants are being utilized to enhance patient outcomes. These devices integrate sensor technology to monitor various parameters, providing valuable data that can be used to tailor postoperative care and rehabilitation [1]. In spinal surgery, the application

of smart implants is emerging as a promising innovation. These devices are designed to monitor parameters such as load distribution and alignment, providing real-time data that can assist surgeons in optimizing implant placement and postoperative care [17].

In the realm of trauma and sports medicine, smart implants hold significant potential for transforming patient care. In fracture management, for instance, smart implants can monitor the stability of the fixation and the progress of bone healing, allowing for timely interventions if complications arise. In sports medicine, smart implants can provide data on joint loading and movement patterns, aiding in the optimization of rehabilitation protocols and the prevention of re-injury [30, 31].

Challenges and Limitations

The advancement of smart orthopedic implants introduces several challenges and limitations that must be addressed to ensure their efficacy and safety. Key concerns include biocompatibility and long-term durability of integrated sensors, battery life and energy efficiency of the implants, and data privacy alongside cybersecurity issues [32].

Biocompatibility is a critical factor in the development of smart implants. The integration of sensors and electronic components within these devices necessitates materials that are not only functional but also compatible with human tissue. Materials such as polyethylene, titanium, and parylene have been utilized due to their favorable biocompatibility profiles [33]. However, the presence of electronic components can elicit foreign body reactions, including inflammatory responses and fibrous encapsulation, which may compromise sensor functionality over time [34]. For instance, histological changes in the tissue surrounding the implant, such as inflammation and fibrous tissue formation, can impair biosensor activity, leading to potential device failure. Additionally, concerns have been raised regarding the potential cytotoxic, genotoxic, or pyrogenic effects of implant failure, particularly in younger patients [35].

The longevity of smart implants is closely tied to their power management systems. Many devices rely on batteries to power integrated sensors and communication modules. Ensuring adequate battery life while maintaining a compact implant size presents a significant engineering challenge [36]. Microelectromechanical systems (MEMS)-based technologies have been employed to reduce the size of sensors and associated circuitry, thereby decreasing power consumption. However, operating at higher frequencies to achieve this reduction can lead to increased energy absorption by surrounding tissues, potentially causing heating and signal attenuation [37]. Exploring alternative power sources, such as energy harvesting from body movements or wireless power transmission, may offer solutions but also introduce additional complexities in design and safety considerations [38].

Data privacy and cybersecurity are paramount concerns in the deployment of smart implants. These devices collect and transmit sensitive patient data, including physiological parameters and activity levels, which must be protected from unauthorized access and breaches [39]. The increasing prevalence of cyber threats in healthcare necessitates robust security measures to safeguard this information. Ethical considerations also arise regarding the ownership and use of the data generated by these implants. Ensuring compliance with data protection regulations and maintaining patient trust are critical for the widespread adoption of smart implant technologies [40]. Furthermore, the integration of wireless communication systems within implants introduces potential vulnerabilities that could be exploited, underscoring the need for comprehensive cybersecurity strategies in the design and implementation of these devices [41].

Addressing these challenges requires a multidisciplinary approach, combining expertise in materials science, biomedical engineering, cybersecurity, and clinical practice. Ongoing research and development efforts are focused on enhancing the biocompatibility and durability of implant materials, improving energy efficiency and exploring alternative power solutions, and implementing robust data protection mechanisms. Through these concerted efforts, the potential of smart orthopedic implants to improve patient outcomes can be fully realized [42, 43].

Regulatory and Ethical Considerations

The integration of smart implants into orthopedic practice necessitates careful navigation of regulatory frameworks and ethical considerations to ensure patient safety, data security, and informed consent [44].

Regulatory approval processes for smart implants are complex and multifaceted. In the United States, the Food and Drug Administration (FDA) oversees the evaluation and authorization of these devices. Depending on the risk classification of the implant, different regulatory pathways may be applicabl [45]. For instance, devices deemed to have moderate risk may undergo the 510(k) premarket notification process, which requires demonstrating substantial equivalence to a legally marketed predicate device. This pathway is generally less burdensome than the premarket approval (PMA) process, which is reserved for higher-risk devices and necessitates more extensive clinical evidence [46]. The FDA has been working to provide clearer guidance on the regulatory requirements for smart medical devices, acknowledging the unique challenges they present [47].

Ethical implications of continuous patient monitoring via smart implants are significant. While these devices offer the potential for real-time health monitoring and early detection of complications, they also raise concerns about patient autonomy and the potential for over-surveillance [48]. Continuous data collection may lead to information overload for both patients and healthcare providers, and there is a risk that patients may feel their privacy is being infringed upon. Moreover, the psychological impact of constant health monitoring should not be underestimated, as it may induce anxiety or alter patient behavior. It is essential to balance the benefits of continuous monitoring with respect for patient autonomy and privacy [49, 50].

Addressing patient consent and data ownership is crucial in the deployment of smart implants. Patients must be fully informed about what data will be collected, how it will be used, who will have access to it, and the measures in place to protect their privacy [51]. Clear and comprehensive consent processes are essential to ensure that patients understand and agree to the data practices associated with their implants. Furthermore, issues of data ownership must be clarified; patients should have rights to access their data and control its use [52]. This includes the ability to withdraw consent and have their data deleted if they so choose. Healthcare providers and device manufacturers must navigate these issues carefully to maintain trust and comply with data protection regulations [53].

Future Directions and Research Gaps

The field of smart orthopedic implants is poised for significant advancements, driven by emerging technologies and interdisciplinary collaboration. Innovations such as self-healing materials, bioelectronics, and bioprinting are at the forefront of research, aiming to enhance implant functionality and patient outcomes [54].

Self-healing materials represent a promising avenue in orthopedic implant development. These materials have the intrinsic ability to repair damage without external intervention, potentially extending the lifespan of implants and reducing the need for revision surgeries [55]. Incorporating self-healing polymers or composites into implant design could allow for the automatic repair of microcracks or other minor damages that occur over time, maintaining the structural integrity and performance of the implant. Research in this area is ongoing, with studies exploring various self-healing mechanisms and their applicability to load-bearing orthopedic devices [56].

Bioelectronics is another emerging field with significant implications for smart implants. The integration of electronic components with biological systems enables real-time monitoring and therapeutic interventions [57]. For instance, bioelectronic implants can be designed to monitor bone healing processes and deliver electrical stimulation to promote tissue regeneration. Recent advancements have led to the development of multifunctional bone implants that combine sensing capabilities with therapeutic actuation systems, offering a comprehensive approach to patient care [58, 59].

Bioprinting, particularly three-dimensional (3D) bioprinting, holds significant potential in creating custom smart implants tailored to individual patient anatomies. This technology allows for the precise fabrication of complex structures using bioinks composed of cells and biomaterials [60].

In orthopedic applications, 3D bioprinting can be utilized to produce scaffolds that mimic the native bone architecture, facilitating better integration and promoting tissue regeneration. Moreover, bioprinting enables the customization of implants to match patient-specific defect sites, potentially improving surgical outcomes and reducing recovery times [61].

The successful development and implementation of these advanced technologies necessitate close collaboration between orthopedic surgeons, engineers, and data scientists. Surgeons provide critical clinical insights and define the functional requirements of implants, while engineers contribute expertise in materials science, biomechanics, and device design [62]. Data scientists play a pivotal role in analyzing the vast amounts of data generated by smart implants, developing algorithms to interpret sensor outputs, and creating predictive models to inform clinical decision-making [63]. This interdisciplinary approach ensures that smart implants are designed with a comprehensive understanding of both clinical needs and technological capabilities, ultimately leading to more effective and personalized patient care [64].

Despite these promising developments, several research gaps remain. Further studies are needed to optimize the properties of self-healing materials for orthopedic applications, ensuring they can withstand the mechanical demands of load-bearing implants. The long-term biocompatibility and stability of bioelectronic components within the human body require thorough investigation [65]. Additionally, while bioprinting has demonstrated potential, challenges related to the vascularization of printed tissues and the scalability of the technology must be addressed. Ongoing research and collaboration across disciplines will be essential to overcome these challenges and fully realize the potential of smart orthopedic implants [66].

CONCLUSION

In conclusion, smart orthopedic implants represent a groundbreaking innovation at the intersection of medicine, engineering, and data science, offering a transformative approach to joint replacement and musculoskeletal care. By integrating advanced sensors, wireless communication, and real-time data analytics, these implants provide unprecedented capabilities for monitoring wear, detecting complications, and optimizing treatment outcomes. The incorporation of emerging technologies, such as self-healing materials, bioelectronics, and bioprinting, alongside interdisciplinary collaboration, underscores the vast potential of smart implants to enhance orthopedic care and improve patient quality of life. Despite challenges related to biocompatibility, data security, and regulatory hurdles, the ongoing evolution of smart implant technologies highlights a promising future where personalized, data-driven, and patient-centered solutions become the cornerstone of healthcare. Embracing these innovations will not only redefine orthopedic practices but also pave the way for a new era of intelligent healthcare systems designed to deliver better outcomes and quality of life for patients worldwide.

Conflict of interest *The authors declare that they have no competing interests.*

Funding *Not applicable.*

Ethics approval and consent to participate *Not applicable.*

Consent for publication *Not applicable.*

Availability of data and material *Data sharing not applicable to this article as no data-sets were generated or analyzed during the current study.*

REFERENCES

1. Abyzova E, Dogadina E, Rodriguez RD, et al. Beyond Tissue replacement: The Emerging role of smart implants in healthcare. *Mater Today Bio*. 2023;22:100784. doi: 10.1016/j.mtbio.2023.100784.
2. Yogev D, Goldberg T, Arami A, et al. Current state of the art and future directions for implantable sensors in medical technology: Clinical needs and engineering challenges. *APL Bioeng*. 2023;7(3):031506. doi: 10.1063/5.0152290.
3. Wu Y, Liu J, Kang L, et al. An overview of 3D printed metal implants in orthopedic applications: Present and future perspectives. *Heliyon*. 2023;9(7):e17718. doi: 10.1016/j.heliyon.2023.e17718.
4. Hossain N, Mahmud MZA, Hossain A, et al. Advances of materials science in MEMS applications: A review. *Results Eng*. 2024;22(2):102115. doi: 10.1016/j.rineng.2024.102115.
5. Luo Y. Toward Fully Automated Personalized Orthopedic Treatments: Innovations and Interdisciplinary Gaps. *Bioengineering (Basel)*. 2024;11(8):817. doi: 10.3390/bioengineering11080817.

6. Iyengar KP, Kariya AD, Botchu R, et al. Significant capabilities of SMART sensor technology and their applications for Industry 4.0 in trauma and orthopaedics. *Sensors Int*. 2022;(3):100163. doi: 10.1016/j.sintl.2022.100163.
7. Kelmers E, Szuba A, King SW, et al. "Smart Knee Implants: An Overview of Current Technologies and Future Possibilities". *Indian J Orthop*. 2022;57(5):635-642. doi: 10.1007/s43465-022-00810-5.
8. Wang J, Chu J, Song J, Li Z. The application of impantable sensors in the musculoskeletal system: a review. *Front Bioeng Biotechnol*. 2024;12:1270237. doi: 10.3389/fbioe.2024.1270237.
9. Abd-Elaziem W, Darwish MA, Hamada A, Daoush WM. Titanium-Based alloys and composites for orthopedic implants Applications: A comprehensive review. *Materials & Design*. 2024;241:112850. doi: 10.1016/j.matdes.2024.112850.
10. Juanola-Feliu E, Miribel-Català PL, Páez Avilés C, et al. Design of a customized multipurpose nano-enabled implantable system for in-vivo theranostics. *Sensors (Basel)*. 2014;14(10):19275-19306. doi: 10.3390/s141019275.
11. Cao Z, Chen P, Ma Z, et al. Near-Field Communication Sensors. *Sensors (Basel)*. 2019;19(18):3947. doi: 10.3390/s19183947.
12. Serrano LP, Maita KC, Avila FR, et al. Benefits and Challenges of Remote Patient Monitoring as Perceived by Health Care Practitioners: A Systematic Review. *Perm J*. 2023;27(4):100-111. doi: 10.7812/TPP/23.022.
13. Windolf M, Varjas V, Gehweiler D, et al. Continuous Implant Load Monitoring to Assess Bone Healing Status-Evidence from Animal Testing. *Medicina (Kaunas)*. 2022;58(7):858. doi: 10.3390/medicina58070858.
14. Fulton II MR, Zubair M, Taghavi S. Laboratory Evaluation of Sepsis. 2023. In: *StatPearls [Internet]*. Treasure Island (FL): StatPearls Publishing; 2023. Available at: https://www.ncbi.nlm.nih.gov/books/NBK594258/. Accessed Feb 5, 2025.
15. Gaobotse G, Mbunge E, Batani J, Muchemwa B. Non-invasive smart implants in healthcare: Redefining healthcare services delivery through sensors and emerging digital health technologies. *Sensors Int*. 2022;3:100156. doi: 10.1016/j.sintl.2022.100156.
16. Eghan-Acquah E, Bavil AY, Bade D, et al. Enhancing biomechanical outcomes in proximal femoral osteotomy through optimised blade plate sizing: A neuromusculoskeletal-informed finite element analysis. *Comput Methods Programs Biomed*. 2024;257:108480. doi: 10.1016/j.cmpb.2024.108480.
17. Ledet EH, Liddle B, Kradinova K, Harper S. Smart implants in orthopedic surgery, improving patient outcomes: a review. *Innov Entrep Health*. 2018;5:41-51. doi: 10.2147/IEH.S133518.
18. Tariq A, Gill AY, Hussain HK. Evaluating the potential of artificial intelligence in orthopedic surgery for value-based healthcare. *Int J Multidisc Sci Arts*. 2023;2(2):27-35. doi: 10.47709/ijmdsa.v2i1.2394.
19. Vora LK, Gholap AD, Jetha K, et al. Artificial Intelligence in Pharmaceutical Technology and Drug Delivery Design. *Pharmaceutics*. 2023;15(7):1916. doi: 10.3390/pharmaceutics15071916.
20. Wang C, He T, Zhou H, et al. Artificial intelligence enhanced sensors - enabling technologies to next-generation healthcare and biomedical platform. *Bioelectron Med*. 2023;9(1):17. doi: 10.1186/s42234-023-00118-1.
21. Sumner J, Lim HW, Chong LS, et al. Artificial intelligence in physical rehabilitation: A systematic review. *Artif Intell Med*. 2023;146:102693. doi: 10.1016/j.artmed.2023.102693.
22. Chirayath A, Dhaniwala N, Kawde K. A Comprehensive Review on Managing Fracture Calcaneum by Surgical and Non-surgical Modalities. *Cureus*. 2024;16(2):e54786. doi: 10.7759/cureus.54786.
23. Adeniyi NO, Arowoogun JO, Chidi R, et al. The impact of electronic health records on patient care and outcomes: A comprehensive review. *World J Adv Res Rev*. 2024;21(2):1446-1455. doi: 10.30574/wjarr.2024.21.2.0592
24. Ghazizadeh E, Naseri Z, Deigner HP, et al. Approaches of wearable and implantable biosensor towards of developing in precision medicine. *Front Med (Lausanne)*. 2024;11:1390634. doi: 10.3389/fmed.2024.1390634.
25. Andriollo L, Picchi A, Iademarco G, et al. The Role of Artificial Intelligence and Emerging Technologies in Advancing Total Hip Arthroplasty. *J Pers Med*. 2025;15(1):21. doi: 10.3390/jpm15010021.
26. Akhtar MN, Haleem A, Javaid M, et al. Artificial intelligence-based orthopaedic perpetual design. *J Clin Orthop Trauma*. 2024;49:102356. doi: 10.1016/j.jcot.2024.102356.
27. Iyengar KP, Gowers BTV, Jain VK, et al. Smart sensor implant technology in total knee arthroplasty. *J Clin Orthop Trauma*. 2021;22:101605. doi: 10.1016/j.jcot.2021.101605.
28. Abdulmalek S, Nasir A, Jabbar WA, et al. IoT-Based Healthcare-Monitoring System towards Improving Quality of Life: A Review. *Healthcare (Basel)*. 2022;10(10):1993. doi: 10.3390/healthcare10101993.
29. Li X, He Y, Wang D, Rezaei MJ. Stroke rehabilitation: from diagnosis to therapy. *Front Neurol*. 2024;15:1402729. doi: 10.3389/fneur.2024.1402729.
30. Jeyaraman M, Jayakumar T, Jeyaraman N, Nallakumarasamy A. Sensor Technology in Fracture Healing. *Indian J Orthop*. 2023;57(8):1196-1202. doi: 10.1007/s43465-023-00933-3.
31. Al-Shalawi FD, Mohamed Ariff AH, Jung DW, et ak. Biomaterials as Implants in the Orthopedic Field for Regenerative Medicine: Metal versus Synthetic Polymers. *Polymers (Basel)*. 2023;15(12):2601. doi: 10.3390/polym15122601.
32. Kim SJ, Wang T, Pelletier MH, Walsh WR. 'SMART' implantable devices for spinal implants: a systematic review on current and future trends. *J Spine Surg*. 2022;8(1):117-131. doi: 10.21037/jss-21-100.
33. Teo AJT, Mishra A, Park I, et al. Polymeric Biomaterials for Medical Implants and Devices. *ACS Biomater Sci Eng*. 2016;2(4):454-472. doi: 10.1021/acsbiomaterials.5b00429.
34. Capuani S, Malgir G, Chua CYX, Grattoni A. Advanced strategies to thwart foreign body response to implantable devices. *Bioeng Transl Med*. 2022;7(3):e10300. doi: 10.1002/btm2.10300.
35. Noskovicova N, Hinz B, Pakshir P. Implant Fibrosis and the Underappreciated Role of Myofibroblasts in the Foreign Body Reaction. *Cells*. 2021;10(7):1794. doi: 10.3390/cells10071794.
36. Roy S, Azad ANMW, Baidya S, et al. Powering solutions for biomedical sensors and implants inside the human body: A comprehensive review on energy harvesting units, energy storage, and wireless power transfer techniques. *IEEE Transa Power Electron*. 2022;37(10):12237-12263. doi: 10.1109/tpel.2022.3164890.
37. Nazir S, Kwon OS. Micro-electromechanical systems-based sensors and their applications. *Appl Sci Converg Technol*. 2022;31:40-45. doi: 10.5757/ASCT.2022.31.2.40.
38. Ávila BYL, Vázquez CAG, Baluja OP, et al. Energy harvesting techniques for wireless sensor networks: A systematic literature review. *Energy Strategy Reviews*. 2025;57:101617. doi: 10.1016/j.esr.2024.101617.

39. Jaime FJ, Muñoz A, Rodríguez-Gómez F, Jerez-Calero A. Strengthening Privacy and Data Security in Biomedical Microelectromechanical Systems by IoT Communication Security and Protection in Smart Healthcare. *Sensors (Basel)*. 2023;23(21):8944. doi: 10.3390/s23218944.
40. Alanazi AT. Clinicians' Perspectives on Healthcare Cybersecurity and Cyber Threats. *Cureus*. 2023;15(10):e47026. doi: 10.7759/cureus.47026.
41. Williams PA, Woodward AJ. Cybersecurity vulnerabilities in medical devices: a complex environment and multifaceted problem. *Med Devices (Auckl)*. 2015;8:305-316. doi: 10.2147/MDER.S50048.
42. Subramaniam S, Akay M, Anastasio MA, et al. Grand Challenges at the Interface of Engineering and Medicine. *IEEE Open J Eng Med Biol*. 2024;5:1-13. doi: 10.1109/OJEMB.2024.3351717.
43. Anyanwu EC, Osasona F, Akomolafe OO, et al. Biomedical engineering advances: A review of innovations in healthcare and patient outcomes. *Int J Sci Res Arch*. 2024;11(1):870-882. doi: 10.30574/ijsra.2024.11.1.0139
44. Rovere G, Bosco F, Miceli A, et al. Adoption of blockchain as a step forward in orthopedic practice. *Eur J Transl Myol*. 2024;34(2):12197. doi: 10.4081/ejtm.2024.12197.
45. Jazowski SA, Winn AN. The Role of the FDA and Regulatory Approval of New Devices for Diabetes Care. *Curr Diab Rep*. 2017;17(6):40. doi: 10.1007/s11892-017-0871-6.
46. Premarket notification [510(k)]. In: Wreh E. *Medical Device Regulation*. Elsevier; 2023:57-89.
47. *U.S. Food and Drug Administration. FDA proposes framework to advance credibility of AI models used for drug and biological product submissions*. 2025. Available at: https://www.fda.gov/news-events/press-announcements/fda-proposes-framework-advance-credibility-ai-models-used-drug-and-biological-product-submissions. Accessed Feb 5, 2025.
48. Cohen IG, Gerke S, Kramer DB. Ethical and Legal Implications of Remote Monitoring of Medical Devices. *Milbank Q*. 2020;98(4):1257-1289. doi: 10.1111/1468-0009.12481.
49. Nijor S, Rallis G, Lad N, Gokcen E. Patient Safety Issues From Information Overload in Electronic Medical Records. *J Patient Saf*. 2022;18(6):e999-e1003. doi: 10.1097/PTS.0000000000001002.
50. Zhong L, Cao J, Xue F. The paradox of convenience: how information overload in mHealth apps leads to medical service overuse. *Front Public Health*. 2024;12:1408998. doi: 10.3389/fpubh.2024.1408998.
51. Camara C, Peris-Lopez P, Tapiador JE. Security and privacy issues in implantable medical devices: A comprehensive survey. *J Biomed Inform*. 2015;55:272-289. doi: 10.1016/j.jbi.2015.04.007.
52. Shah P, Thornton I, Kopitnik NL, Hipskind JE. Informed Consent. 2024. In: *StatPearls [Internet]*. Treasure Island (FL): StatPearls Publishing; 2025. Available at: https://www.ncbi.nlm.nih.gov/books/NBK430827/. Accessed Feb 5, 2025.
53. Chiruvella V, Guddati AK. Ethical Issues in Patient Data Ownership. *Interact J Med Res*. 2021;10(2):e22269. doi: 10.2196/22269.
54. Intravaia JT, Graham T, Kim HS, et al. Smart Orthopedic Biomaterials and Implants. *Curr Opin Biomed Eng*. 2023;25:100439. doi: 10.1016/j.cobme.2022.100439.
55. Bandyopadhyay A, Mitra I, Goodman SB, et al. Improving Biocompatibility for Next Generation of Metallic Implants. *Prog Mater Sci*. 2023;133:101053. doi: 10.1016/j.pmatsci.2022.101053.
56. Kanu NJ, Gupta E, Vates UK, et al. Self-healing composites: A state-of-the-art review. *Compos A Appl Sci Manuf*. 2019;121:474-486. doi: 10.1016/j.compositesa.2019.04.012.
57. Yao G, Gan X, Lin Y. Flexible self-powered bioelectronics enables personalized health management from diagnosis to therapy. *Sci Bull (Beijing)*. 2024;69(14):2289-2306. doi: 10.1016/j.scib.2024.05.012.
58. Luo S, Zhang C, Xiong W, et al. Advances in electroactive biomaterials: Through the lens of electrical stimulation promoting bone regeneration strategy. *J Orthop Translat*. 2024;47:191-206. doi: 10.1016/j.jot.2024.06.009.
59. Boys AJ, & Keene ST. Bioelectronic interfacial matching for superior implant design. *Cell Rep Phys Sci*. 2024;5(8):101877. doi: 10.1016/j.xcrp.2024.101877.
60. Mirshafiei M, Rashedi H, Yazdian F, et al. Advancements in tissue and organ 3D bioprinting: Current techniques, applications, and future perspectives. *Materials & Design*. 2024;240:112853. doi: 10.1016/j.matdes.2024.112853.
61. Selim M, Mousa HM, Abdel-Jaber G, et al. Innovative designs of 3D scaffolds for bone tissue regeneration: Understanding principles and addressing challenges. *Eur Polym J*. 2024;215:113251. doi: 10.1016/j.eurpolymj.2024.113251.
62. Kulkarni PG, Paudel N, Magar S, et al. Overcoming Challenges and Innovations in Orthopedic Prosthesis Design: An Interdisciplinary Perspective. *Biomed Mater Devices*. 2023:1-12. doi: 10.1007/s44174-023-00087-8.
63. Shajari S, Kuruvinashetti K, Komeili A, Sundararaj U. The Emergence of AI-Based Wearable Sensors for Digital Health Technology: A Review. *Sensors (Basel)*. 2023;23(23):9498. doi: 10.3390/s23239498.
64. Schrimpff C, Link E, Fisse T, et al. Mental Models of Smart Implant Technology: A Topic Modeling Approach to the Role of Initial Information and Labeling. *Health Commun*. 2025:1-13. doi: 10.1080/10410236.2024.2447548.
65. Shekhawat D, Singh A, Banerjee M, et al. Bioceramic composites for orthopaedic applications: A comprehensive review of mechanical, biological, and microstructural properties. *Ceram Int*. 2020;47(3):3013–3030. doi: 10.1016/j.ceramint.2020.09.214.
66. Yuan X, Wang Z, Che L, et al. Recent developments and challenges of 3D bioprinting technologies. *Int J Bioprinting*. 2024;10:1752. doi: 10.36922/ijb.1752.

The article was submitted 29.01.2025; approved after reviewing 04.02.2025; accepted for publication 31.03.2025.

Information about the author:

Eskandar Kirolos — BSc, MBBCh, and MA, kiroloss.eskandar@gmail.com, https://orcid.org/0000-0003-0085-3284.

Professor Dyachkov Alexander Nikolaevich (75th birthday anniversary)

Professor Alexander Nikolaevich Dyachkov, MD, Chief Researcher of the Educational Department of the Ilizarov Center, celebrated his 75th birthday on May 27, 2025.

His road to the medical profession began with graduation from the Omsk Medical Institute. He continued his career in emergency surgery. The young doctor Alexander Dyachkov came to Kurgan in 1976 and was chosen by competition for the position of junior research fellow in the experimental department. All his thoughts were devoted to research work, and he worked in a well-coordinated team of like-minded people.

Successful results of the research into the effectiveness of the transosseous osteosynthesis method, conducted under the supervision of G.A. Ilizarov, allowed Alexander Dyachkov to take a new approach to solving the problem of muscle defect management and became the basis for his candidate's dissertation, which he brilliantly defended in 1985. The work was the first to evaluate the reparative processes in muscle tissue during defect management. Translation of the experimental results into clinical practice had a significant effect and could reduce disability in severe orthopedic pathology and injuries.

Later, A.N. Dyachkov became interested in studying the potential of using the Ilizarov method in craniosurgery. The concept he developed became the basis for preparing a dissertation for doctor of medical sciences degree, which he successfully defended in 1997.

Alexander Nikolaevich has dedicated more than 40 years to work at the Ilizarov Center and has come a long professional path. For many years, he worked as the Scientific Secretary of the Center and made a great contribution to the development and implementation of scientific research planning. Professor Dyachkov was the Scientific Secretary of several dissertation councils organized on the basis of the Ilizarov Center for many years. His assistance to dozens of applicants in preparing scientific papers and theses is invaluable. More than 10 candidate and doctoral dissertations were defended under his direct supervision. A.N. Dyachkov is the author and co-author of more than 250 printed works, 25 inventions and utility models. In 2010, A.N. Dyachkov was appointed acting director of the Center, and then deputy director for scientific work.

For high performance in scientific and clinical activities, he was awarded the medal of the Order of Merit for the Fatherland.

The medical dynasty of the Dyachkovs at the Center can also be considered his special merit. Currently, his son and grandson work at the Ilizarov Center. They are also successful in their profession and are known for their scientific achievements.

The staff of the Center and the editorial board of the journal Genij Ortopedii congratulate the Honorary Professor of the Ilizarov Center Alexander Nikolaevich Dyachkov on his anniversary and wish him good health, family well-being, peace of mind and strength to implement new scientific ideas, support young scientists and continue the traditions established by Academician G.A. Ilizarov.

Professor Ulrich Eduard Vladimirovich (1937 – 2025)

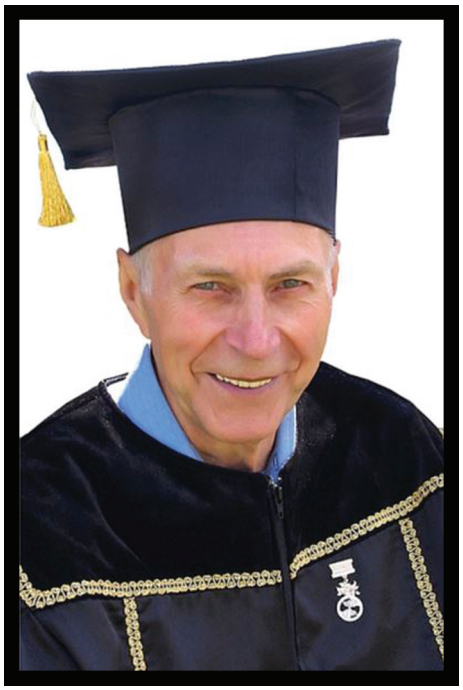

An outstanding pediatric surgeon, one of the founders of the Russian surgical vertebrology, founder of the St. Petersburg School of Pediatric Vertebrologists, Honorary professor of the Ilizarov Center, doctor of medical sciences, professor Eduard Vladimirovich Ulrich passed away on June 2, 2025. He was only 87 years old. “Only”, because his clear and sharp mind, strong handshake, brilliant erudition, unbending will, colossal performance, selfless devotion to his favorite work and intuition in determining advanced trends in spinal surgery did not depend on age.

The beginning of Eduard Vladimirovich's professional way a of a series of tests. His childhood coincided with the siege of Leningrad and evacuation; his father was repressed during Stalin's rule and was rehabilitated only in 2011. By the way, Eduard Vladimirovich spent 12 years fighting for this rehabilitation. The choice of profession was predetermined by the war years and observation of evacuation hospitals, but even after successfully passing the entrance exams, the commission had questions for the son of a repressed person with a German surname.

After graduating from Leningrad Pediatric Medical Institute (LPMI) in 1961, he worked for two years as a surgeon in the district hospital of the Arkhangelsk region together with experienced operating nurses who had gone through the Great Patriotic War, and in practice he knew "the difference between Esmarch's mug and Esmarch's mask." Later, he recalled this time as a period of professional happiness. Returning to Leningrad in 1963, Eduard Vladimirovich connected his whole life with the Department of Pediatric Surgery of LPMI, going from a postgraduate student and assistant to the head of the department.

In 1967, Eduard Vladimirovich Ulrich defended his candidate's of medical sciences dissertation on the topic of "Surgical treatment of post-traumatic deformities of the bones of the upper extremities in children under the supervision of G.A. Bairov, a famous pediatric surgeon, corresponding member of the Academy of Medical Sciences." At a time when pediatric surgery required universe approach, he dealt with emergency and planned thoracic and abdominal surgery, issues of pediatric anesthesiology and proctology. In the 1970s, Eduard Vladimirovich began to study the topic that was completely unknown at that time, congenital deformities of the spine, and in 1985 he successfully defended his doctoral dissertation on the topic of "Surgical treatment of malformations of the spine in children."

There was no computerization yet, but he systematized data on more than 500 patients and created a classification of congenital anomalies of the spine and spinal canal. At a time when special spinal instruments were unavailable in our country, Eduard Vladimirovich created the first original metal instrumentation for the correction of spinal deformities in young children using his own drawings, developed unique operations for hemivertebrae, vertebral segmentation disorders, thoracic insufficiency syndromes and spinal cord splitting, focusing on finding methods for correcting such defects. During the same period, research was initiated on combined extravertebral pathology, methods of contrasting the spinal canal and anesthetic protection of the spinal cord. It were the years when CT and MRI had just started to be introduced into medical practice, and most surgical decisions were made based on only X-ray spondylography.

Professor E.V. Ulrich was ahead of his time, having organized the first training course in pediatric vertebrology in Russia in the mid-1990s (the creation of this specialty was only just discussed) and having put forward the idea of creating a specialized emergency vertebrology service

in St. Petersburg. He did not find support in the city administration at that time, but almost 10 years later this idea was finally implemented by the director of the Turner Children's Orthopedic Institute A.G. Baindurashvili within the framework of the regional center for spinal injuries in children.

The merits of Professor E.V. Ulrich have been recognized by leading world specialists. In 1999, E.V. Ulrich together with Professor J. Dubousset (France), with whom they had been friends for many years, organized the GICD (Cotrel-Dubousset Group) congress in St. Petersburg, which was attended by more than 100 vertebrologists from Europe, Asia and Africa. In the early 2000s, under his leadership, a comprehensive program was prepared that united researchers, doctors and teachers of medical universities and actually determined the creation of the school of pediatric vertebrologists in St. Petersburg, from which many specialists emerged and now head the leading medical centers, institutes and clinics of our country.

Eduard Vladimirovich's active life position was reflected in the advancement of knowledge and in the education of young people. In 2004, he became the first laureate of the Ternovsky Award for Services to Children's Surgery. At the same time, he joined the staff of the newly created scientific and practical journal "Spine Surgery" and published in its very first issue an article devoted to the classification of vertebral anomalies together with R. Winter and J. Lonstein. E.V. Ulrich was a member of the editorial boards of several surgical and orthopedic journals, the author of seven monographs, numerous patents, and the supervisor and scientific consultant of three doctoral and 19 candidate dissertations.

He gradually limited his practical work with age but Eduard Vladimirovich remained a person to whom everyone, regardless of age and experience, could turn for help. Anyone who was lucky enough to communicate with him remembers the sincere joy that Professor Ulrich experienced when talking about the ideas and successes of colleagues and students. His presence in the operating room, calm voice and practical advice made them work more confidently and set seemingly unattainable goals, and successfully solve the most unusual situations.

Eduard Vladimirovich Ulrich passed away at the age of 87, but he remains in our memory as a wise Teacher, Colleague, Scientist and a Man with a capital letter. Thank you, Eduard Vladimirovich, for the fact that all those years we had the happiness of being with you …

Students and colleagues of Professor E.V. Ulrich,
editorial board of the journal Genij Orthopedii

Главный редактор А.В. Бурцев

Компьютерная верстка М.А. Беляева

Журнал зарегистрирован Федеральной службой по надзору в сфере связи,
информационных технологий и массовых коммуникаций
ПИ № ФС77-68207 от 30 декабря 2016 года

Территория распространения: Российская Федерация, зарубежные страны

Подписано в печать 17.06.2025. Дата выхода 26.06.2025
Формат 60 × 84 1/8. Усл. печ. л. 16,04
Тираж 75 экз. Заказ № 15516. Свободная цена

Адрес издателя, редакции журнала «Гений ортопедии»
640014, Россия, г. Курган, ул. М. Ульяновой, 6
http://ilizarov-journal.com

Отпечатано в Типографии «Эталон». 198097, г. Санкт-Петербург, ул. Трефолева, 2 литера БН, помещение 3-Н, офис 1